SINGLE, DUAL AND TRIPLE DISCHARGE FROM A LARGE, STRATIFIED, TWO-PHASE REGION THROUGH SMALL BRANCHES

By

Ibrahim Galal Ibrahim Hassan

A Thesis

Submitted to the Faculty of Graduate Studies

in Partial Fulfillment of the Requirements

for the Degree of

Doctor of Philosophy

Department of Mechanical and Industrial Engineering

University of Manitoba

Winnipeg, Manitoba, Canada

1995

ISBN 0-612-13177-7

Name ________

Dissertation Abstracts International is arranged by broad, general subject categories. Please select the one subject which most nearly describes the content of your dissertation. Enter the corresponding four-digit code in the spaces provided.

Heat and Thermodynamics — SUBJECT TERM

0348 — SUBJECT CODE

UMI

Subject Categories

THE HUMANITIES AND SOCIAL SCIENCES

COMMUNICATIONS AND THE ARTS
- Architecture ... 0729
- Art History ... 0377
- Cinema ... 0900
- Dance ... 0378
- Fine Arts ... 0357
- Information Science ... 0723
- Journalism ... 0391
- Library Science ... 0399
- Mass Communications ... 0708
- Music ... 0413
- Speech Communication ... 0459
- Theater ... 0465

EDUCATION
- General ... 0515
- Administration ... 0514
- Adult and Continuing ... 0516
- Agricultural ... 0517
- Art ... 0273
- Bilingual and Multicultural ... 0282
- Business ... 0688
- Community College ... 0275
- Curriculum and Instruction ... 0727
- Early Childhood ... 0518
- Elementary ... 0524
- Finance ... 0277
- Guidance and Counseling ... 0519
- Health ... 0680
- Higher ... 0745
- History of ... 0520
- Home Economics ... 0278
- Industrial ... 0521
- Language and Literature ... 0279
- Mathematics ... 0280
- Music ... 0522
- Philosophy of ... 0998
- Physical ... 0523
- Psychology ... 0525
- Reading ... 0535
- Religious ... 0527
- Sciences ... 0714
- Secondary ... 0533
- Social Sciences ... 0534
- Sociology of ... 0340
- Special ... 0529
- Teacher Training ... 0530
- Technology ... 0710
- Tests and Measurements ... 0288
- Vocational ... 0747

LANGUAGE, LITERATURE AND LINGUISTICS
- Language
  - General ... 0679
  - Ancient ... 0289
  - Linguistics ... 0290
  - Modern ... 0291
- Literature
  - General ... 0401
  - Classical ... 0294
  - Comparative ... 0295
  - Medieval ... 0297
  - Modern ... 0298
  - African ... 0316
  - American ... 0591
  - Asian ... 0305
  - Canadian (English) ... 0352
  - Canadian (French) ... 0355
  - English ... 0593
  - Germanic ... 0311
  - Latin American ... 0312
  - Middle Eastern ... 0315
  - Romance ... 0313
  - Slavic and East European ... 0314

PHILOSOPHY, RELIGION AND THEOLOGY
- Philosophy ... 0422
- Religion
  - General ... 0318
  - Biblical Studies ... 0321
  - Clergy ... 0319
  - History of ... 0320
  - Philosophy of ... 0322
- Theology ... 0469

SOCIAL SCIENCES
- American Studies ... 0323
- Anthropology
  - Archaeology ... 0324
  - Cultural ... 0326
  - Physical ... 0327
- Business Administration
  - General ... 0310
  - Accounting ... 0272
  - Banking ... 0770
  - Management ... 0454
  - Marketing ... 0338
- Canadian Studies ... 0385
- Economics
  - General ... 0501
  - Agricultural ... 0503
  - Commerce-Business ... 0505
  - Finance ... 0508
  - History ... 0509
  - Labor ... 0510
  - Theory ... 0511
- Folklore ... 0358
- Geography ... 0366
- Gerontology ... 0351
- History
  - General ... 0578
  - Ancient ... 0579
  - Medieval ... 0581
  - Modern ... 0582
  - Black ... 0328
  - African ... 0331
  - Asia, Australia and Oceania 0332
  - Canadian ... 0334
  - European ... 0335
  - Latin American ... 0336
  - Middle Eastern ... 0333
  - United States ... 0337
- History of Science ... 0585
- Law ... 0398
- Political Science
  - General ... 0615
  - International Law and Relations ... 0616
  - Public Administration ... 0617
- Recreation ... 0814
- Social Work ... 0452
- Sociology
  - General ... 0626
  - Criminology and Penology ... 0627
  - Demography ... 0938
  - Ethnic and Racial Studies ... 0631
  - Individual and Family Studies ... 0628
  - Industrial and Labor Relations ... 0629
  - Public and Social Welfare ... 0630
  - Social Structure and Development ... 0700
  - Theory and Methods ... 0344
- Transportation ... 0709
- Urban and Regional Planning ... 0999
- Women's Studies ... 0453

THE SCIENCES AND ENGINEERING

BIOLOGICAL SCIENCES
- Agriculture
  - General ... 0473
  - Agronomy ... 0285
  - Animal Culture and Nutrition ... 0475
  - Animal Pathology ... 0476
  - Food Science and Technology ... 0359
  - Forestry and Wildlife ... 0478
  - Plant Culture ... 0479
  - Plant Pathology ... 0480
  - Plant Physiology ... 0817
  - Range Management ... 0777
  - Wood Technology ... 0746
- Biology
  - General ... 0306
  - Anatomy ... 0287
  - Biostatistics ... 0308
  - Botany ... 0309
  - Cell ... 0379
  - Ecology ... 0329
  - Entomology ... 0353
  - Genetics ... 0369
  - Limnology ... 0793
  - Microbiology ... 0410
  - Molecular ... 0307
  - Neuroscience ... 0317
  - Oceanography ... 0416
  - Physiology ... 0433
  - Radiation ... 0821
  - Veterinary Science ... 0778
  - Zoology ... 0472
- Biophysics
  - General ... 0786
  - Medical ... 0760

EARTH SCIENCES
- Biogeochemistry ... 0425
- Geochemistry ... 0996
- Geodesy ... 0370
- Geology ... 0372
- Geophysics ... 0373
- Hydrology ... 0388
- Mineralogy ... 0411
- Paleobotany ... 0345
- Paleoecology ... 0426
- Paleontology ... 0418
- Paleozoology ... 0985
- Palynology ... 0427
- Physical Geography ... 0368
- Physical Oceanography ... 0415

HEALTH AND ENVIRONMENTAL SCIENCES
- Environmental Sciences ... 0768
- Health Sciences
  - General ... 0566
  - Audiology ... 0300
  - Chemotherapy ... 0992
  - Dentistry ... 0567
  - Education ... 0350
  - Hospital Management ... 0769
  - Human Development ... 0758
  - Immunology ... 0982
  - Medicine and Surgery ... 0564
  - Mental Health ... 0347
  - Nursing ... 0569
  - Nutrition ... 0570
  - Obstetrics and Gynecology ... 0380
  - Occupational Health and Therapy ... 0354
  - Ophthalmology ... 0381
  - Pathology ... 0571
  - Pharmacology ... 0419
  - Pharmacy ... 0572
  - Physical Therapy ... 0382
  - Public Health ... 0573
  - Radiology ... 0574
  - Recreation ... 0575
  - Speech Pathology ... 0460
  - Toxicology ... 0383
- Home Economics ... 0386

PHYSICAL SCIENCES

Pure Sciences
- Chemistry
  - General ... 0485
  - Agricultural ... 0749
  - Analytical ... 0486
  - Biochemistry ... 0487
  - Inorganic ... 0488
  - Nuclear ... 0738
  - Organic ... 0490
  - Pharmaceutical ... 0491
  - Physical ... 0494
  - Polymer ... 0495
  - Radiation ... 0754
- Mathematics ... 0405
- Physics
  - General ... 0605
  - Acoustics ... 0986
  - Astronomy and Astrophysics ... 0606
  - Atmospheric Science ... 0608
  - Atomic ... 0748
  - Electronics and Electricity ... 0607
  - Elementary Particles and High Energy ... 0798
  - Fluid and Plasma ... 0759
  - Molecular ... 0609
  - Nuclear ... 0610
  - Optics ... 0752
  - Radiation ... 0756
  - Solid State ... 0611
- Statistics ... 0463

Applied Sciences
- Applied Mechanics ... 0346
- Computer Science ... 0984
- Engineering
  - General ... 0537
  - Aerospace ... 0538
  - Agricultural ... 0539
  - Automotive ... 0540
  - Biomedical ... 0541
  - Chemical ... 0542
  - Civil ... 0543
  - Electronics and Electrical ... 0544
  - Heat and Thermodynamics ... 0348 —
  - Hydraulic ... 0545
  - Industrial ... 0546
  - Marine ... 0547
  - Materials Science ... 0794
  - Mechanical ... 0548
  - Metallurgy ... 0743
  - Mining ... 0551
  - Nuclear ... 0552
  - Packaging ... 0549
  - Petroleum ... 0765
  - Sanitary and Municipal ... 0554
  - System Science ... 0790
- Geotechnology ... 0428
- Operations Research ... 0796
- Plastics Technology ... 0795
- Textile Technology ... 0994

PSYCHOLOGY
- General ... 0621
- Behavioral ... 0384
- Clinical ... 0622
- Developmental ... 0620
- Experimental ... 0623
- Industrial ... 0624
- Personality ... 0625
- Physiological ... 0989
- Psychobiology ... 0349
- Psychometrics ... 0632
- Social ... 0451

SINGLE, DUAL AND TRIPLE DISCHARGE FROM A LARGE, STRATIFIED, TWO-PHASE REGION THROUGH SMALL BRANCHES

BY

IBRAHIM GALAL IBRAHIM HASSAN

A Practicum submitted to the Faculty of Graduate Studies of the University of Manitoba in partial fulfillment of the requirements of the degree of

DOCTOR OF PHILOSOPHY

I hereby declare that I am the sole author of this thesis.

I authorize the University of Manitoba to lend this thesis to other institutions or individuals for the purpose of scholarly research.

ABSTRACT

The development of experimental correlations and theoretical models for the accurate prediction of the flow rate and quality during two-phase discharge through small branches in pipes has received considerable attention in the recent literature. This interest is due to the relevance of this topic to many industrial applications, such as the flow distribution in the cooling headers of CANDU nuclear reactors (CANDU is derived from CANada, Deuterium and Uranium) during postulated Loss-Of-Coolant Accidents ($LOCA$).

A few experimental investigations for the onsets of gas and liquid entrainment, mass flux and quality have been reported for the case of a single discharge (e.g., Smoglie and Reimann, 1986; Schrock et al., 1986; Yonomoto and Tasaka, 1988 and 1991). Experimental data and correlations were also developed for the onsets of gas and liquid entrainment during dual discharge from a large reservoir (Parrott et al., 1991; Armstrong et al., 1992). However, no information exists currently on the mass flux and quality during dual discharge. For three or more branches, design information is completely lacking.

In the present investigation, extensive data were generated for the mass flow rate and quality of two-phase (air-water) discharge from a large stratified region (at a pressure P_o) through small side branches ($d = 6.35\ mm$). Four groups of data were generated; each group corresponds to a particular branch configuration. Group

no.1 contains the data for a single side branch, group no. 2 corresponds to two side branches separated by a distance L center-to-center with the centerlines in the same horizontal plane. and group no. 3 corresponds to two side branches separated by a distance L center-to-center with centerlines in the same vertical plane. All branches in group nos. 1 to 3 were mounted on a flat vertical wall with their axes horizontal and parallel to each other. Group no. 4 corresponds to three side branches installed on a semicircular wall. Dimensions of the wall-branches assembly in group no. 4 were selected to be in direct proportion to the CANDU header-feeder system. The test matrix in this group was designed to include data of a single discharge, dual discharge and triple discharge. The cases of dual and triple discharge in group nos. 2-4 were investigated under the conditions of equal hydraulic resistance R for the branches and equal pressure drop ΔP across the branches.

In each of the four groups, the mass flow rate $\dot{m}_{TP}$ and quality x were measured at different liquid levels within the range giving two-phase flow in the branches. The independent variables P_o, ΔP, R and L/d (if applicable) were varied in a systematic fashion in order to isolate the influence of each variable. The following ranges were covered: P_o =316 and 516 kPa, ΔP =37 to 229 kPa, $L/d = 1.5, 2, 3$ and 8 and $R =$ 900 to 3000 $(kg.m)^{-1/2}$. Normalized plots are shown to be capable of absorbing the effects of some independent variables within the tested range of operating conditions. Empirical relations were developed for $\dot{m}_{TP}$ and x (in group nos. 1 to 3) in terms of normalized parameters. These relations agree well with the experimental data.

A theoretical model was developed for predicting the critical height at the onset of liquid entrainment during dual discharge from a stratified two-phase region through branches of finite size mounted on an inclined flat wall. A previous analysis by Armstrong et al. (1992), in which the branches were simulated by point sinks on a vertical wall, has been extended to account for the finite size of the branches and the wall inclination. The present model approaches the correct limit for the onset of liquid entrainment at low values of Froude number at the upper and lower branches, Fr_1 and Fr_2, respectively and it converges to the Armstrong et al.'s predictions at high Fr_1 and Fr_2. The present analysis applies to any two immiscible fluids with the term " liquid entrainment" referring to the appearance of the heavier fluid through the lower branch. Some experimental verification of the present theoretical trend is also provided.

ACKNOWLEDGMENTS

I would like to acknowledge and thank the many people who have provided assistance over the course of this investigation. Special thanks go to the author's supervisors, Dr. H. M. Soliman and Dr. G. E. Sims, both of whom provided continuous encouragement and guidance throughout the entire research process. The technical support provided by Dr. J. E. Kowalski of the Whiteshell Laboratories, AECL Research is greatly appreciated. The assistance of Mr. M. Kapitoler and Mr. J. Finken in constructing and maintaining the apparatus is gratefully acknowledged.

The financial support provided by the Natural Science and Engineering Research Council of Canada, the CANDU Owners Group, and the University of Manitoba is sincerely acknowledged as well.

Finally, I would like to thank my family and my wife for their sincere support and encouragement. I am also grateful to my home country Egypt for providing me with this special opportunity of undertaking this higher education.

TABLE OF CONTENTS

CHAPTER PAGE

LIST OF FIGURES

FIGURE PAGE

FIGURE PAGE

FIGURE PAGE

FIGURE PAGE

FIGURE PAGE

FIGURE **PAGE**

LIST OF TABLES

TABLE PAGE

NOMENCLATURE

a_α	coefficient, defined by Equation (2.18)
b_α	coefficient, defined by Equation (2.21)
Bo	Bond number, defined by Equation (2.12)
c	empirical parameter used in Equations (2.6) and (2.11)
c_p	specific heat at constant pressure, $J/kg \cdot K$
c_α	coefficient, defined by Equation (2.22)
d	branch diameter, m
D	diameter of semicircular surface for data group no. 4, m
Fr	Froude number, defined by Equations (2.4) and (2.5)
Fr^*	Froude number, defined by Equation (5.3)
g	gravitational acceleration, m/s^2
h	vertical distance between the flat part of the water surface and the centerline of a branch, m
h^*	liquid level, defined in Figures 4.36 and 4.53, m
h_b	critical height at the BLE or BGE used in Equations (2.6) and (2.11), m
h_b^*	liquid level, defined by Equation (2.26), m
$h_{BLE,O}$	critical height at the BLE obtained from Equation (5.2), used in Figures 5.5 and 5.6, m

H	normalized liquid level, defined by Equation (4.1)
k	ratio of specific heats
L	distance between the centerlines of two branches, m
$\dot{m}$	mass flow rate, kg/s
M	normalized mass flow rate, defined by Equation (4.2)
N_μ	viscosity number, defined by Equation (2.12)
P	pressure, Pa
r	coefficient, defined by Equation (2.7)
R	hydraulic resistance given by Equation (3.1), $(kg \cdot m)^{-1/2}$
R'	ideal gas constant, $J/kg \cdot K$
s	distance, defined in Figure (5.1), m
t	deflection of the interface, m
T	temperature, K
x	quality
X, Y, Z	coordinates in the Cartesian system used in Chapter 5, m
v	specific volume, m^3/kg
V	velocity, m/s
V_d	mean velocity of the continuous phase through the branch (which is the gas during BLE and the liquid during BGE), m/s
V_L^*	mean liquid velocity in the main pipe (downstream from the branch) used

in Equation (2.29), m/s

Greek Letters

α	void fraction
$\delta(\ )$	uncertainty in ( )
δ^*	meniscus height used in Equation (2.30), m
θ	wall inclination angle, defined in Figure 5.1
μ	dynamic viscosity, $N \cdot s/m^2$
ρ	density, kg/m^3
ρ_m	homogeneous density, defined in Equation (2.27), kg/m^3
σ	surface tension, N/m

Subscripts

$1, 2$	lower or upper branch during dual discharge (used in Chapter 5)
A, B or C	branches A, B or C
BGE	beginning of gas entrainment
BLE	beginning of liquid entrainment

c	choking conditions
G	gas phase
L	liquid phase
o	large reservoir condition
s	separator condition
TP	two phase
x, y, z	components in X-, Y- and Z-directions, respectively, used in Chapter 5

CHAPTER 1

INTRODUCTION

Several industrial applications involve two-phase flow discharging from a stratified region through single or multiple branches. Examples of these applications include the flow through small breaks in horizontal cooling channels of nuclear reactors during postulated loss-of-coolant accidents, the flow distribution in CANDU header-feeder systems (multiple branches) during accident scenarios and two-phase distribution headers in general, where a certain incoming stream fed into a large header is divided among a number of discharging streams. Knowledge of the flow phenomena involved, as well as the mass flow rate and quality of all discharging streams is obviously essential for the design and/or performance prediction of such systems.

For the case of single discharge from a large flow channel under stratified flow conditions, Zuber (1980) pointed out that during such flows two distinct phenomena may occur, depending on the location of the gas-liquid interface relative to the branch. If the interface is located above the branch, gas can be entrained (by vortex or vortex-free motion) into the predominantly liquid flow through the branch. On the other hand, if the interface is located below the branch, liquid may be entrained into the predominantly gas flow. He proposed simplified correlations for the onsets of these phenomena in terms of relevant system parameters and branch orientation (top, bottom or side). Later, detailed experiments were reported on the onsets of gas and liquid entrainment, two-phase mass flux and quality during discharge from a large stratified region (with or without main flow) through a single branch with different orientations (e.g., Smoglie and Reimann, 1986; Schrock et al., 1986; Yonomoto and Tasaka, 1988 and 1991; Micaelli and Memponteil, 1989).

In situations where multiple discharge takes place simultaneously from several branches, the existing single-branch correlations may not apply. Initial steps towards understanding these systems were undertaken by Parrott et al. (1991) and Armstrong et al. (1992) who investigated the onsets of gas and liquid entrainment, respectively, during discharge from stratified two-phase regions through two side branches. However, no information exists currently on the mass flux and quality during dual discharge. For three or more branches , information is completely lacking.

The objective of this thesis is to address the current deficiency in the literature by taking a number of steps towards creating new knowledge that would ultimately lead to the proper design of two-phase headers with multiple discharge. In more explicit terms, the objectives of the present study are:

1. To develop experimental data and correlations for determining the two-phase mass flux and quality during single and dual discharge from a large stratified

region through small branches mounted on a vertical flat wall. For the dual discharge case, the centerlines of the branches are to be located in either (i) a horizontal plane, or (ii) a vertical plane.

2. To develop experimental data for determining the two-phase mass flux and quality during discharge from a large stratified region through small branches mounted on a semicircular wall. Dimensions of the wall-branches assembly were chosen to be in direct proportion to the CANDU header-feeder system. The test matrix was designed to include data of single discharge, dual discharge and triple discharge.

3. To perform a visual study of the different flow phenomena (such as the onset of gas entrainment, the onset of liquid entrainment, or a combination of both) that may occur during dual and triple discharge. The flow loop was designed to facilitate this investigation.

4. To develop a theoretical model for determining the onset of liquid entrainment during dual discharge from a large stratified region through small side branches mounted on an inclined flat wall. The derivation technique used in this study may help in the future for modeling similar flow phenomena that may occur during multiple two-phase discharge.

CHAPTER 2

LITERATURE REVIEW

2.1 Single-Discharge Investigations

Studies of two-phase flow through small branches in horizontal pipes under stratified-flow conditions have gained importance due to their relevance to many engineering applications. The importance of this problem has motivated significant research, conducted mostly during the past ten years. Smoglie and Reimann (1986) performed experiments using stratified air-water flow at 200 to 500 kPa in a horizontal pipe (20.6 cm in diameter) with different branch sizes (d = 6, 8, 12 and 20 mm) and different orientations (top, bottom or side) for each branch. The branches were simulated by pipe stubs (0.055 m in length) with sharp-edged entrances and the flow through the branch was controlled by a throttle valve. These results indicated an insignificant effect of the branch size on the onsets of gas and liquid entrainment and the quality at the branch. The onsets of entrainment were detected by the noise in the differential-pressure signals across the branch.

Correlations were developed by Smoglie and Reimann (1986) based on their experimental data to predict the onsets of entrainment and quality of discharge. For the side- and bottom-orientation cases (most relevant cases for the present work), the critical heights corresponding to the Onset or Beginning of Gas Entrainment (BGE) and the Beginning of Liquid Entrainment (BLE) were given in terms of Froude number as follows:

For the side-orientation case,

$$\frac{h_{BGE}}{d} = 0.681 \;\; Fr_{BGE}^{0.4} \tag{2.1}$$

and

$$\frac{|h_{BLE}|}{d} = 0.626 \;\; Fr_{BLE}^{0.4}. \tag{2.2}$$

For the bottom-orientation case,

$$\begin{aligned} \frac{h_{BGE}}{d} &= 1.816 \;\; Fr_{BGE}^{0.4}, && \text{for vortex flow,} \\ &= 0.626 \;\; Fr_{BLE}^{0.4}, && \text{for vortex-free flow,} \end{aligned} \tag{2.3}$$

with

$$Fr_{BGE} = \frac{4 \;\; \dot{m}_{L,BGE}}{\pi\sqrt{gd^5\rho_L(\rho_L - \rho_G)}} \tag{2.4}$$

and

$$Fr_{BLE} = \frac{4 \;\; \dot{m}_{G,BLE}}{\pi\sqrt{gd^5\rho_G(\rho_L - \rho_G)}}, \tag{2.5}$$

where h is the vertical distance between the water surface and the centerline of the branch (positive in the upward direction), ρ_G is the density of the gas, ρ_L is the density of the liquid, g is the gravitational acceleration, and $\dot{m}$ is the mass flow rate at the onset.

The quality of discharge was correlated for the region $h_{BLE} \leq h \leq h_{BGE}$ ($h_{BLE} = 0$ for the bottom branch). For the side branch, it was given by

$$x = r^{\left(1.0+c\,\frac{h}{h_b}\right)}\left[1.0 - 0.5\left(\frac{h}{h_b}\right)\left(1.0+\frac{h}{h_b}\right)r^{\left(1.0-\frac{h}{h_b}\right)}\right]^{0.5}, \tag{2.6}$$

with $$r = \frac{1.15}{1.0 + \sqrt{\frac{\rho_L}{\rho_G}}}, \tag{2.7}$$

where $c = 1.09$, $h_b = h_{BGE}$ when $h > 0$, and $c = 1.00$, $h_b = |h_{BLE}|$ when $h < 0$.

For the bottom branch, the quality was given by

$$x = r^{(2.5\ h/h_{BGE})} \left[1.0 - 0.5 \left(\frac{h}{h_{BGE}} \right) \left(1.0 + \frac{h}{h_{BGE}} \right) r^{(1.0 - h\ /h_{BGE})} \right]^{0.5}. \tag{2.8}$$

Schrock et al. (1986) performed experiments using both air-water and steam-water as the working fluids. The experiments were performed at system pressures up to 1.07 MPa in a horizontal pipe (10.2 cm in diameter) with different branch sizes ($d = 4$, 6 and 10 mm) and different orientations for each branch. The branches were simulated by tubes 123 mm in length. Viewing windows were placed at the branch section and in the pipe just upstream and downstream of the branch to allow visual observation of the flow phenomena. They concluded that the BGE (side and bottom orientations) was affected by surface tension and viscosity in addition to Froude number. The BGE data for the side orientation did not agree with the data of Smoglie and Reimann (1986). No explanation was given for this disagreement. Their data on discharge quality, together with data from other studies were correlated in terms of a normalized interface level. The correlations for h_{BGE}, h_{BLE} and x of side branches were given by

$$\frac{h_{BGE}}{d} = \sqrt{\frac{\sigma}{g d^2 \Delta\rho}} \left(\frac{1}{40.6} Fr_{BGE} Bo^2 N_\mu^{-0.5} \right)^{0.476}, \tag{2.9}$$

$$\frac{|h_{BLE}|}{d} = 0.624\ \ Fr_{BLE}^{0.4} \tag{2.10}$$

and

$$x = 0.06^{\left(1.0+\frac{h}{h_b}\right)^{0.7}} \left[1.0 - c\left(\frac{h}{h_b}\right)\left(1.0 + \frac{h}{h_b}\right)\right], \tag{2.11}$$

with $$Bo = d\sqrt{\frac{g\Delta\rho}{\sigma}}, \quad \text{and} \quad N_\mu = \frac{\mu_L\,(g\Delta\rho)^{0.25}}{\sigma^{0.75}\rho_L^{0.5}}, \tag{2.12}$$

where Bo is the Bond number, N_μ is the viscosity number, σ is the surface tension, $\Delta\rho$ is the density difference between the phases, μ_L is the liquid viscosity, ($c = 0.5$, $h_b = h_{BGE}$) when $h > 0$ and ($c = 0$, $h_b = |h_{BLE}|$) when $h < 0$. For bottom branches, h_{BGE} and x were given by

$$\frac{h_{BGE}}{d} = \sqrt{\frac{\sigma}{gd^2\Delta\rho}}\left(\frac{1}{19.4}Fr_{BGE}Bo^2N_\mu^{-0.5}\right)^{0.454} \tag{2.13}$$

and $$x = \left[1.0 - \left(\frac{h}{h_{BGE}}\right)^2\right]^{3.5} exp\left[-3.1\left(\frac{h}{h_{BGE}}\right)\right]. \tag{2.14}$$

Yonomoto and Tasaka (1988) developed a simple analytical model to study two-phase flow through small branches. Air-water experiments at a maximum pressure of 700 kPa were also conducted. A horizontal, square duct (19 cm x 19 cm) was used in the experiments instead of a round pipe. The branch was simulated by a sharp-edged junction ($d = 10$ and 20 mm). The characterization of BGE and BLE was determined by visual observation. Their model defined a two-phase interface profile having a conical shape near the branch. Therefore, the mass flow rate and quality of the two-phase discharge through the branch were expressed as a function of the void fraction α, defined as a ratio of gas flow area to total flow area in this conical region

$$\dot{m}_{TP} = \alpha\ \dot{m}_{G,BGE} + (1.0 - \alpha)\ \dot{m}_{L,BGE} \tag{2.15}$$

and
$$x = \frac{\alpha\ \dot{m}_{G,BGE}}{\dot{m}_{TP}}. \tag{2.16}$$

The void fraction α for the side branch was given by

$$\alpha = (1.0 - a_\alpha)\left(\frac{h}{h_{BLE}}\right) + a_\alpha, \qquad \text{for } h < 0$$

and
$$\alpha = -a_\alpha\left(\frac{h}{h_{BGE}}\right) + a_\alpha, \qquad \text{for } h > 0, \tag{2.17}$$

where
$$a_\alpha = \frac{1.0}{1.0 + \left(\frac{\dot{m}_{G,BLE}}{\dot{m}_{L,BGE}}\right)\sqrt{\frac{\rho_L}{\rho_G}}}, \tag{2.18}$$

$$\frac{h_{BGE}}{d} = 0.682\ Fr_{BGE}^{0.4} \quad \text{and} \quad \frac{|h_{BLE}|}{d} = 0.558\ Fr_{BLE}^{0.4}. \tag{2.19}$$

For the bottom branch, α was given by

$$\alpha = 0.9\ b_\alpha, \qquad \text{for } 0 \leq\ b_\alpha \leq 0.6$$

and
$$\alpha = 1.15\ b_\alpha - 0.15, \qquad \text{for } 0.6 <\ b_\alpha \leq 1.0, \tag{2.20}$$

where

$$b_\alpha = 1.0 - \left[c_\alpha + \left({c_\alpha}^2 + \frac{\dot{m}_{G,BLE}}{\dot{m}_{L,BGE}}\sqrt{\frac{\rho_L}{\rho_G}}\left(\frac{h}{h_{BGE}}\right)^{2.5}\right)^{0.5}\right], \tag{2.21}$$

with
$$c_\alpha = 0.5\left(1.0 - \frac{\dot{m}_{G,BLE}}{\dot{m}_{L,BGE}}\sqrt{\frac{\rho_L}{\rho_G}}\right)\left(\frac{h}{h_{BGE}}\right)^{2.5} \tag{2.22}$$

and $$\frac{h_{BGE}}{d} = 0.909 \ Fr_{BGE}^{0.4}. \tag{2.23}$$

Good agreement was obtained between their model and their experimental data for discharge quality on the liquid- entrainment side ($h < 0$) and an empirical correction factor was incorporated in the model on the gas-entrainment side ($h > 0$). A modified mathematical model was developed later by Yonomoto and Tasaka (1991) which improved the agreement with the experimental data.

Micaelli and Memponteil (1989) performed experiments using steam-water mixtures. A wide range of parameters was covered (system pressures of 2 to 7 MPa, main pipe diameters of 80 and 135 mm, and branch diameters of 12 and 20 mm). The correlations for the BGE and BLE were based on their experimental data as well as those of Smoglie and Reimann (1986), and Schrock et al. (1986). A semi-empirical correlation was developed for the branch quality based on simple theoretical approaches adjusted by their own experimental data as well as other experimental data in the literature.

In their final correlation, the quality x for the side-branch case was given as a function of the void fraction α at the branch inlet over the whole range $h_{BLE} \leq h \leq h_{BGE}$ as follows:

$$x = \frac{\alpha}{\alpha + \sqrt{\frac{\rho_L}{\rho_G}}(1.0 - \alpha)}, \tag{2.24}$$

where

$$\alpha = 1.0 - 0.5\left(1.0 + \frac{h}{h_b^*}\right)^2 \qquad \text{for } h < 0$$

and

$$\alpha = 0.5\left(1.0 - \frac{h}{h_b^*}\right)^2, \qquad \text{for } h > 0, \tag{2.25}$$

with

$$h_b^* = 0.69\left[\frac{\dot{m}_{TP}^2}{g\rho_m(\rho_L - \rho_G)}\right]^{0.2} \tag{2.26}$$

and ρ_m is the homogeneous density given by

$$\rho_m = \left[\frac{x}{\rho_G} + \frac{(1.0 - x)}{\rho_L}\right]^{-1}. \tag{2.27}$$

For the bottom branch, x was also correlated by Equation (2.24) with α given by

$$\alpha = 1.0 - \frac{h}{h_{BGE}} \tag{2.28}$$

and

$$h_{BGE} = \left[1.0 - \left(\frac{V_L^*}{V_d}\right)^{0.4}\right]\left[\frac{\dot{m}_{L,BGE}^2}{g\rho_L(\rho_L - \rho_G)}\right]^{0.2}, \tag{2.29}$$

where V_d and V_L^* are the mean liquid velocities in the branch and in the main pipe (downstream from the branch), respectively.

2.2 Multiple-Discharge Investigations

The common feature among the investigations mentioned above is that fluid discharge was always induced through one branch (top, bottom or side). In situations where discharge takes place simultaneously from multiple branches at the same cross-section, such as the case with the flow distribution headers of CANDU nuclear reactors or two-phase distribution headers in general, these existing models of single discharge may not apply.

Kowalski and Krishnan (1987) reported experiments with steam-water flow in a test section typical of the CANDU header-feeder system. In general, the CANDU heat-transport system contains large horizontal headers, approximately 10 to 12m in length and 0.3 to 0.4m in diameter, connected to the fuel channels by a number of feeders, typically 50.8 mm in diameter, attached to the side walls of the header. Normally, the feeders are arranged in banks at different cross-sections along the header with five feeders in each bank. Kowalski and Krishnan found that the experimental values of the critical heights at BGE and BLE were significantly underpredicted by the correlations of Smoglie and Reimann (1986) .

Initial steps towards understanding the reasons for the disagreement between the single and multiple discharge results were taken by Parrott (1993). He investigated experimentally the phenomena of BGE and BLE for the condition of simultaneous discharge from two small branches oriented vertically with respect to each other on the side of a high -pressure reservoir containing a stratified air-water mixture. The study was performed with system pressures of 0.5 MPa during BGE experiments and 0.3 MPa during BLE experiments. Both onsets were determined by visual observation. Parrott concluded that the critical heights corresponding to the onsets can be strongly influenced by the vertical distance separating the centerlines of the branches.

Parrott et al. (1991) developed an empirical correlation for the critical height for BGE at the upper branch during dual discharge given by

$$\frac{h_{BGE}+\delta^*}{d} = 0.887\left[Fr_1 + Fr_2\ exp\left(-2.52\left(\frac{L}{d}\right)^{1.1} Fr_1^{-0.22} Fr_2^{-0.16}\right)\right]^{0.334}, \quad (2.30)$$

where h_{BGE} is the vertical distance between the flat interface and the centerline of the upper branch, Fr_1 and Fr_2 are the Froude numbers at the upper and lower branches and δ^* is the meniscus height (estimated to be about 3.3 mm). Since correlation (2.30) is purely empirical, its use was recommended only for geometries , fluid properties and flow conditions similar to those considered in their experimental investigation.

Following Parrott et al. (1991), Armstrong et al. (1992) developed a theoretical model to predict the critical height for BLE during dual discharge. In their simplified theoretical analysis, Armstrong et al. (1992) neglected the effects of viscosity and surface tension, assumed potential flow throughout the field and treated each branch as a point sink. With these simplifications, h_{BLE}/L was obtained as a function of $Fr_1\left(\frac{L}{d}\right)^{-2.5}$ and $Fr_2\left(\frac{L}{d}\right)^{-2.5}$. The model will be discussed further in Chapter 5.

The above review shows that some information exists in the literature on the flow phenomena and critical heights for the BGE and BLE during dual discharge. However, no information exists currently on the mass flux and quality during dual discharge. For multiple discharge, design information is completely lacking. The objective of this thesis is to address the current deficiency in the literature by taking a number of steps towards creating new knowledge that would ultimately lead to the proper design of two-phase headers with multiple discharge.

CHAPTER 3

EXPERIMENTAL INVESTIGATION

3.1 Scope

The data taken in this investigation are categorized into four groups. Each group corresponds to a particular branch configuration. Group no. 1 presents the data of a single branch (diameter d); group no. 2 corresponds to two side branches of equal diameter d and a horizontal separating distance L center-to-center; group no. 3 corresponds to two side branches of equal diameter d and a vertical separating distance L center-to-center. All branches in group nos. 1 to 3 were mounted on a flat vertical surface with their centerlines horizontal, as shown in Figure 3.1. Group no.4 corresponds to three side branches of equal diameter d installed on a semicircular surface. Dimensions of the semicircular surface and branches were chosen to be in direct proportion to those of the CANDU header-feeder system.

The experiments of dual and triple discharge were conducted under the conditions that the branches have the same hydraulic resistance R, and the pressure drop is the same across the branches.

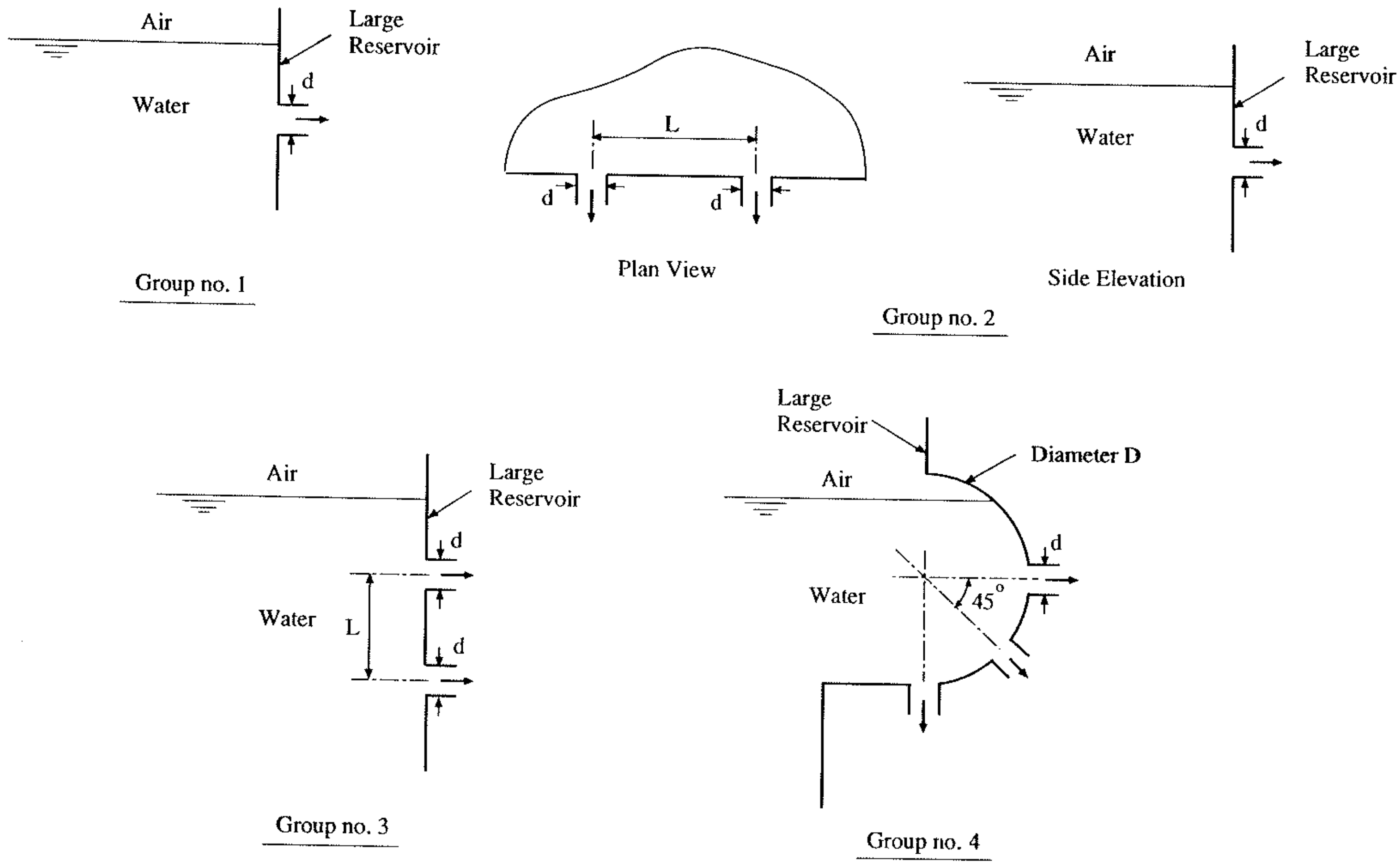

Figure 3.1: Branch geometries for group nos. 1 to 4

Group nos. 1 to 4 could serve as benchmark data for testing safety codes of CANDU nuclear reactors and in general would guide future research on two-phase distribution headers.

3.2 Experimental Parameters

The geometrical and flow parameters relevant to the most elaborate case of triple discharge are shown in Figure 3.2. The modifications applicable to the other cases of single and dual discharge are given at the end of this section.

Figure 3.2 shows a semicircular surface with three branches (A, B and C) of equal internal diameter d placed on the side of a large reservoir containing stratified layers of air and water at a pressure P_o. One stream (could be A, B or C) was directed to a measuring separator where air and water flow rates were measured downstream, and the remaining two streams were directed to an auxiliary (non-measuring) separator. Both separators were kept at P_s; thus the pressure drop across all branches, ΔP, was kept the same. Even though each experiment would have to be repeated three times in order to measure the flow from all three branches, this was found preferable to using three separators due to the difficulty in maintaining all separators at a preset pressure throughout testing. Another condition that was imposed in this study is equal hydraulic resistance R for all branches. The hydraulic resistance of a branch was based on single-phase liquid flow conditions, as defined

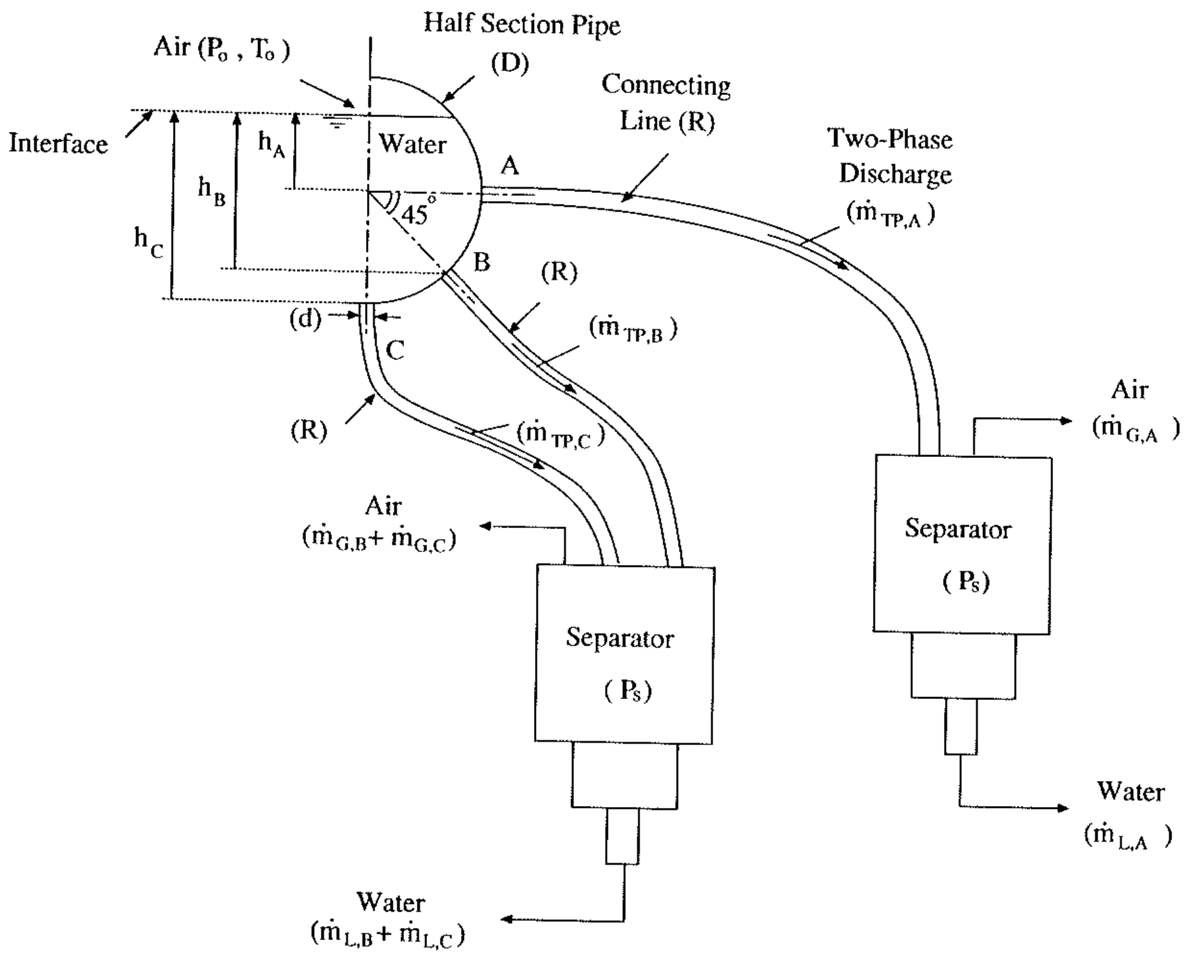

Figure 3.2: Relevant experimental parameters for group no. 4

later.

Under these conditions, the mass flow rate and quality of the three discharging streams are expected to depend on P_o, ΔP, R and the location of the air-water interface relative to the branches. For fixed values of P_o, ΔP and R, let us consider the dependence of flow from the three branches on the location of the interface. At high interface levels above branch A, the discharge from the three branches will be in the form of single-phase liquid with essentially equal mass flow rates, $\dot{m}_{L,A} = \dot{m}_{L,B} = \dot{m}_{L,C}$. Lowering the interface level, a critical height is reached where the BGE occurs at branch A ($h_A = h_{BGE,A}$ and $\dot{m}_{L,A} = \dot{m}_{BGE,A}$). For $h_A > h_{BGE,A}$, the four quantities $\dot{m}_{L,BGE,A}$, $\dot{m}_{L,A}$, $\dot{m}_{L,B}$ and $\dot{m}_{L,C}$ are essentially equal. The hydraulic resistance for any branch is defined as

$$R = \frac{\sqrt{\Delta P}}{\dot{m}_{L,BGE}}. \tag{3.1}$$

A further lowering of the interface results in a two-phase discharge at branch A at a rate $\dot{m}_{TP,A}$, while the single-phase liquid flow at branches B and C remains unchanged. The two-phase flow from branch A is split in the measuring separator into liquid and gas components, whereby

$$\dot{m}_{TP,A} = \dot{m}_{L,A} + \dot{m}_{G,A} \tag{3.2}$$

and the quality is given by

$$x_A = \frac{\dot{m}_{G,A}}{\dot{m}_{TP,A}}. \tag{3.3}$$

As h decreases, $\dot{m}_{TP,A}$ decreases while x_A increases. Four other onsets are encountered with further lowering of the interface: (1) the BLE at branch A corresponding to $h_A = h_{BLE,A}$, $x_A = 1.0$ and $\dot{m}_{G,A} = \dot{m}_{G,BLE,A}$ (although on lowering the interface level, at any BLE the flow changes from there being liquid entrained in the branch to there being no liquid entrained in the branch, the term "onset" or "beginning" is used, rather than "end", in keeping with the existing literature), (2) the BGE at branch B corresponding to $h_B = h_{BGE,B}$ and $\dot{m}_{L,B} = \dot{m}_{L,BGE,B}$, (3) the BLE at branch B with $h_B = h_{BLE,B}$, $x_B = 1.0$ and $\dot{m}_{G,B} = \dot{m}_{G,BLE,B}$ and (4) the BGE at branch C with $h_C = h_{BGE,C}$ and $\dot{m}_{L,C} = \dot{m}_{L,BGE,C}$. The order in which these onsets are encountered as the interface is lowered depends on the values of $P_o, \Delta P$ and R. Finally at $h_C = 0.0$, the discharge from the three branches will be in the form of single-phase gas with flow rates $\dot{m}_{G,A} = \dot{m}_{G,B} = \dot{m}_{G,C} = \dot{m}_{G,BLE,A} = \dot{m}_{G,BLE,B} = \dot{m}_{G,BLE,C}$.

In the case of experiments with a single discharge in group nos. 1 and 4, the active branch was directed to the measuring separator and the auxiliary separator was left inactive. Two onsets were encountered, and the independent parameters for mass flow rate and quality were P_o, ΔP, R and h. For the dual discharge experiments in group nos. 2 to 4, four onsets were encountered, and the independent parameters were P_o, ΔP, R, h as well as the configuration of the two branches. The geometrical parameters relevant to group nos. 1 to 3 are shown in Figure 3.1. Both separators were activated as measuring separators in the experiments of group nos. 2 and 3.

The objective of this investigation is to focus on the two-phase discharge region between the two extreme onsets and to investigate the behavior of $\dot{m}_{TP}$ and x within this region. The experimental data were sought in a systematic fashion so that the influence of each independent parameter could be assessed individually.

3.3 Experimental Test Facility

3.3.1 Flow Loop

A schematic diagram of the flow loop is shown in Figure 3.3. An immersion-type circulating pump was used to supply distilled water to the test section at a rate adjusted by a by-pass line. The temperature of the water was held steady during the experiment by a cooling coil, as shown in Figure 3.3. The large reservoir was connected to an air supply equipped with a feed-back pressure controller which maintained a steady pressure P_o in the test section throughout the experiment.

The two-phase flows leaving the test section through the branches were directed to their respective separators where the air and water were split by centrifugal action. The flow rates of air and water leaving the measuring separator(s) were each measured by a bank of four variable-area-type flowmeters with overlapping ranges. Each of these flow-measuring stations covered the range of 15 cm^3/min to 0.0415 m^3/min on the water side and 198 cm^3/min to 1.3 m^3/min at standard conditions on the air side.

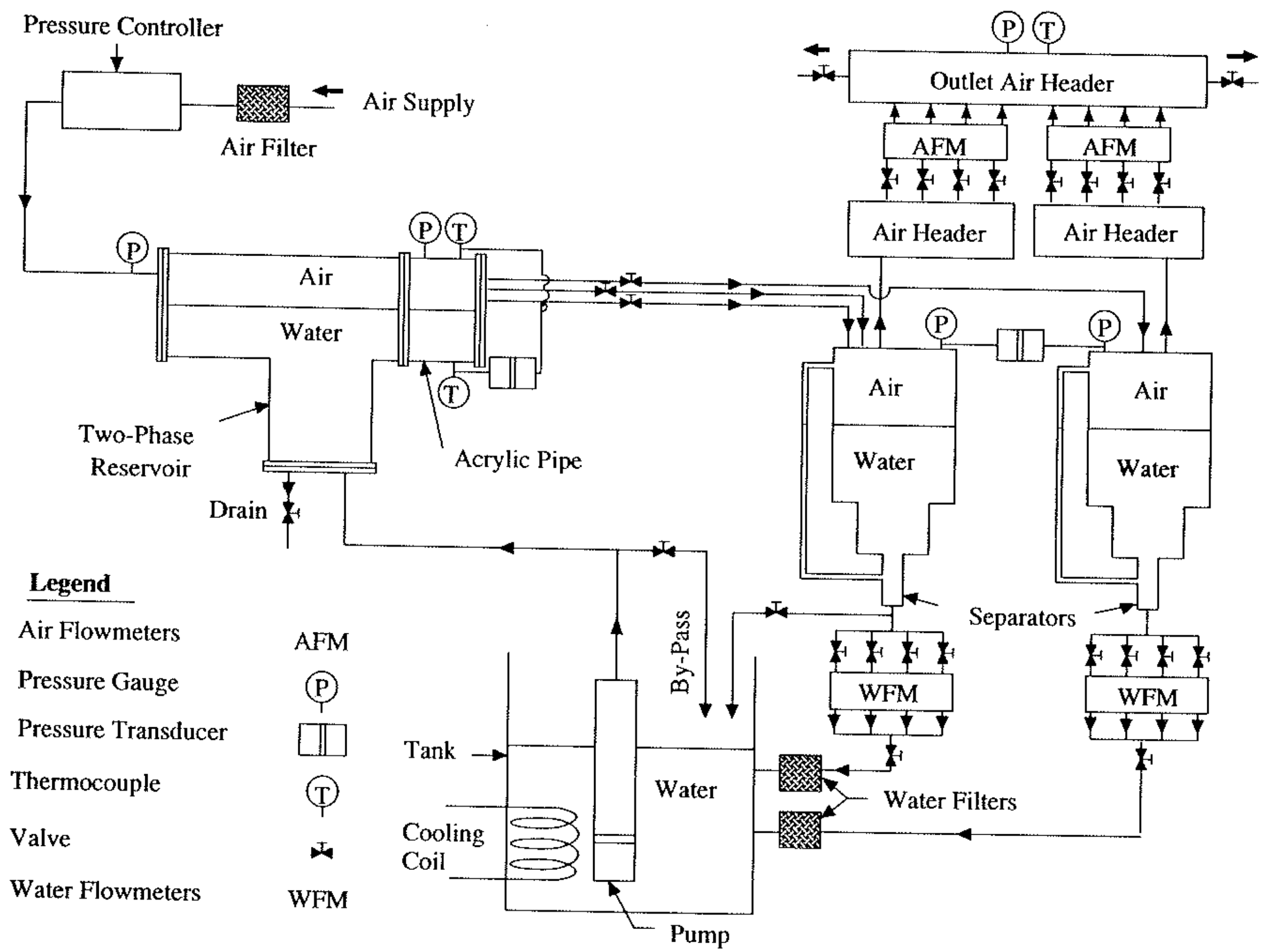

Figure 3.3: Schematic diagram of the experimental test facility

The temperature and pressure within the large reservoir, as well as other locations within the loop, were recorded during the experiment. All flow meters, thermocouples and pressure gauges were calibrated before testing began (see Appendix A).

3.3.2 Two-Phase Reservoir

Details of the large reservoir are shown in Figure 3.4 with water entering through the bottom flange, air entering through the left flange and discharge through the right flange. The geometrical design of the reservoir is similar to that used by Parrott et al. (1991). The reservoir was manufactured from type 304 stainless-steel sections, except for a clear acrylic pipe section near the outlet flange for visual observation of the flow phenomena. The acrylic pipe was held firmly between two machined flanges by four tie-rods and sealed with an O-ring at each end. The air and water entering through the reservoir were dispersed into a number of streams to prevent any waves or ripples on the gas-liquid interface. The attainment of a smooth interface was essential in eliminating fluctuations in the differential pressure transducer signal used to measure the liquid level height. Details of the inlet air and water dispersers are shown in Figures 3.5 and 3.6, respectively. Each disperser was mounted onto the inner face of the corresponding flange.

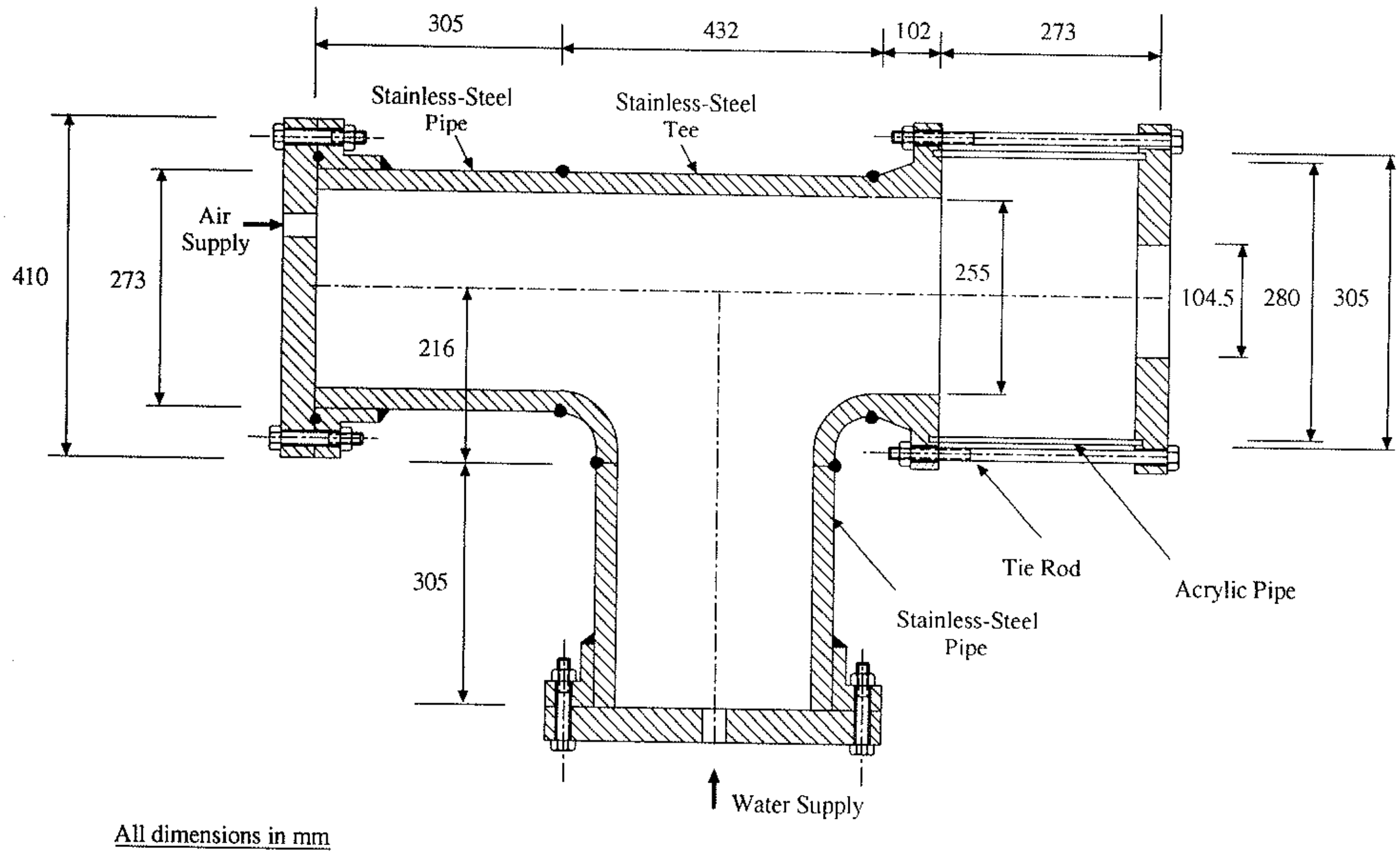

Figure 3.4: Cross-sectional view of the two-phase reservoir

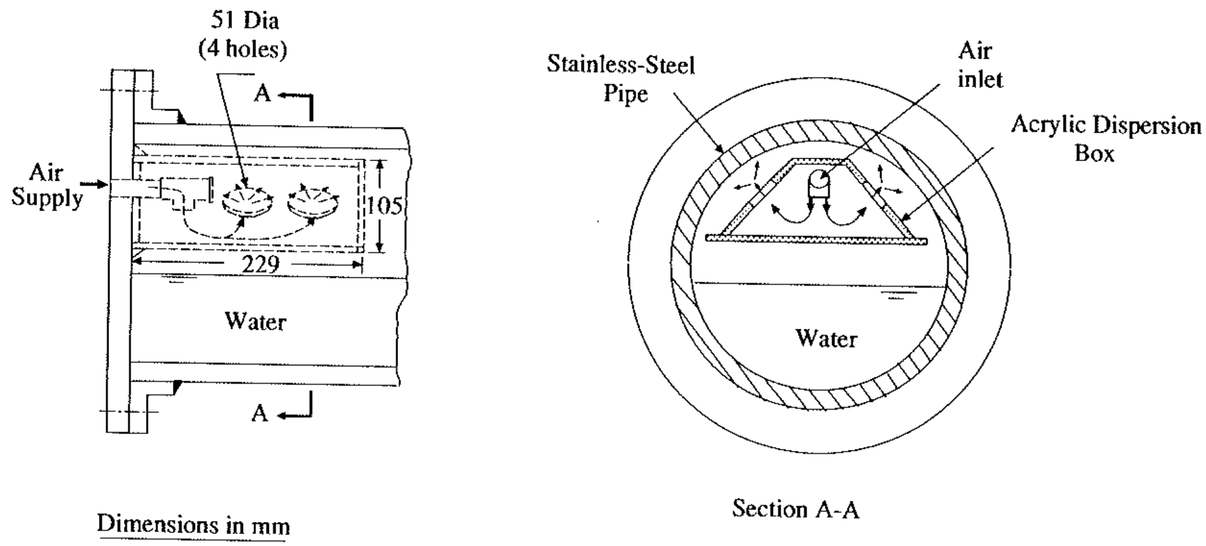

Figure 3.5: Details of the air disperser

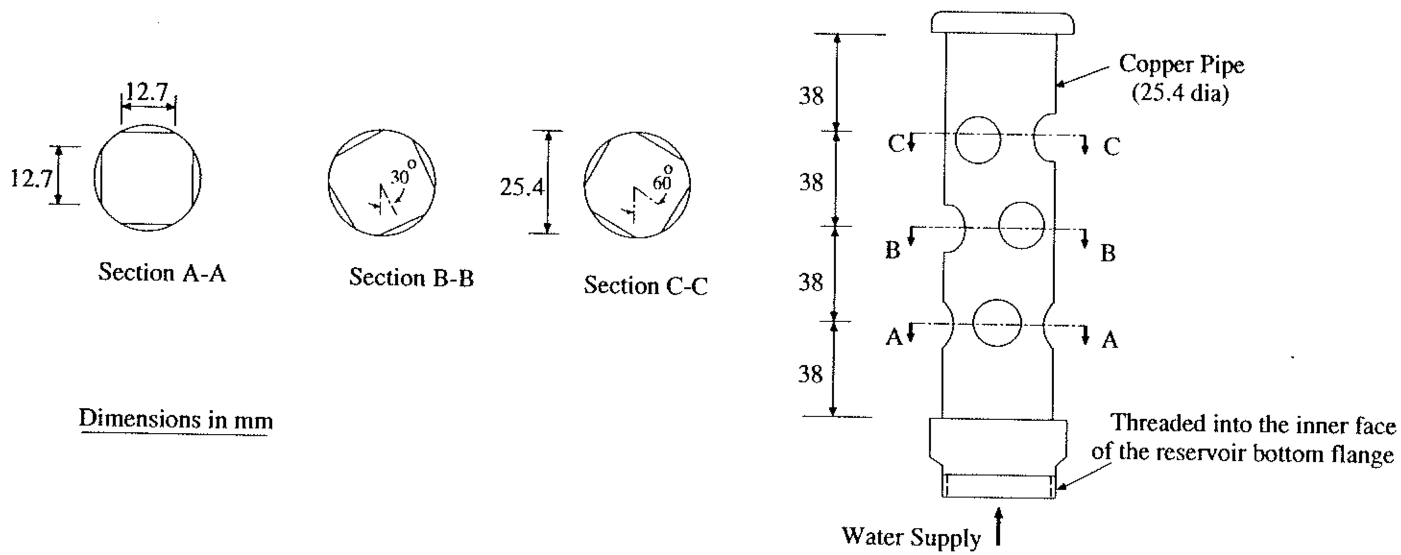

Figure 3.6: Details of the water disperser

3.3.3 Test Sections

A schematic diagram of a test section used in group nos. 1 to 3 is shown in Figure 3.7 . The first part of the discharge branches were holes , 6.35 mm in diameter and 127 mm long, machined in a brass block and bolted to the stainless-steel outlet flange. Thus, each branch had a straight length of 20 diameters before any bends or area changes were incorporated. Two brass blocks were machined to provide L/d = 1.5, 2, 3 and 8. A surveying transit was used to ensure that the faces of the outlet flange and the brass block were vertical and that the centerlines of the test branches fell on a straight (horizontal in group no. 2 and vertical in group no. 3) line. Of course, only one branch was active in group no. 1 experiments.

The test section used in group no. 4 is shown in Figure 3.8. A semicircular shape of diameter 50.8 mm and length 50.8 mm was machined in a brass block and three branches were drilled and connected to the semicircular surfaces at angles 0, 45° and 90° from the horizontal, as shown in the figure. The branches started out with a diameter d = 6.35 mm, were maintained at this size for a length of at least 4 diameters and were subsequently enlarged to a diameter 9.53 mm, as shown in Figure 3.8. The brass block was bolted to a stainless-steel blind flange and the semicircular surface and branches were exposed to a large, stratified, air-water region.

In the early stages of the investigation, consideration was given to a circular (full

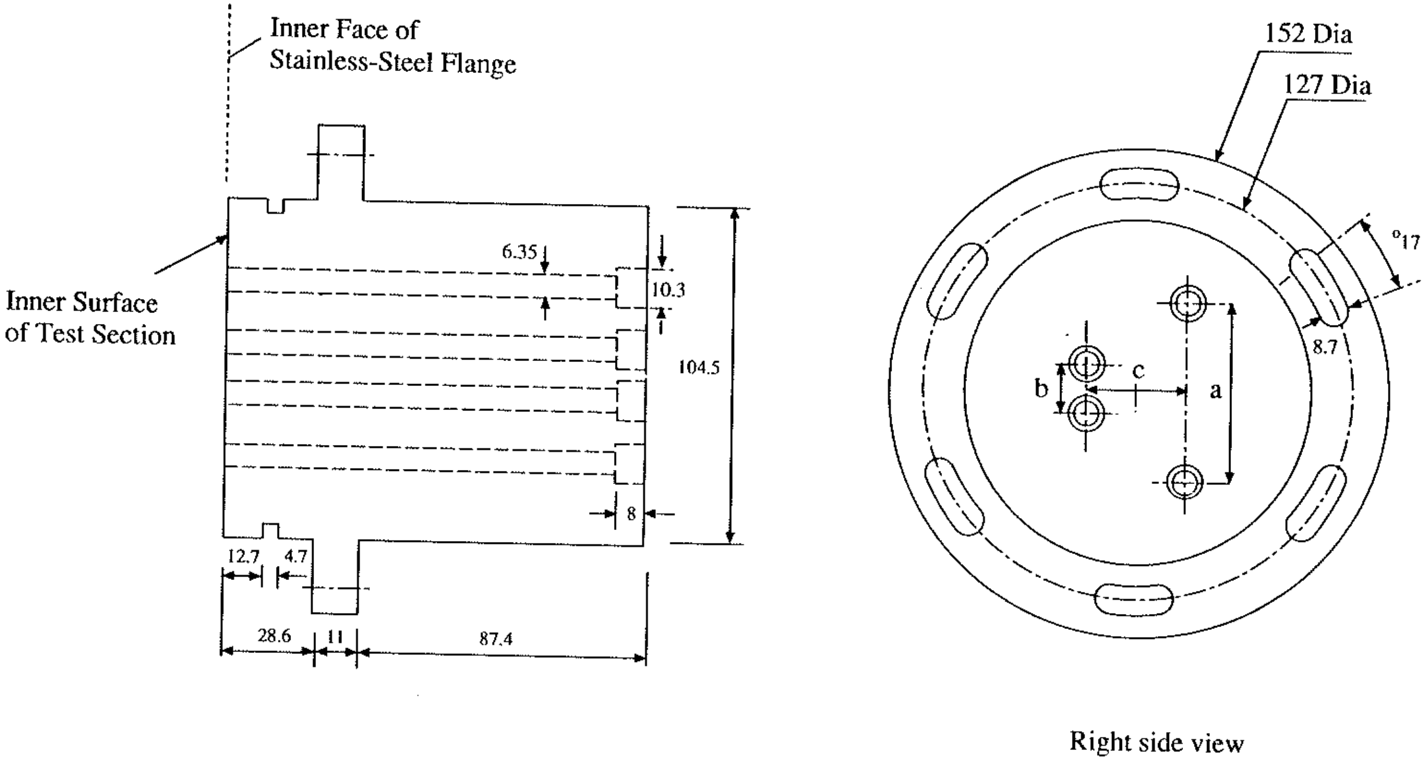

Length	Test Section no. 1	Test Section no. 2
a	50.8	19.05
b	12.7	10.30
c	25.4	38.10

All dimensions in mm

Figure 3.7: Details of test sections for group nos. 1 to 3

(Two test sections were used with different values of a,b and c)

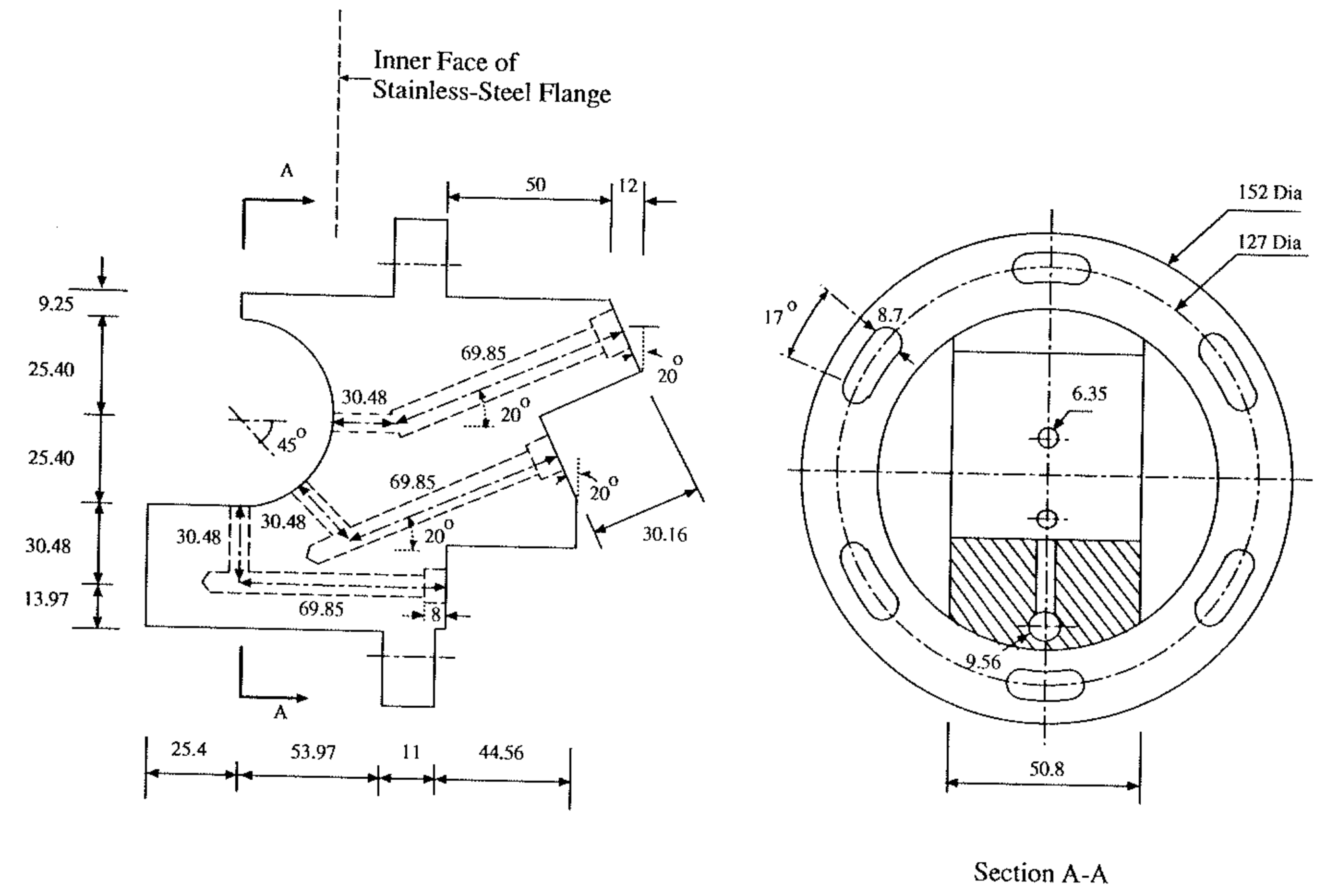

All dimensions in mm

Figure 3.8: Details of the test section for group no. 4

header) test section with 5 branches. However, a careful analysis of the expected flow conditions revealed that the flow rates leaving the branches would have to be kept fairly small if stratified conditions were to be maintained in the header. Due to the interest in a wide range of branch flow rates, a semicircular (half header) test section that is open to a large volume was adopted instead. Of course, certain conditions would have to be satisfied if the results of the semicircular section are to be considered applicable to the circular geometry. As shown later in Section 4.4, the flow out of branch C (see Figure 3.2) was found to be essentially independent of whether or not there was flow out of branches A and B within the tested range. Therefore, it is unlikely that the two missing branches from the circular section would affect the results of branch C in a circular section. As well, the two missing branches would have been too far from branches A and B to cause significant effects there. As a result, the data from the present test section should be representative of those for a full-header geometry.

3.3.4 Separation Tanks

The two-phase flows leaving the test section through the branches were directed to separators where the air and water were split by centrifugal action. This was achieved by forcing the flow through two 60.0 mm diameter nozzles angled to discharge the flow in a downward spiraling direction, as shown in Figure 3.9. Water exiting from the nozzles flowed along the tank wall where it drained downward.

The air flowed out through the top of the separation tank. A baffle located above the gas-liquid interface isolated the interface from the flow above it. The baffle, a circular disk perforated with many small holes, 5.5 mm in diameter, has a diameter slightly smaller than that of the separation tank; this left a gap of about 4 mm on the tank wall.

The tank incorporated abrupt changes in cross-sectional area as shown in Figure 3.9. If the liquid flow rate was too low, the gas-liquid interface in the tank was maintained in the smallest diameter cross-section. On the other hand, for the high liquid flow rate, the interface was maintained in the largest diameter cross-section. This procedure decreased the errors resulting from small changes in the height of the interface with time.

Each separation tank was constructed from type 304 stainless-steel sections with flanges welded and bolted to each end. A 640 mm long-sight-glass was used to observe visually the liquid level in the tank. A pressure tap was installed on the air side of each separator and connected to a differential pressure transducer. The reading of this transducer during the dual and triple discharge experiments was monitored continuously and adjustments were made (if necessary) for the outlet flow rates in order to ensure that the pressure difference between the two separators was at or near zero.

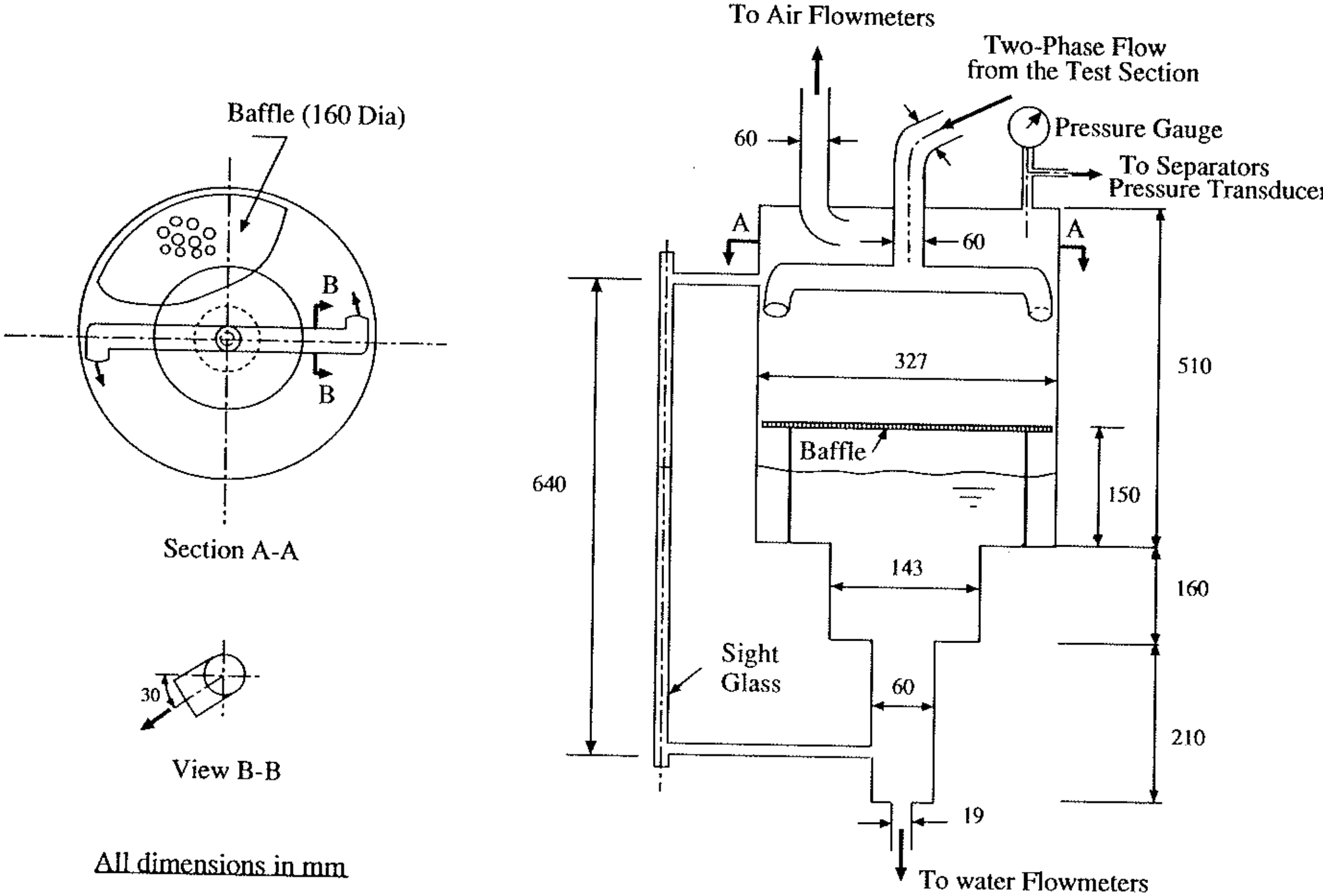

Figure 3.9: Details of a separation tank

3.3.5 Liquid Level Measurement

Two pressure taps, as shown in Figure 3.10, one on the air side and the other on the water side, were installed on the outlet flange and connected to a differential pressure transducer (Rosemount model 1151 DP) in order to measure the liquid height in the test section from which the value of h was determined. A 24 VDC power supply was connected to the transducer which produced an electrical current that varied linearly with the differential pressure. The current was passed through a resistor and the voltage drop across the resistor was measured with a digital voltmeter. Calibration of the transducer (see Appendix A) provided a measurement of 0 to 254 mm water height over the range of 2 to 10 volts as measured by a voltmeter with a resolution of $1mV$. Therefore, very small changes in the liquid level could be easily detected.

3.4 Experimental Procedure

A total of 100 data sets were collected in this investigation, Fourteen data sets for group no. 1, thirty-two data sets for group no. 2, thirty-two data sets for group no. 3 and twenty-two data sets for group no. 4. Each set corresponds to a certain combination of P_o, ΔP, R as well as the configuration of the branch(es). Before starting the experiments with a new branch configuration, the hydraulic resistances of the connecting lines were set nearly equal (not necessary for single discharge experiments in group nos. 1 and 4). This was done by performing adjustments

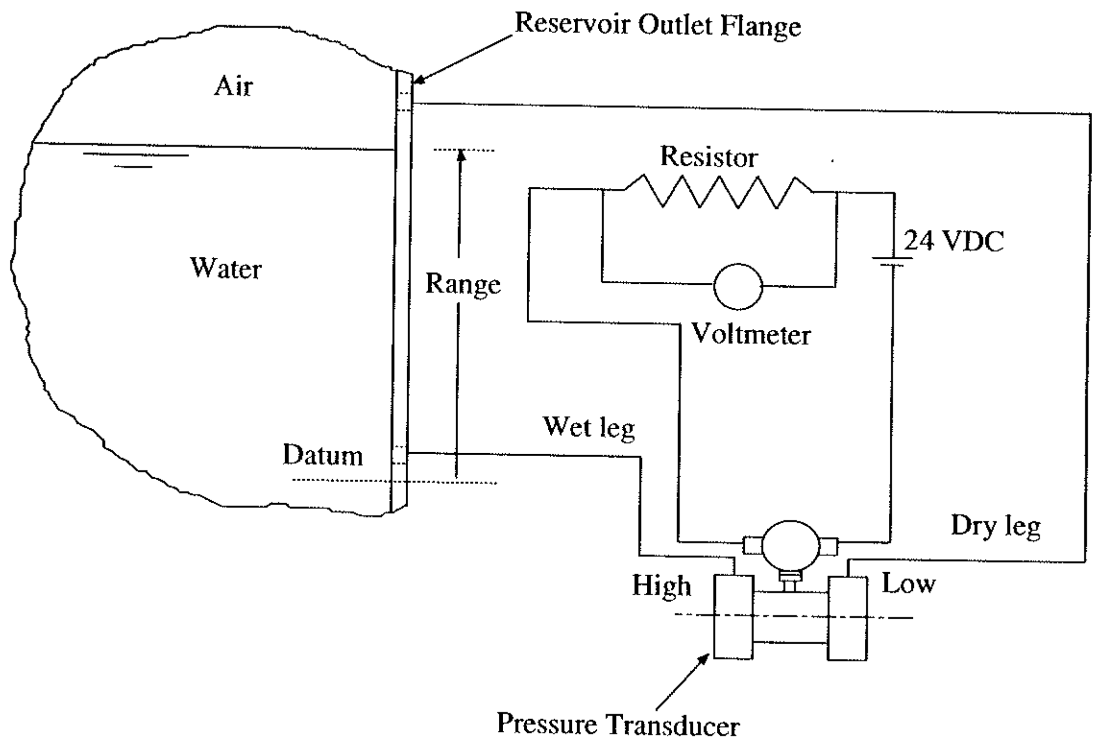

Figure 3.10: Installation for liquid-level measurement

on one or all lines until the deviation between the single-phase liquid flow rates from all branches was 3 % (all sets) or less. The deviation between the single-phase gas flow rates from the all branches was 6.8 % or less for data set nos. 3-3, 4-21 and 4-22, while for the other 97 data sets, it was 4.3 % or less. After adjusting R for a given configuration, appropriate values of P_o and ΔP were fixed and an experimental procedure was followed in collecting the data of each group. Following is the procedure followed for dual-discharge experiments (branches one above the other) in group no. 3 (see Figure 3.1) and group no.4 (could be branches A and B, A and C or B and C); the modifications for the single-discharge experiments in group nos. 1 and 4, dual discharge experiments (branches side by side) in group no. 2, and the triple discharge experiments in group no. 4 are pointed out at the end of this section:

1. The conditions at the BGE at the upper branch (interface level and mass flow rate) were established first. The air-water interface location (height) was set at a high value and was reduced in small steps, at which the liquid flow rate was measured under steady conditions. As the onset was approached, the liquid level was slowly lowered further until gas was suddenly entrained at the branch; this onset was observed visually through the transparent part of the test section. The steady-state flow rate just before the onset and the reading of the pressure transducer immediately following the onset were recorded.

2. Knowing that the magnitudes of the critical height for BGE at the upper branch and the critical height for $theBLE$ at the lower branch are roughly equal, the vertical distance between these two locations was divided into a number (in the range of 20 to 30) of equal intervals. The experiment was then conducted at decreasing values of h. At each h, the liquid level was held constant for a sufficient period of time that allowed the flow into each separator to be split and measured accurately.

3. Three other onsets were encountered with decreasing h; these were the BLE at the upper branch, and the BGE and the BLE at the lower branch. All these onsets were detected visually. As each one of these onsets was approached, the liquid level was lowered in fine increments so that the corresponding h and $\dot{m}$ were accurately determined. With the water level just slightly above that for the condition of the BLE at either branch, a stream of water was seen to be pulled up from the interface through the branch. Decreasing the level caused this stream to become thinner until it suddenly disappeared at the "onset".

For single-discharge experiments in group nos. 1 and 4, the procedure was similar, except for the fact that two onsets were present in this case. In dual-discharge experiments in group no. 2 (branches side by side), identical conditions were measured for both branches at the BGE and also at the BLE due to symmetry (same ΔP, same R and same distance from the interface). Therefore, only two onsets were relevant to tests in group no. 2, as in group no. 1.

For triple discharge experiments in group no. 4, as pointed out earlier, one stream (could be A, B or C) was directed to a measuring separator where air and water were measured downstream, and the remaining two streams were directed to the auxiliary separator. Each experiment was repeated three times in order to measure the flow from all three branches. The experimental procedure was similar to that of dual discharge, except for the fact that measurements were made only between the two onsets of a given branch.

3.5 Data Reduction

The recorded data for each test run included the air and water flow rates, the liquid level, the stagnation conditions within the large reservoir, P_o and T_o, as well as the pressure and temperature in the separators and other locations within the loop. Strictly speaking, there was some finite air velocity in the large reservoir; however, the cross-sectional area was so large that this velocity was below 0.6 m/s at the highest discharge rates. All parameters presented in the following chapter are based on directly measured quantities, except for Fr_{BLE}. In order to determine Fr_{BLE}, the inlet conditions at the branch(es) had to be determined. This was done by applying the following procedure (similar to that used by Armstrong et al., 1992):

1. Treating the air as an ideal gas, assuming isentropic flow and applying an energy balance between the stagnation conditions and the branch inlet, we get

$$c_p T_o = c_p T + \frac{V_d^2}{2}, \tag{3.4}$$

where c_p is the constant-pressure specific heat, T is the temperature at branch inlet and V_d is the mean discharge velocity.

2. From mass conservation, we have

$$\dot{m}_{G,BLE} = \frac{\pi}{4} d^2 \rho_G V_d, \tag{3.5}$$

where the density ρ_G is given by

$$\rho_G = \frac{P}{R'T}, \tag{3.6}$$

P is the pressure at the branch inlet and R' is the ideal gas constant for air.

3. The isentropic expansion from the stagnation conditions to the branch inlet is given by

$$\frac{T}{T_o} = \left(\frac{P}{P_o}\right)^{\frac{k-1}{k}} \tag{3.7}$$

where k is the ratio of specific heats.

Equations (3.4) to (3.7) were solved iteratively (with T_o and $\dot{m}_{G,BLE}$ as known) for the values of P, T, ρ_G and V_d. Equation (2.5) was then used for the evaluation of

Fr_{BLE}. The assumption of isentropic expansion was carefully assessed by Parrott (1993). It was found that this assumption had a small influence on the value of Fr_{BLE}, mainly because the differences $(T - T_o)$ and $(P - P_o)$ were small.

3.6 Experimental Uncertainty

An estimate of the uncertainties in the independent and dependent variables was made in the fashion described by Moffat (1988), and Kline and McClintock (1953). All uncertainties quoted here are at "odds" of 20 to 1. The uncertainties are meant to accommodate: the accuracy of the calibrating device, the error in fitting an equation (for computer data reduction) to the calibration data, discrimination uncertainties in the measuring instruments and unsteadiness in the process. Pressure gauges were calibrated using a deadweight tester, thermocouples using a standard mercury-in-glass thermometer, gas rotameters using wet test meters and venturi meters (in turn the calibrations of which were traceable to National Institute of Standards and Technology) and liquid rotameters using a weigh- and-time method. The pressure transmitter used for measuring h was calibrated against a micromanometer and the digital voltmeter used in the calibration was subsequently used in the normal running of the experiments; for both calibration and subsequent experiments the sensitivity was approximately 35 mV per mm of water; the discrimination on the digital voltmeter was ± 1 mV.

The results of the uncertainty analysis vary slightly among the four groups and the highest uncertainties for each variable are given here. The uncertainty in P_o (absolute pressure) was ± 0.9 %; the uncertainty in ΔP for data sets with $\Delta P = 40$ kPa (the smallest ΔP) was ± 7.9 %, while for the other data sets (higher ΔP) it was ± 3.9 % or less. The maximum uncertainty in the flow rates $\dot{m}_G$, $\dot{m}_L$ and $\dot{m}_{TP}$ was ± 4.0 %, ± 2.5 % and ± 4.7 %, respectively. The uncertainty in temperature measurements was $\pm 0.25°C$. The maximum uncertainty in the quality x was ± 4.7 %. The maximum uncertainty in R was ± 4.7 %. The maximum absolute uncertainties in h, h_{BGE} and h_{BLE} were ± 0.15 mm, ± 0.38 mm and ± 0.38 mm, respectively.

For the dimensionless quantity H (defined later in Chapter 4, used in the analysis of the data of group nos. 1 to 3 and having a range of 0 to 1), in the range $0.2 \leq H \leq 1$, the maximum uncertainty in $\delta H/H$ was ± 8.0 % ; the uncertainty in $\delta H/H$ increased with decreasing H, was a maximum of $\pm 13.5\%$ at $H = 0.1$ and increased to large values as H approached zero. For the dimensionless quantity M (defined later in Chapter 4, used in the analysis of the data of group nos. 1 to 3 and having a range of 0 to 1), δM varied between approximately ± 0.003 and ± 0.038, smaller values being associated with small M and larger values being associated with large M; in the range of $0.1 \leq M \leq 1$, the maximum uncertainty in $\delta M/M$ was ± 6 %; the uncertainty in $\delta M/M$ increased with decreasing M and at the smallest finite M (=0.05) was $\pm 10\%$.

CHAPTER 4

EXPERIMENTAL RESULTS AND DISCUSSION

4.1 Single Discharge from a Branch on a Flat, Vertical Wall

4.1.1 Presentation of Data and Trends

The operating conditions for the fourteen sets of experimental data generated in this group are listed in Table 4.1. It is obvious from this table that the independent variables P_o, ΔP and R were varied in a systematic fashion whereby the influence of each independent parameter was considered separately while the other two variables were held constant. Set nos. 1-1 to 1-3 and set nos. 1-4 to 1-6 explore the effect of ΔP at fixed values of P_o and R. The influence of R at fixed values of P_o and ΔP can be examined using set nos. 1-1, 1-11 and 1-12, or set nos. 1-4, 1-13 and 1-14. Finally, the influence of P_o at fixed values of ΔP and R can be examined from set nos. 1-7 to 1-10. A complete tabulation of all experimental data in this group can be found in Appendix B.

Table 4.1: Nominal operating conditions for group no. 1 (single discharge)

Data Set No.	P_o (kPa)	ΔP (kPa)	R $(kg.m)^{-1/2}$
1-1 1-2 1-3	316	123 82 40	1000
1-4 1-5 1-6	517	235 166 97	
1-7 1-8 1-9 1-10	316 378 448 517	127	
1-11 1-12	316	123	1660 3000
1-13 1-14	517	235	1600 3000

Figures 4.1 and 4.2 show typical results for $\dot{m}_{TP}$ and x, respectively. Within each data set (fixed P_o, ΔP, and R), $\dot{m}_{TP}$ decreases from $\dot{m}_{L,BGE}$ to $\dot{m}_{G,BLE}$ and x increases from 0 to 1 as h decreases from h_{BGE} to h_{BLE}. As the independent parameters P_o, ΔP and R were varied during the experimental program, significant effects were noted on the measured dependent parameters. Increasing R at the same P_o and ΔP gave decreasing in $\dot{m}_{L,BGE}$, $\dot{m}_{G,BLE}$, h_{BGE}, and $|h_{BLE}|$, as shown in Figure 4.3; similar trends were obtained on decreasing ΔP at the same P_o and R. Increasing P_o at the same ΔP and R had essentially no effect on h_{BGE} and $\dot{m}_{L,BGE}$ while $\dot{m}_{G,BLE}$ and $|h_{BLE}|$ increased, as shown in Figure 4.4.

Normalized plots are shown in Figures 4.5 to 4.10 using the following definitions for the normalized liquid level and the normalized mass flow rate, respectively:

$$H = \frac{h - h_{BLE}}{h_{BGE} - h_{BLE}}, \tag{4.1}$$

and

$$M = \frac{\dot{m}_{TP} - \dot{m}_{G,BLE}}{\dot{m}_{L,BGE} - \dot{m}_{G,BLE}}. \tag{4.2}$$

Figures 4.5 to 4.10 show that when the present data are plotted in terms of M versus H and x versus H, the effects of P_o, ΔP, and R are largely absorbed within the present tested range of parameters. This observation is based on experimental data corresponding to a finite range of parameters and thus, should not be extended outside the present range without considerable thought. For example, Figure 4.10 suggests a very small but consistent effect of P_o on x. This effect may become more

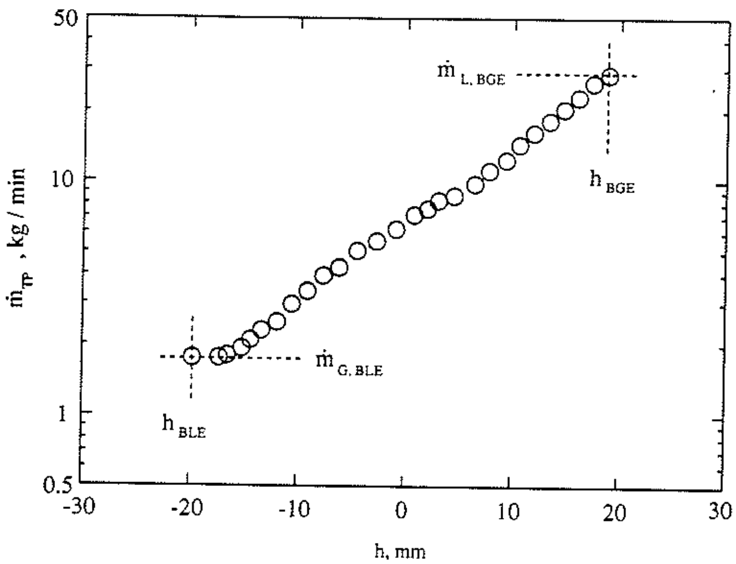

Figure 4.1: Two-phase mass flow rate for data set no. 1-4

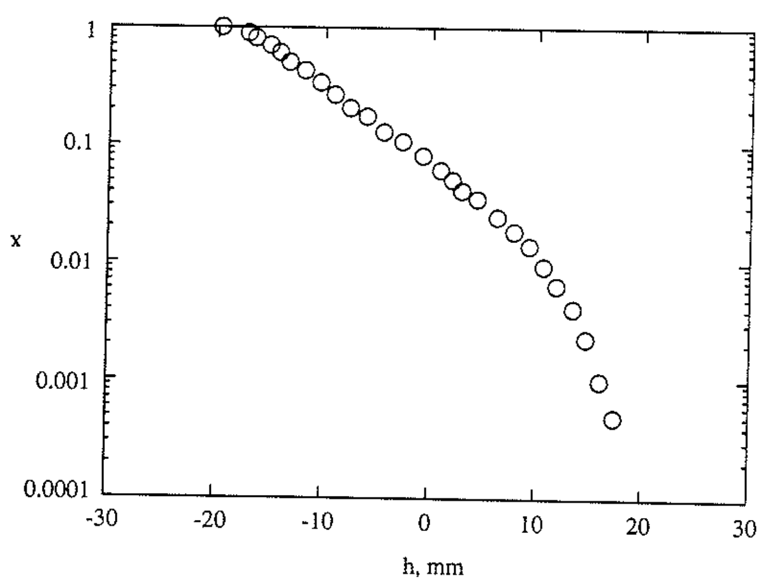

Figure 4.2: Discharge quality for data set no. 1-4

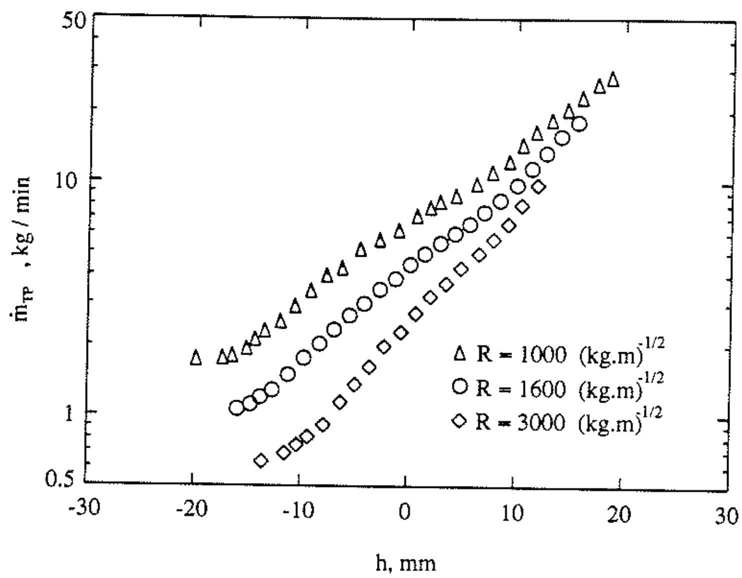

Figure 4.3: Effect of R on $\dot{m}_{TP}$ from data set nos. 1-4, 1-13 and 1-14

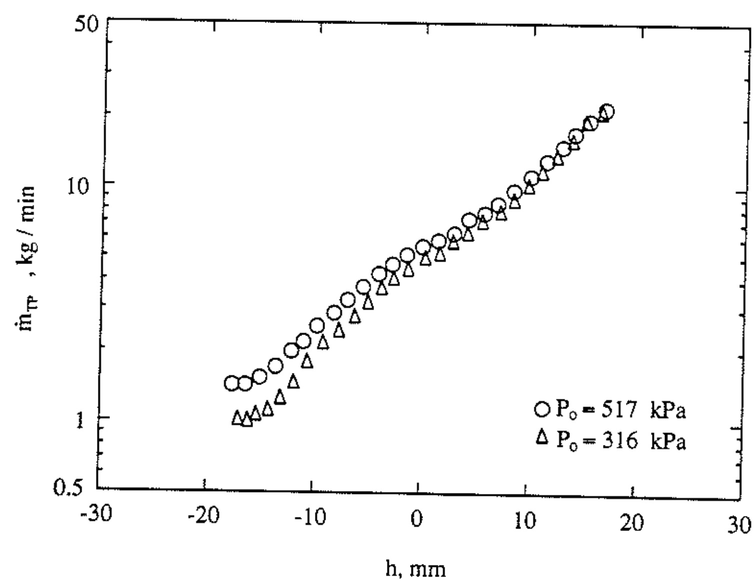

Figure 4.4: Effect of P_o on $\dot{m}_{TP}$ from data set nos. 1-7 and 1-10

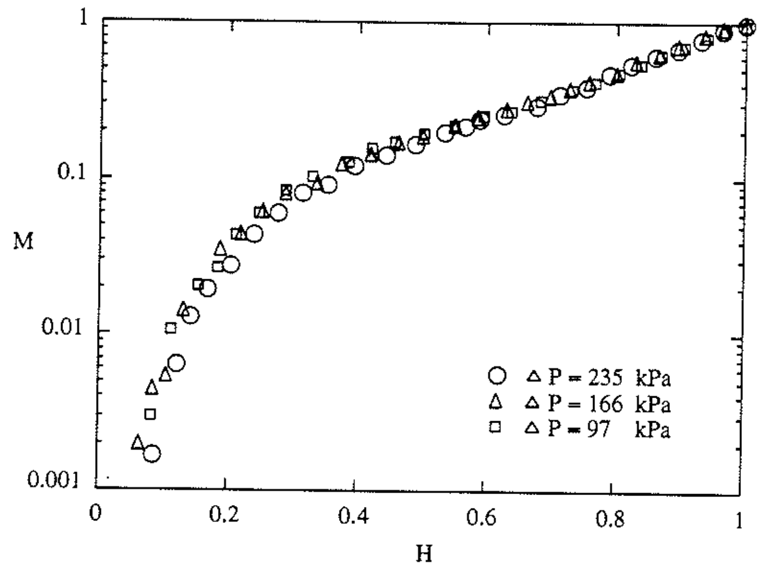

Figure 4.5: Values of M for different ΔP using data set nos. 1-4 to 1-6

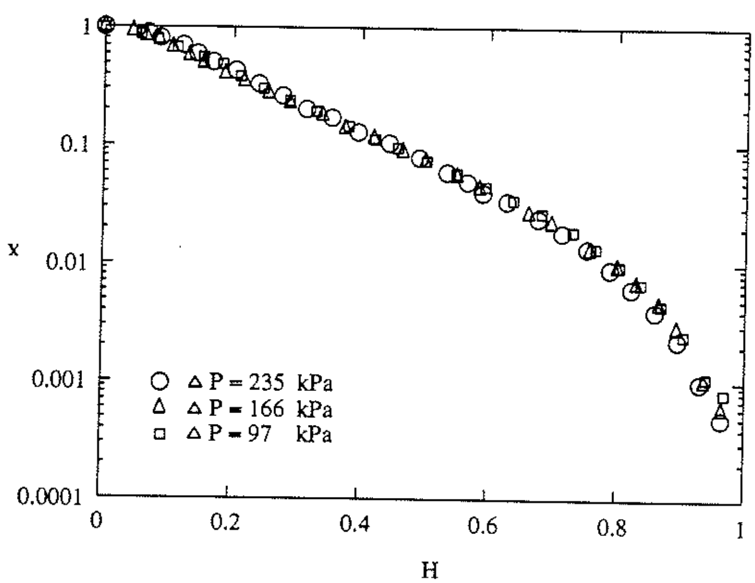

Figure 4.6: Values of x for different ΔP using data set nos. 1-4 to 1-6

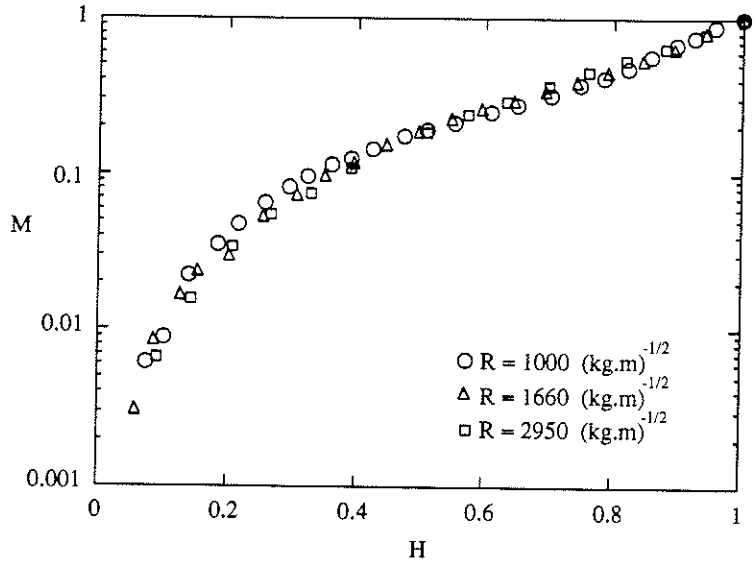

Figure 4.7: Values of M for different R using data set nos. 1-1, 1-11 and 1-12

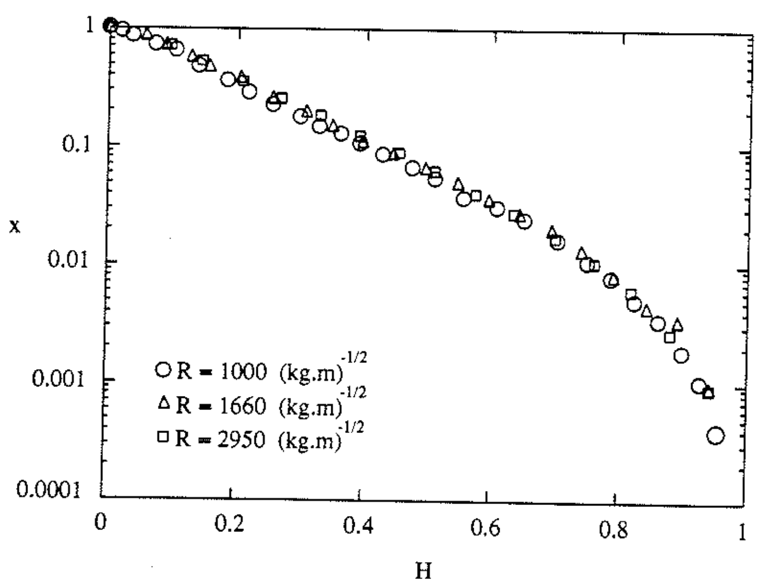

Figure 4.8: Values of x for different R using data set nos. 1-1, 1-11 and 1-12

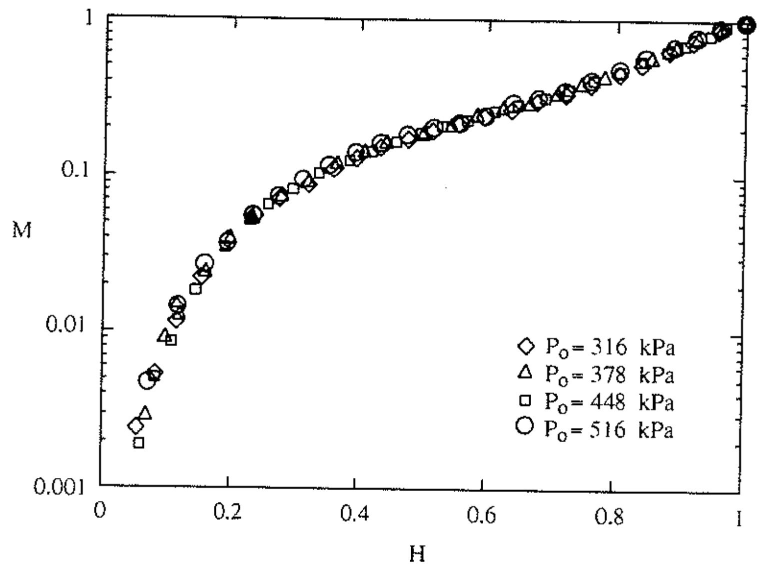

Figure 4.9: Values of M for different P_o using data set nos. 1-7 to 1-10

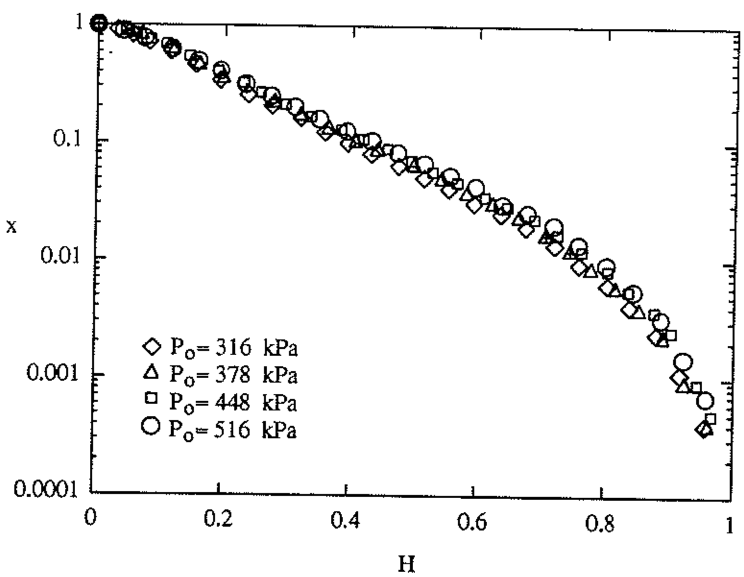

Figure 4.10: Values of x for different P_o using data set nos. 1-7 to 1-10

visible if the range of P_o is considerably widened.

4.1.2 Comparisons with Existing Correlations

Comparisons were conducted between the present results and those of previous investigations. Figures 4.11 and 4.12 relate to the height of the interface at the BGE and BLE , respectively (correlations used in these figures are given in Chapter 2, except for that of Armstrong et al. which is given in Chapter 5). These critical heights are correlated in terms of Fr_{BGE} and Fr_{BLE} given by Equations (2.4) and (2.5), respectively. Significant deviations can be seen among different correlations for the case of h_{BGE} in Figure 4.11, where the present results appear to be closest to those of Micaelli and Memponteil (1989) and Parrott et al. (1991). The correlation by Schrock et al. (1986) includes viscosity and Bond numbers (in addition to Froude number) which were evaluated at the present experimental conditions.

The deviations between the present h_{BLE} results (Figure 4.12) and the correlations are not very significant. The manner by which the experiment is conducted can influence h_{BLE} . In the present experiment, all values of h_{BLE} were measured with a slowly decreasing liquid level whereby the area of the metal face between the interface and the branch was wet. Additional results were obtained with a slowly rising liquid level (i.e., dry face of test section) and they are shown in Figure 4.12. Some deviation appears between the two sets of experimental results; however, these deviations are small, as well as the deviations among the different

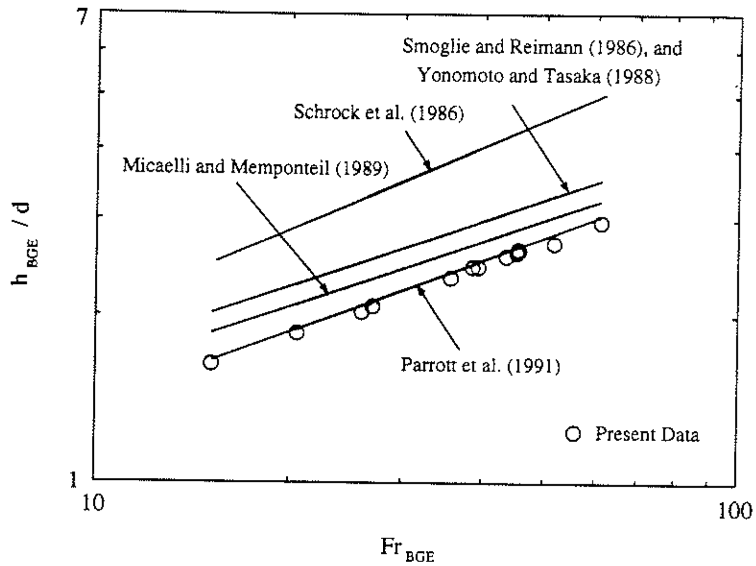

Figure 4.11: Interface level at the *BGE* for group no. 1

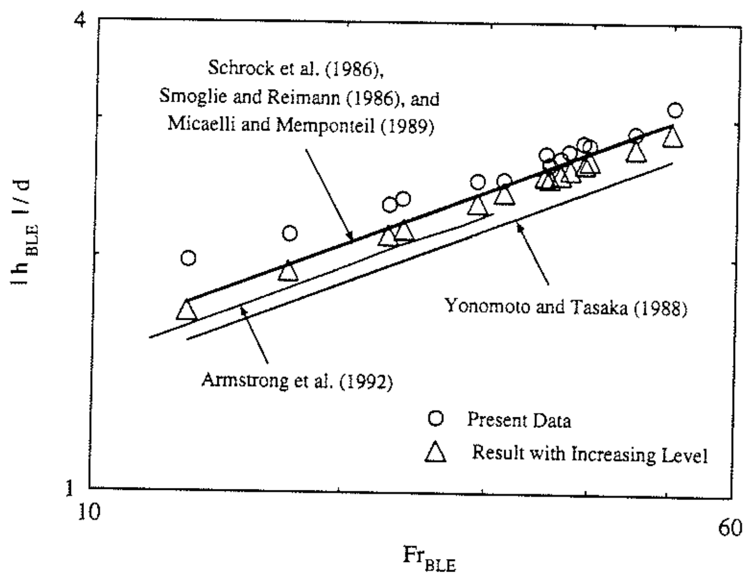

Figure 4.12: Interface level at the *BLE* for group no. 1

correlations for h_{BLE}.

The present values of x were compared with existing correlations and a representative sample of the results is shown in Figures 4.13 to 4.15 for data set no. 1-4 (where the mass flow rates are highest). Figures 4.13 and 4.14 show significant deviations among the correlations of Smoglie and Reimann (1986), Schrock et al. (1986), and Yonomoto and Tasaka (1988), given by (2.6), (2.11) and (2.16), respectively. As well, the data are underpredicted by the correlations at high values of x and overpredicted at low values of x. These three correlations provide x as a function of h/h_{BGE} for $h > 0$ and $h/|h_{BLE}|$ for $h < 0$.

The best agreement was obtained with the correlation of Micaelli and Memponteil (1989), given by (2.24). In this correlation, the quality x was given as a function of h/h_b^* over the whole range $h_{BLE} \leq h \leq h_{BGE}$. Figure 4.15 shows good agreement between data set no. 1-4 and the correlation of Micaelli and Memponteil throughout the whole range of x. The trends illustrated in Figures 4.13 to 4.15 for set no. 1-4 were found to be the same for all the other data sets.

Although the correlation of Micaelli and Memponteil (1989) has the widest data base among all existing correlations, and it resulted in the best agreement with the present data, this correlation is not in a suitable form for predicting x. This is because of the dependence on h_b^* (given by Equation (2.26)), which in turn, requires a knowledge of $\dot{m}_{TP}$, a quantity not known *a priori*. Rather than requiring $\dot{m}_{TP}$ for the determination of x, it would be useful to provide separate correlations for

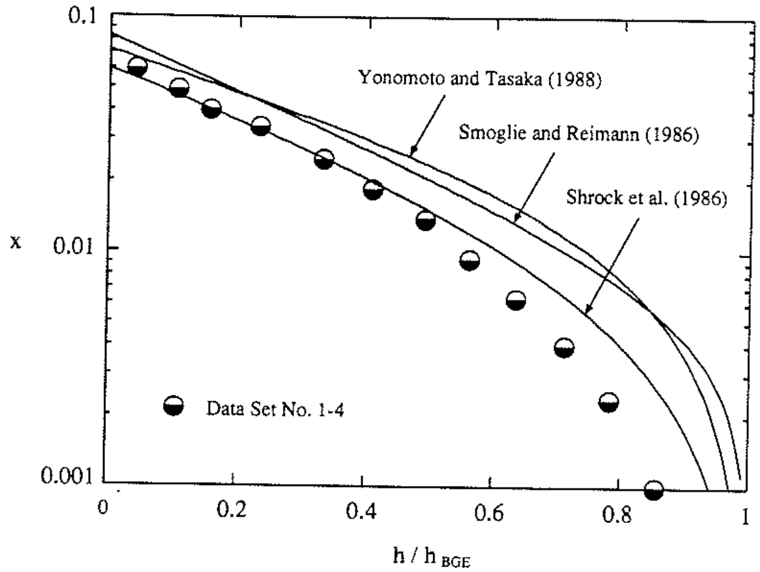

Figure 4.13: Comparison between data set no. 1-4 and previous correlations ($h \geq 0$)

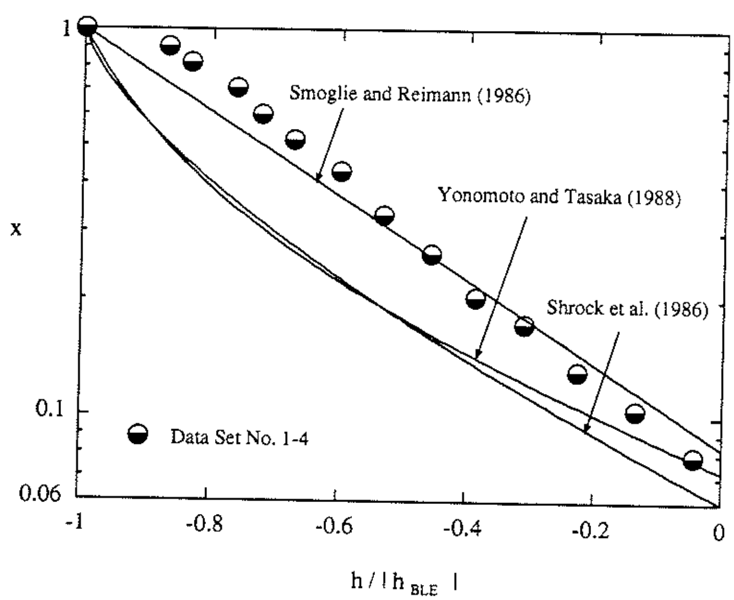

Figure 4.14: Comparison between data set no. 1-4 and previous correlations ($h \leq 0$)

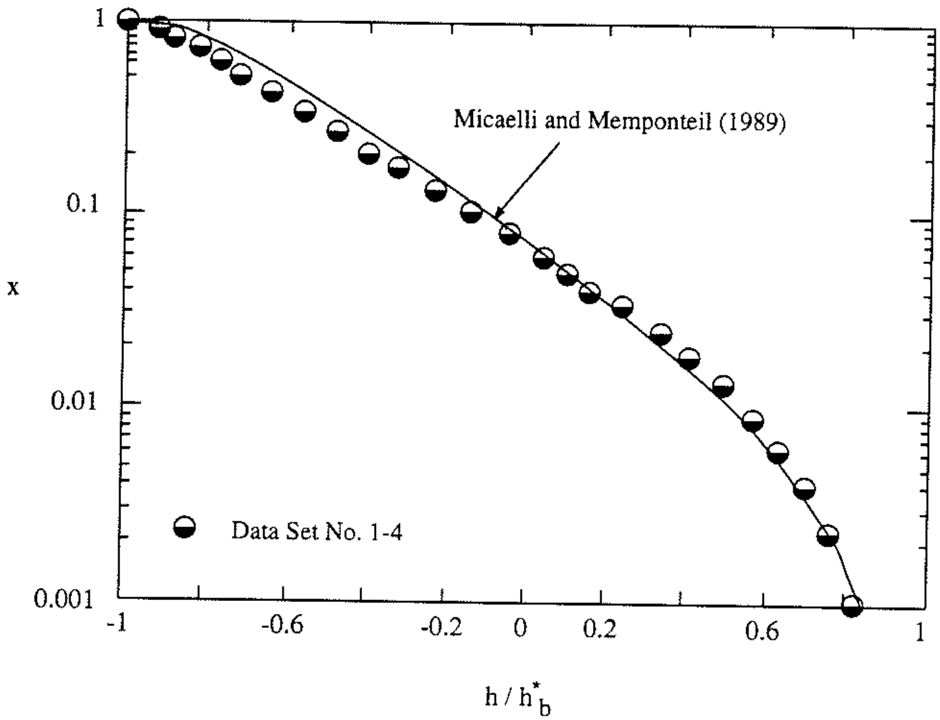

Figure 4.15: Comparison between data set no. 1-4 and the correlation of Micaelli and Memponteil (1989)

determining $\dot{m}_{TP}$ and x independently.

4.1.3 Correlation of Present Data

Correlations were developed based on the present experimental data. They consist of the following relations:

$$\frac{h_{BGE}}{d} = 0.57 \ \ Fr_{BGE}^{0.4}, \tag{4.3}$$

$$\frac{|h_{BLE}|}{d} = 0.87 \ \ Fr_{BLE}^{0.31}, \tag{4.4}$$

$$\begin{aligned} x \ = \ & 0.2 \ \ exp\left[6 \ \ H\left(\frac{1-11.67H}{1-H}\right)\right] + \\ & 0.8 \ \ \left(1-H^2\right)^{1.3} \ \ \left[-0.0122 + \frac{0.42}{1.0+\sqrt{\frac{\rho_L}{\rho_G}}}\right]^{H} \end{aligned} \tag{4.5}$$

and

$$M = H^2 \ \ exp\left[\ -1.84 \ H^2 \ \left(1.0 - H^2\right)^{1.318}\ \right]. \tag{4.6}$$

For given values of ρ_L, ρ_G, d, h, P_o, R and ΔP (from which corresponding values of $\dot{m}_{L,BGE}$ and $\dot{m}_{G,BLE}$ can be determined for the particular system under consideration), $\dot{m}_{TP}$ and x can be easily determined from the above relations.

Equation (4.3) correlates the present data of h_{BGE} within ± 5 % and its predictions are very close to those of Parrott et al. (1991), as can be seen in Figure 4.11. Equation (4.4) correlates the present data of h_{BLE} (for decreasing liquid level) within ± 5 % and its predictions are close to those of existing correlations, as shown in Figure 4.12. Equations (4.5) and (4.6) converge to the appropriate limits at $H = 0$ and 1. They are consistent with the trends shown in Figures 4.5-4.10, whereby x and M are functions of H with a slight dependence of x on P_o or (ρ_L/ρ_G).

Figures 4.16 and 4.17 show comparisons between all the data in group no. 1 and the correlating equations for x and M, respectively. Very good agreement can be seen in these figures. Quantitatively, the experimental values of x were predicted with a root-mean-square error of 8.1 % over the range $0.001 \leq x \leq 1$. As well, the experimental values of M were predicted with a root-mean-square error of 13.2 % over the range $0.001 \leq M \leq 1.0$ and a root-mean-square error of 8.2 % over the range $0.01 \leq M \leq 1.0$. It should be emphasized that these correlating equations are empirical and thus, their accuracy can only be assured within the range of conditions covered in this investigation.

4.1.4 Comparison with Critical Two-Phase Models

In order to know the type of flow (subcritical or supercritical) through the branches, a comparison was made between the experimental data of $\dot{m}_{TP}$ and the results of two models available in the literature for predicting the critical $\dot{m}_{TP}$. These two models are the "homogeneous frozen model" and the Henry-Fauske model. The first model is that given by Whalley (1987) for homogeneous frozen flow as follows:

$$\dot{m}_{TP,c}^2 = \frac{\pi^2 d^4 P_o k}{16 v_{G,o} x} \left(\frac{2}{k+1}\right)^{\left(\frac{k+1}{k-1}\right)} \tag{4.7}$$

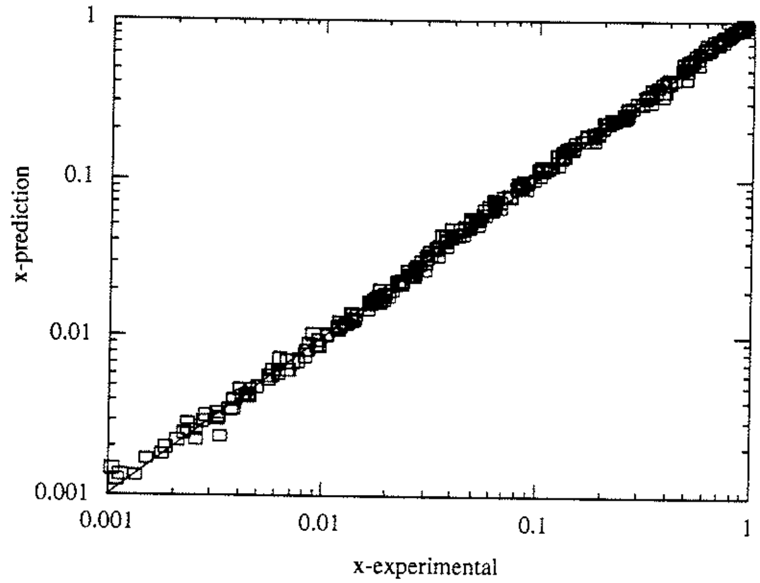

Figure 4.16: Comparison between the present data for x and the proposed correlation

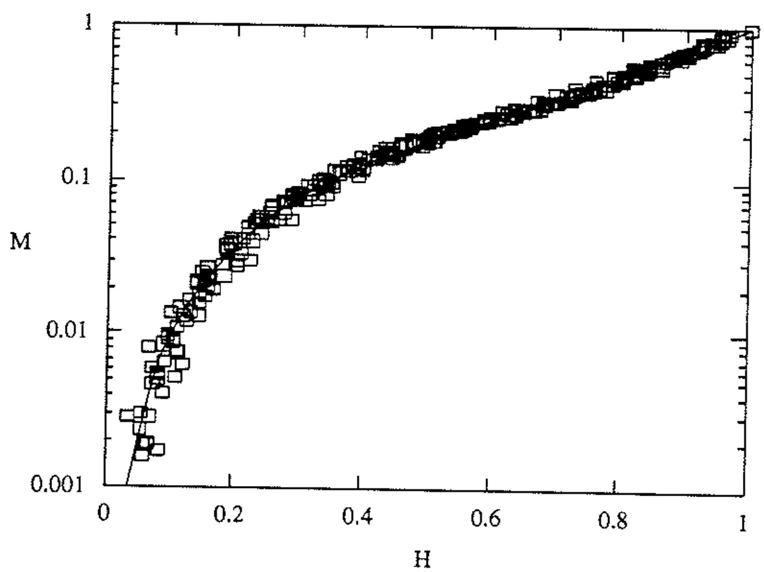

Figure 4.17: Comparison between the present data for M and the proposed correlation

where $\dot{m}_{TP,c}$ is the critical two-phase flow rate, x is the quality (constant within the pipe) and P_o and $v_{G,o}$ are the pressure and gas specific volume at the stagnation conditions upstream of the choking plane.

The second model is that given by Henry and Fauske (1971) for non-homogeneous flow, as follows:

$$\dot{m}^2_{TP,c} = \left(\frac{\pi^2 d^4}{8}\right) \left[\frac{(1-x)v_{L,o}(P_o - P_c) + \left(\frac{xk}{k-1}\right)(P_o v_{G,o} - P_c v_{G,c})}{((1-x)v_{L,o} + x v_{G,c})^2}\right], \qquad (4.8)$$

with

$$v_{G,c} = v_{G,o}[\frac{P_c}{P_o}]^{-1/k}, \qquad (4.9)$$

where $v_{L,o}$ is the liquid specific volume at the stagnation conditions upstream of the choking plane, P_c and v_{gc} are the the pressure and the gas specific volume at the choking plane.

The measured values of $\dot{m}_{TP}$ were compared with the predictions of Equations (4.7) and (4.8) at the present operating conditions. The pressure and temperature in the large reservoir were taken as the stagnation conditions in Equations (4.7) and (4.8), while the pressure in the separation tank was assumed to be the choking pressure. These assumptions will give the lowest prediction for the two-phase critical flow at the present values of P_o and P_s. Figures 4.18 and 4.19 show the comparison for data set nos. 1-1 and 1-4 (where the mass flow rates are highest at two different values of P_o). It is clear from these figures that the present values of $\dot{m}_{TP}$ are smaller than predicted critical values at the same conditions. An experimental

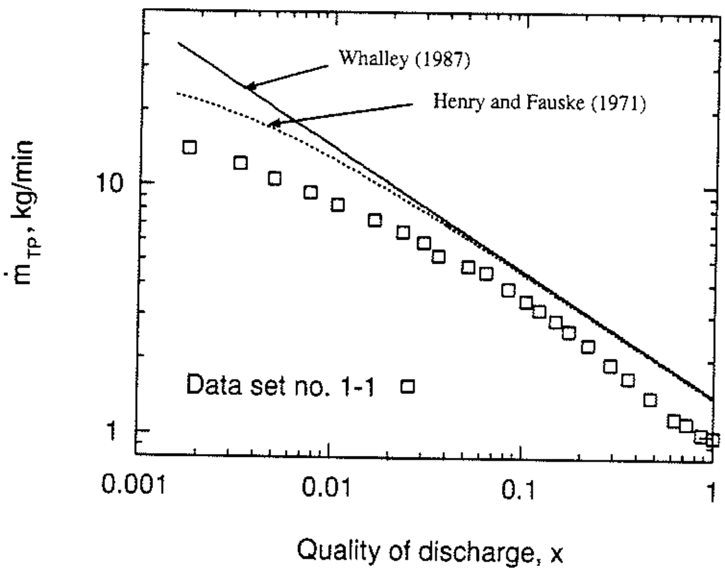

Figure 4.18: Comparison between $\dot{m}_{TP}$ for data set no. 1-1 and critical flow correlations

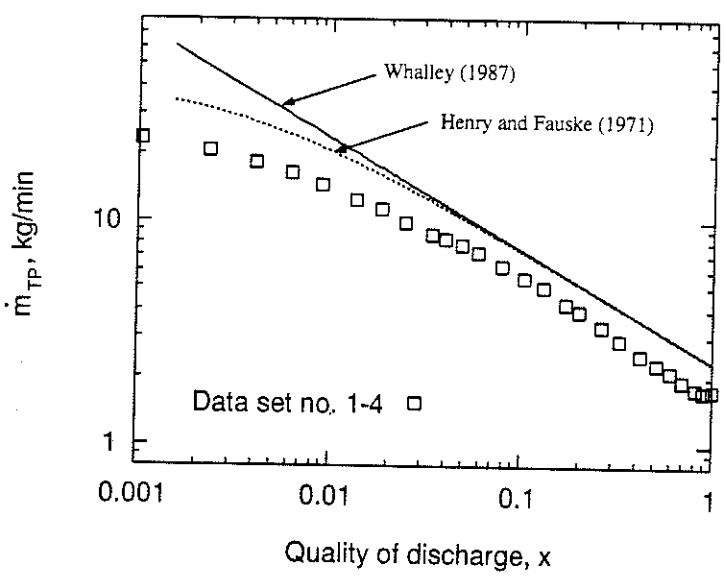

Figure 4.19: Comparison between $\dot{m}_{TP}$ for data set no. 1-4 and critical flow correlations

check was conducted for the limiting case of single-phase air flow by increasing ΔP beyond the maximum value otherwise used in the experiments and no choking occurred. These trends, showing subcritical flow, were found to be the same for the remaining data sets in the present group as well as in the other three groups.

4.2 Dual Discharge from Branches on a Flat Side Wall, the Centerlines Lying in a Horizontal Plane

The operating conditions for the 32 data sets generated in this group are listed in Table 4.2. For $L/d = 1.5$, set nos. 2-1 to 2-3 and set nos. 2-6 to 2-8 explore the effect of ΔP at fixed P_o and R. The influence of R at fixed P_o and ΔP can be examined from set nos. 2-1, 2-4 and 2-5, or set nos. 2-6, 2-9 and 2-10. A similar test matrix was followed for $L/d = 2$. However, for $L/d = 3$ and 8, it was decided not to include the influence of R at fixed P_o and ΔP because sufficient information on this effect had been gained from the results of $L/d = 1.5$ and 2. Values of P_o, ΔP and R used in this investigation are practically identical to those used in group no. 1 (see Table 4.1) ; therefore, influences of the discharge at the second branch can be clearly isolated. A complete tabulation of the data in this group is given in Appendix C.

Table 4.2 Nominal operating conditions for group no. 2
(dual discharge-branch centerlines lying in a horizontal plane)

Set No.	L/d	P_o (kPa)	ΔP (kPa)	R $(kg.m)^{-1/2}$
2-1	1.5	316	123	1000
2-2			82	
2-3			40	
2-4			123	1670
2-5				3000
2-6		517	235	1000
2-7			166	
2-8			97	
2-9			235	1670
2-10				3000
2-11	2.0	316	123	1000
2-12			82	
2-13			40	
2-14			123	1670
2-15				3000
2-16		517	235	1000
2-17			166	
2-18			97	
2-19			235	1670
2-20				3000
2-21	3.0	316	123	1000
2-22			82	
2-23			40	
2-24		517	235	
2-25			166	
2-26			97	
2-27	8.0	316	123	1000
2-28			82	
2-29			40	
2-30		517	235	
2-31			166	
2-32			97	

4.2.1 Flow Phenomena

The flow phenomena will be described in terms of the mass flow rate of each phase at each branch (Figure 4.20) and the appearance of the interface (Figure 4.21); these are functions of h (the vertical distance measured upward from the centerlines of the branches to the flat part of the interface, as shown in Figure 4.21(b)). The interface shape will be sketched approximately to scale for $L/d = 8$ (simple case) and $L/d = 2$ (complex case) , both with large ΔP and small R. The term "simple case" means that the branches act essentially independently of each other; this situation arises for some combination of large L/d and/or small ΔP and/or large R. The term "complex case", means that there is interaction between the two branches and it arises with the opposite combination of L/d (small), ΔP (large) and R (small). The sketches marked "side elevation" in Figure 4.21 depict the interface outline an observer would see from the side of the test section and perpendicular to the centerlines of the branches (for the simple case, the sketches then show the interface along a vertical plane through the centerline of one of the two branches; this is not the situation for the complex case).

The Simple Case:

$h \geq h_{BGE}$ (see region 1 in Figure 4.20)

Let us begin with an interface level well above the two branches. Each branch will be flowing liquid only, $\dot{m}_L$, and the interface will be flat, as shown in Figure 4.21(a).

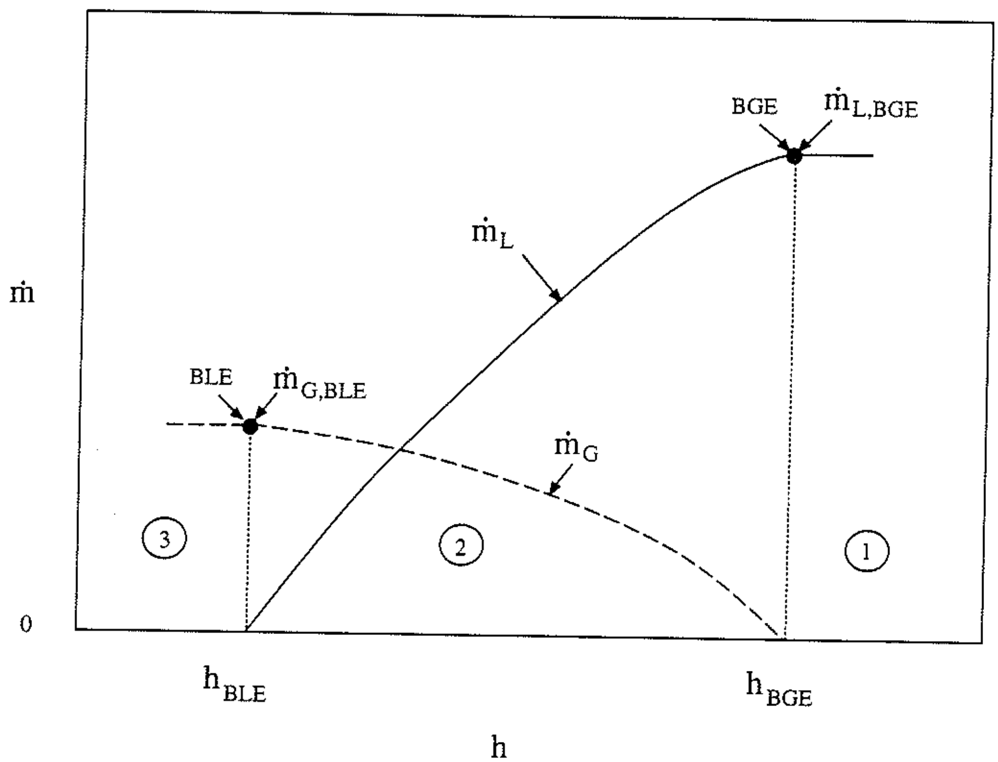

Figure 4.20: Qualitative mass flow rates at either branch
(centerlines in horizontal plane)

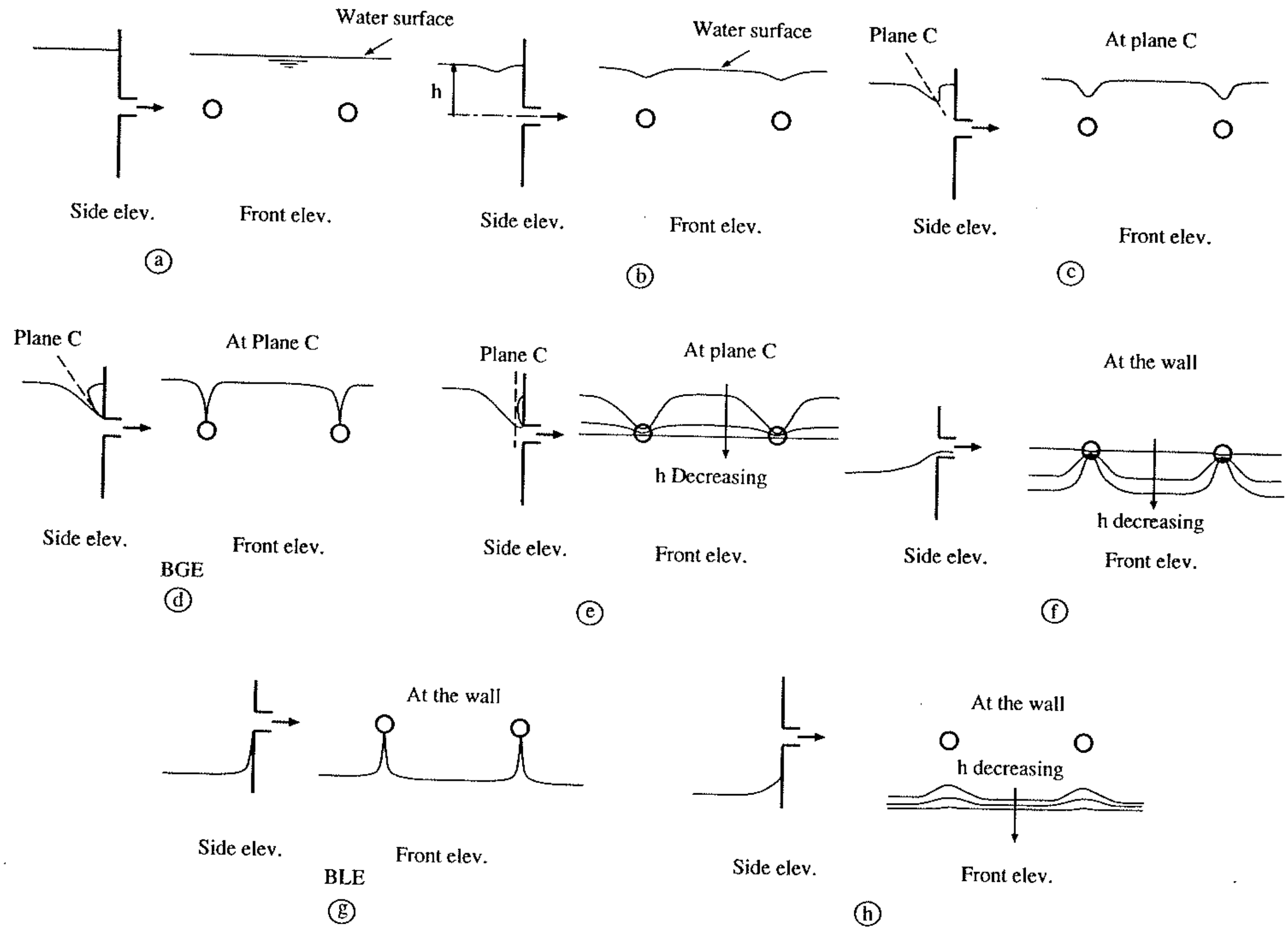

Figure 4.21: Sketches of interface shapes , (branch centerlines in horizontal plane)

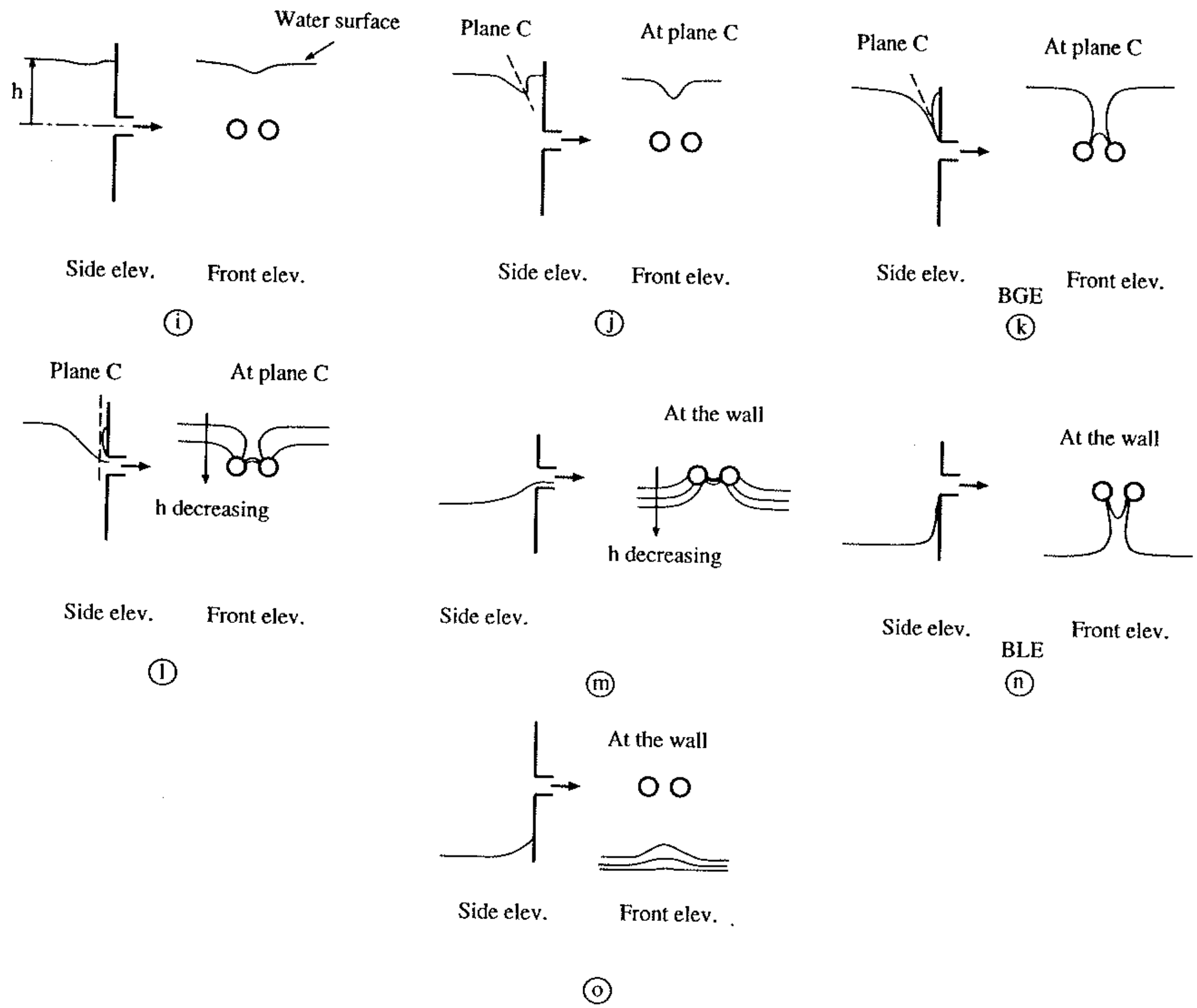

Figure 4.21(cont.): Sketches of interface shapes (branch centerlines in horizontal plane)

As h is lowered and approaches h_{BGE} , two "dimples" begin to form in the interface (Figure 4.21(b)). These depressions become more pronounced (Figure 4.21(c)) and cone-like until the tips of the two cones suddenly extend to the branches; this is the BGE at the branches (Figure 4.21(d)), the corresponding h is h_{BGE} and the flow rate is $\dot{m}_L = \dot{m}_{L,BGE}$. Identical conditions of entrainment in this region (as well, in the all other regions) were observed at both branches due to symmetry (same ΔP, same R and same distance from the interface).

$h_{BGE} > h \geq h_{BLE}$ (see region 2 in Figure 4.20)

In this range, as h decreases, the liquid mass flow rate decreases and the gas mass flow rate increases at each branch. The interface shape is shown through Figures 4.21(e) and (f) until at (g) liquid is no longer entrained at the two branches (this is the BLE at the branches);i.e., $\dot{m}_L = 0$ and $h = h_{BLE}$ while the corresponding gas flow rate at each branch is $\dot{m}_{G,BLE}$.

$h < h_{BLE}$ (see region 3 in Figure 4.20)

In this range, the interface shape would be as depicted in Figure 4.21(h); when $|h|$ is sufficiently large the interface is flat. The flow rate in this region at each branch is $\dot{m}_G = \dot{m}_{G,BLE}$.

The Complex Case:

$h \geq h_{BGE}$ (see region 1 in Figure 4.20)

As h is lowered and approaches h_{BGE}, a "dimple" begins to form in the middle of the interface between the two branches (Figure 4.21(i)). This depression becomes more pronounced with decreasing h (Figure 4.21(j)) and cone-like until the bottom of the cone is suddenly divided into two small cones, each extending to a branch as shown in Figure 4.21(k). This is the BGE at the branches, the corresponding h is h_{BGE} (larger than that of simple case) and the flow rate is $\dot{m}_L = \dot{m}_{L,BGE}$ (same as for the simple case).

$h_{BGE} > h \geq h_{BLE}$ (see region 2 in Figure 4.20)

As with the simple case, in this range as h decreases, $\dot{m}_L$ decreases and $\dot{m}_G$ increases at each branch. The interface shapes are shown in Figure 4.21(l) and (m); for $h > 0$ gas is fed to both branches from a single region above and between the two branches; for $h < 0$ liquid is fed to both branches from a single region below and between the two branches. As h approaches h_{BLE}, the streams feeding liquid to both branches become thinner until the flow of liquid into both branches ceases ($\dot{m}_L = 0$); this is at h_{BLE} (larger in magnitude than that of the simple case) with the interface shown in Figure 4.21(n) and $\dot{m}_G = \dot{m}_{G,BLE}$ (same as for the simple case).

$h < h_{BLE}$ (see region 3 in Figure 4.20)

The interface shapes are depicted in Figure 4.21(o); when $|h|$ is sufficiently large the interface is flat. The flow rate in this region at each branch is $\dot{m}_G = \dot{m}_{G,BLE}$ (same as for the simple case).

4.2.2 Onsets of Gas and Liquid Entrainment

The critical heights corresponding to the BGE and BLE at both branches were measured in each of the 32 data sets. A segment of these results corresponding to $L/d = 1.5$, 3 and 8 is shown in Figures 4.22 and 4.23. Since the critical heights measured at both branches were nearly identical, only the results from one of the two branches are shown in Figures 4.22 and 4.23. These results are correlated in terms of their respective Froude numbers as defined in Equations (2.4) and (2.5).

Two lines corresponding to the limiting cases $L/d = 0$ and ∞ are also shown in Figures 4.22 and 4.23. For $L/d = \infty$, the flow situation reduces to that of a single side branch for which the critical heights at the onsets may be correlated by Equations (4.3) and (4.4). For the limiting case $L/d = 0$, the flow situation again reduces to that of a single branch with double the amount of flow discharge. Thus, the lines marked $L/d = 0$ in Figures 4.22 and 4.23 were also obtained from Equations (4.3) and (4.4), respectively, by doubling the values of Froude number.

It is clear from Figures 4.22 and 4.23 that the lines of $L/d = 0$ and ∞ form an envelope for the present data if we allow for the expected experimental errors. The magnitudes of the critical heights for both onsets increase as L/d decreases. The data for $L/d = 8$ are very close to the line $L/d = \infty$, suggesting that at $L/d = 8$, the branches are practically behaving as two independent single branches.

Empirical relations were developed based on the present data for $1.5 \leq L/d \leq 8$.

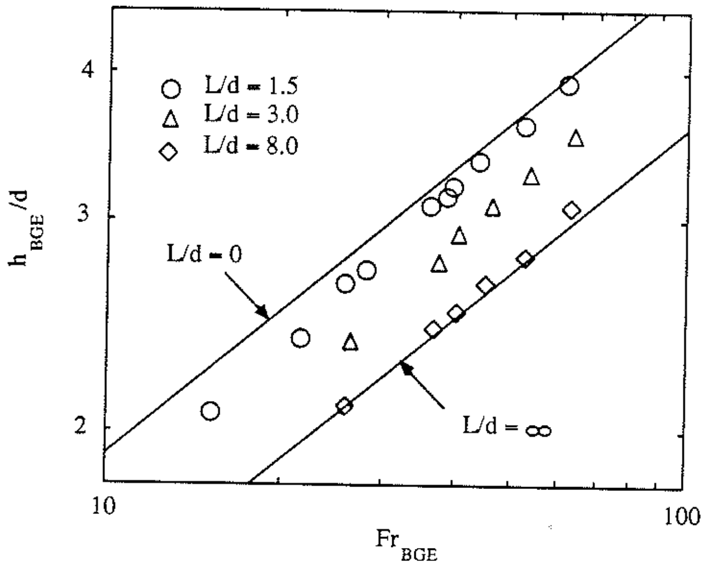

Figure 4.22: The *BGE* for group no. 2

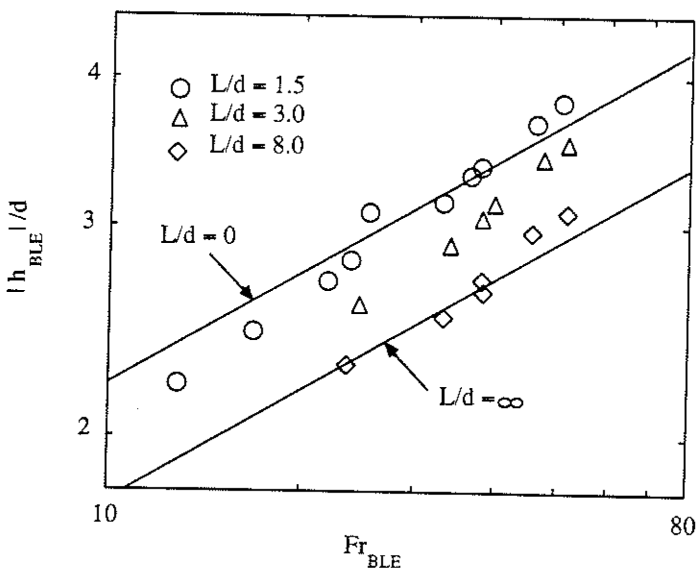

Figure 4.23: The *BLE* for group no. 2

These relations are given by

$$\frac{h_{BGE}}{d} = 0.57 \ (\ A \ Fr_{BGE})^{0.4} \tag{4.10}$$

and

$$\frac{|h_{BLE}|}{d} = 0.87 \ (B \ Fr_{BGE})^{0.31}, \tag{4.11}$$

where

$$A = 1.0 + exp\left[-0.613 \ (\frac{L}{d})^{1.5} \ (Fr_{BGE})^{-0.40}\right] \tag{4.12}$$

and

$$B = 1.0 + exp\left[-2.06 \ (\frac{L}{d})^{2.54} \ (Fr_{BLE})^{-1.2}\right]. \tag{4.13}$$

Equations (4.10) to (4.13) converge to the correct limits at $L/d = 0$ and ∞. As well, these equations predict the data with root-mean-square errors of 1.8 % in h_{BGE} and 3.77 % in h_{BLE}.

4.2.3 Mass Flow Rate and Quality

In order to explain the trends from the current results, the presentation is made first in terms of dimensional quantities. Measured values of $\dot{m}_G$, $\dot{m}_L$, $\dot{m}_{TP}$ and x for data set no. 2-6 are presented in Figures 4.24 to 4.27, respectively. This data set corresponds to the highest P_o and ΔP and the lowest R, a combination that results in the highest gas and liquid flow rates. In addition, this set corresponds to the smallest L/d; therefore, the effects due to dual discharge seen in Figures 4.24 to 4.27 are the most pronounced in this study. Results from group no. 1 for single discharge at the same P_o, ΔP and R (set no. 1-4) are shown for comparison.

Figures 4.24 to 4.27 confirm the geometrical and flow symmetry applied at the two branches in the present study by showing that all results of mass flow rate

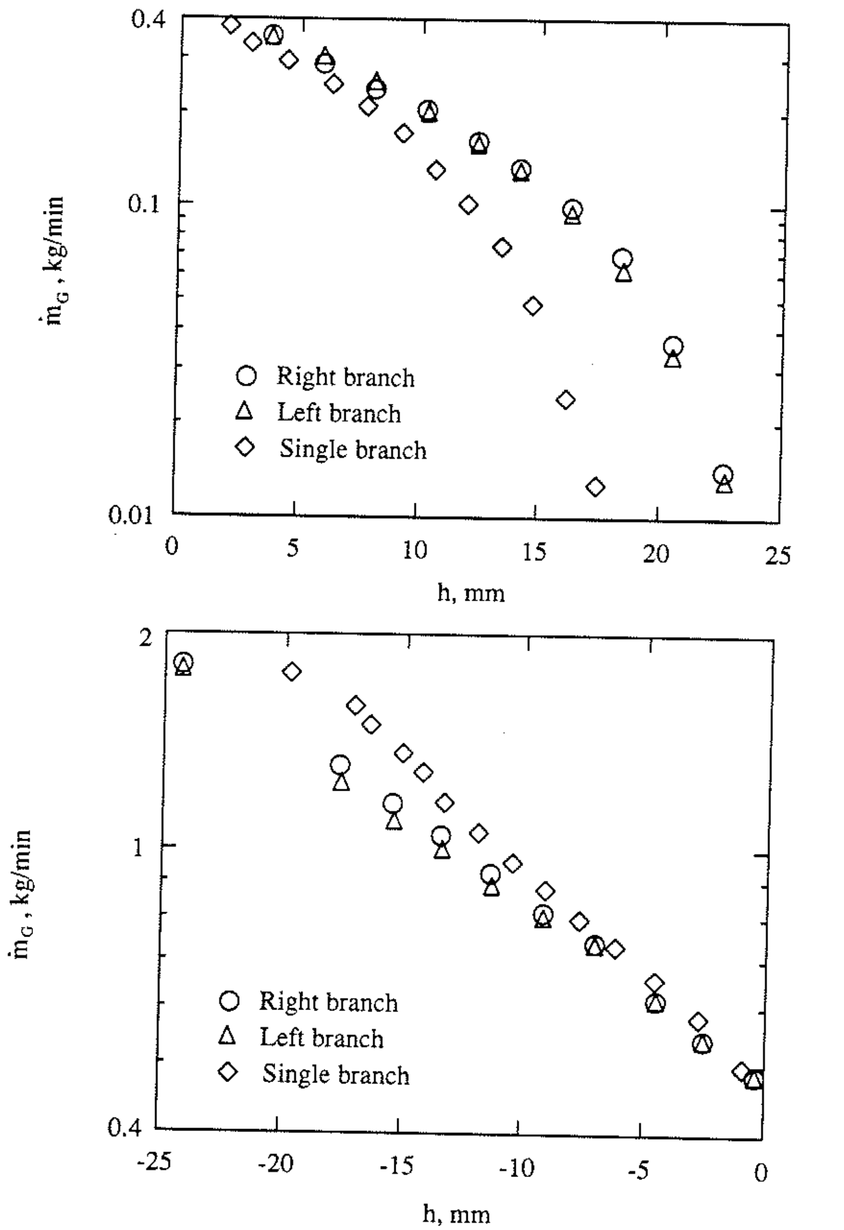

Figure 4.24: Gas mass flow rate for data set no. 2-6

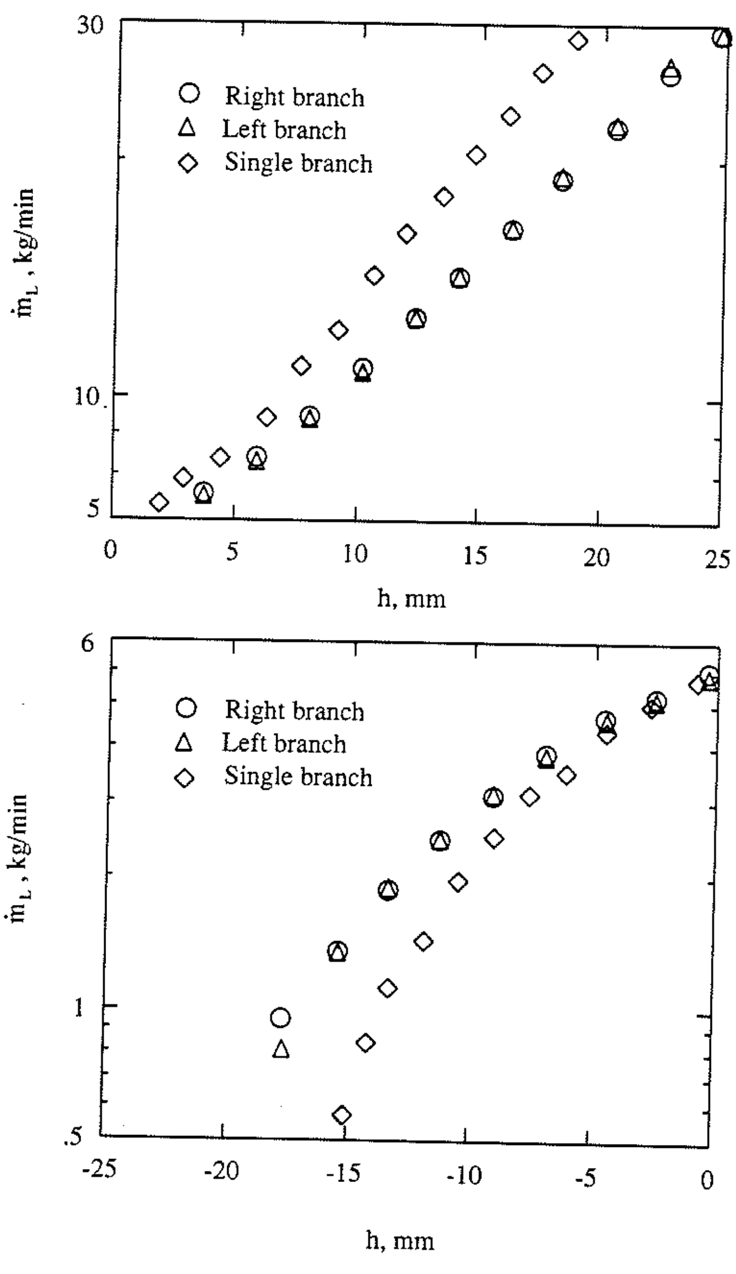

Figure 4.25: Liquid mass flow rate for data set no. 2-6

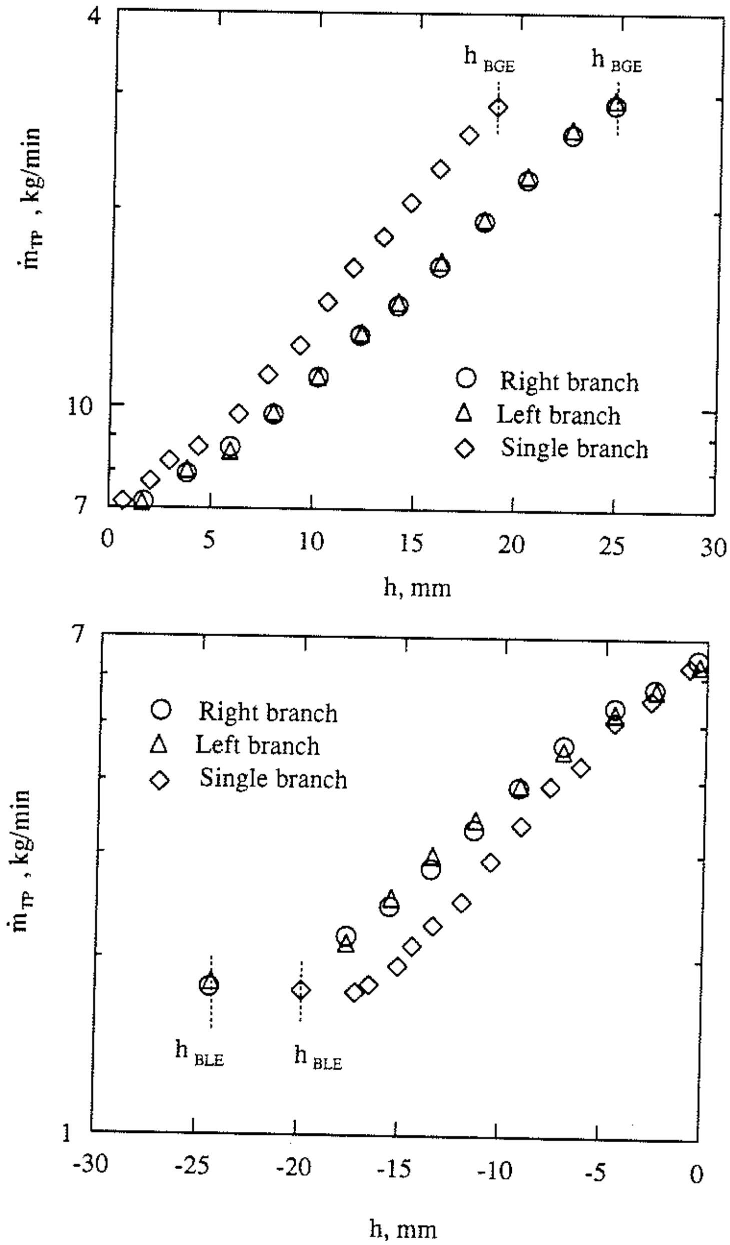

Figure 4.26: Two-phase mass flow rate for data set no. 2-6

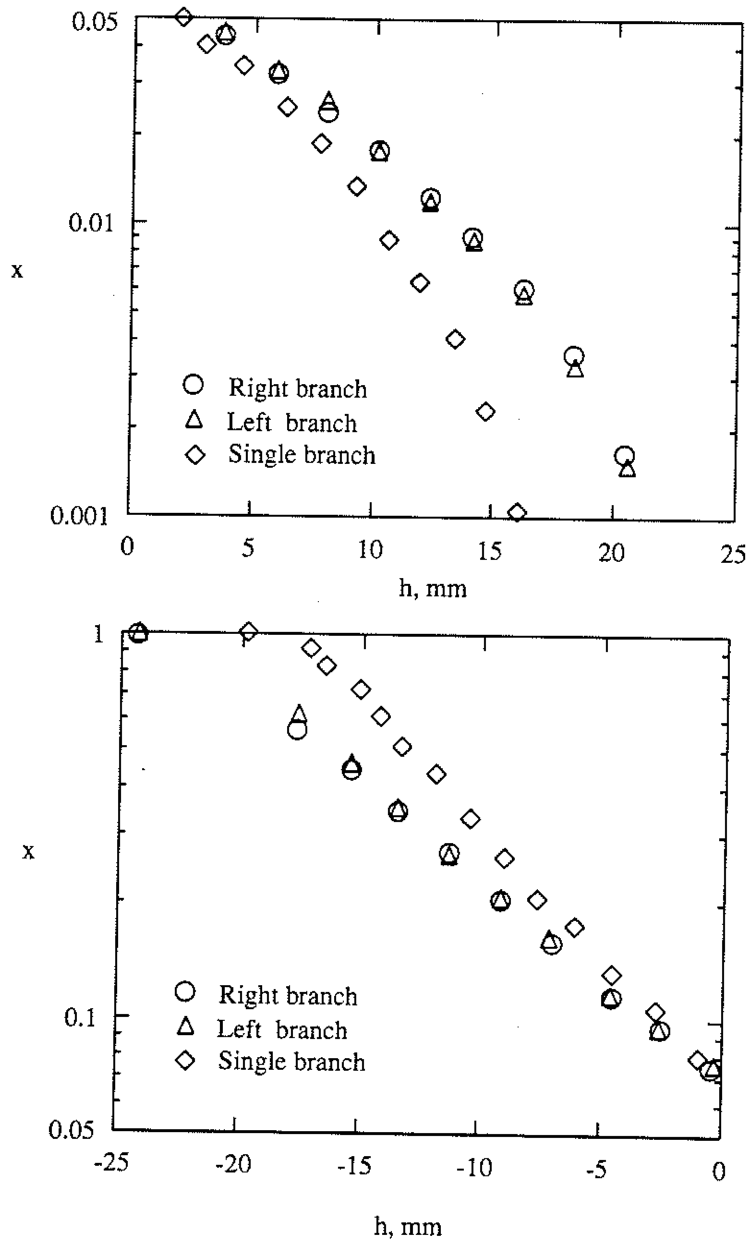

Figure 4.27: Discharge quality for data set no. 2-6

and quality are nearly identical for the two branches. However, there is significant deviation between the present dual-discharge results and those of group no. 1 for a single discharge. For $h > 0$, Figure 4.24 shows that $\dot{m}_G$ is generally higher for the dual-discharge case at any given h. This increase in $\dot{m}_G$ is accompanied by a decrease in $\dot{m}_L$, as shown in Figure 4.25 for $h > 0$. These opposite trends are in fact consistent and can be explained by observing that all the data (of single and dual discharge) in Figures 4.24 to 4.27 correspond to the same ΔP and thus, an increase in $\dot{m}_G$ would require a decrease in $\dot{m}_L$. For $h < 0$, these trends reverse, i.e., $\dot{m}_G$ decreases and $\dot{m}_L$ increases for the dual-discharge case. The results of $\dot{m}_{TP}$ and x for data set no. 2-6 shown in Figures 4.26 and 4.27 follow easily from the data in Figures 4.24 and 4.25.

The trends shown in Figures 4.24 to 4.27 for data set no. 2-6 are typical of all data sets. The magnitude of the deviation between the results of single and dual discharge were found to decrease with an increase in L/d or R, or a decrease in ΔP. For data set nos. 2-27 to 2-32 corresponding to $L/d = 8$, insignificant differences between single- and dual-discharge results were obtained for all values of P_o, ΔP and R tested in this study.

An attempt was made to plot the data in a normalized fashion in order to absorb the deviations seen in the dimensional plots of Figures 4.24 to 4.27. This was done using the normalized liquid level and the normalized mass flow rate defined in Equations (4.1) and (4.2).

Figures 4.28 and 4.29 show that the data of quality and mass flow rate, respectively, from set no. 2-6 collapse on the respective single-discharge results from group no. 1 at the same P_o, ΔP and R. This is very significant since the results for data set no. 2-6 deviated the most from the single-discharge results for the same conditions (as seen in Figures 4.24 to 4.27).

The ability of the normalized parameters of Equations (4.1) and (4.2) to absorb the effects of other independent parameters is shown in Figures 4.30 and 4.31. Sixteen data sets corresponding to P_o = 316 kPa with all tested combinations of ΔP, R and L/d are shown to be largely collapsed in these plots. The same behavior was also found for the other half of the data (P_o = 517 kPa). However, one small effect remains due to the system pressure P_o. Figure 4.32 shows a slight increase in x with P_o at the same ΔP, R and L/d. On the other hand, the effect of P_o on M was found to be insignificant, as illustrated in Figure 4.33.

Similar trends were reported in Section 4.1 for the case of single-branch discharge whereby M was found to be a function of H only (for all P_o, ΔP and R tested) and x was found to be dependent on H and P_o (for all ΔP and R tested).

In view of the similarity in trends between the present data and those in group no. 1 and the data collapse shown in Figures 4.28 and 4.29, it was decided to test the validity of Equations (4.5) and (4.6) for the present data. This comparison resulted in excellent agreement, as shown in Figures 4.34 and 4.35. Quantitatively, the quality x was predicted with a root-mean-square error of 8.5 % over the range

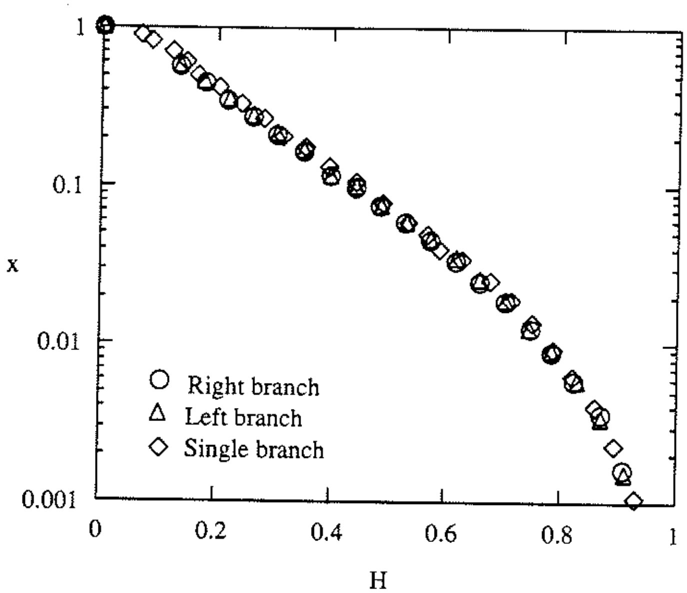

Figure 4.28: Normalized plot of x versus H
for data set no. 2-6

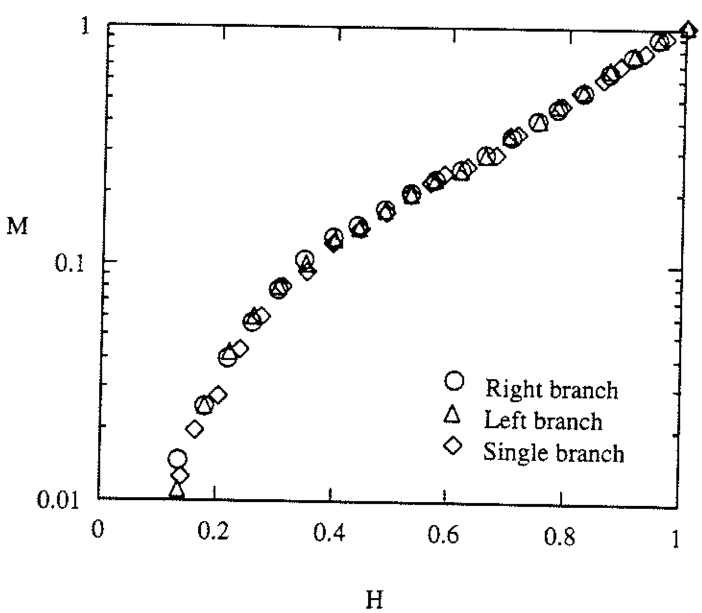

Figure 4.29: Normalized plot of M versus H
for data set no. 2-6

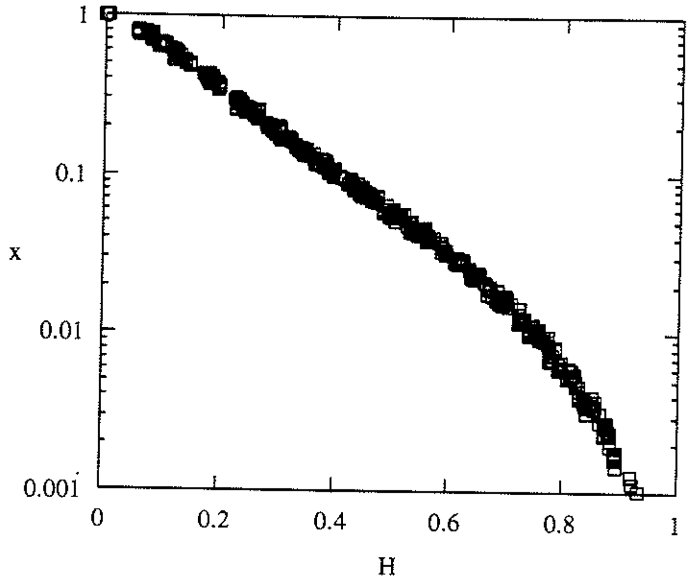

Figure 4.30: Normalized plot of x versus H
for all data sets at $P_o = 316\ kPa$

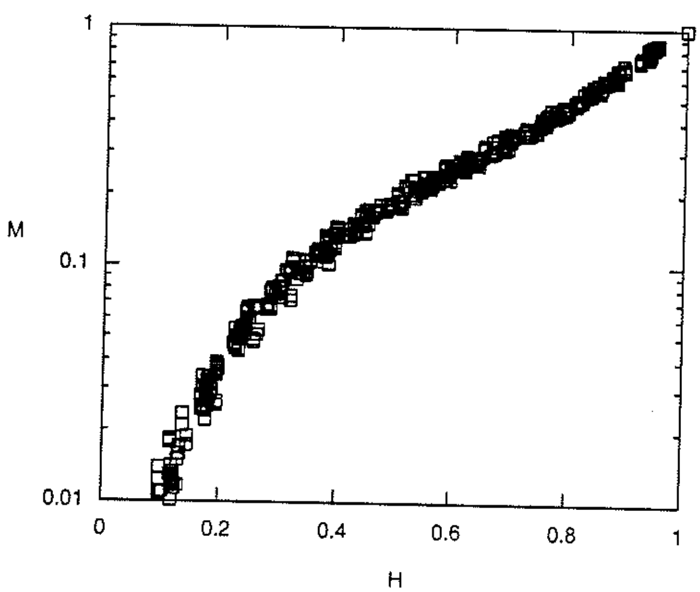

Figure 4.31: Normalized plot of M versus H
for all data sets at $P_o = 316\ kPa$

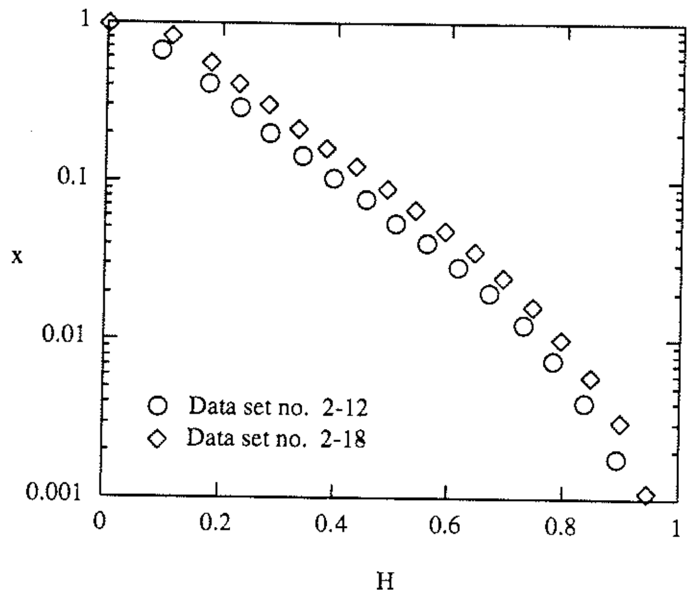

Figure 4.32: Effect of P_o on the $x - H$ relation

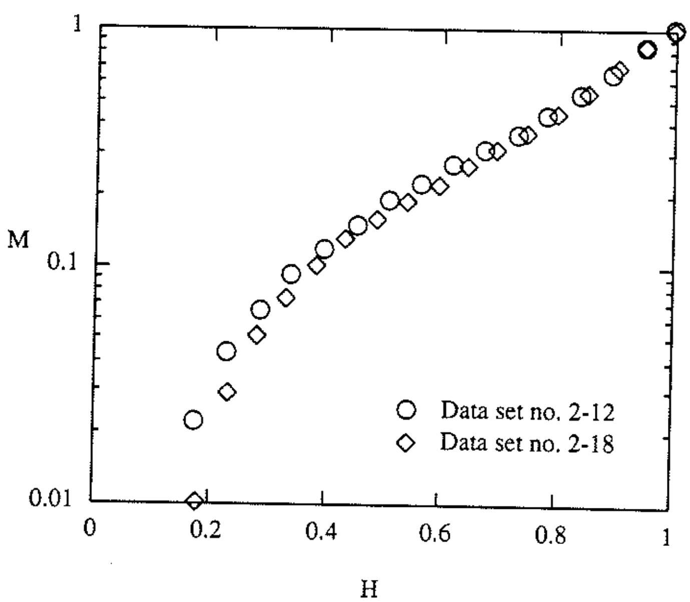

Figure 4.33: Effect of P_o on the $M - H$ relation

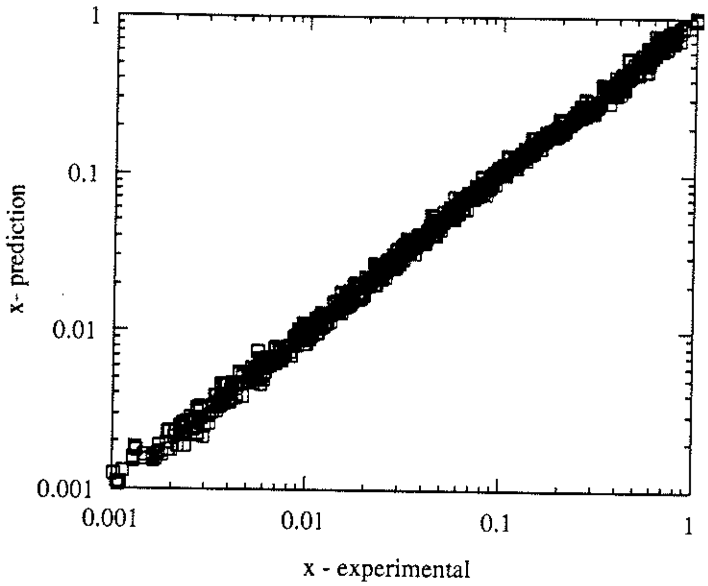

Figure 4.34: Comparison between all data of x and correlation (4.5)

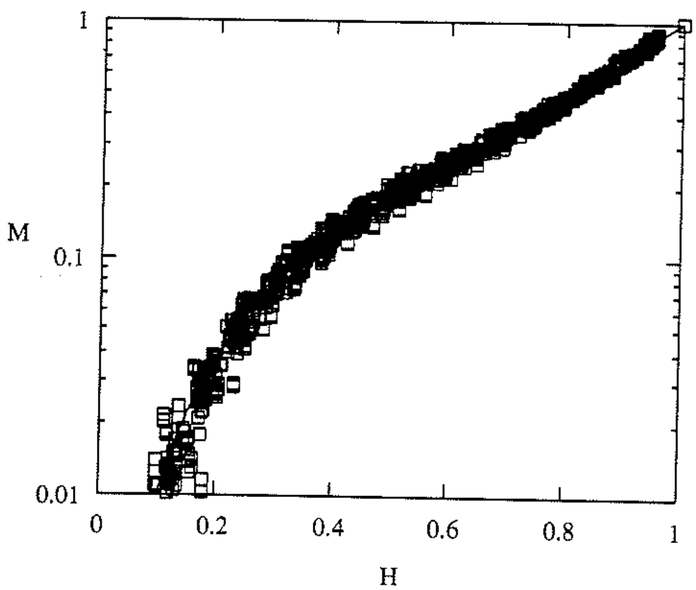

Figure 4.35: Comparison between all data of M and correlation (4.6)

$0.001 \leq x \leq 1$. The dimensionless two-phase discharge M was predicted with a root-mean-square error of 14.2 % over the range $0.01 \leq M \leq 1$ and the accuracy of prediction improved significantly if very low values of M were not considered. For example, the root-mean-square error reduces to 7 % in the range $0.05 \leq M \leq 1$. Since correlations (4.5) and (4.6) are empirical, their accuracy can only be assured within the range of conditions covered in this investigation.

4.3 Dual Discharge from Branches on a Flat Side Wall, the Centerlines Lying in a Vertical Plane

The operating conditions for the 32 data sets generated in this group are listed in Table 4.4. The test matrix was purposely designed to be identical to that of group no. 2 in order to isolate the effect of orientation of the branches. A complete tabulation of the data in this group is given in Appendix D.

4.3.1 Flow Phenomena

The flow phenomena are described in terms of the mass flow rate of each phase and the appearance of the interface, these as a function of h^*, where h^* is the distance of the flat part of the interface above some datum located arbitrarily well below the lower branch; this definition of h^* is shown in Figure 4.36(a). The terms "simple case" and "complex case" are used and mean those situations where

Table 4.3: Nominal operating conditions for group no. 3 (dual discharge-branch centerlines lying in a vertical plane)

Set No.	L/d	P_o (kPa)	ΔP (kPa)	R $(kg.m)^{-1/2}$
3-1	1.5	316	123	1000
3-2			82	
3-3			40	
3-4			123	1670
3-5				3000
3-6		517	235	1000
3-7			166	
3-8			97	
3-9			235	1670
3-10				3000
3-11	2.0	316	123	1000
3-12			82	
3-13			40	
3-14			123	1670
3-15				3000
3-16		517	235	1000
3-17			166	
3-18			97	
3-19			235	1670
3-20				3000
3-21	3.0	316	123	1000
3-22			82	
3-23			40	
3-24		517	235	
3-25			166	
3-26			97	
3-27	8.0	316	123	1000
3-28			82	
3-29			40	
3-30		517	235	
3-31			166	
3-32			97	

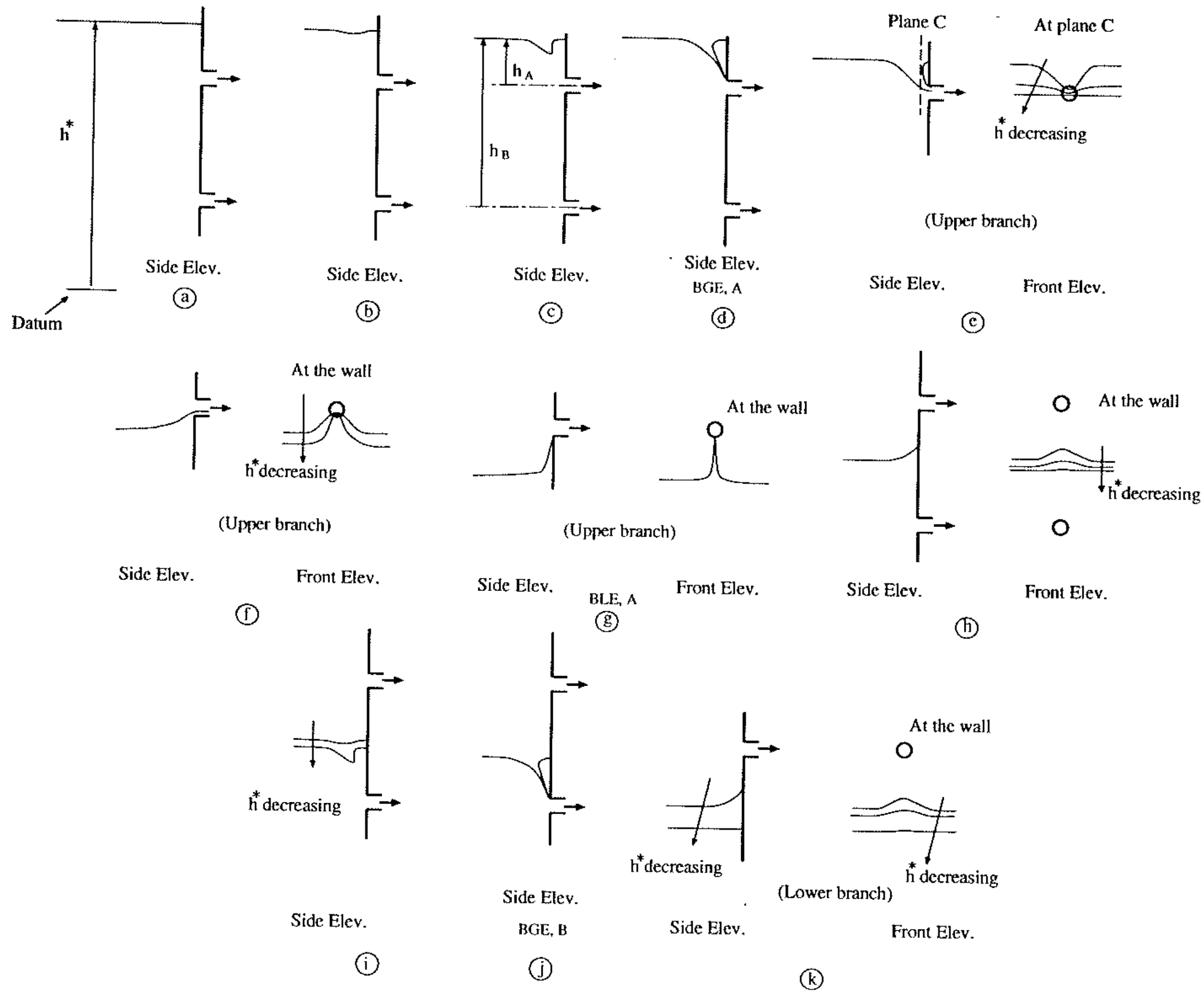

Figure 4. 36: Sketches of interface shapes (branch centerlines in vertical plane)

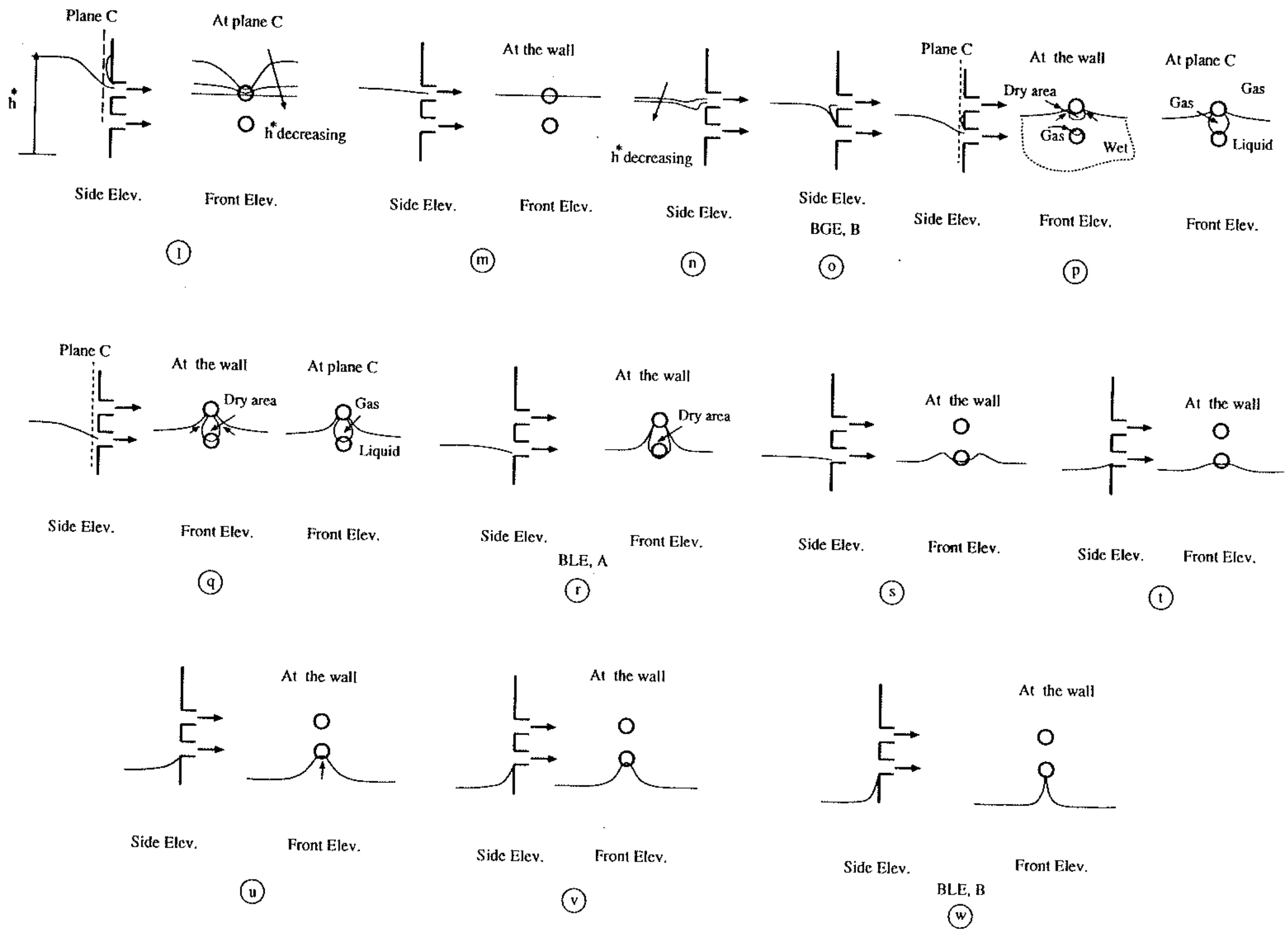

Figure 4.36 (cont.): Sketches of interface shapes (branch centerlines in vertical plane)

$h^*_{BLE,A} > h^*_{BGE,B}$ and $h^*_{BLE,A} < h^*_{BGE,B}$, respectively, where subscript A refers to the upper branch and subscript B refers to the lower branch. The interface shape will be sketched approximately to scale for $L/d = 8$ (simple case) and $L/d = 2$ (complex case) , both with large ΔP and small R.

The Simple Case ($h^*_{BLE,A} > h^*_{BGE,B}$):

$h^* \geq h^*_{BGE,A}$ (see region 1 in Figure 4.37(a))

Let us begin with an interface level well above the upper branch. Both branches will be flowing liquid only, the flow rates of which will be essentially the same, i.e., $\dot{m}_{L,A} = \dot{m}_{L,B}$ as shown in Figure 4.37(a), and the interface will be flat as shown in Figure 4.36(a). As h^* is lowered and approaches $h^*_{BGE,A}$, a "dimple" begins to form in the interface (Figure 4.36(b)). This dimple depression becomes more pronounced (Figure 4.36(c)) and cone-like until the bottom of the cone suddenly extends to the upper branch; this is the BGE at the upper branch BGE, A (Figure 4.36(d)); the corresponding h^* is $h^*_{BGE,A}$ and the flow rates are $\dot{m}_{L,A} = \dot{m}_{L,B} = \dot{m}_{L,BGE,A}$. In Figure 4.36, sketches marked "side elevation" are taken along a vertical plane through the centerlines of the two branches.

$h^*_{BGE,A} > h^* \geq h^*_{BLE,A}$ (see region 2 in Figure 4.37(a))

In this range, the lower branch continues to flow only liquid at the rate $\dot{m}_{L,B} = \dot{m}_{L,BGE,A}$. At the upper branch $\dot{m}_{L,A}$ decreases and $\dot{m}_{G,A}$ increases as h^* decreases. The interface shape is shown through Figure 4.36(e) and (f) until at (g) liquid is

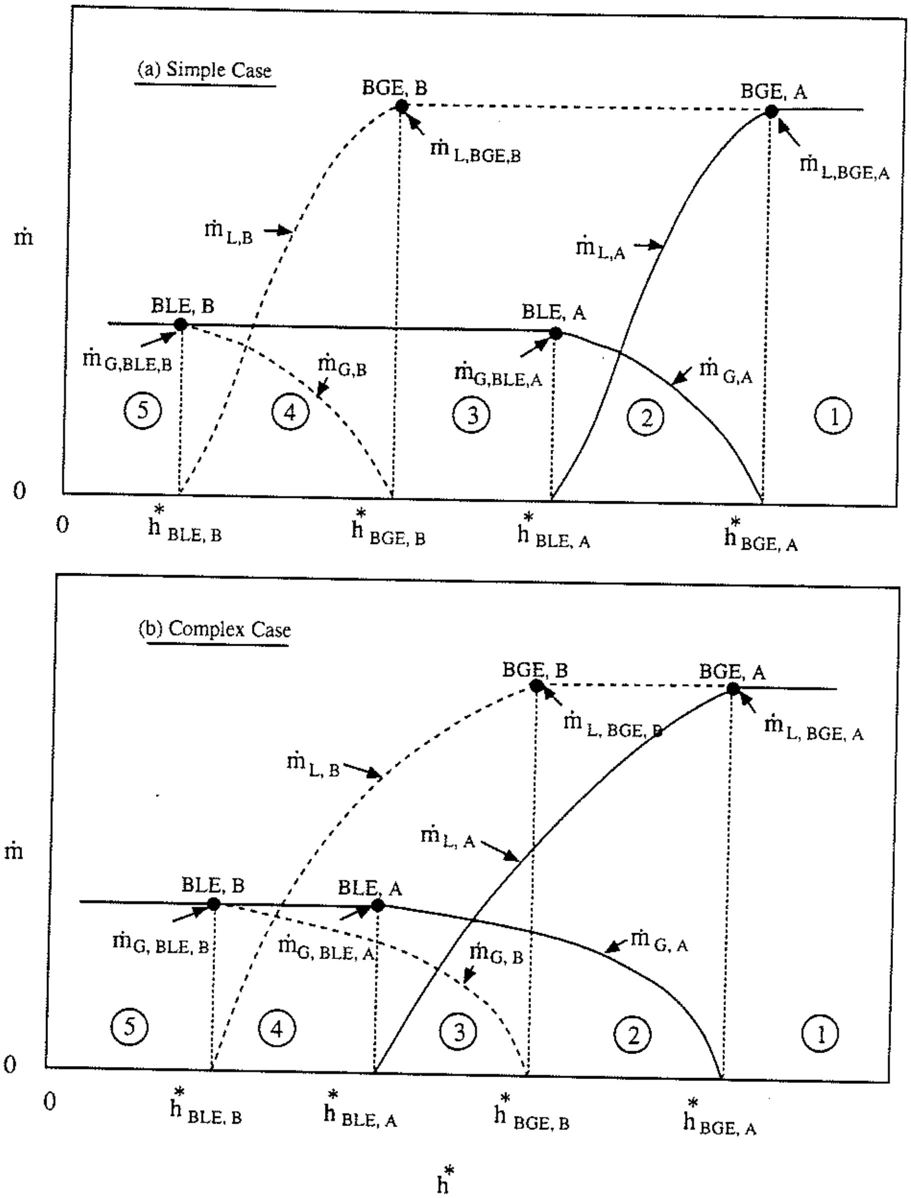

Figure 4.37: Qualitative mass flow rates for dual discharge (branch centerlines in vertical plane)

no longer entrained at the upper branch, i.e. $\dot{m}_{L,A} = 0$ and $h^* = h^*_{BLE,A}$ while the corresponding gas flow rate at the upper branch is $\dot{m}_{G,BLE,A}$.

<u>$h^*_{BLE,A} > h^* \geq h^*_{BGE,B}$ (see region 3 in Figure 4.37(a))</u>

As h^* is reduced below $h^*_{BLE,A}$, the upper branch flows only gas at the rate of $\dot{m}_{G,A} = \dot{m}_{L,BLE,A}$. The lower branch continues to flow only liquid at the rate of $\dot{m}_{L,B} = \dot{m}_{L,BGE,A}$. With decreasing h^*, the interface is depicted in Figure 4.36(h) and (i). In (i) a dimple in the interface has begun to form, becomes more pronounced and cone-like and finally the tip of the cone extends to the lower branch, as depicted in Figure 4.36(j). This is the *BGE* at the lower branch; the h^* is $h^*_{BGE,B}$ and the various flow rates are $\dot{m}_{G,A} = \dot{m}_{G,BLE,A}$, $\dot{m}_{L,A} = 0$, $\dot{m}_{G,B} = 0$ (onset) and $\dot{m}_{L,B} = \dot{m}_{L,BGE,B}$ $(= \dot{m}_{L,BGE,A})$.

<u>$h^*_{BGE,B} > h^* \geq h^*_{BLE,B}$ (see region 4 in Figure 4.37(a))</u>

In this range, the interface shape would be as depicted in Figure 4.36(e), (f) and (g), excepting, of course, at the lower branch. The BLE, B is at $h^*_{BLE,B}$ at which the various flow rates are $\dot{m}_{G,A} = \dot{m}_{G,BLE,A}$,$\dot{m}_{L,A} = 0$, $\dot{m}_{G,B} = \dot{m}_{G,BLE,B}$ $(= \dot{m}_{G,BLE,A})$, $\dot{m}_{L,B} = 0$ (onset).

<u>$h^* < h^*_{BLE,B}$ (see region 5 in Figure 4.37(a))</u>

In this range, the interface shape would be as depicted in Figure 4.36(k); when h^* is sufficiently small the interface is flat. The flow rates in this region are $\dot{m}_{G,A} =$

$\dot{m}_{G,B} = \dot{m}_{G,BLE,A} = \dot{m}_{G,BLE,B}$ and $\dot{m}_{L,A} = \dot{m}_{L,B} = 0$.

The Complex Case ($h^*_{BLE,A} < h^*_{BGE,B}$):

$h^* \geq h^*_{BGE,A}$ (see region 1 in Figure 4.37(b))

The description is the same as for the simple case, including references to the sketches (except for the distance between the branches and $h^*_{BGE,A}$ being larger in the present case).

$h^*_{BGE,A} > h^* \geq h^*_{BGE,B}$ (see region 2 in Figure 4.37(b))

In this range, the lower branch continues to flow only liquid at the rate $\dot{m}_{L,B} = \dot{m}_{L,BGE,A}$ while at the upper branch $\dot{m}_{L,A}$ decreases (from a value of $\dot{m}_{L,BGE,A}$) and $\dot{m}_{G,A}$ increases as h^* decreases. The interface shape is shown in Figure 4.36(l), (m) and (n) with a cone being formed at the lower values of h^* until at (o) the tip of the cone extends to the lower branch when $h^* = h^*_{BGE,B}$.

$h^*_{BGE,B} > h^* \geq h^*_{BLE,A}$ (see region 3 in Figure 4.37(b))

In this range, both branches are flowing a two-phase mixture. As h^* is lowered, the liquid flow rate $\dot{m}_{L,A}$ and gas flow rate $\dot{m}_{G,A}$ at the upper branch continue to decrease and increase, respectively. Similarly, for the lower branch $\dot{m}_{L,B}$ decreases while $\dot{m}_{G,B}$ increases. Liquid is fed to the upper branch in two streams from the sides of the branch. A "trough" of gas feeds gas to the lower branch. The interface shapes are sketched in Figure 4.36(p) and (q). The streams feeding liquid to the upper branch become thinner as h^* is decreased until the flow of liquid into the upper branch ceases ($\dot{m}_{L,A} = 0$) ; this is at $h^*_{BLE,A}$ and the interface is sketched in Figure 4.36(r); at this point $\dot{m}_{G,A} = \dot{m}_{G,BLE,A}$, the maximum $\dot{m}_{G,A}$.

$h^*_{BLE,A} > h^* \geq h^*_{BLE,B}$ (see region 4 in Figure 4.37(b))

Here the upper branch is flowing gas only at $\dot{m}_{G,A} = \dot{m}_{G,BLE,A}$ while the lower is flowing a two-phase mixture. The interface shapes are shown in Figure 4.36(s) to (v) as h^* is decreased. The liquid sucked up the wall as in (v) diminishes to zero as h^* is decreased to $h^*_{BLE,B}$; this is shown in Figure 4.36(w) at which point $\dot{m}_{L,B} = 0$ and $\dot{m}_{G,B} = \dot{m}_{G,BLE,B}(= \dot{m}_{G,BLE,A})$, the maximum gas flow rate in the lower branch.

$h^* < h^*_{BLE,B}$ (see region 5 in Figure 4.37(b))

Here both branches are flowing gas only and the various flow rates are $\dot{m}_{L,A} = \dot{m}_{L,B} = 0$ and $\dot{m}_{G,A} = \dot{m}_{G,B} = \dot{m}_{BLE,A} = \dot{m}_{BLE,B}$. The interface shapes are essentially as shown in Figure 4.36(k).

4.3.2 Onsets of Gas and Liquid Entrainment

The critical heights at the BGE and BLE were measured for both branches in each of the 32 data sets. A sample of these results is shown in Figure 4.38 (gas entrainment) and Figure 4.39 (liquid entrainment). Data for $L/d = 1.5$ and 8 are shown in both figures; the trend for intermediate values of L/d is monotonic. The

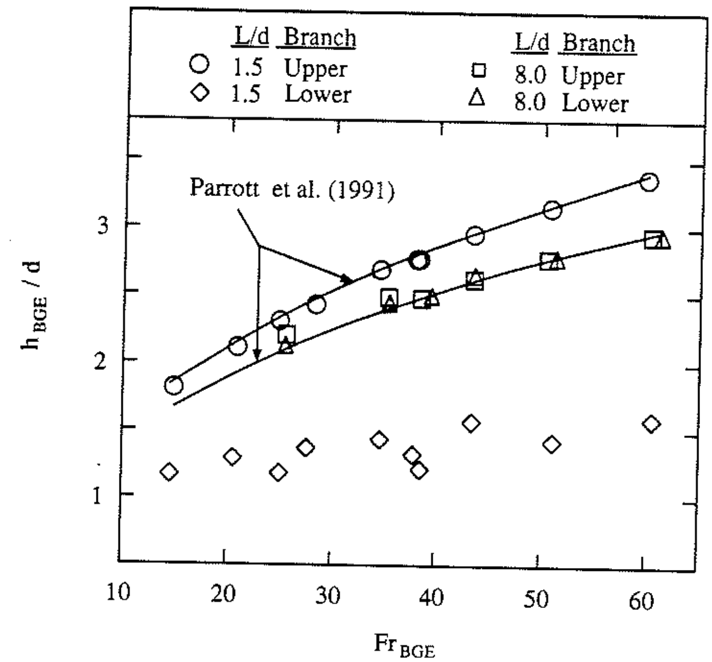

Figure 4.38: The *BGE* for group no.3

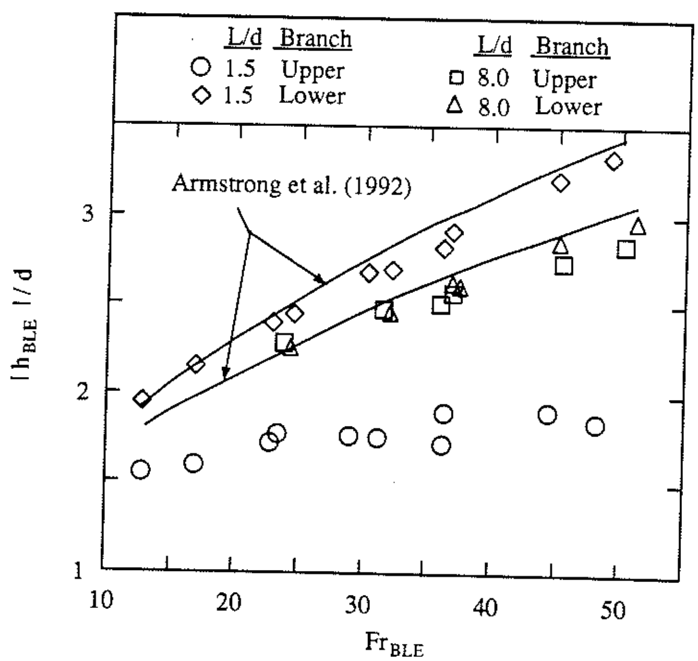

Figure 4.39: The *BLE* for group no.3

predicted values of $h_{BGE,A}$ from the empirical correlation of Parrott et al. (1991), given by Equation (2.30), are shown in Figure 4.38 and the predicted values of $h_{BLE,B}$ from the theoretical analysis of Armstrong et al. (1992), given later by Equation (5.2), are shown in Figure 4.39. The results in Figures 4.38 and 4.39 are presented in terms of Fr_{BGE} and Fr_{BLE} defined by Equations (2.4) and (2.5), respectively.

Figure 4.38 shows that $h_{BGE,A}$ and $h_{BGE,B}$ are nearly identical for L/d = 8, which suggests very little interaction between the branches at this separating distance. The interaction between the branches intensifies as L/d decreases and as a consequence, $h_{BGE,A}$ increases while $h_{BGE,B}$ decreases. This trend is consistent with the observation that just before the BGE at the upper branch, both branches are fully submerged in liquid and the lower branch would thus assist the upper branch in entraining gas from higher interface locations, while on the other hand, just before the BGE at the lower branch, only the lower branch is fully submerged in liquid and thus the upper branch competes with (rather than assists) the lower branch for gas flow. The deviation between $h_{BGE,A}$ and $h_{BGE,B}$ increases continuously up to the values shown in Figure 4.38 for L/d = 1.5. The correlation of Parrott et al. (1991) is in excellent agreement with the present data of $h_{BGE,A}$ for L/d = 1.5 and 8 (as well as for L/d = 2 and 3).

Figure 4.39 also shows that the interaction between the branches is small at L/d = 8 with nearly identical values of $h_{BLE,A}$ and $h_{BLE,B}$. The deviation between these two critical heights increases continuously as L/d decreases. However, the trend in this case is for $|h_{BLE,A}|$ to decrease and $|h_{BLE,B}|$ to increase as L/d decreases. This trend is also consistent with the observation that just before the BLE at the lower branch, both branches are receiving pure gas flow and the upper branch would thus assist the lower branch in entraining liquid from deeper interface locations, while on the other hand, just after the BLE at the upper branch, only the upper branch is receiving pure gas flow and thus the lower branch competes with the upper branch for liquid flow. The theoretical predictions of Armstrong et al. (1992) are in good agreement with the present data of $h_{BLE,B}$ for L/d = 1.5 and 8 (as well as for $L/d = 2$ and 3).

Empirical correlations were developed for the critical heights at all four onsets based on the present data. These correlations, obtained by least square fitting, are given by the following relations:

$$\frac{h_{BGE,A}}{d} = 0.57 \ (A_1 \ Fr_{BGE})^{0.4}, \tag{4.14}$$

$$\frac{h_{BGE,B}}{d} = 0.57 \ (Fr_{BGE})^{A_2}, \tag{4.15}$$

$$\frac{|h_{BLE,A}|}{d} = 0.87 \ (Fr_{BLE})^{A_3} \tag{4.16}$$

and

$$\frac{|h_{BLE,B}|}{d} = 0.87 \ (A_4 \ Fr_{BLE})^{0.31}, \tag{4.17}$$

where,

$$A_1 = 1.0 + exp\left[-1.96 \left(\frac{L}{d}\right)^{1.2} (Fr_{BGE})^{-0.32}\right], \tag{4.18}$$

$$A_2 = 0.4 - 0.223\, exp\left[-0.415\, \left(\frac{L}{d}\right)^{1.5} (Fr_{BGE})^{-0.2}\right], \quad (4.19)$$

$$A_3 = 0.31 - 0.13\, exp\left[-0.209\, \left(\frac{L}{d}\right)^{1.5} (Fr_{BLE})^{-0.2}\right] \quad (4.20)$$

and

$$A_4 = 1.0 + exp\left[-2.27\, \left(\frac{L}{d}\right)^{1.2} (Fr_{BLE})^{-0.32}\right]. \quad (4.21)$$

The above relations converge to the correct limits at the two extremes of L/d. For $L/d = \infty$, we get $A_1 = A_4 = 1$, $A_2 = 0.4$ and $A_3 = 0.31$, and Equations (4.14) to (4.17) converge to the single-branch relations given by Equations (4.3) and (4.4). For $L/d = 0$, we get $A_1 = A_4 = 2$, and Equations (4.14) and (4.17) reduce to the single-branch relations with twice the values of Froude number; i.e., a single branch with twice the flow rate.

The predictive relations given by Equations (4.14) to (4.17) are in excellent agreement with the present data. The root-mean-square values of the deviation between the present data and (4.14) to (4.17) are 1.9 %, 4.4 %, 3.8 % and 2.9 %, respectively.

4.3.3 Mass Flow Rate and Quality

In order to explain the trends from the current results, the presentation is made first in terms of dimensional quantities. Measured values of $\dot{m}_G$, $\dot{m}_L$, $\dot{m}_{TP}$ and x for data set no. 3-6 are presented in Figures 4.40 to 4.43, respectively. For the dual discharge case, the h of the abscissa on these figures is h_A for the upper branch and h_B for the lower branch (h_A and h_B are defined as the distances from the centerlines of

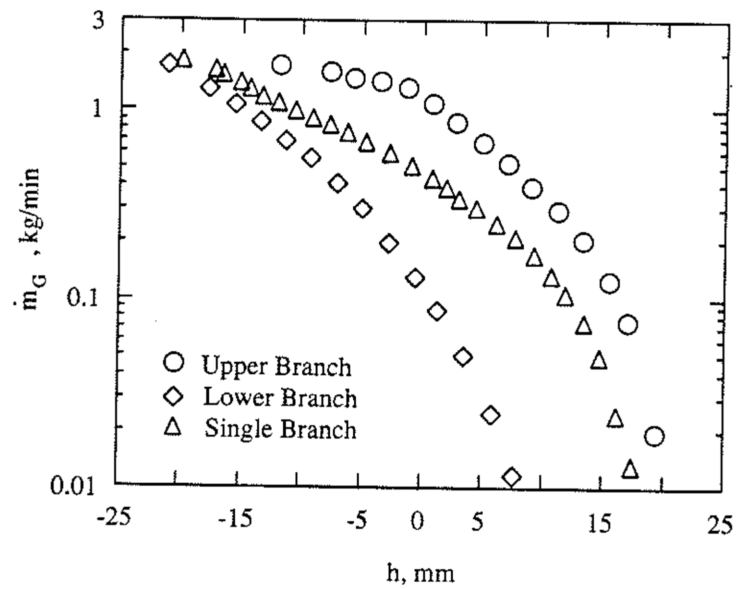

Figure 4.40: Gas mass flow rate for data set no. 3-6

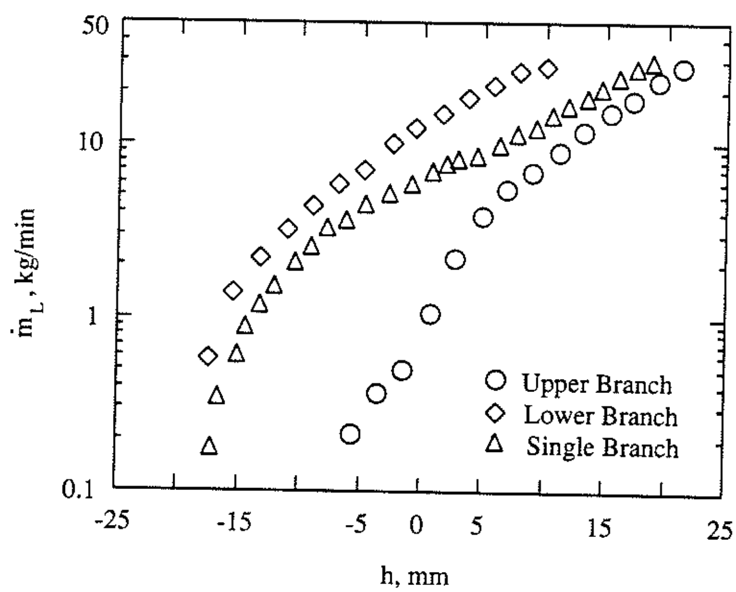

Figure 4.41: Liquid mass flow rate for data set no. 3-6

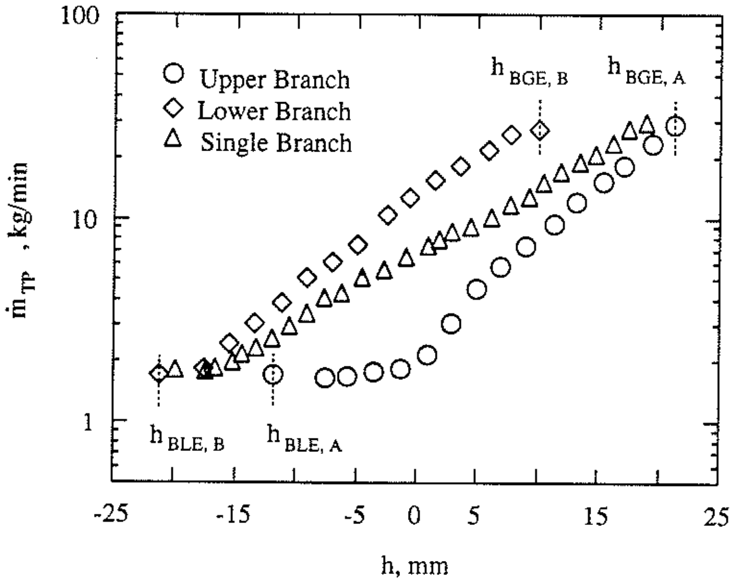

Figure 4.42: Two-phase mass flow rate for data set no. 3-6

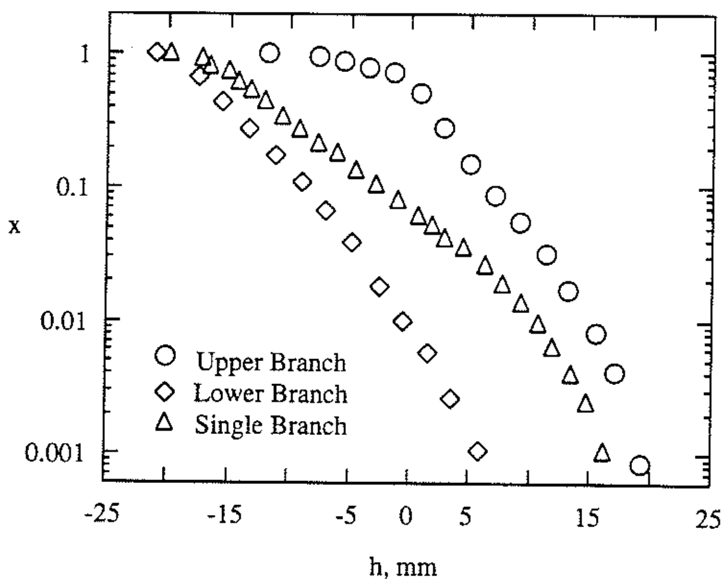

Figure 4.43: Discharge quality for data set no. 3-6

upper and lower branches, respectively, to the flat part of the interface, as shown in Figure 4.36(c). This data set corresponds to the highest P_o and ΔP and lowest R, a combination that results in the highest gas and liquid flow rates. In addition, this set corresponds to the smallest L/d; therefore, the effects due to dual discharge seen in Figures 4.40 to 4.43 are the most pronounced in this study. Results from group no. 1 for single discharge at the same P_o, ΔP and R are shown for comparison. Figure 4.40 shows an increase in air flow rate at the upper branch and a decrease at the lower branch relative to the single-branch case. Figure 4.41 shows that $\dot{m}_L$ follows an opposite trend to that of $\dot{m}_G$. These opposite trends are in fact consistent and can be explained by observing that all the data in Figures 4.40 and 4.41 correspond to the same ΔP and thus, an increase in $\dot{m}_G$ at one branch would require a decrease in $\dot{m}_L$ at the same branch. The results in Figures 4.42 and 4.43 follow easily from those in Figures 4.40 and 4.41. It is clear from Figures 4.40 to 4.43 that the results for dual discharge cannot be predicted from those of single discharge and thus the need for the present data is justified.

The trends shown in Figures 4.40 to 4.43 for data set no. 3-6 are typical of all data sets. The magnitude of the deviation between the results at the upper and lower branches were found to decrease with an increase in L/d or R, or a decrease in ΔP. For data set nos. 3-27 to 3-32 corresponding to $L/d = 8$, insignificant differences between upper, lower and single branch results were obtained for all values of P_o, ΔP and R tested in this study.

An attempt was made to plot the data in a normalized fashion as in the case where the two branch centerlines lie in a horizontal plane so that the influences of some independent variables may be absorbed. This was done using the previous definitions (4.1) and (4.2) for the normalized liquid level and the normalized mass flow rate for the results of each branch (e.g., $H_A = (h_A - h_{BLE,A})/(h_{BGE,A} - h_{BLE,A})$). The discharge quality at the upper branch for set nos. 3-6 to 3-10 is shown in Figure 4.44 and the normalized two-phase flow rate from the lower branch for set nos. 3-1 to 3-5 is shown in Figure 4.45. These results show that the influences of ΔP and R can be absorbed (within the tested range) by plotting x versus H and M versus H. However, the collapsed data in both figures deviate from the single-branch results.

It must be pointed out that for any value of L/d, the results for x and M at both branches should approach the single-branch results at sufficiently low values of ΔP and/or high values of R. As pointed out earlier in Section 4.3.1, the two branches will behave essentially as two independent single branches if the onset of liquid entrainment at the upper branch corresponds to a higher interface level than that for the BGE at the lower branch. However, for the results in Figures 4.44 and 4.45 ($L/d = 1.5$), this would require a very low ΔP of approximately 0.1 kPa at $P_o = 517\ kPa$ and $R = 1000\ (kg.m)^{-1/2}$. All the results in data set nos. 3-1 to 3-26 correspond to sufficiently high values of ΔP for which the interface level at the BLE at the upper branch is lower than the interface level at the BGE at the lower branch. Thus, these data sets correspond to the condition where there is mutual

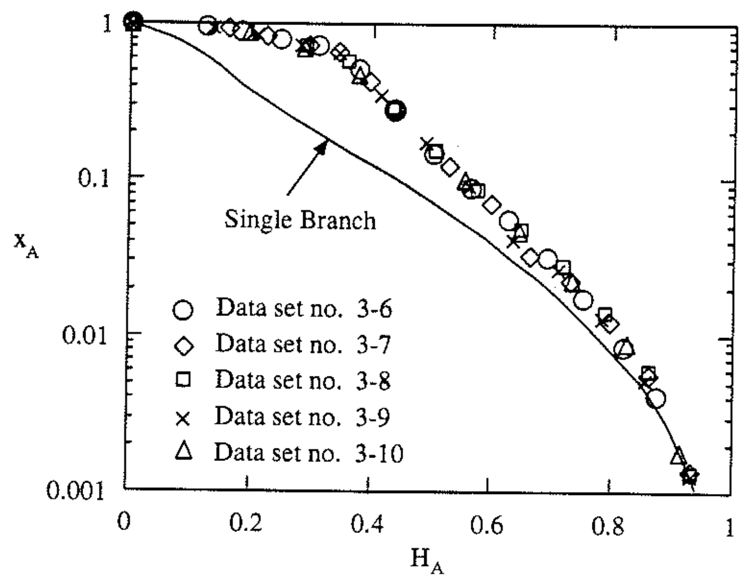

Figure 4.44: Values of x_A for data set nos. 3-6 to 3-10

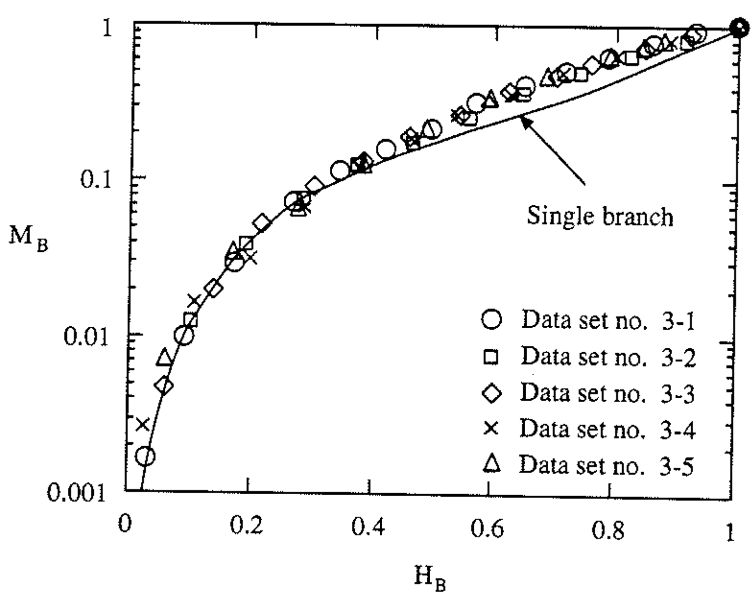

Figure 4.45: Values of M_B for data set nos. 3-1 to 3-5

interaction between the upper and lower branches. The trends in Figures 4.44 and 4.45 showing the collapse of data for various ΔP and R are typical of all data in set nos. 3-1 to 3-26.

An effect that could not be absorbed by these normalized plots is that of L/d. Figures 4.46 and 4.47 show normalized plots of discharge quality and mass flow rate, respectively, for data set no. 3-1 corresponding to $L/d = 1.5$. Very significant differences can be seen between the results for the upper branch and those for the lower branch. The upper-branch results converge to those of a single branch at high H and the lower-branch results converge to those of a single branch at low H. The difference between upper and lower branch results was found to decrease as L/d was increased while maintaining the same P_o, ΔP and R. Figures 4.48 and 4.49 show that the results for both branches in data set no. 3-30 ($L/d = 8$) collapse on top of the single-branch data. This behavior is typical of all data in set nos. 3-27 to 3-32. All these data correspond to the condition where the BLE at the upper branch occurs at a considerably higher interface level than that for the BGE at the lower branch and the two branches function as independent single branches.

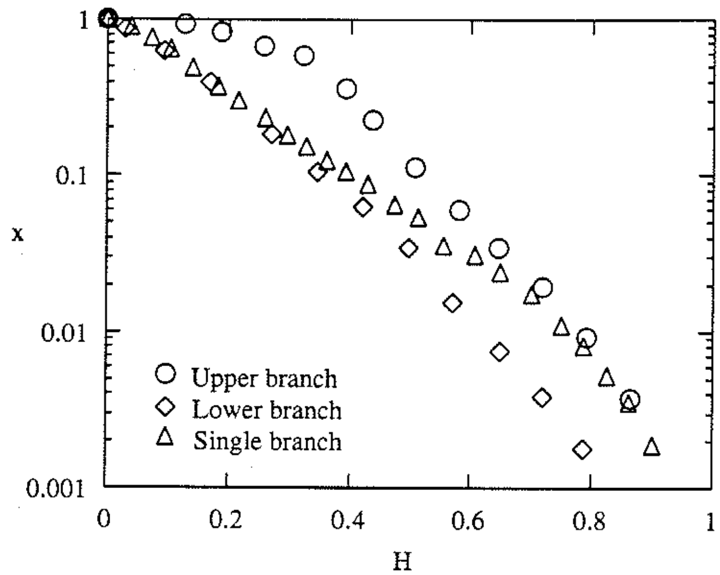

Figure 4.46: Discharge quality for data set no. 3-1

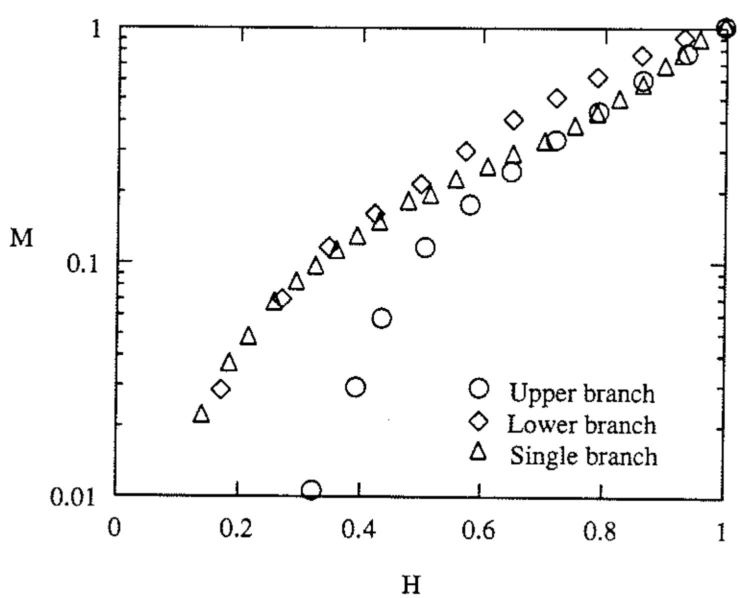

Figure 4.47: Normalized two-phase discharge for data set no. 3-1

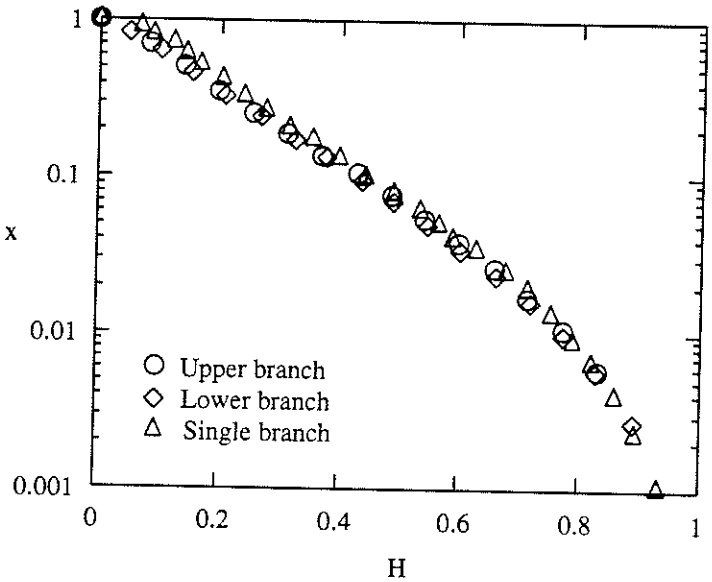

Figure 4.48: Discharge quality for data set no. 3-30

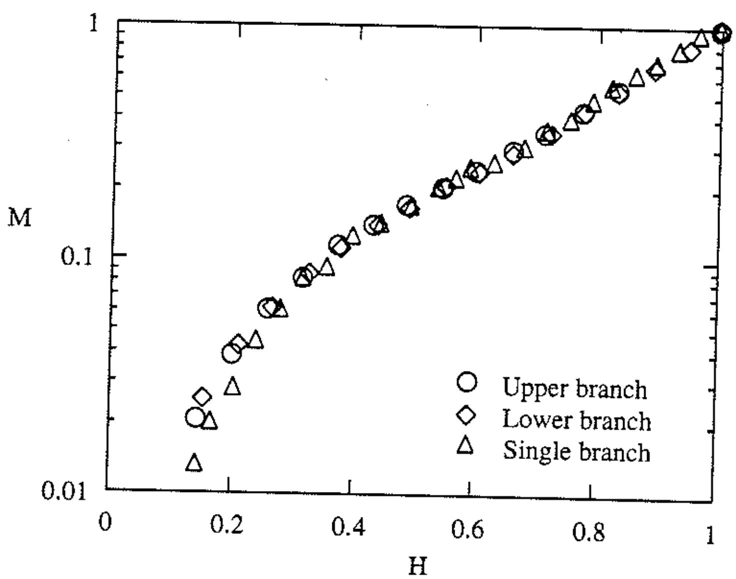

Figure 4.49: Normalized two-phase discharge for data set no. 3-30

4.3.4 Correlation of Present Data

An attempt was made to develop empirical relations for the prediction of x and M at both branches resulting in the following relations:

$$x_A = 0.2\ exp\left[6\ H_A\ \left(\frac{1 - B_1 H_A}{1 - H_A}\right)\right] + 0.8\left(1 - H_A^2\right)^{1.3}(B_2 E)^{H_A}, \tag{4.22}$$

$$x_B = 0.2\ exp\left[6\ H_B\left(\frac{1 - C_1 H_B}{1 - H_B}\right)\right] + 0.8\left(1 - H_B^2\right)^{1.3}(C_2 E)^{H_B}, \tag{4.23}$$

$$M_A = H_A^{[2+B_3(1-H_A^3)]}\ exp\left[-1.84\ H_A^2\ \left(1.0 - H_A^2\right)^{1.318}\right] \tag{4.24}$$

and

$$M_B = H_B^2\ exp\left[-1.84\ H_B^2\ \left(1.0 - H_B^2\right)^{C_3}\right], \tag{4.25}$$

where,

$$B_1 = 11.67 - 9.67\ exp\left[-0.01\left(\frac{L}{d}\right)^3\right], \tag{4.26}$$

$$B_2 = 1 + 0.92\ exp\left[-0.75\left(\frac{L}{d}\right)\right], \tag{4.27}$$

$$B_3 = 6.68\ exp\left[-0.027\left(\frac{L}{d}\right)^4\right], \tag{4.28}$$

$$C_1 = 11.67 - 3.03\ exp\left[-0.016\left(\frac{L}{d}\right)^3\right], \tag{4.29}$$

$$C_2 = 1 - 0.71\ exp\left[-0.03\left(\frac{L}{d}\right)^4\right], \tag{4.30}$$

$$C_3 = 1.318 + 5.78\ exp\left[-0.37\left(\frac{L}{d}\right)^2\right] \tag{4.31}$$

and

$$E = -0.0122 + 0.42\left(1 + \sqrt{\frac{\rho_L}{\rho_G}}\right)^{-1}. \tag{4.32}$$

At the limit $L/d = \infty$, the above relations converge to $B_1 = C_1 = 11.67$, $B_2 = C_2 = 1$, $B_3 = 0$ and $C_3 = 1.318$ and consequently, Equations (4.22) to (4.25) converge to the single-branch relations for x and M reported earlier in Section 4.1. Within the range $1.5 \leq L/d \leq 8$, the above empirical model is in good agreement with the present data, as exemplified in Figures 4.50 and 4.51. Quantitatively, the discharge quality at the upper branch is predicted with a root-mean-square error of 16.7 % over the range $0.001 \leq x_A \leq 1$, the discharge quality at the lower branch is predicted with a root-mean-square error of 18.1 % over the range $0.001 \leq x_B \leq 1$, the normalized two-phase discharge at the upper branch is predicted with a root-mean-square error of 23.3 % over the range $0.01 \leq M_A \leq 1$ and the normalized two-phase discharge at the lower branch is predicted with a root-mean-square error of 11.3 % over the range $0.01 \leq M_B \leq 1$. All errors were found to decrease considerably when the segment of data corresponding to the smallest values of x and M was not considered.

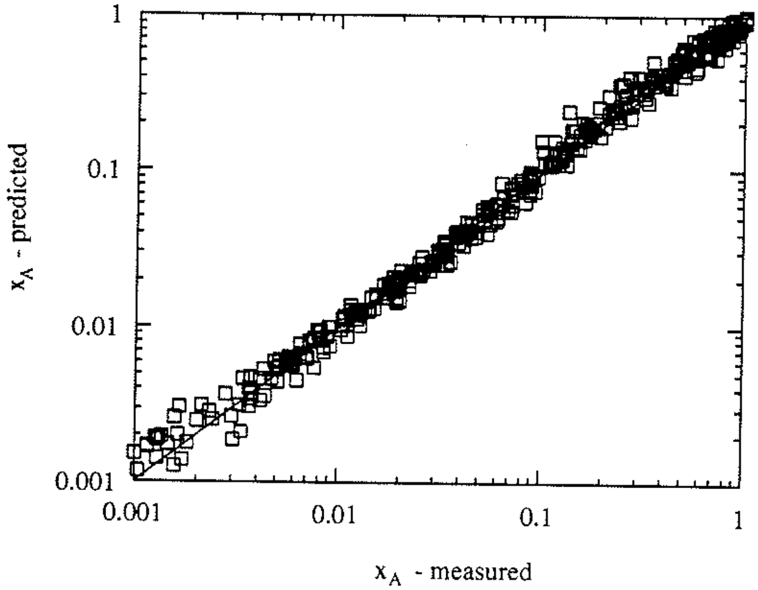

Figure 4.50: Predicted versus measured values of x_A

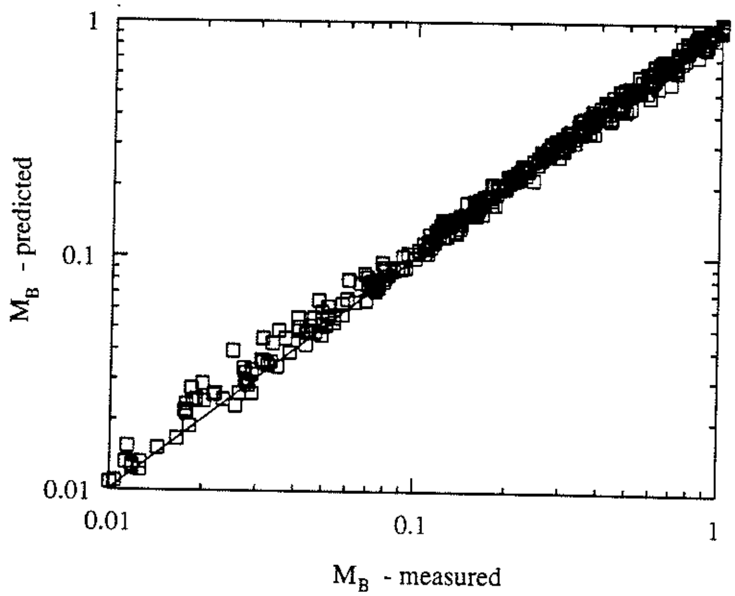

Figure 4.51: Predicted versus measured values of M_B

4.4 Single, Dual and Triple Discharge from Branches on a Semicircular Side Wall

The motivation for this part of the experimental investigation was discussed earlier in Chapter 3 and the results presented here apply to the specific geometry shown in Figure 3.2. The test matrix performed in this part (data group no. 4) consists of 22 data sets, as given in Table 4.7.

Data set nos. 4-1 to 4-3 correspond to a single discharge from a side branch. Comparisons between these three sets and the corresponding data from group no. 1 can demonstrate the effect of wall curvature. For dual discharge, the effect of wall curvature can be explored through comparisons between set nos. 4-10 to 4-12 and the corresponding data from group no. 3. Data set nos. 4-7 to 4-9 for a single discharge from the bottom branch correspond to a previously tested geometry (e.g., Smoglie and Reimann, 1986; Schrock et al., 1986; Yonomoto and Tasaka, 1991) with the difference being no superimposed main flow in the present study. However, all the present data of dual and triple discharge, as well as single discharge from branch B, correspond to new (and previously untested) branch geometries.

No attempt was made at correlating the data in this section. Wider ranges of geometries and operating conditions need to be covered before reliable correlations can be developed. However, the present data are very valuable as they can serve the following purposes: (a) investigating the effect of wall curvature, (b) demonstrating

Table 4.4: Nominal operating conditions for group no. 4

Set. No.	Activated line(s)	P_o (kPa)	ΔP (kPa)	R $(kg.m)^{-1/2}$
4-1	A only	316	123	1000
4-2			40	
4-3		517	235	
4-4	B only	316	123	
4-5			40	
4-6		517	235	
4-7	C only	316	123	
4-8			40	
4-9		517	235	
4-10	A and B	316	123	
4-11			40	
4-12		517	235	
4-13	A and C	316	123	
4-14			40	
4-15		517	235	
4-16	C and B	316	123	
4-17			40	
4-18		517	235	
4-19	A, B and C	316	123	
4-20			82	
4-21			40	
4-22		517	123	

the effects of additional discharge(s) on the flow from a particular branch, and (c) providing a data base for validation of existing thermal- hydraulics codes. A complete tabulation of all data in this section can be found in Appendix E.

4.4.1 Flow Phenomena

In the present section, the flow phenomena will be described for the triple discharge case. The interface shape will be sketched approximately to scale for data set no. 4-19 as a function of h^* (h^* in this case is measured upward from the bottom of the semicircular test section, as shown in Figure 4.52(b). The other three data sets of triple discharge (set nos. 4-20 to 4-22) have similar sketches for the interface shape and similar order in which the onsets were encountered as in set no. 4-19. The sketches marked "side elevation" in Figure 4.52 depict the interface outline an observer would see from the side of the test section and perpendicular to the centerlines of the branches (except for the flat interface surface far away from the plane of the centerline toward or away from the observer).

$h^* \geq h^*_{BGE,A}$ (see region 1 in Figure 4.53)

Let us begin with an interface level well above branch A. The three branches will be flowing liquid only , the flow rates will be essentially the same, i.e. $\dot{m}_{L,A} = \dot{m}_{L,B} = \dot{m}_{L,C}$ as shown in Figure 4.53, and the interface will be flat as shown in Figure 4.52(a). As h^* is lowered and approaches $h^*_{BGE,A}$ a "dimple" begins to form in the interface (Figure 4.52(b)). This depression becomes more pronounced and cone-like

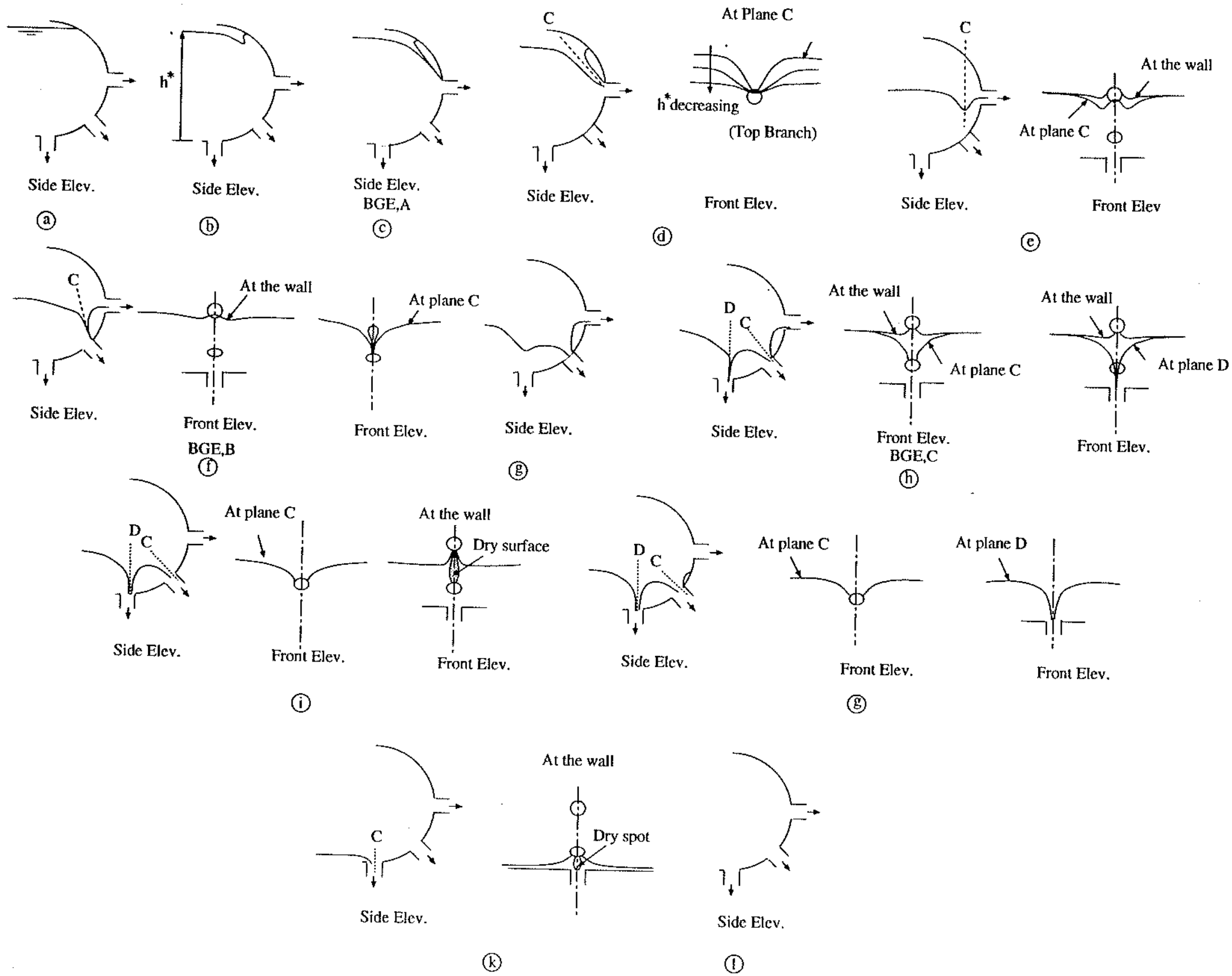

Figure 4.52: Sketches of interface shapes during triple discharge

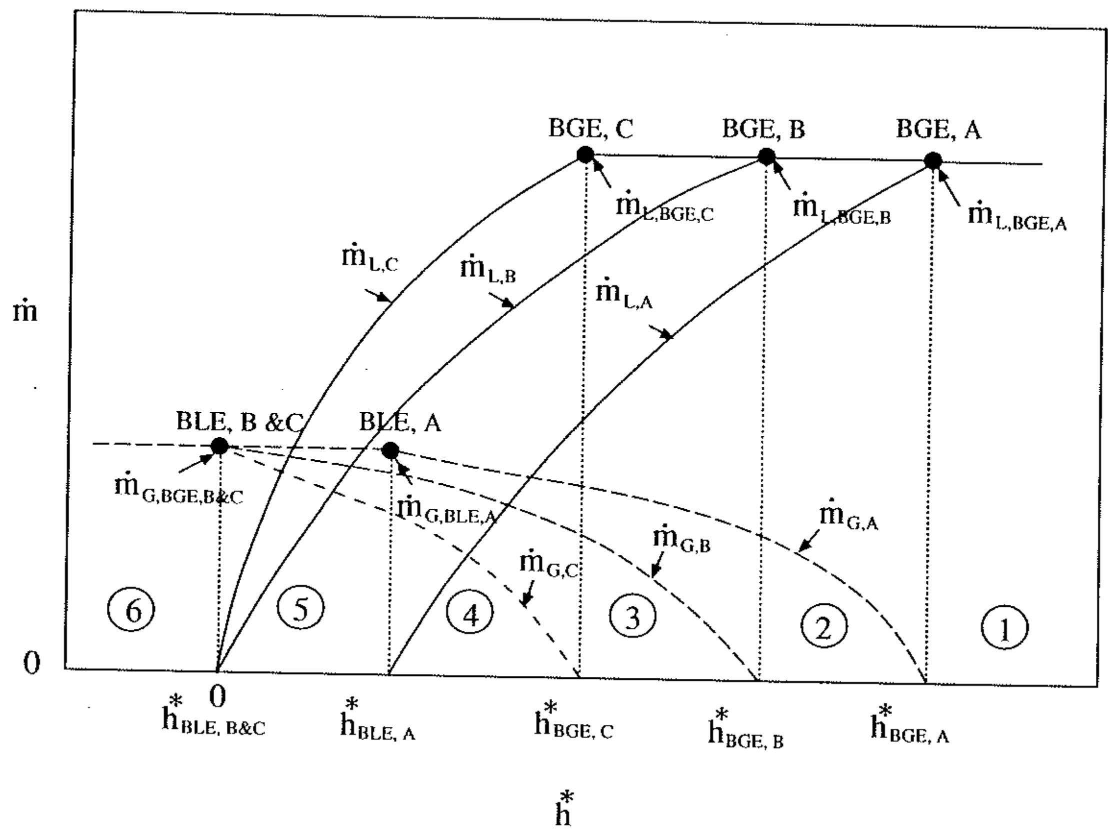

Figure 4.53: Qualitative mass flow rates during triple discharge

until the tip of the cone suddenly extends to branch A; this is the BGE at branch A (Figure 4.52(c)); the corresponding h^* is $h^*_{BGE,A}$ and the flow rates are $\dot{m}_{L,A} = \dot{m}_{L,B} = \dot{m}_{L,C} = \dot{m}_{L,BGE,A}$.

$h^*_{BGE,A} > h^* \geq h^*_{BGE,B}$ (see region 2 in Figure 4.53)

In this range the two branches B and C continue to flow liquid at the rate $\dot{m}_{L,B} = \dot{m}_{L,C} = \dot{m}_{L,BGE,A}$. At branch A, $\dot{m}_{L,A}$ decreases (from a value $\dot{m}_{L,BGE,A}$) and $\dot{m}_{G,A}$ increases as h^* decreases. The interface shape is shown in Figure 4.52(d). As h^* is lowered and approaches $h^*_{BGE,B}$ two cones begin to form above branch B (Figure 4.52(e)) and become more pronounced until their tips suddenly extend to branch B (Figure 4.52(f)); this is the BGE at branch B.

$h^*_{BGE,B} > h^* \geq h^*_{BGE,C}$ (see region 3 in Figure 4.53)

In this range branch C continues to flow only liquid at the rate $\dot{m}_{L,C} = \dot{m}_{L,BGE,A}$ $= \dot{m}_{L,BGE,B}$ while branches A and C are flowing a two-phase mixture. As h^* is lowered, the liquid flow rate $\dot{m}_{L,A}$ and gas flow rate $\dot{m}_{G,A}$ at branch A continue to decrease and increase, respectively. Similarly for branch B, $\dot{m}_{L,B}$ decreases while $\dot{m}_{G,B}$ increases. A "trough" of gas feeds gas to branch B, around which at the wall, the water flows up at each side to branch A. As h^* is lowered further and approaches $h^*_{BGE,C}$, a cone begins to form above branch C from the bottom of the trough, as shown in Figure 4.52(g). This cone becomes more pronounced as h^* decreases until its tip suddenly extends to branch C. This is the BGE at branch C (Figure 4.52(h)).

$h^*_{BGE,C} > h^* \geq h^*_{BLE,A}$ (see region 4 in Figure 4.53)

In this range, the three branches are flowing a two-phase mixture. A trough feeds gas to branch B while a cone from the bottom of the trough feeds gas to C. At the wall a dry spot begins to form between branches A and B with liquid being fed to the branch A in two streams from the sides ; the two streams become thinner as h^* decreases until the flow of liquid into branch A ceases ($\dot{m}_{L,A} = 0$). This is the $h^*_{BLE,A}$ (Figure 4.52(i)); at this point $\dot{m}_{G,A} = \dot{m}_{G,BLE,A}$, the maximum $\dot{m}_{G,A}$.

$h^*_{BLE,A} > h^* \geq h^*_{BLE,C}$ (see region 5 in Figure 4.53)

Here, branch A is flowing gas only at $\dot{m}_G = \dot{m}_{G,BLE,A}$ while branches B and C are flowing a two-phase mixture . A trough feeds gas to branch B while a cone from the bottom of the trough feeds gas to branch C (Figure 4.52(g)). As h^* is decreased, a dry spot form between B and C at the wall. Liquid is fed to branch B through two streams (Figure 4.52(k)) and these become thinner until the flow of liquid into branches B ceases ($\dot{m}_{L,B} = 0$); this is the BLE at branch B. Within the present conditions, the BLE at branch B and the BLE at branch C occurred at the same liquid level ($h^*_{BLE,C} = h^*_{BLE,B}$, $\dot{m}_{L,C} = 0$). This occurs at $h^* = 0$.

$h^* < h^*_{BLE,C}$ (see region 6 in Figure 4.53)

Here, the three branches are flowing gas only and the various flow rates are $\dot{m}_{L,A} = \dot{m}_{L,B} = \dot{m}_{L,C} = 0$ and $\dot{m}_{G,A} = \dot{m}_{G,B} = \dot{m}_{G,C} = \dot{m}_{G,BLE,A} = \dot{m}_{G,BLE,B} = \dot{m}_{G,BLE,C}$.

It should be pointed out that the order in which the onsets in triple discharge are encountered as the interface is lowered depends on the values of ΔP and R. At small values of ΔP and/or large values of R, branch A could act independently of the other two branches B and C (i.e., $h^*_{BGE,B} < h^*_{BLE,A}$), or the three branches could act independently of each other (i.e., $h^*_{BGE,B} < h^*_{BLE,A}$ and $h^*_{BGE,C} < h^*_{BLE,B}$). However, such conditions were never observed at the present values of P_o, ΔP and R.

4.4.2 Single Discharge

The effect of wall curvature on two-phase discharge from a single side branch is explored in Figure 4.54 by comparing data set no. 4-3 (semicircular wall) with data set no. 1-4 (flat wall). Both sets correspond to the highest P_o and ΔP, and the lowest R, a combination that gives the highest gas and liquid flow rates. The deviation between the two sets is fairly small, as shown in Figure 4.54. Comparisons between set nos. 4-1 and 4-2, and the corresponding data from group no. 1 produced even smaller deviations due to curvature. There is no need to compare set nos. 4-1 to 4-3 against existing correlations from the literature, since comparisons were made in Section 4.1.2 against the data of single side discharge from a flat wall, and the wall curvature is shown to have little effect for branch A.

A comparison between the present data of a single discharge from branch C and existing correlations is shown in Figure 4.55 (for the BGE) and Figure 4.56 (for

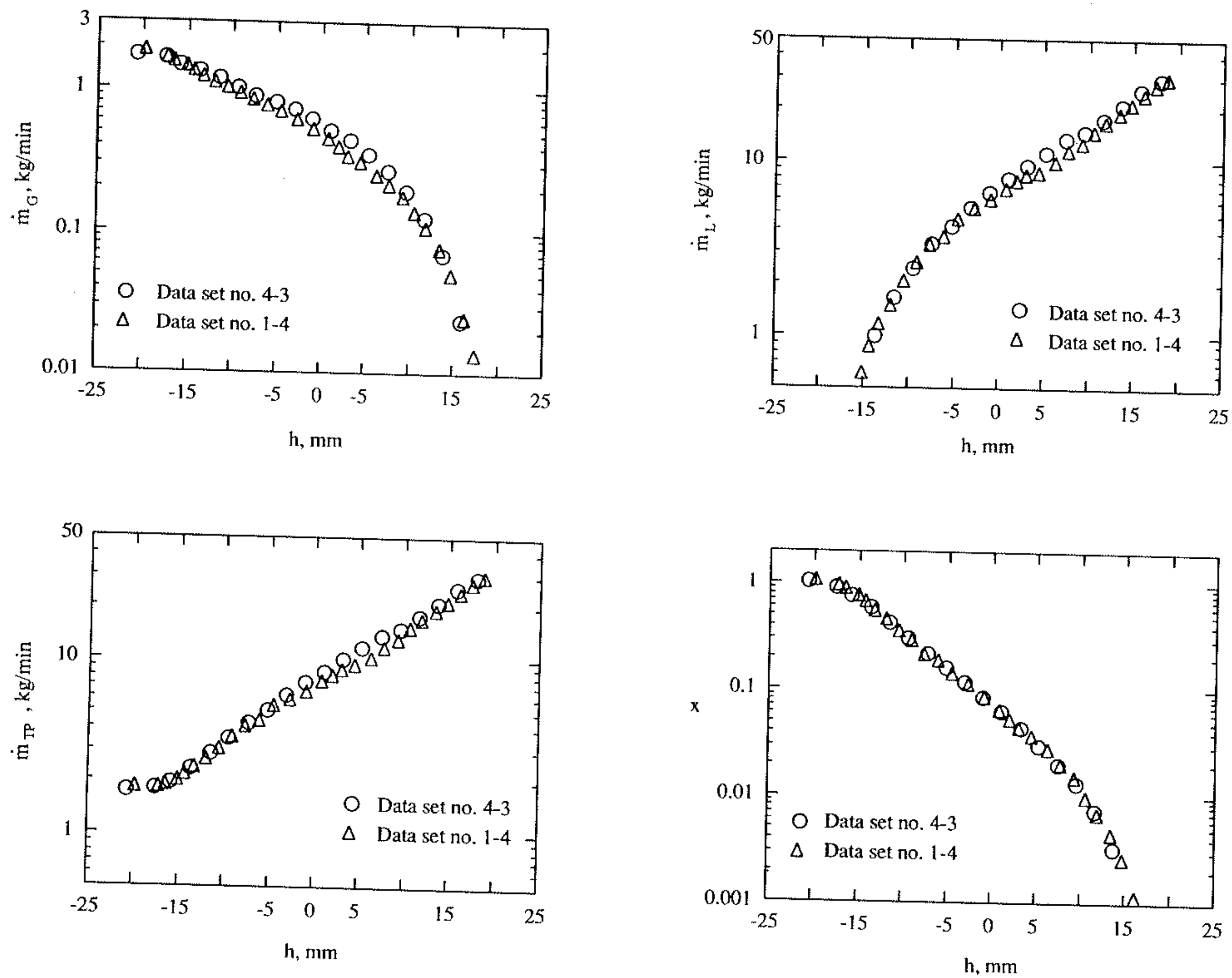

Figure 4.54: Effect of wall curvature on single discharge from a side branch

the discharge quality). These results show that significant deviation can be found among the existing correlations. The present data of discharge quality agree best with the correlation of Smoglie and Reimann (1986). In the present experiments, it was not possible to confirm whether the flow mode at BGE was vortex or vortex free. However, it is easy to state that the superimposed velocity in the tank was insignificant. Figure 4.55 shows that the present data of h_{BGE} are in best agreement with Smoglie and Reimann (1986) for vortex-free flow with no superimposed velocity.

A comparison between the data of a single discharge from branches A, B and C is shown in Figure 4.57. For the same value of h (location of the interface relative to the branch centerline), the data suggest significant deviations among the flow rates and qualities measured at the three branches. The value of h_{BGE} increases as we go around the branches from A to B to C. As well, $\dot{m}_G$ at the same h increases from A to B to C. The opposite is true for the critical height for liquid entrainment and $\dot{m}_L$. For branch C, the BLE has no physical meaning ($h_{BLE} = 0$) and for branch B, the onset of liquid entrainment coincided with "dry-out" conditions at the bottom of the semicircular cross-section. The term "dry-out" refers to the condition when the flat part of the water surface is that the same level as the bottom of the semicircular test section.

The results in Figure 4.57 indicate that it is easier for the gas to reach branches B and C than it is to reach branch A. This trend has some bearing on the following results where discharge from more than one branch is activated simultaneously.

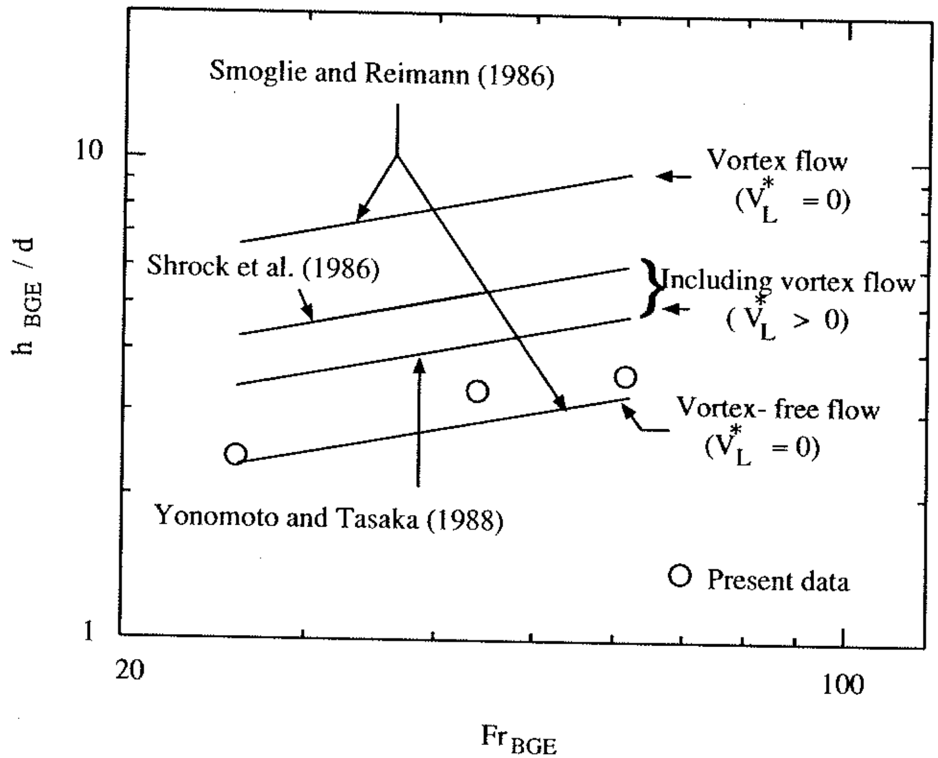

Figure 4.55: Comparison between the data of BGE at branch C and existing correlations

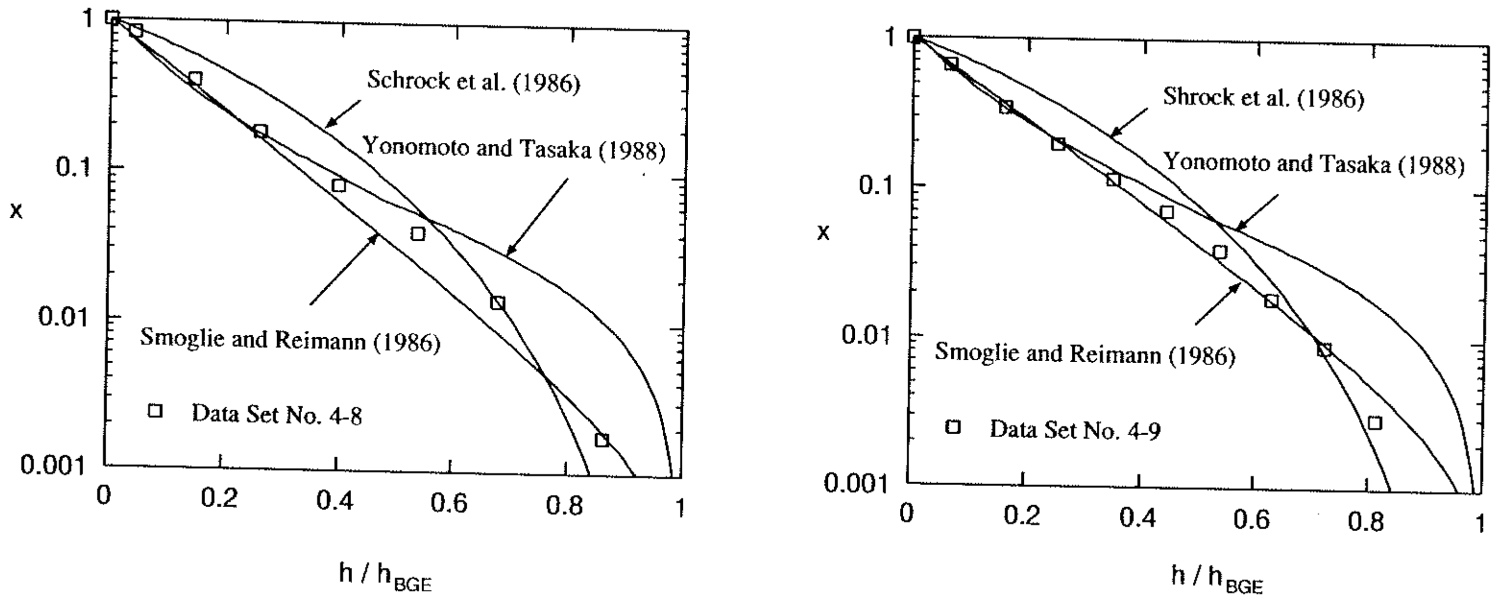

Figure 4.56: Comparison between the data of quality during single discharge from branch C and existing correlations

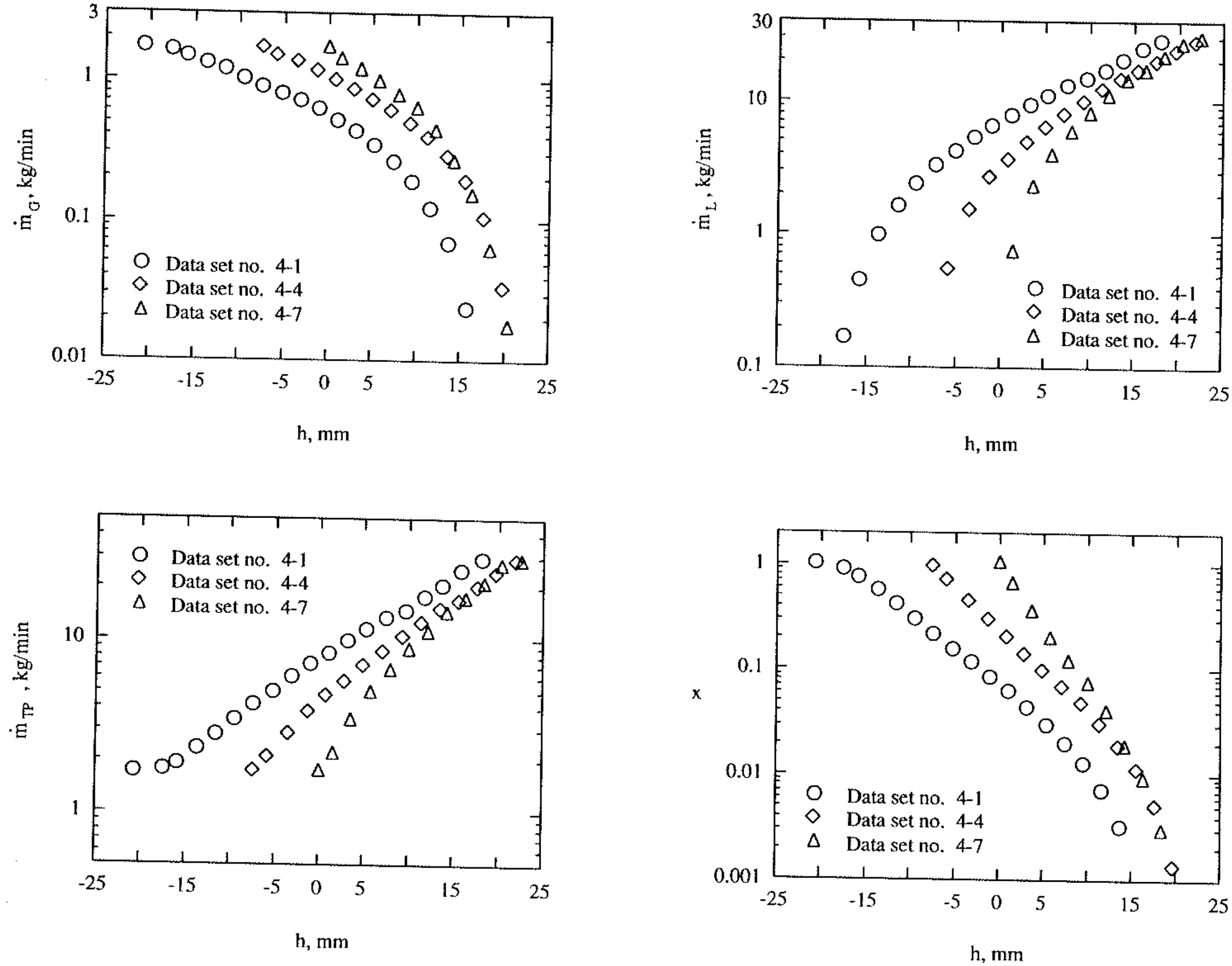

Figure 4.57: Single discharge from branches A, B and C

4.4.3 Dual and Triple Discharge

Figure 4.58 shows a comparison between data of dual discharge from branches A and B (semicircular wall) and data of dual discharge from group no. 3 (flat vertical wall). The vertical separating distance between branches A and B is 2.78 d; therefore, the comparisons are made using data of $L/d = 2$ and 3 from group no. 3; the main objective of this comparison is to explore the effect of wall curvature.

The effect of pipe curvature at the upper branch appears to be small. Figure 4.58 shows that values of $\dot{m}_{TP}$ and x at the upper branch in data set no. 4-12 are bounded by data set no. 3-16 ($L/d = 2$) and data set no. 3-24 ($L/d = 3$). However, at the lower branch, more significant effects of wall curvature can be seen. The BGE in set no. 4-12 occurs at higher interface levels than in set nos. 3-16 and 3-24. Following the onset of gas entrainment, the lower branch in the semicircular section continues to receive higher quality and lower $\dot{m}_{TP}$ than the lower branch in the flat-wall case all the way until the BLE.

The critical height for the BLE at the lower branch is significantly different between set no. 4-12 and set no. 3-16 (or 3-24). However, it must be pointed out that the onset of liquid entrainment for branch B in set no. 4-12 coincided with dry-out conditions at the bottom of the pipe. Therefore, it is fair to conclude that the results at or near this limit may be affected by the pipe-to-branch diameter ratio.

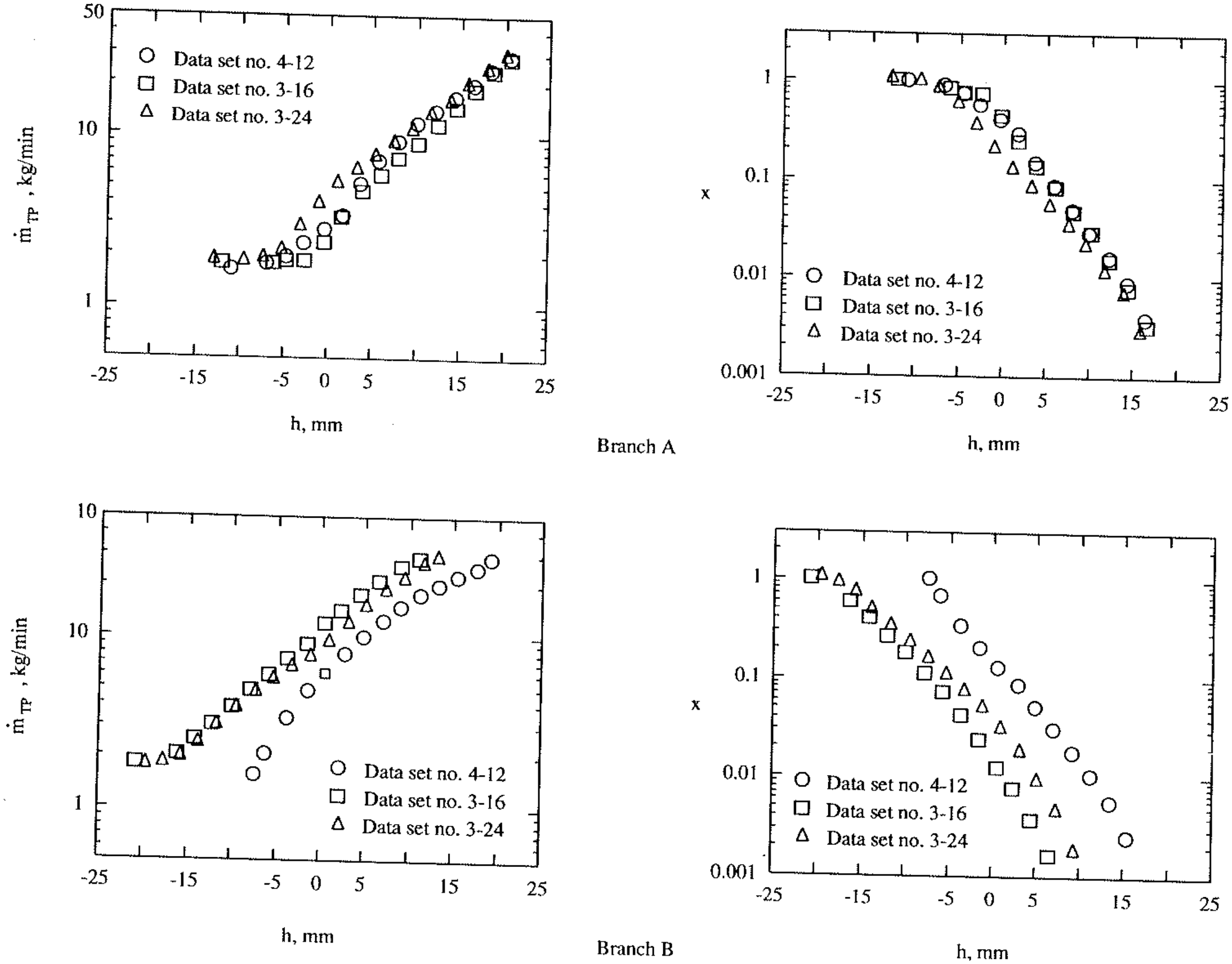

Figure 4.58: Effect of wall curvature on dual discharge from side branches

Figures 4.59 to 4.61 were prepared in order to cast some light on the possible influences on the different flow parameters as we go from a single to a dual to a triple flow discharge. For example, Figure 4.59 compares single discharge from branch A with discharge from A while branch B is active, discharge from A while C is active, and discharge from A while B and C are active. It is clear from this figure that flow from B has a strong effect on the flow from A, while the flow from C has a small effect on the flow from A. The results indicate also that, when branch B is already activated, whether or not branch C is active does not have significant effects on the flow from branch A. Activating branch B resulted in more gas and less liquid at branch A. This trend is similar to that in group no. 3.

Another interesting examination of trends is shown in Figure 4.60. In this figure, a comparison in made between single discharge from branch B and discharge from B while A is active, discharge from B while C is active and discharge from B while A and C are active. The four data sets produce significantly different results. Activating A pulls the gas away from B while activating C brings more gas into B. The opposite is true for the liquid. Again, these trends are similar to those observed in group no. 3 for the flat vertical wall. The deviations seen in Figure 4.60 among single, dual and triple discharge are a clear demonstration of the need for the present data.

Finally, Figure 4.61 illustrates the effects of additional discharges on the flow from branch C. It is clear that the addition of discharges from A, or B, or A and

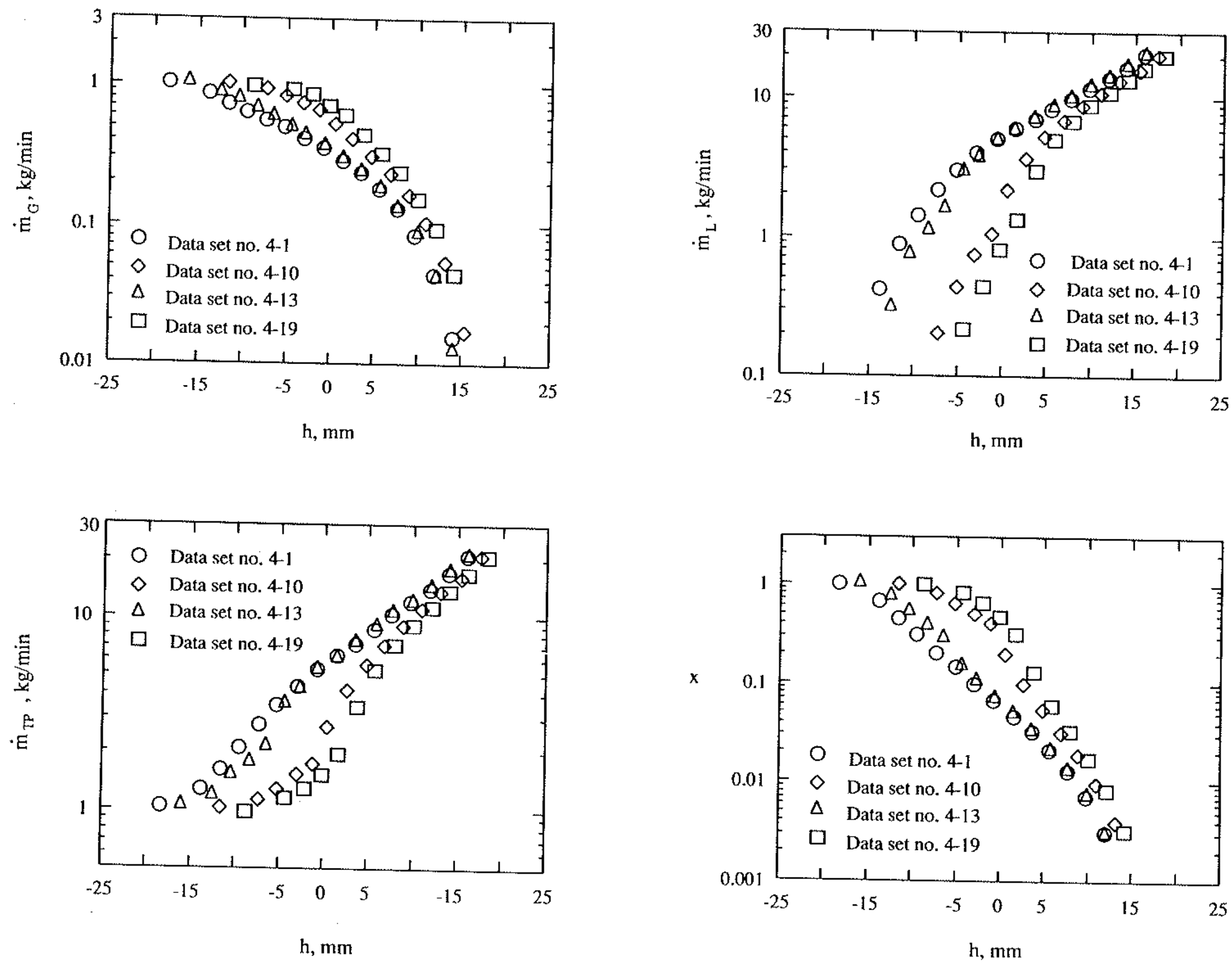

Figure 4.59: Effects of additional discharges on the flow from branch A

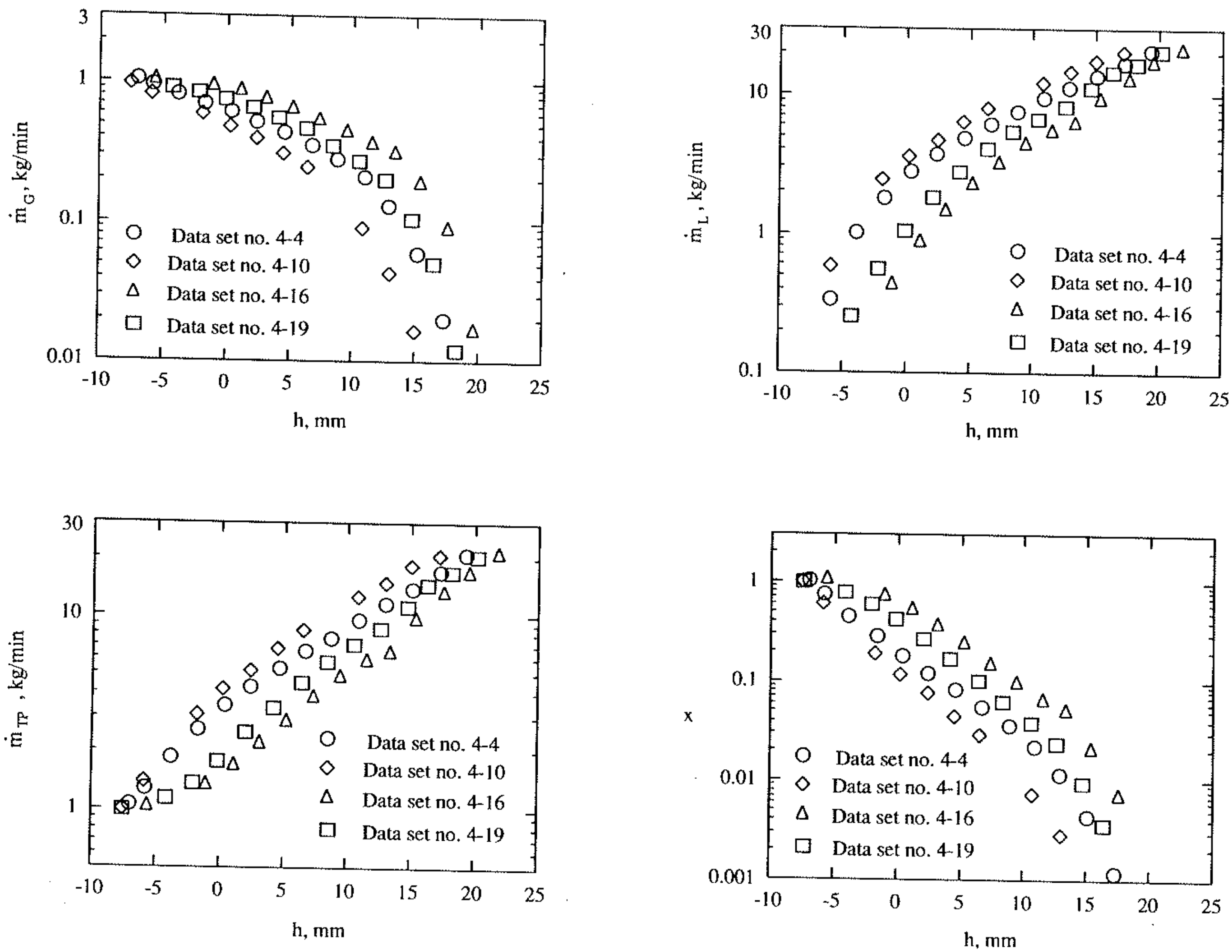

Figure 4.60: Effects of additional discharges on the flow from branch B

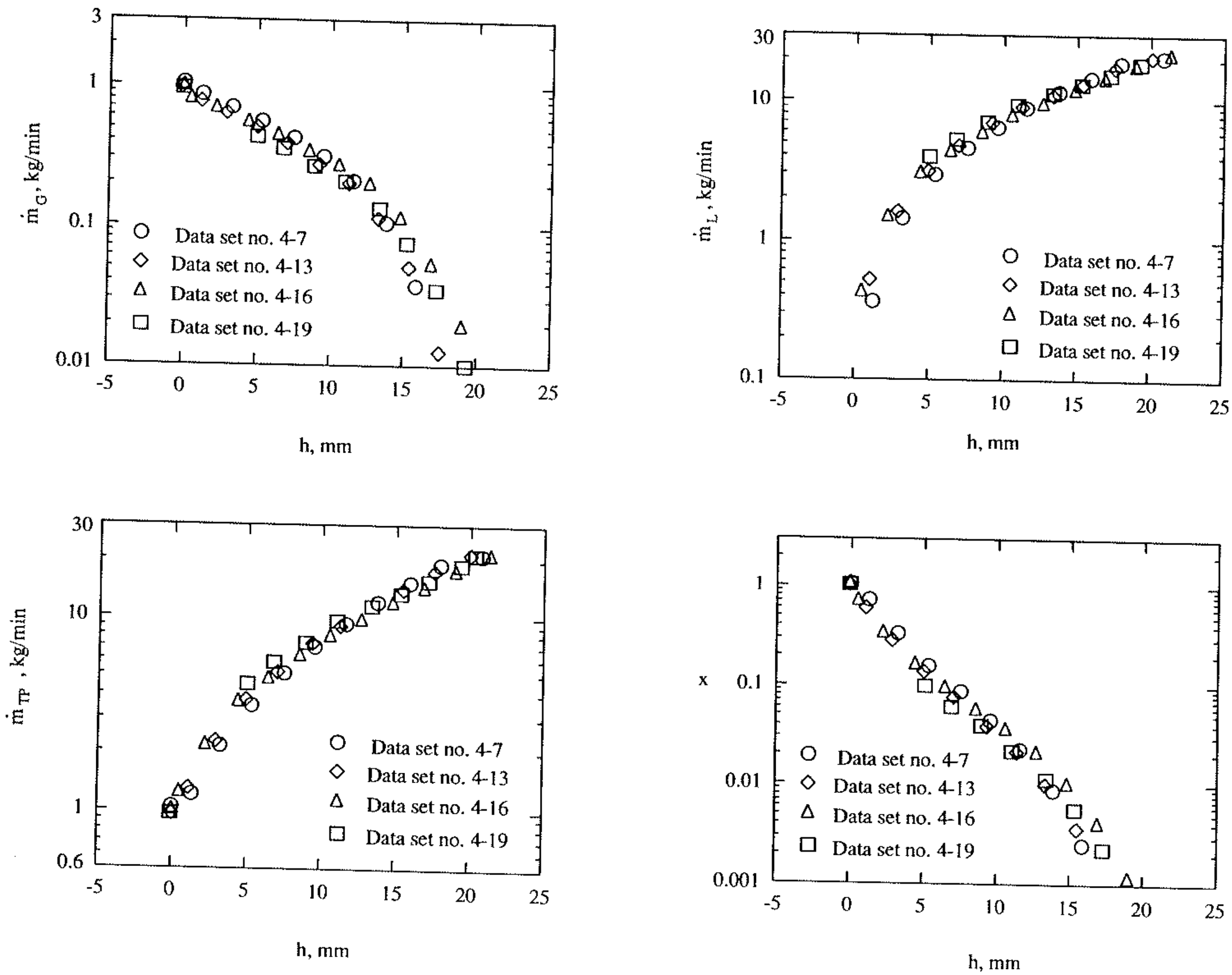

Figure 4.61: Effects of additional discharges on the flow from branch C

B does not change the flow parameters at C by appreciable amounts.

CHAPTER 5

THEORETICAL ANALYSIS OF THE ONSET OF LIQUID ENTRAINMENT DURING DISCHARGE FROM TWO BRANCHES ON AN INCLINED, FLAT SIDE WALL

5.1 Introductory Remarks

Two important phenomena were identified in Chapter 4 that can have a strong influence on the discharging flow through branches; these are the BGE and BLE phenomena. For the case of single discharge, a few theoretical formulae were reported recently to predict these two phenomena as well as the discharging flow rate and quality (see literature review).

In situations where multiple discharge takes place simultaneously from several branches, there is only one model in the literature developed by Armstrong et al. (1992). The model predicts the BLE during dual discharge from two small branches located on a vertical wall of a large reservoir. In their simplified theoretical analysis, Armstrong et al. neglected the effects of viscosity and surface tension, assumed potential flow throughout the field and treated each branch as a point sink. With these simplifications, the following relations were obtained:

$$\left[\frac{Fr_1^*}{(s/L)^2} + \frac{Fr_2^*}{(s/L+1)^2}\right]\left[\frac{Fr_1^*}{(s/L)^3} + \frac{Fr_2^*}{(s/L+1)^3}\right] = 32 \quad (5.1)$$

and

$$h_{BLE}/L = s/L + \frac{1}{4}\left[\frac{Fr_1^*/(s/L)^2 + Fr_2^*/(s/L+1)^2}{Fr_1^*/(s/L)^3 + Fr_2^*/(s/L+1)^3}\right], \quad (5.2)$$

where h_{BLE} is the critical height at the BLE at the lower branch (treated as a positive quantity throughout this chapter), s is the corresponding distance between the tip of the deflected interface and the branch centerline (as shown in Figure 5.1) and Fr^* is given by

$$Fr^* = \frac{4\dot{m}}{\pi\sqrt{g\rho\Delta\rho L^5}}. \quad (5.3)$$

During dual discharge, for any values of Fr_1^* and Fr_2^*, the corresponding h_{BLE}/L and s/L values can be obtained from Equations (5.1) and (5.2). At the limit $Fr_1^* = 0$ and $Fr_2^* = 0$, Equations (5.1) and (5.2) predict $h = s = 0$. Evidently, these are not the appropriate limits since the physics of the problem suggest $h_{BLE} = s = d/2$ at $Fr_1^* = Fr_2^* = 0$. Therefore, the accuracy of Equations (5.1) and (5.2) is doubtful at low values of Fr_1^* and Fr_2^*. Also, Equations (5.1) and (5.2) predict h_{BLE} when the side wall is a vertical plane (i.e., $\theta = 0$). For applications corresponding to $0 < \theta < 90°$, no analysis has been proposed yet.

The points of concern raised above provided the motivation to continue the analysis of BLE phenomenon. The main objectives are to determine the boundary

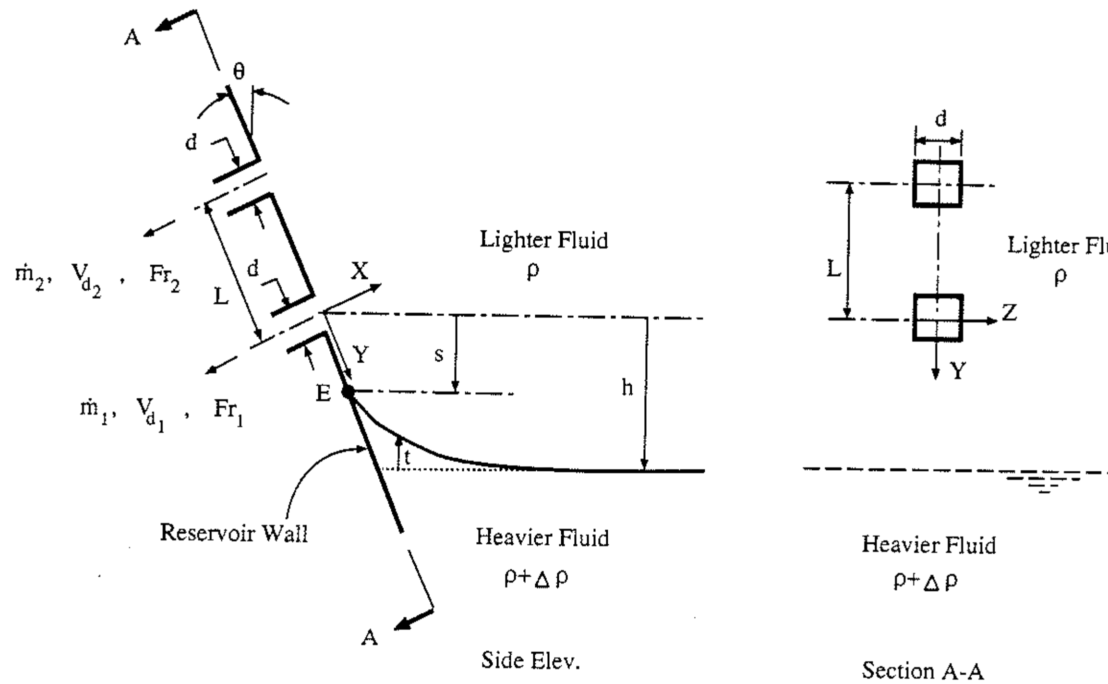

Figure 5.1: Geometry and coordinate system

beyond which Equations (5.1) and (5.2) can provide good accuracy and to determine the effect of reservoir wall inclination on the BLE at the lower branch. In doing so, a more complete three dimensional model has been developed following the Armstrong et al. (1992) approach while eliminating the point-sink assumption and adding the effect of reservoir wall inclination. The present analysis applies to any two immiscible fluids with the term "BLE" referring to the appearance of the heavier fluid in the predominantly lighter fluid through the lower branch.

5.2 Analysis

The configuration under consideration in the present analysis is shown in Figure 5.1. Stratified layers of immiscible fluids with densities ρ and $\rho + \Delta\rho$ are contained in a large reservoir with two side branches of square cross section (dxd) separated by a distance L center-to-center. The dominant forces are the inertia and gravity forces, while the effects of viscosity and surface tension are assumed to be negligible. The flow in the lighter fluid is assumed to be steady incompressible potential flow, and equilibrium of the interface is controlled by a balance between inertia and gravity forces. In the present analysis, as in the Armstrong et al.(1992) approach, equilibrium of the interface and the velocity field in the lighter fluid are initially determined. Equality of the velocity and its gradient at linking point E, shown in Figure 5.1 are later imposed as conditions for the BLE at the lower branch.

5.2.1 Equilibrium of the Interface

Equilibrium of the interface is controlled by a balance between inertia and gravity forces. Therefore, by applying the Bernoulli equation on a streamline coincident with the interface from both sides of the lighter and heavier fluids, we get

$$\frac{V^2}{2} = \frac{\Delta\rho}{\rho} g\, t, \tag{5.4}$$

where V is the local velocity along the interface and t is the local deflection measured from the flat interface. Point E, shown in Figure 5.1, is the linking point between the interface and the reservoir wall. This point corresponds to $t = h - s$, therefore

$$\frac{V_E^2}{2} = \frac{\Delta\rho}{\rho} g(h - s). \tag{5.5}$$

5.2.2 Velocity Field in the Lighter Fluid

In developing the velocity field in the lighter fluid, the presence of the stationary heavier fluid is ignored. The flow field in the medium extends over $0 \leq X \leq \infty$, $-\infty \leq Y \leq \infty$ and $\infty \leq Z \leq \infty$, as shown in Figure 5.1. Flow within the medium is caused by discharges with uniform velocities, V_{d_1} from the lower branch (situated at $X = 0$, $Y = \pm d/2$ and $Z = \pm d/2$) and V_{d_2} from the upper branch (situated at $X = 0$, $Y = -L \pm d/2$ and $Z = \pm d/2$). Consequently there is a three-dimensional problem with V_x, V_y and V_z representing the velocity components in the X-, Y- and Z-direction, respectively. Based on the assumptions stated earlier, the flow field within the medium can be derived from the potential flow theory.

Applying the continuity equation, we get

$$\frac{\partial V_x}{\partial X} + \frac{\partial V_y}{\partial Y} + \frac{\partial V_z}{\partial Z} = 0. \qquad (5.6)$$

Introducing a scalar potential function ϕ, such that

$$V_x = \frac{\partial \phi}{\partial X}, \quad V_y = \frac{\partial \phi}{\partial Y} \quad \text{and} \quad V_z = \frac{\partial \phi}{\partial Z}, \qquad (5.7)$$

we get the well known Laplace equation

$$\frac{\partial^2 \phi}{\partial X^2} + \frac{\partial^2 \phi}{\partial Y^2} + \frac{\partial^2 \phi}{\partial Z^2} = 0. \qquad (5.8)$$

Equation (5.8) is subject to the following list of boundary conditions:

$$\text{at X} = 0 \qquad \begin{aligned} \frac{\partial \phi}{\partial X} &= -V_{d1} & \frac{-d}{2} \le Y \le \frac{d}{2} \qquad & \frac{-d}{2} \le Z \le \frac{d}{2} \\ &= -V_{d2} & -L - \frac{d}{2} \le Y \le -L + \frac{d}{2} \qquad & \frac{-d}{2} \le Z \le \frac{d}{2} \\ &= 0 & \text{other values of Y and Z} \qquad & \end{aligned} \qquad (5.9)$$

$$\text{at Z} = 0 \qquad \frac{\partial \phi}{\partial Z} = 0 \qquad (5.10)$$

$$\text{at X} \longrightarrow \infty \quad or \quad Y \longrightarrow \infty \quad or \quad Z \longrightarrow \infty, \qquad \phi \text{ is finite.} \qquad (5.11)$$

Based on the method of separation of variables, a solution for Equation (5.8) satisfying boundary conditions (5.10) and (5.11) can be written as

$$\phi = \frac{1}{\pi} \int_0^\infty \int_0^\infty \left[A(\alpha, \beta) \cos(\alpha Y) + B(\alpha, \beta) \sin(\alpha Y)\right] \bullet$$

$$\cos(\beta Z) \exp\left(-\sqrt{\alpha^2 + \beta^2}\, X\right) \, d\alpha \, d\beta, \qquad (5.12)$$

where $A(\alpha,\beta)$ and $B(\alpha,\beta)$ are arbitrary functions . In order to determine $A(\alpha,\beta)$ and $B(\alpha,\beta)$, we substitute the remaining boundary conditions from Equation (5.9) into Equation (5.12) as follows:

The derivative of ϕ with respect to X at $X = 0$ can be written as

$$\begin{aligned} -\frac{\partial\phi}{\partial X} &= \frac{1}{\pi}\int_0^\infty\int_0^\infty \sqrt{\alpha^2+\beta^2}[A(\alpha,\beta)\cos(\alpha Y) \\ &+ B(\alpha,\beta)\sin(\alpha Y)]\cos(\beta Z)\,d\alpha\,d\beta. \end{aligned} \tag{5.13}$$

Adopting the definition

$$\int_0^\infty \sqrt{\alpha^2+\beta^2}[A(\alpha,\beta)\cos(\alpha Y)+B(\alpha,\beta)\sin(\alpha Y)]\,d\alpha = f(Y,\alpha,\beta) \tag{5.14}$$

and substituting from Equation (5.14) into Equation (5.13) using the Fourier cosine transformation, we get

$$f(Y,\alpha,\beta) = \int_{-\infty}^\infty -\frac{\partial\phi}{\partial X}\cos(\beta Z)\,dZ. \tag{5.15}$$

In order to determine $f(Y,\alpha,\beta)$, we substitute Equation (5.9) into Equation (5.15) and do the necessary integration. Thus

$$\begin{aligned} f(Y,\alpha,\beta) &= \frac{2V_{d1}}{\beta}\sin(\beta\frac{d}{2}) && \frac{-d}{2}\le Y\le\frac{d}{2} \\ &= \frac{2V_{d2}}{\beta}\sin(\beta\frac{d}{2}) && -L-\frac{d}{2}\le Y\le -L+\frac{d}{2} \\ &= 0 && \text{other values of Y.} \end{aligned} \tag{5.16}$$

Now, $A(\alpha,\beta)$ and $B(\alpha,\beta)$ can be determined by applying Fourier sine and cosine transforms to Equation (5.14) as follows:

$$A(\alpha,\beta)\sqrt{\alpha^2+\beta^2} = \frac{1}{\pi}\int_{-\infty}^\infty f(Y,\alpha,\beta)\cos(\alpha Y)\,dY$$

and $$B(\alpha,\beta)\sqrt{\alpha^2+\beta^2} = \frac{1}{\pi}\int_{-\infty}^{\infty} f(Y,\alpha,\beta)\sin(\alpha Y)\, dY. \qquad (5.17)$$

Substituting Equation (5.16) into Equation (5.17) and doing the necessary integrations, we can write the arbitrary functions $A(\alpha,\beta)$ and $B(\alpha,\beta)$ as

$$\begin{aligned} A(\alpha,\beta) &= \frac{1}{\sqrt{\alpha^2+\beta^2}}\left[\frac{4V_{d1}}{\pi\alpha\beta}\sin(\frac{\beta d}{2})\sin(\frac{\alpha d}{2}) + \frac{4V_{d2}}{\pi\alpha\beta}\sin(\frac{\beta d}{2})\sin(\frac{\alpha d}{2})\cos(\alpha L)\right] \\ B(\alpha,\beta) &= \frac{1}{\sqrt{\alpha^2+\beta^2}}\left[\frac{-4V_{d2}}{\pi\alpha\beta}\sin(\frac{\beta d}{2})\sin(\alpha L)\sin(\frac{\alpha d}{2})\right]. \end{aligned} \qquad (5.18)$$

Now, substituting Equation (5.18) into Equation (5.12), we get the following final formulation of the potential function within the fluid

$$\begin{aligned} \phi &= \int_0^{\infty}\int_0^{\infty} \frac{4}{\pi^2\alpha\beta\sqrt{\alpha^2+\beta^2}}\left[V_{d1}\cos(\alpha Y)\cos(\beta Z)\sin(\frac{\alpha d}{2})\sin(\frac{\beta d}{2}) + \right. \\ & \left. V_{d2}\ \cos(\beta Z)\sin(\frac{\alpha d}{2})\sin(\frac{\beta d}{2})\cos(\alpha(L+Y))\right]\exp\left(-\sqrt{\alpha^2+\beta^2}\ X\right)\, d\alpha\, d\beta \end{aligned} \qquad (5.19)$$

The quantity that we are primarily interested in is the velocity component V along the wall (at $X = Z = 0$). This can be obtained by substituting Equation (5.19) into Equation (5.7), thus:

$$\begin{aligned} V_y|_{X=Z=0} &= \int_0^{\infty}\int_0^{\infty} \frac{-4}{\pi^2\beta\sqrt{\alpha^2+\beta^2}}\left[V_{d1}\sin(\alpha Y)\sin(\frac{\alpha d}{2})\sin(\frac{\beta d}{2})\right. \\ &+ \left. V_{d2}\sin(\frac{\alpha d}{2})\sin(\frac{\beta d}{2})\sin(\alpha(L+Y))\right]\, d\alpha\, d\beta. \end{aligned} \qquad (5.20)$$

Using tables of integral transforms by Bateman (1954) and performing the necessary integrations, we can obtain the integral of Equation (5.20) in the following closed form:

$$
\begin{aligned}
V_y|_{X=Z=0} &= \frac{V_{d1}\Gamma^2(\frac{1}{2})}{2\pi^2}\left[\left(\frac{Y}{d}+0.5\right)^{-1} {}_2F_1\left(\frac{1}{2},\,\frac{1}{2},\,\frac{3}{2};\,-\left(\frac{2Y}{d}+1\right)^{-2}\right)\right. \\
&- \left.\left(\frac{Y}{d}-0.5\right)^{-1} {}_2F_1\left(\frac{1}{2},\,\frac{1}{2},\,\frac{3}{2};-\left(\frac{2Y}{d}-1\right)^{-2}\right)\right] \\
&+ \frac{V_{d2}\Gamma^2(\frac{1}{2})}{2\pi^2}\left[\left(\frac{Y}{d}+\frac{L}{d}+0.5\right)^{-1} {}_2F_1\left(\frac{1}{2},\,\frac{1}{2},\,\frac{3}{2};\,-\left(\frac{2Y}{d}+\frac{2L}{d}+1\right)^{-2}\right)\right. \\
&- \left.\left(\frac{Y}{d}+\frac{L}{d}-0.5\right)^{-1} {}_2F_1\left(\frac{1}{2},\,\frac{1}{2},\,\frac{3}{2};\,-\left(\frac{2Y}{d}+\frac{2L}{d}-1\right)^{-2}\right)\right], \qquad (5.21)
\end{aligned}
$$

where ${}_2F_1(a,\ b,\ c;\ w)$ is the complex hypergeometric function of variable w with the parameters a, b, and c. The function is the solution of the hypergeometric equation (Press et al., 1992), given by

$$
w\,(1-w)\frac{\partial^2\,({}_2F_1)}{\partial w^2} = a\,b\,({}_2F_1) - [\,c - (a+b+1)\,w]\frac{\partial\,({}_2F_1)}{\partial w}. \qquad (5.22)
$$

Equation (5.22) has three singular points at $w = 0,\ 1$, and ∞ which correspond to $Y = \infty$, imaginary value, and $\pm(d/2)$ or $(-L \pm d/2)$ (the edges of the two branches), respectively which fortunately, do not pose any problem in the subsequent analysis.

Using the velocity profile given by Equation (5.21), we can determine the kinetic energy $V_E^2/2$ at linking point E, located at $X = Z = 0$ and $Y = S = s/cos\theta$. Therefore,

$$
\begin{aligned}
V_y|_{X=Z=0} &= \frac{V_{d1}\Gamma^2(\frac{1}{2})}{2\pi^2}\left[\left(\frac{S}{d}+0.5\right)^{-1} {}_2F_1\left(\frac{1}{2},\,\frac{1}{2},\,\frac{3}{2};\,-\left(\frac{2S}{d}+1\right)^{-2}\right)\right. \\
&- \left.\left(\frac{S}{d}-0.5\right)^{-1} {}_2F_1\left(\frac{1}{2},\,\frac{1}{2},\,\frac{3}{2};-\left(\frac{2S}{d}-1\right)^{-2}\right)\right] \\
&+ \frac{V_{d2}\Gamma^2(\frac{1}{2})}{2\pi^2}\left[\left(\frac{S}{d}+\frac{L}{d}+0.5\right)^{-1} {}_2F_1\left(\frac{1}{2},\,\frac{1}{2},\,\frac{3}{2};\,-\left(\frac{2S}{d}+\frac{2L}{d}+1\right)^{-2}\right)\right. \\
&- \left.\left(\frac{S}{d}+\frac{L}{d}-0.5\right)^{-1} {}_2F_1\left(\frac{1}{2},\,\frac{1}{2},\,\frac{3}{2};\,-\left(\frac{2S}{d}+\frac{2L}{d}-1\right)^{-2}\right)\right]. \qquad (5.23)
\end{aligned}
$$

5.3 The Critical Height at the BLE

We now have two expressions for ${V_E}^2/2$, obtainable from Equations (5.5) and (5.23), applicable at point E which links the interface with the wall of the reservoir. Figure 5.2 shows a graphical representation of these two expressions for fixed values of V_{d_1} , V_{d_2} , g ,L, d , θ, ρ and $\Delta\rho$. Under these conditions Equation (5.23) provides a specific relation between $V_E^2/2$ and s represented by the curve in Figure 5.2, while Equation (5.5) produces a series of parallel straight lines depending on the values of h. For large values of h, the straight line and the curve do not intersect, while two points of intersection are possible with small values of h. There is one value of h that produces a single intersection with the straight line given by Equation (5.5) forming a tangent to the curve given by Equation (5.23). The hypothesis in this analysis (similar to Armstrong et al., 1992; Soliman and Sims, 1992) is that this value of h corresponding to the critical height for the BLE can be determined by equating $V_E^2/2$ given by Equations (5.5) and (5.23) and their first derivative with respect to s. Therefore, the BLE is characterized by the following two equations:

$$\frac{\Delta\rho}{\rho}\; g\; (h_{BLE} - s) =$$

$$\frac{1}{2}\left\{\frac{V_{d1}\Gamma^2(\frac{1}{2})}{2\pi^2}\left[\left(\frac{S}{d}+0.5\right)^{-1}\; {}_2F_1\left(\frac{1}{2},\frac{1}{2},\frac{3}{2};\,-\left(\frac{2S}{d}+1\right)^{-2}\right)\right.\right.$$
$$\left. - \left(\frac{S}{d}-0.5\right)^{-1}\; {}_2F_1\left(\frac{1}{2},\frac{1}{2},\frac{3}{2};-\left(\frac{2S}{d}-1\right)^{-2}\right)\right]$$
$$+\frac{V_{d2}\Gamma^2(\frac{1}{2})}{2\pi^2}\left[\left(\frac{S}{d}+\frac{L}{d}+0.5\right)^{-1}\; {}_2F_1\left(\frac{1}{2},\frac{1}{2},\frac{3}{2};\,-\left(\frac{2S}{d}+\frac{2L}{d}+1\right)^{-2}\right)\right.$$

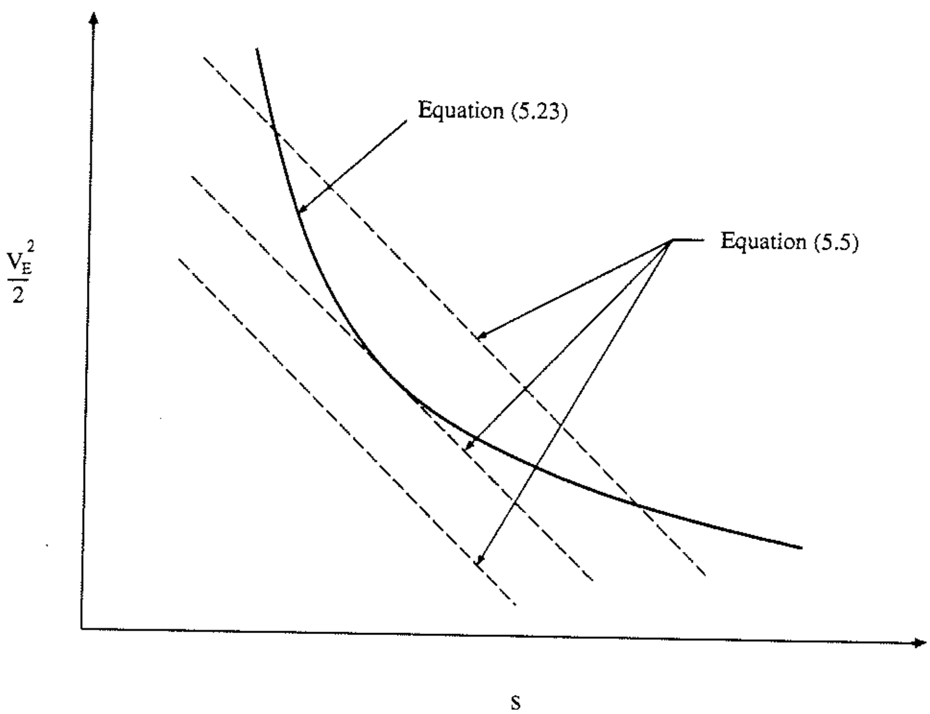

Figure 5.2: Behavior of $\frac{V_E^2}{2}$ versus s

$$- \left(\frac{S}{d} + \frac{L}{d} - 0.5\right)^{-1} {}_2F_1\left(\frac{1}{2},\, \frac{1}{2},\, \frac{3}{2};\, -\left(\frac{2S}{d} + \frac{2L}{d} - 1\right)^{-2}\right)\Bigg]\Bigg\}^2 \qquad (5.24)$$

and

$$\frac{-\Delta\rho}{\rho} \quad g \quad cos(\theta) = \frac{1}{2}\left\{\left(\frac{\Gamma^2(\frac{1}{2})}{2\pi^2}\right)^2 \left[\frac{-2F_2^2}{d} S_2^{-3} + 2F_2 S_2^{-2}\,\frac{\partial F_2}{\partial S} + \frac{4S}{d^2} F_1 F_2 \left(S_1 S_2\right)^{-2}\right.\right.$$
$$\left. - \quad 2\left(S_1 S_2\right)^{-1}\left(F_2 \frac{\partial F_1}{\partial S} + F_1 \frac{\partial F_2}{\partial S}\right) - \frac{2F_1^2}{d} S_1^{-3} + 2F_1 S_1^{-2}\,\frac{\partial F_1}{\partial S}\right] V_{d_1}^2$$

$$+ \quad 2\left(\frac{\Gamma^2(\frac{1}{2})}{2\pi^2}\right)^2 \left[\left(\frac{F_3}{S_3} - \frac{F_4}{S_4}\right)\left(\frac{F_2}{d} S_2^{-2} - S_2^{-1}\frac{\partial F_2}{\partial S} - \frac{F_1}{d} S_1^{-2} + S_1^{-1}\frac{\partial F_1}{\partial S}\right) + \right.$$
$$\left.\left(\frac{F_1}{S_1} - \frac{F_2}{S_2}\right)\left(\frac{F_4}{d} S_4^{-2} - S_4^{-1}\frac{\partial F_4}{\partial S} - \frac{F_3}{d} S_3^{-2} + S_3^{-1}\frac{\partial F_3}{\partial S}\right)\right] V_{d_1}\ V_{d_2}$$

$$+ \quad \left(\frac{\Gamma^2(\frac{1}{2})}{2\pi^2}\right)^2 \left[\frac{-2F_4^2}{d} S_4^{-3} + 2F_4 S_4^{-2}\,\frac{\partial F_4}{\partial S} + 4\left(\frac{S}{d^2} + \frac{L}{d^2}\right) F_3 F_4 (S_3 S_4)^{-2}\right.$$
$$\left.\left. - \quad 2(S_3 S_4)^{-1}\left(F_4 \frac{\partial F_3}{\partial S} + F_3 \frac{\partial F_4}{\partial S}\right) - \frac{2F_3^2}{d}\ S_3^{-3} + 2F_3 S_3^{-2}\,\frac{\partial F_3}{\partial S}\right] V_{d_2}^2 \ \right\}, \quad (5.25)$$

where

$$S = s/\cos\theta,$$

$$S_1 = \frac{S}{d} + 0.5,$$

$$S_2 = \frac{S}{d} - 0.5,$$

$$S_3 = \frac{S}{d} + \frac{L}{d} + 0.5,$$

$$S_4 = \frac{S}{d} + \frac{L}{d} - 0.5,$$

$$F_1 = {}_2F_1\left(\frac{1}{2}, \frac{1}{2}, \frac{3}{2}; -\left(\frac{2S}{d} + 1\right)^{-2}\right),$$

$$F_2 = {}_2F_1\left(\frac{1}{2}, \frac{1}{2}, \frac{3}{2}; -\left(\frac{2S}{d} - 1\right)^{-2}\right),$$

$$F_3 = {}_2F_1\left(\frac{1}{2}, \frac{1}{2}, \frac{3}{2}; -\left(\frac{2S}{d} + \frac{2L}{2d} + 1\right)^{-2}\right),$$

$$F_4 = {}_2F_1\left(\frac{1}{2}, \frac{1}{2}, \frac{1}{2}; -\left(\frac{2S}{d} + \frac{2L}{d} - 1\right)^{-2}\right),$$

$$\frac{\partial F_1}{\partial S} = \left(\frac{2}{3d}\right)\left(\frac{2S}{d} + 1\right)^{-3} {}_2F_1\left(\frac{3}{2}, \frac{3}{2}, \frac{5}{2}; -\left(\frac{2S}{d} + 1\right)^{-2}\right),$$

$$\frac{\partial F_2}{\partial S} = \left(\frac{2}{3d}\right)\left(\frac{2S}{d} - 1\right)^{-3} {}_2F_1\left(\frac{3}{2}, \frac{3}{2}, \frac{5}{2}; -\left(\frac{2S}{d} - 1\right)^{-2}\right),$$

$$\frac{\partial F_3}{\partial S} = \left(\frac{2}{3d}\right)\left(\frac{2S}{d} + \frac{2L}{d} + 1\right)^{-3} {}_2F_1\left(\frac{3}{2}, \frac{3}{2}, \frac{5}{2}; -\left(\frac{2S}{d} + \frac{2L}{d} + 1\right)^{-2}\right)$$

and

$$\frac{\partial F_4}{\partial S} = \left(\frac{2}{3d}\right)\left(\frac{2S}{d} + \frac{2L}{d} - 1\right)^{-3} {}_2F_1\left(\frac{3}{2}, \frac{3}{2}, \frac{5}{2}; -\left(\frac{2S}{d} + \frac{2L}{d} - 1\right)^{-2}\right).$$

Introducing Froude number given by Equation (2.5) and knowing that for a square branch $\dot{m} = \rho d^2 V_d$, we get

$$Fr = \frac{4V_d}{\pi\sqrt{g\ d\ \Delta\rho/\rho}}. \tag{5.26}$$

Using Equation (5.26), we can write Equations (5.24) and (5.25) as:

$$\begin{aligned}
\frac{h_{BLE}}{d} - \frac{s}{d} = \frac{1}{2}\Bigg\{ & \frac{Fr_1\Gamma^2(\frac{1}{2})}{8\pi}\Bigg[\left(\frac{S}{d}+0.5\right)^{-1} {}_2F_1\left(\frac{1}{2},\frac{1}{2},\frac{3}{2};-\left(\frac{2S}{d}+1\right)^{-2}\right) \\
& - \left(\frac{S}{d}-0.5\right)^{-1} {}_2F_1\left(\frac{1}{2},\frac{1}{2},\frac{3}{2};-\left(\frac{2S}{d}-1\right)^{-2}\right)\Bigg] \\
& + \frac{Fr_2\Gamma^2(\frac{1}{2})}{8\pi}\Bigg[\left(\frac{S}{d}+\frac{L}{d}+0.5\right)^{-1} {}_2F_1\left(\frac{1}{2},\frac{1}{2},\frac{3}{2};-\left(\frac{2S}{d}+\frac{2L}{d}+1\right)^{-2}\right) \\
& - \left(\frac{S}{d}+\frac{L}{d}-0.5\right)^{-1} {}_2F_1\left(\frac{1}{2},\frac{1}{2},\frac{3}{2};-\left(\frac{2S}{d}+\frac{2L}{d}-1\right)^{-2}\right)\Bigg]\Bigg\}^2
\end{aligned} \qquad (5.27)$$

and

$$-\frac{32\,cos(\theta)}{\pi^2} = \left[\; C_1\; Fr_1^2 \;+\; C_2\; Fr_1\; Fr_2 \;+\; C_3\; Fr_2^2 \;\right], \qquad (5.28)$$

where C_1, C_2, and C_3 are given by the following equations:

$$\begin{aligned}
C_1 = & \left(\frac{\Gamma^2(\frac{1}{2})}{2\pi^2}\right)^2 \Bigg\{-2F_2^2S_2^{-3} + 2F_2S_2^{-2}\left(d\,\frac{\partial F_2}{\partial S}\right) + \frac{4S}{d}F_1F_2\,(S_1S_2)^{-2} \\
& - 2\,(S_1S_2)^{-1}\left[F_2\left(d\,\frac{\partial F_1}{\partial S}\right) + F_1\left(d\,\frac{\partial F_2}{\partial S}\right)\right] - 2F_1^2S_1^{-3} + 2F_1S_1^{-2}\left(d\,\frac{\partial F_1}{\partial S}\right)\Bigg\},
\end{aligned}$$

$$\begin{aligned}
C_2 = & \; 2\left(\frac{\Gamma^2(\frac{1}{2})}{2\pi^2}\right)^2 \Bigg\{\left(\frac{F_3}{S_3}-\frac{F_4}{S_4}\right)\left[F_2S_2^{-2} - S_2^{-1}\left(d\,\frac{\partial F_2}{\partial S}\right) - F_1S_1^{-2} + S_1^{-1}\left(d\,\frac{\partial F_1}{\partial S}\right)\right] \\
& + \left(\frac{F_1}{S_1}-\frac{F_2}{S_2}\right)\left[F_4S_4^{-2} - S_4^{-1}\left(d\frac{\partial F_4}{\partial S}\right) - F_3S_3^{-2} + S_3^{-1}\left(d\,\frac{\partial F_3}{\partial S}\right)\right]\Bigg\}
\end{aligned}$$

and

$$\begin{aligned}
C_3 = & \left(\frac{\Gamma^2(\frac{1}{2})}{2\pi^2}\right)^2 \Bigg\{-2F_4^2S_4^{-3} + 2F_4S_4^{-2}\left(d\frac{\partial F_4}{\partial S}\right) + 4\left(\frac{S}{d}+\frac{L}{d}\right)F_3F_4(S_3S_4)^{-2} \\
& - 2(S_3S_4)^{-1}\left[F_4\left(d\,\frac{\partial F_3}{\partial S}\right) + F_3\left(d\,\frac{\partial F_4}{\partial S}\right)\right] - 2F_3^2\,S_3^{-3} + 2F_3S_3^{-2}\left(d\,\frac{\partial F_3}{\partial S}\right)\Bigg\}.
\end{aligned}$$

Equations (5.27) and (5.28) provide the necessary relations for determining h_{BLE}/d and s/d corresponding to any given values of Fr_1, Fr_2, L/d and θ. For given values of Fr_1, Fr_2, L/d and θ, an iteration procedure is necessary for determining s/d from Equation (5.28), which is then substituted in Equation (5.27) for evaluating h_{BLE}/d.

During the iteration procedure, the hypergeometric function ${}_2F_1(a,\ b,\ c;\ w)$ at $|w| \leq 1/2$ can be calculated from the following hypergeometric series which in general converges rapidly in this range (the series converge only within $|w| < 1$)

$$
{}_2F_1(a,\ b,\ c;\ w) = 1 + \frac{ab}{c}\ \frac{w}{1!} + \frac{a(a+1)b(b+1)}{c(c+1)}\ \frac{w^2}{2!} + \cdots + \frac{a(a+1)\cdots(a+J-1)b(b+1)\cdots(b+J-1)}{c(c+1)\cdots(c+J-1)}\ \frac{w^J}{J!} + \cdots \qquad (5.29)
$$

Otherwise ($|w| > 1/2$), the hypergeometric function was evaluated by integrating Equation (5.22) in the complex plane. A detailed discussion with computer subroutines for the integration procedure can be found in the Numerical Recipes by Press et al. (1992).

5.4 Results and Discussion

The objectives of this section are to compare the results of the present model at $\theta = 0$ with those of Armstrong et al. (1992) in order to determine quantitively the values of Fr_1 , Fr_2, and L/d beyond which Equations (5.1) and (5.2) are applicable, and to study the effect of θ on h_{BLE}.

Figure 5.3 shows the velocity profile along the reservoir wall beneath the lower branch for $L/d = 2$, $\theta = 0$, $Fr_1 = 5$ and different values of Fr_2. The profiles given by the present model approach infinity at the edge of the branch and they converge to the point sink profile away from the branch. From Figure 5.3, it is clear that the two models give practically identical results beyond $Y/d > 2.5$. Other cases show the same trend. Figure 5.4 shows the prediction of h_{BLE}/d at $L/d = 2$, $\theta = 0$ and different values of Fr_1 and Fr_2.

The present prediction of h_{BLE}/d approaches the appropriate limit of 0.5 as Fr_1 and Fr_2 approach zero and the respective prediction from Armstrong et al. (1992) is approached at high Fr_1 and/or Fr_2. When $Fr_2 = 0$, the deviation between the present predictions of h_{BLE}/d and those of Armstrong et al. is 101% at $Fr_1 = .1$, 26.5% at $Fr_1 = 0.5$, 13.5% at $Fr_1 = 1.0$, and 1.5% at $Fr_1 = 30.0$. This deviation between the two models at $Fr_2 = 0$ decreases with increasing Fr_2 at the same L/d and Fr_1, as shown in Figure 5.4. On the other hand, as shown in Figures 5.5 and 5.6 , the deviation between the two models in terms of $(h_{BLE} - h_{BLE,O})/h_{BLE,O}$, where $h_{BLE,O}$ is the value obtained from Equation (5.1), was found to decrease as L/d was decreased while maintaining the same Fr_1, and Fr_2. Experimentally, over the range of $0 \leq L/d \leq \infty$, $0 \leq Fr_2 \leq 100$, $0.01 \leq Fr_1 \leq 100$, and $\theta = 0$, the deviation between the two models is probably large enough to be detected only within the range of $Fr_1 \leq 30$, especially at large values of L/d and/or small values of Fr_2.

The behavior of s/h_{BLE} for the cases presented in Figure 5.4 is illustrated in

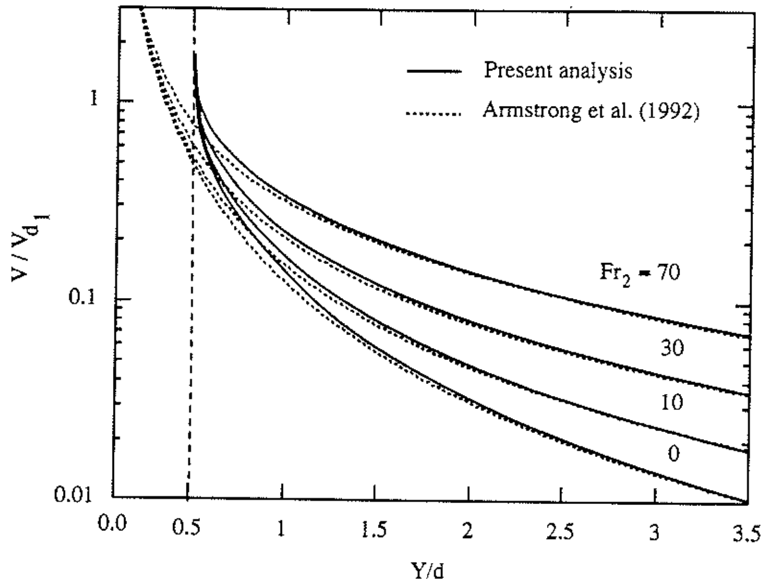

Figure 5.3: Velocity distribution along the reservoir wall at $Fr_1 = 5.0$ and $L/d = 2.0$

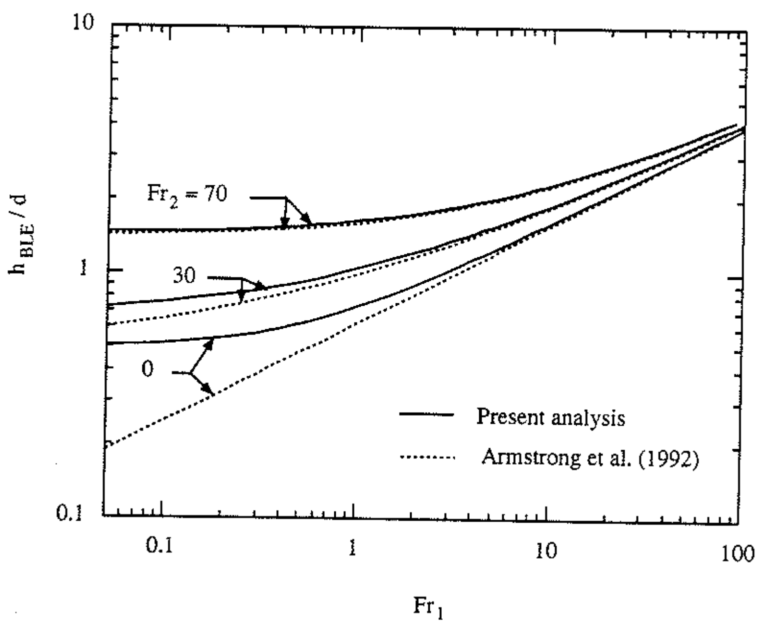

Figure 5.4: Variation of h_{BLE}/d at $L/d = 2.0$

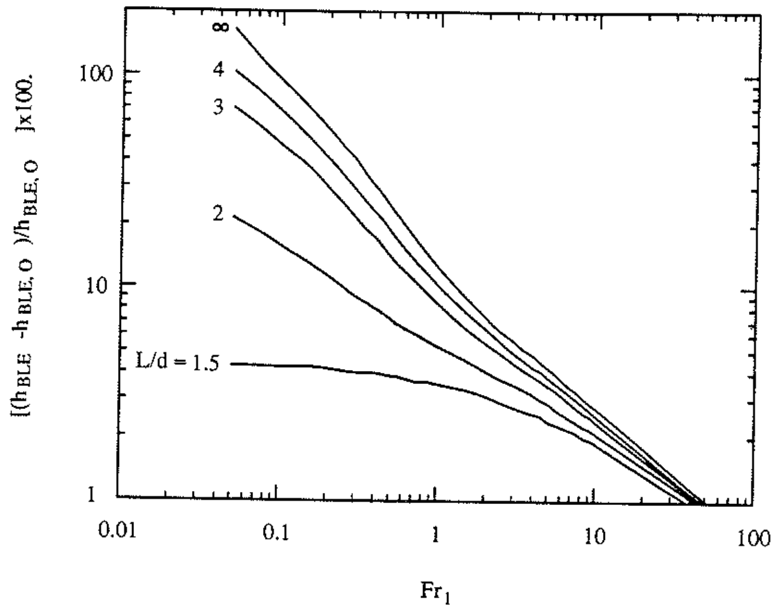

Figure 5.5: Percentage deviation from Armstrong et al. (1992) at $Fr_2 = 30.0$

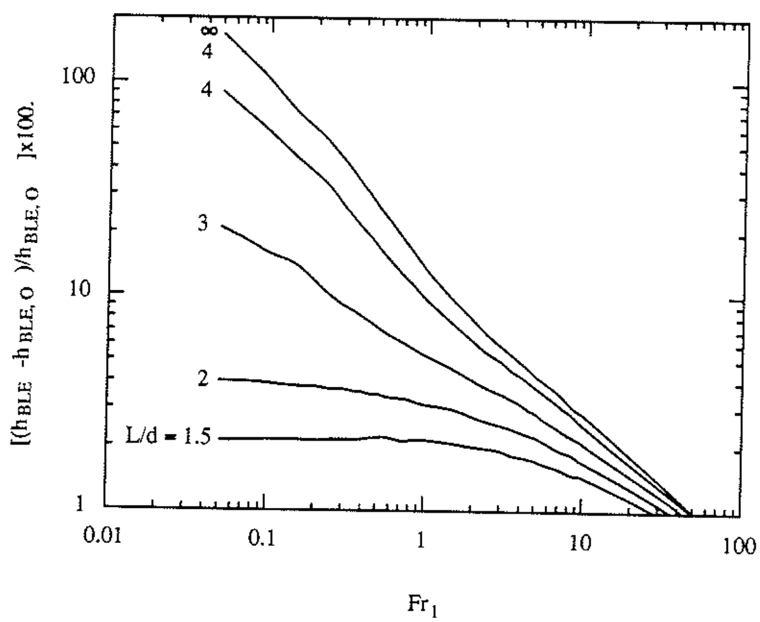

Figure 5.6: Percentage deviation from Armstrong et al. (1992) at $Fr_2 = 70.0$

Figure 5.7. The present predictions of s/h_{BLE} approach the appropriate limit of $s/h = 1.0$ as Fr_1 and Fr_2 approach zero. At large values of Fr_1 and Fr_2, the present model converges to the model given by Armstrong et al. (1992) . Similar trends were observed in other cases. It should be pointed out, that the shape of branch cross-section was found to produce insignificant effects on the results. This can be observed in Figure 5.8 where the present results of single discharge from a square branch are compared with those results from a circular branch developed by Soliman and Sims (1992). The two models give nearly identical results over the whole range of Fr_1.

Figures 5.9 and 5.10 show the prediction of h_{BLE}/d with θ at $L/d = 2.0$ and different values of Fr_1 and Fr_2. With increasing θ, h_{BLE}/d decreases and approaches the physical appropriate limit of $h_{BLE}/d = 0$ at $\theta = 90°$.

5.5 Comparison with Experimental Data

In order to support the present theoretical model at low Fr_1 and Fr_2 values, the experiment of dual discharge in Chapter 3 was extended for test-section pressure ranging from 205 to 516 kPa. A range of discharge flow rates corresponding to $0.05 \leq Fr_1 \leq 60$ at fixed values of $Fr_2 = 1$ at $L/d = 1.5$ and $Fr_2 = 5.0$ at $L/d = 3.0$ were covered (see Table 5.1). As well, experimental data available in the literature which were developed at relatively high values of Froude numbers

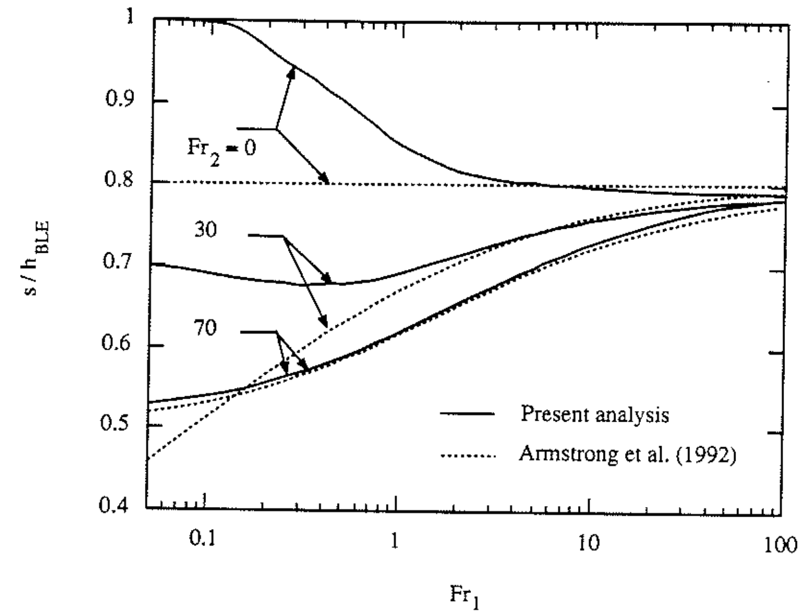

Figure 5.7: Variation of s/h_{BLE} at $L/d = 2.0$

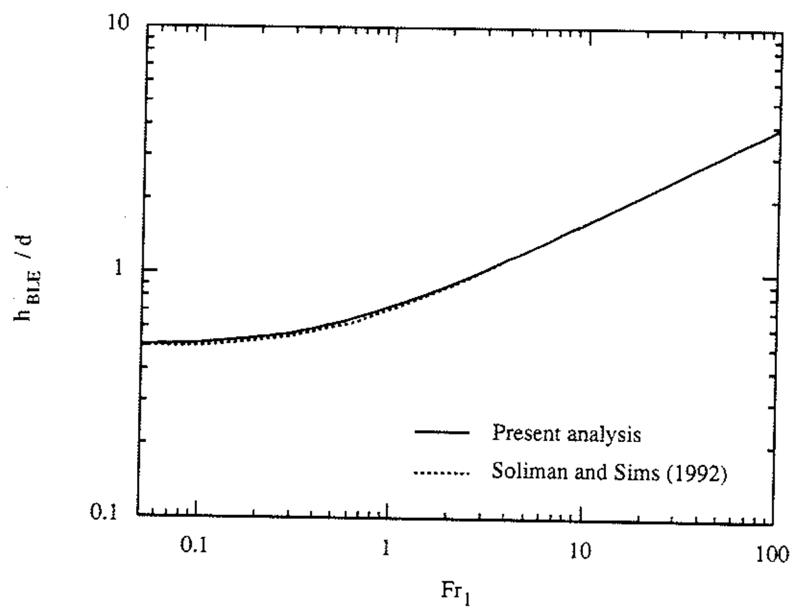

Figure 5.8: Effect of branch cross-section on h_{BLE}/d (single branch)

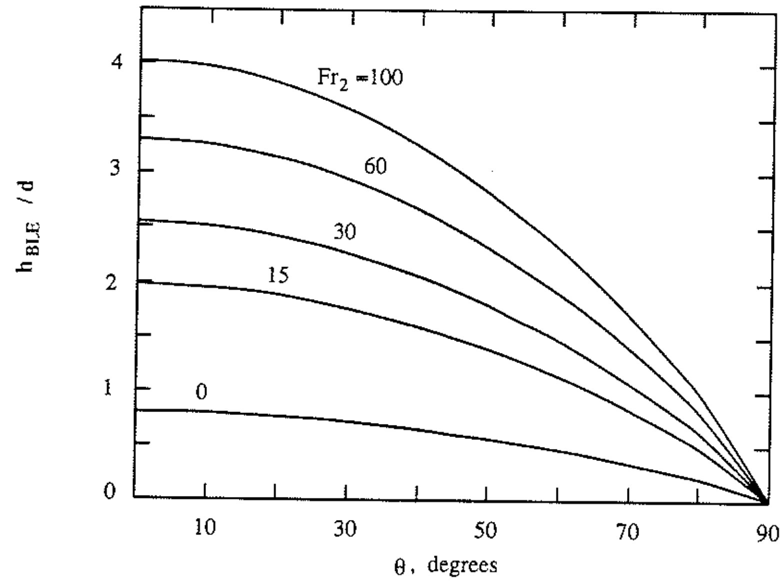

Figure 5.9: Effect of θ on h_{BLE}/d at $Fr_1 = 10$ and $L/d = 2.0$

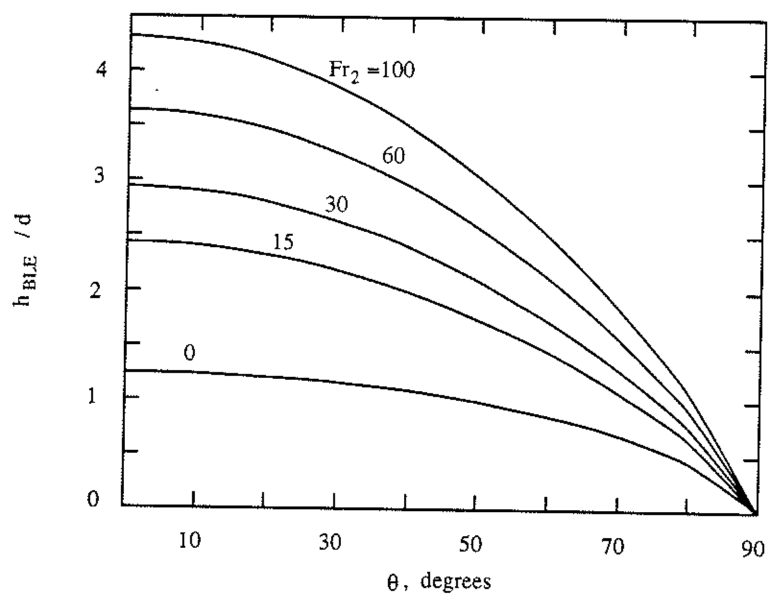

Figure 5.10: Effect of θ on h_{BLE}/d at $Fr_1 = 60$ and $L/d = 2.0$

Table 5.1: Experimental data for BLE at the lower branch

$L/d = 1.5$ and $Fr_2 = 1.0$				$L/d = 3.0$ and $Fr_2 = 5.5$			
P_o [kPa]	T_o [°C]	Fr_1	h_{BLE}/d	P_o [kPa]	T_o [°C]	Fr_1	h_{BLE}/d
204	22.9	0.07	0.63	204	21.7	0.04	0.62
	23.2	0.17	0.64		21.9	0.07	0.61
	23.2	0.31	0.69		21.9	0.14	0.64
	23.5	0.50	0.74		22.2	0.37	0.71
	23.9	1.20	0.82		22.2	0.63	0.77
	24.2	2.77	1.02		22.3	1.59	0.82
	24.3	4.58	1.10		22.5	2.76	0.92
	24.5	7.21	1.34		22.6	5.58	1.23
	24.8	13.45	1.75		22.7	8.38	1.36
	24.8	27.29	2.24		22.7	13.40	1.72
517	25.4	25.79	2.21		22.7	19.81	1.97
	25.4	30.58	2.38		22.7	25.72	2.19
	25.4	41.71	2.66	517	22.8	27.19	2.22
					22.8	30.49	2.37
					22.8	41.52	2.63

were used in the comparison. Figures 5.11 to 5.14 show the comparison between the present analysis at $\theta = 0$ and the experimental data. The trend in the experimental data follows the present theoretical predictions while a significant deviation between the experimental data and the model of Armstrong et al. (1992) can be detected at low Fr_1 and Fr_2, as shown in Figures 5.13 and 5.14. For $\theta > 0$, as far as we know, the only experimental data available to compare with are those present data in set nos. 4-4 to 4-6 for single discharge (branch B) and set nos. 4-10 to 4-12 for dual discharge (branches A and B). Unfortunately, the BLE in the these data sets coincided with the dry-out conditions at the bottom of the pipe as shown in Figures 5.15 and 5.16. Further experiments are recommended to validate the model at $\theta > 0$.

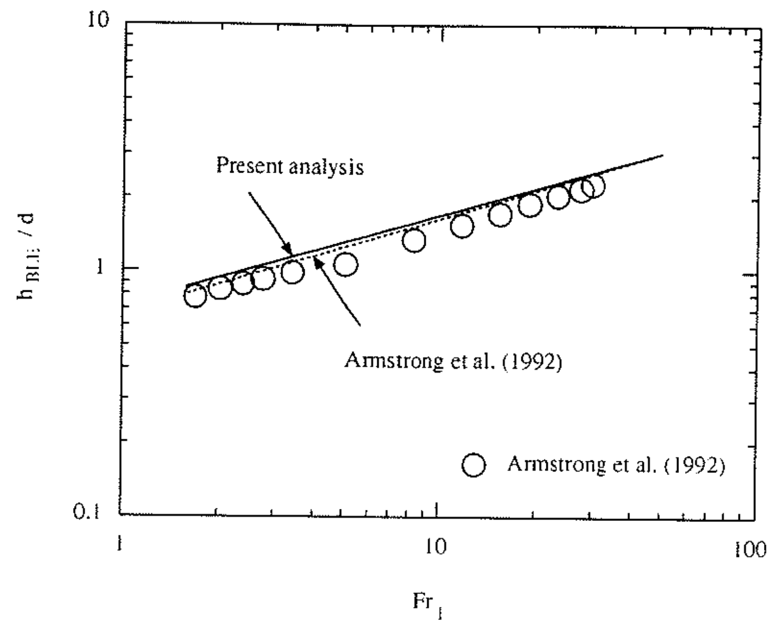

Figure 5.11: Comparison between the present predictions and the experimental data at $L/d = 4$ and $Fr_2 = 15.4$

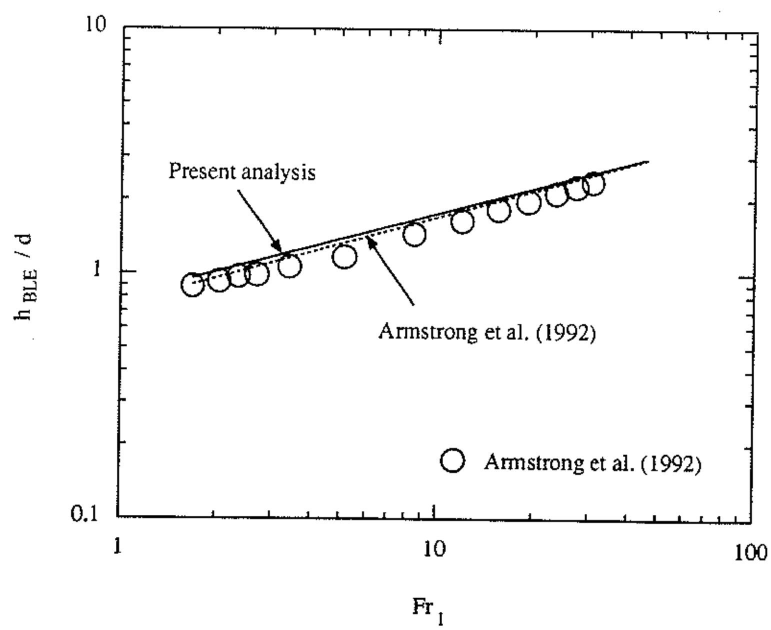

Figure 5.12: Comparison between the present predictions and the experimental data at $L/d = 1.5$ and $Fr_2 = 8.23$

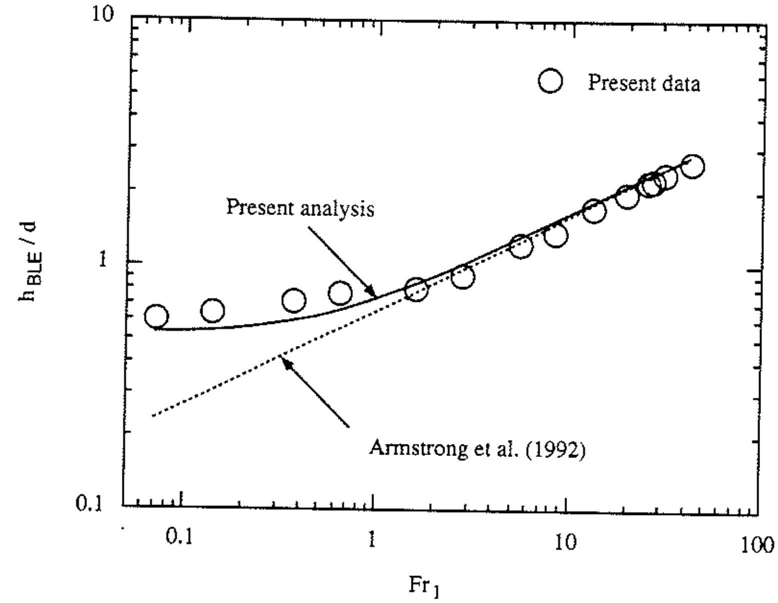

Figure 5.13: Comparison between the present predictions and the experimental data at $L/d = 3$ in Table 5.1

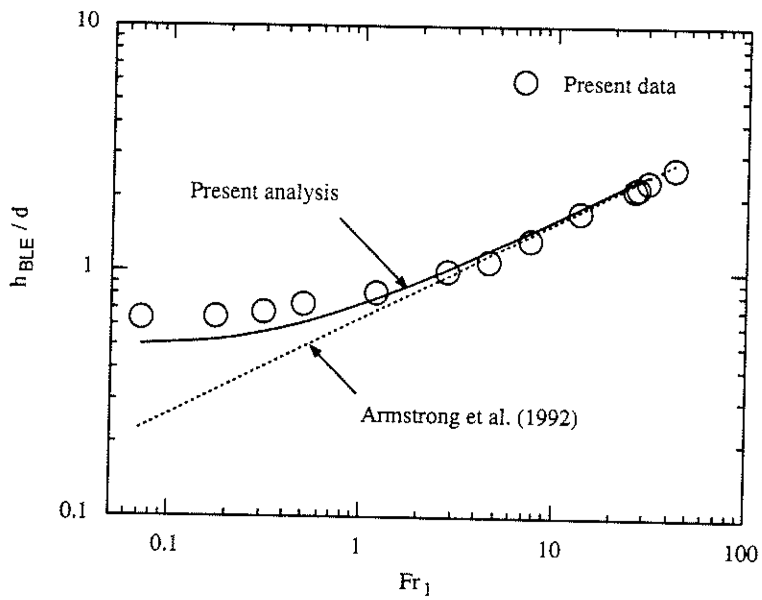

Figure 5.14: Comparison between the present predictions and the experimental data at $L/d = 1.5$ in Table 5.1

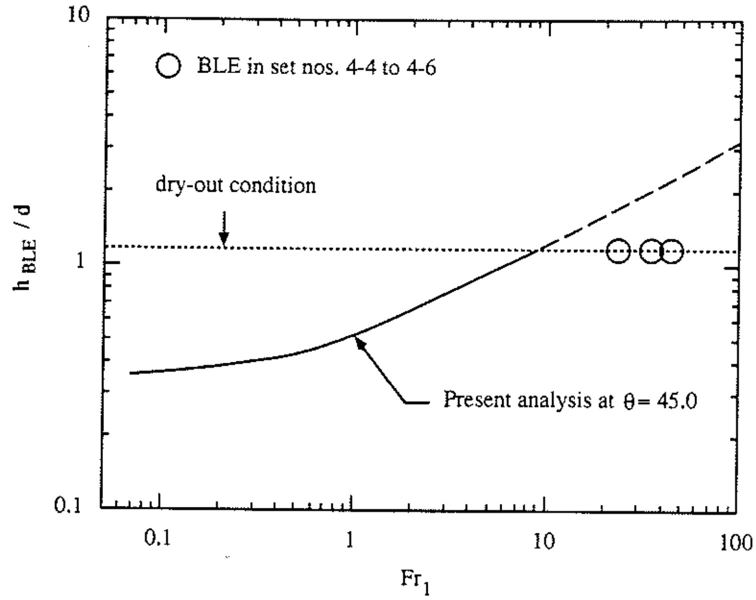

Figure 5.15: Experimental data coinciding with dry-out condition (single discharge)

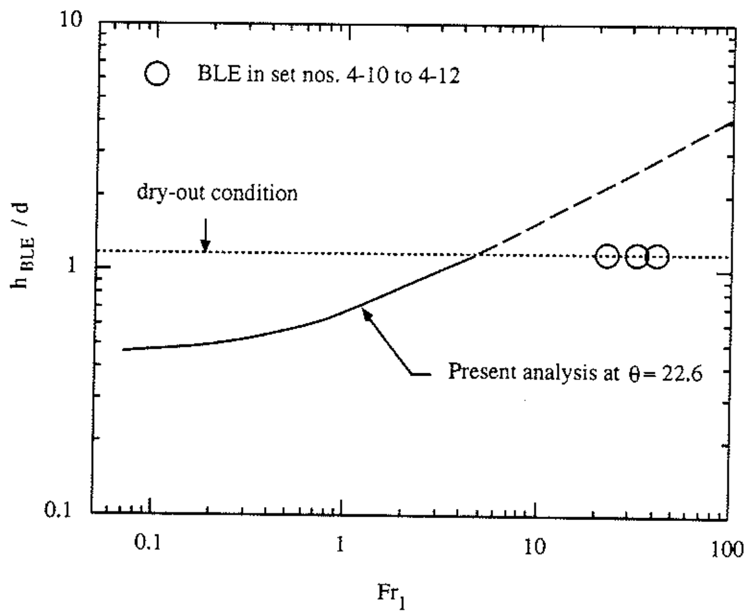

Figure 5.16: Experimental data coinciding with dry-out condition (dual discharge)

CHAPTER 6

CONCLUSIONS

Experimental data are reported on the onsets of gas and liquid entrainment, mass flow rate and quality during discharge from a large stratified region through small side branches ($d = 6.35\ mm$). Four groups of data were generated; each group corresponds to a particular branch configuration. Group no.1 contains the data of a single side branch, group no. 2 corresponds to two side branches separated by a distance L center-to-center with the centerlines in the same horizontal plane, group no. 3 corresponds to two side branches separated by a distance L center-to-center with centerlines in the same vertical plane with the centerlines perpendicular to the wall. All branches in group nos. 1-3 were mounted on a flat vertical wall. Group no. 4 corresponds to three side branches installed on a semicircular wall. Dimensions of the wall-branches assembly in group no. 4 were selected to be in direct proportion to the CANDU header-feeder system. The test matrix in this group was designed to include data of single discharge, dual discharge and triple discharge. The cases of dual and triple discharge in group nos. 2-4 were investigated under the conditions of equal hydraulic resistance R for the branches and equal pressure drop ΔP across the branches.

One hundred data sets were collected in group nos. 1-4 covering the ranges of $316 \leq P_o \leq 517\ kPa$, $40 \leq \Delta P \leq 235\ kPa$, $1000 \leq R \leq 3000\ (kg.m)^{-1/2}$, and different branch configurations. The independent variables were varied in a systematic fashion in order to facilitate the study of the influence of each variable separately. The following conclusions were drawn from group nos. 1-3:

- The results of $\dot{m}_{TP}$ and x for dual discharge (group nos. 2 and 3) can deviate significantly from the corresponding values for single discharge. This deviation increases with an increase in ΔP and/or a decrease in R or L/d.

- Influences of ΔP and R are shown to be largely absorbed (within the present test range) when normalized parameters are used in presenting the data. However, L/d in group no.3 remains as a parameter in these normalized plots. Within the present test range, deviations between dual discharge and single discharge are noted for $L/d = 1.5$, 2 and 3, while for $L/d = 8$, the results for dual discharge collapse on those of single discharge.

- Empirical relations were developed for the prediction of the onsets of gas and liquid entrainment, the two-phase mass flow rate and quality using normalized parameters. Comparisons between these relations and the experimental data base resulted in very good agreement. However, these correlating equations are empirical and thus, their accuracy can only be assured within the range of conditions covered in this investigation.

The experimental investigation of group no.4 revealed some important results. From these results the following conclusions are drawn:

- A comparison between the data of a single discharge and dual discharge (group no.3) from a flat wall and the corresponding data from a semicircular wall showed that the pipe curvature has an insignificant effect on the values of $\dot{m}_{TP}$ and x for single discharge; for dual discharge, it has a small effect on the results at the upper branch and a significant effect on the results at the lower branch. It should be pointed out that the BLE at the lower branch of the semicircular wall coincided with dry-out conditions at the bottom of the pipe. Therefore, it is fair to conclude that the results at or near this limit (BLE) may be affected by pipe-to-branch diameter ratio.

- The flow out of branch A (see Figure 3.2) was found to be dependent on the flow out at B and/or C. The flow from B has a strong effect on the flow from A, while the flow from C has a small effect on the flow from A. The present results indicate also, that, when branch B is already activated, adding branch C does not have significant effects on the flow from A.

- Additional discharge from A and/or C to the flow from B produce significantly different results. Additional discharge from A pulls the gas away from B, while additional discharge from C brings more gas into B. The opposite is true for the liquid (similar trends to those observed in group no.3).

- The flow out of branch C was found to be essentially independent of whether or not there was flow out of branches A and B within the tested range. Therefore, it is unlikely that the two missing branches from the circular section would affect the results of branch C in a circular section. As well, the two missing branches would have been too far from branches A and B to cause significant effects there. As a result, the data from the present test section in group no.4 should be representative of those for a full-header geometry in CANDU reactors.

No attempt was made at correlating the data in group no.4 . Wider ranges of geometries and operating conditions need to be covered before reliable correlations can be developed. However, the present data are very valuable as they could serve the following purposes: (a) investigating the effect of wall curvature, (b) demonstrating the effects of additional discharge(s) on the flow from a particular branch, and (c) providing a data base for validation of existing thermal-hydraulics codes.

The phenomenon of the onset of liquid entrainment was investigated theoretically for the condition of simultaneous discharge from a stratified two-phase region through finite size branches mounted on an inclined flat wall. A previous analysis by Armstrong et al. (1992), in which the branches were simulated by point sinks on a vertical wall, has been extended to account for the finite size of the branches and the wall inclination. According to the present analysis, the critical height corresponding to the onset of liquid entrainment at the lower branch is found to be dependent upon the two discharge rates, the distance separating the centerline of the branches and reservoir wall inclination. Numerical results for vertical walls show that the present model approaches the correct limit for the onset of liquid entrainment at low values of Froude number at the upper and lower branches and it converges to the predictions of Armstrong et al. at high Froude numbers. The present analysis applies to any two immiscible fluids with the term " liquid entrainment" referring to the appearance of the heavier fluid through the lower branch. Some experimental verification of the present theoretical trend is also provided.

REFERENCES

Armstrong, K.F., Parrott, S.D., Sims, G.E., Soliman, H.M. and Krishnan, V.S., "Theoretical and Experimental Study of the Onset of Liquid Entrainment During Dual Discharge from Large Reservoirs", Int. J. Multiphase Flow, 18, 217 - 227 (1992).

Bateman, H., "Tables of Integral Transforms", Vol. 1, McGraw-Hill, New York (1954).

Henry, R.E. and Fauske, H.K., "The Two-Phase Critical Flow of One-Component Mixtures in Nozzles, Orifices and Short Tubes", J. Heat Transfer, 93, 179-187 (1971).

Kline, S.J. and McClintock, F.A., "Describing the Uncertainties in Single-Sample Experiments", Mech. Engg. J., 75, 3 - 8 (1953).

Kowalski, J.E. and Krishnan, V.S., "Two-Phase Flow Distribution in a Large Manifold", AIChE Annual Meeting, New York, November 15-20 (1987).

Micaelli, J.C. and Memponteil, A., "Two-Phase Flow Behavior in a Tee-Junction: The CATHARE Model", Proc. 4th Int. Topical Meeting on Nuclear Reactor Thermal-Hydraulics, Karlsruhe, Germany, 2, 1024 - 1030 (1989).

Moffat, R.J., "Describing the Uncertainties in Experimental Results", Experimental Thermal and Fluid Science , 1, 3 - 17 (1988).

Parrott, S.D., "Experiments on the Onsets of Gas Pull-Through and Liquid Entrainment During Dual Discharge from a Large Reservoir", M.Sc Thesis, University of Manitoba (1993).

Parrott, S.D., Soliman, H.M., Sims, G.E. and Krishnan, V.S., "Experiments on the Onset of Gas Pull-Through During Dual Discharge from a Reservoir", Int. J. Multiphase Flow, 17, 119 - 129 (1991).

Press, W.H., Teukolsky, S.A., Vetterling, W.T. and Flannery, B.P., "Numerical Recipes in Fortran, The Art of Scientific Computer", 2nd Edition, Cambridge (1992).

Schrock, V.E., Revankar, S.T., Mannheimer, R., Wang, C.H. and Jia, D., "Steam-Water Critical Flow Through Small Pipes from Stratified Upstream Regions", Proc. 8th Int. Heat Transfer Conf., San Francisco, 2307 - 2311 (1986).

Smoglie, C. and Reimann, J., "Two-Phase Flow Through Small Branches in a Horizontal Pipe with Stratified Flow", Int. J. Multiphase Flow, 12, 609 - 625 (1986).

Soliman, H.M. and Sims, G.E., "Theoretical Analysis of Onset of Liquid Entrainment for Orifices of Finite Diameters", Int. J. Multiphase Flow, 18, 229-235

(1992).

Yonomoto, T. and Tasaka, K., "New Theoretical Model for Two-Phase Flow Discharged from Stratified Two-Phase Region Through Small Break", J. Nucl. Sci. Tech., 25, 441 - 455 (1988).

Yonomoto, T. and Tasaka, K., "Liquid and Gas Entrainment to a Small Break Hole from a Stratified Two-Phase Region", Int. J. Multiphase Flow, 17, 745 - 765 (1991).

Whalley, P.B., "Boiling, Condensation and Gas-Liquid Flow", Oxford University Press, New York (1987).

Zuber, N., "Problems in Modeling of Small Break LOCA", Nuclear Regulatory Commission Report No. NUREG-0724 (1980).

APPENDICES

APPENDIX A

Instrument Calibration

A.1 Pressure Gauges

Four Bourdon gauges were used in the experiment to give the pressure in the test section, the two separation tanks and the air outlet header (see Figure 3.3). Each pressure gauge was calibrated throughout the entire range (5- 100 psig) using a dead-weight tester. Pressures were imposed by adding weights in increments equivalent to 5 or 10 psig and the gauge readings were recorded along with the actual pressures. After reaching the maximum pressure, the weights were removed in the same increments and the gauge readings were also recorded. The average of the gauge readings was then correlated with the actual pressure. Figures A.1 and A.2 show the calibration results of two gauges. The other two gauges produced similar results.

A.2 Pressure Transducers

Two pressure transducers, Rosemount model 1151 DP, were used in the experiment to measure the liquid level in the test section and the pressure difference between the two separators. Each pressure transducer was calibrated against a micromanometer, as shown in Figure A.3. The digital voltmeter used in

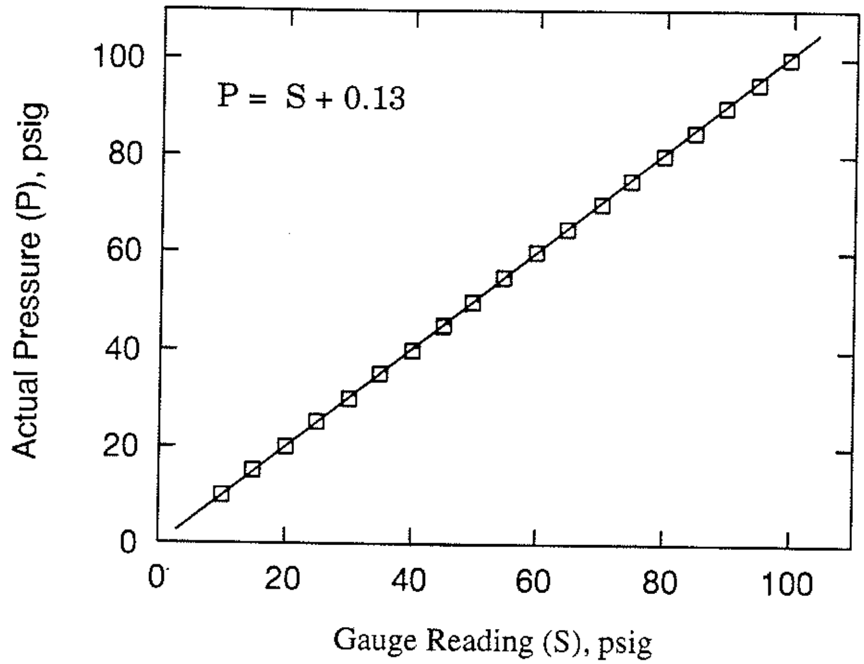

Figure A.1: Calibration results for test-section pressure gauge

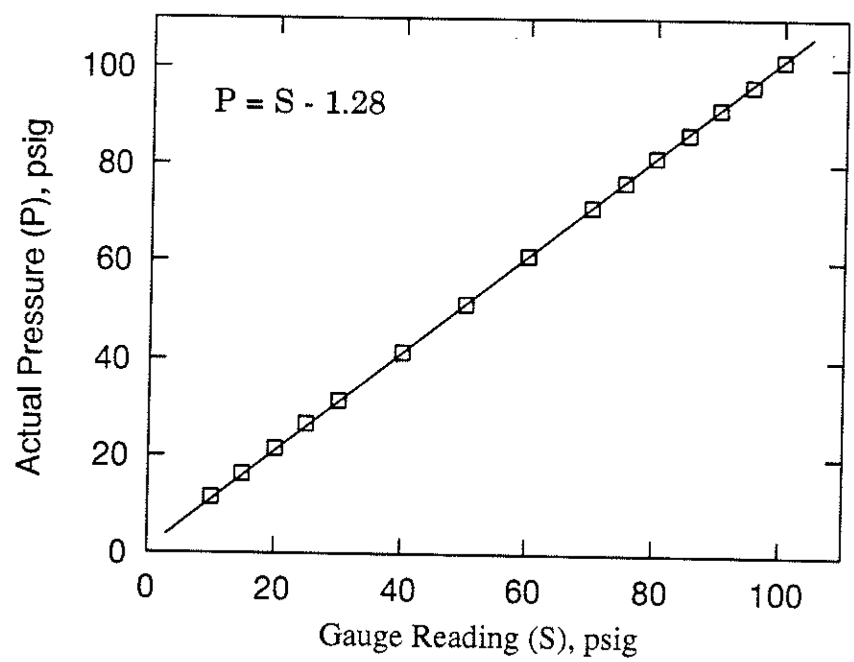

Figure A.2: Calibration results for a separator pressure gauge

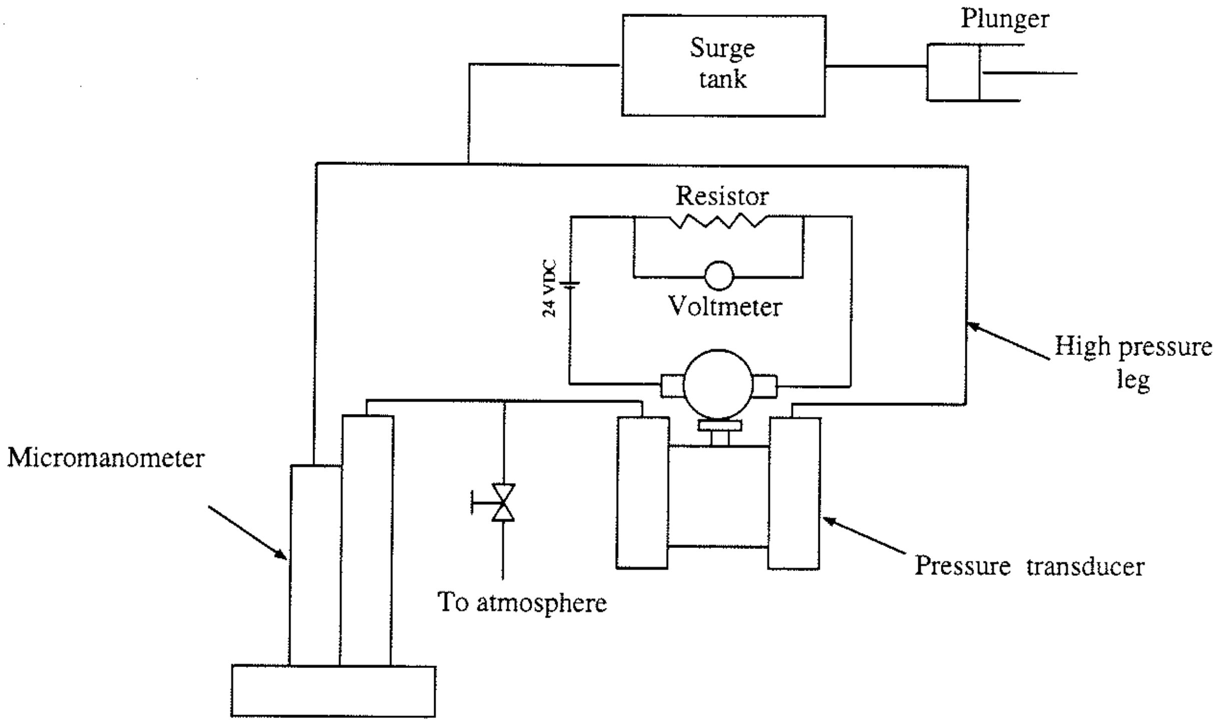

Figure A.3: Pressure transducer calibration apparatus

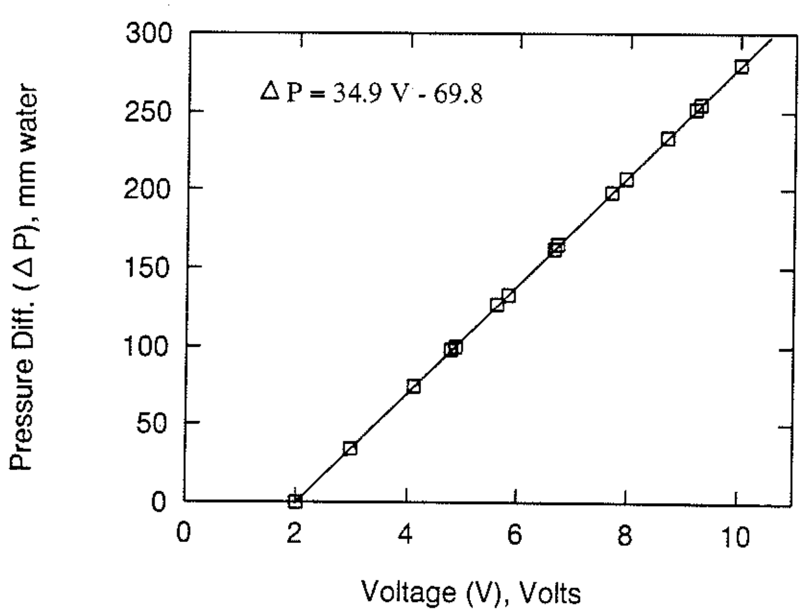

Figure A.4: Calibration results for test-section pressure transducer the calibration was subsequently used in the normal running of the experiments; for both calibration and experiments the sensitivity was approximately 35 μV per mm of water; the discrimination on the digital voltmeter was ± 1 μV. Calibration results of the test-section transducer are shown in Figure A.4. The other transducer had similar results.

A.3 Water Flowmeters

All water flowmeters were calibrated using a weigh-and-time method. Each flowmeter was calibrated between 10 and 100 percent of full scale inclusive, in ascending and descending increments of 10 percent. At each scale reading, an amount of water was collected over a period of time (8 to 15 minutes) while the float remained steady throughout the period. The average actual flow rates were then correlated with the flowmeter scale readings. Figures A.5 and A.6 show the calibration results of two flowmeters. The other flowmeters gave similar results.

A.4 Air Flowmeters

In order to calibrate the air flowmeters over their entire range, a combination of two wet test meters and two venturi meters were used. The two wet test meters (maximum capacity 0.6 and 15 standard m^3/hr) were manufactured by Elster, and the two venturi meters (throat diameter equal to 0.375 and 0.65 $in.$) were manufactured by Fox Valve Development Corp. with calibration traceable to National Institute of Standards and Technology. Comparison between the present calibration and those provided by the manufacturer showed very good agreement.

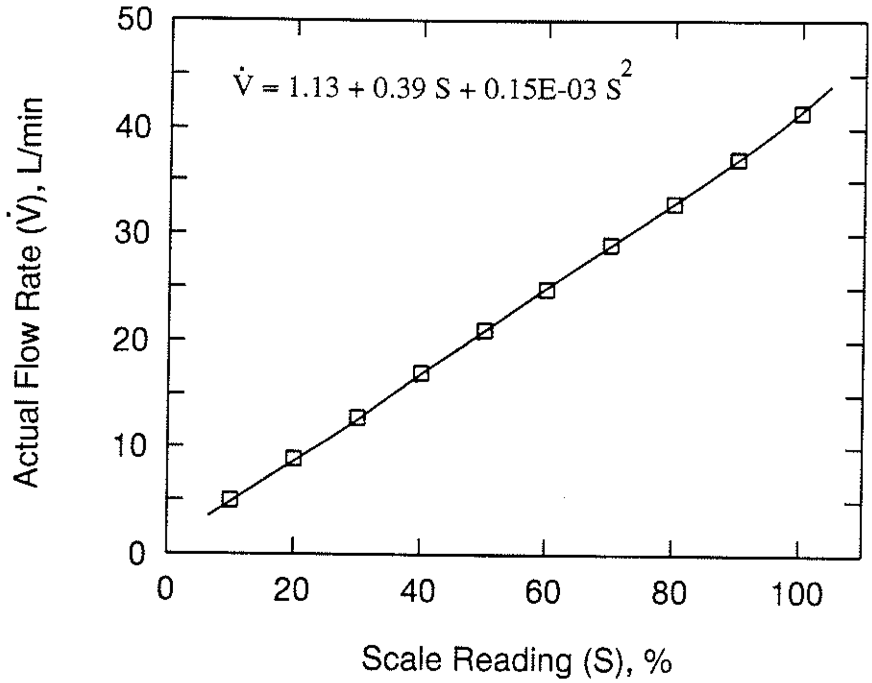

Figure A.5: Calibration results for a water flowmeter (0 - 42 L/min)

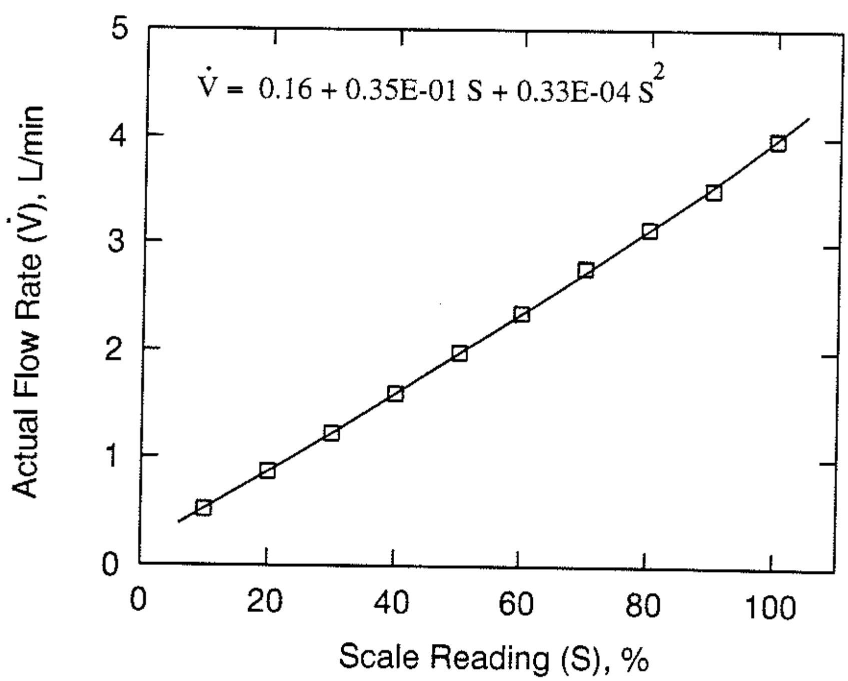

Figure A.6: Calibration results for a water flowmeter (0 - 4.0 L/min)

Deviations were a maximum of about ± 6 % at the lowest flow rates, but were usually within ± 3 %. Therefore, the present calibrations were used in the reduction of all data. Figures A.7 and A.8 show the calibration results of two air flowmeters. The other flowmeters had similar results.

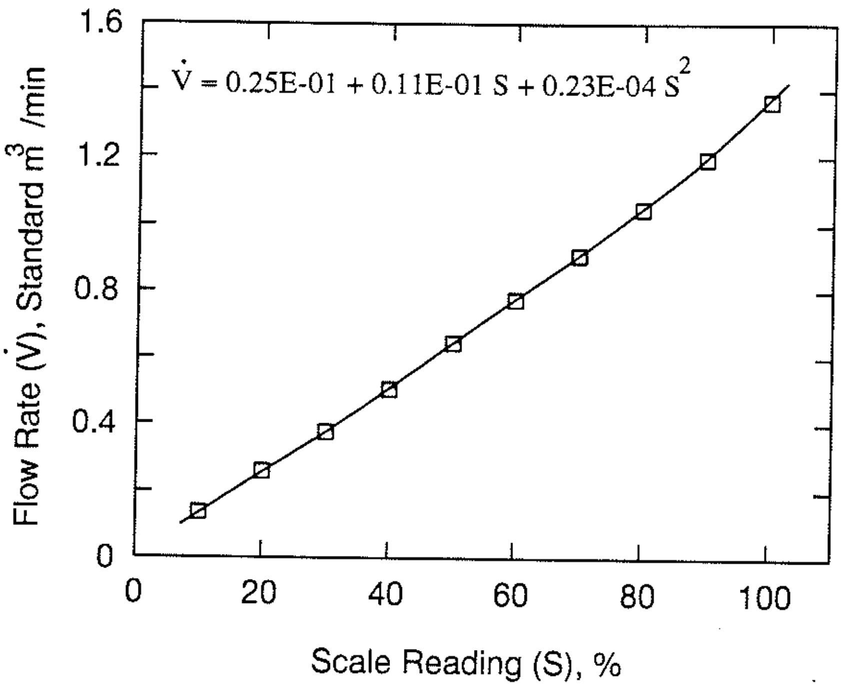

Figure A.7: Calibration results for an air flowmeter
(0 - 1.3 standard m^3/min)

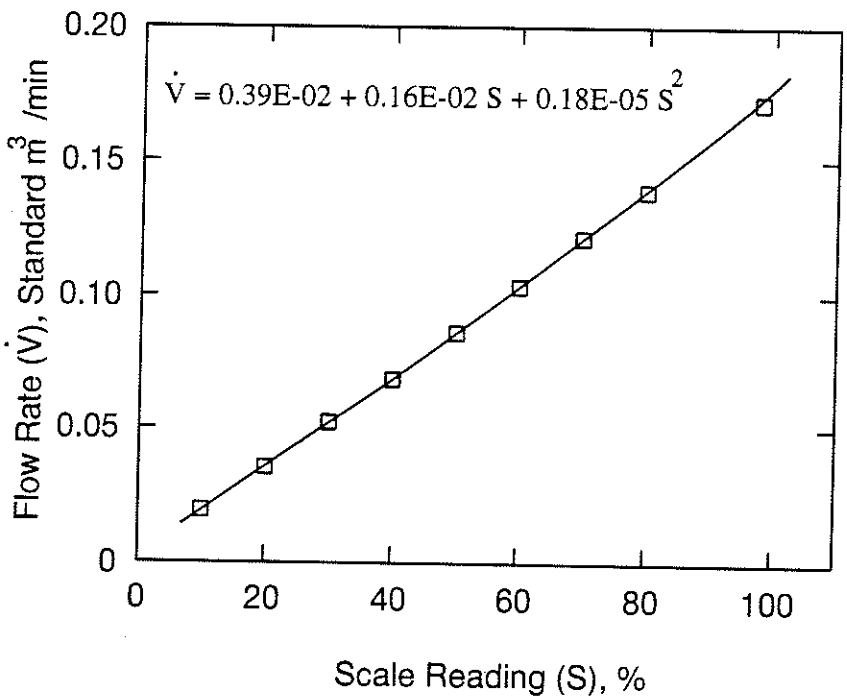

Figure A.8: Calibration results for an air flowmeter
(0 - 0.17 standard m^3/min)

APPENDIX B

Experimental Data for Single Discharge

Table B.1: Experimental data for single discharge

Set No. 1 − 1 P_0 = 316 kPa ΔP = 123 kPa R = 1028 $(kg.m)^{-1/2}$				Set No. 1 − 2 P_0 = 316 kPa ΔP = 82 kPa R = 1029 $(kg.m)^{-1/2}$			
h [mm]	T_o [°C]	$\dot{m}_G$ [kg/min]	$\dot{m}_L$ [kg/min]	h [mm]	T_o [°C]	$\dot{m}_G$ [kg/min]	$\dot{m}_L$ [kg/min]
16.33	20.2	0.00E+00	2.05E+01	14.93	19.3	0.00E+00	1.67E+01
14.86	20.3	8.16E-03	1.82E+01	13.46	20.1	8.91E-03	1.43E+01
13.92	20.4	1.53E-02	1.56E+01	12.30	20.2	1.93E-02	1.21E+01
12.97	20.1	2.50E-02	1.40E+01	11.26	20.3	2.77E-02	1.07E+01
11.75	19.9	3.99E-02	1.20E+01	10.07	20.2	4.09E-02	9.13E+00
10.49	19.7	5.24E-02	1.05E+01	9.08	20.1	5.34E-02	7.91E+00
9.26	19.5	7.11E-02	9.21E+00	7.58	20.0	7.19E-02	7.09E+00
8.07	18.8	8.79E-02	8.27E+00	6.36	19.9	9.00E-02	6.35E+00
6.46	18.4	1.19E-01	7.17E+00	4.95	19.7	1.15E-01	5.56E+00
4.75	18.1	1.52E-01	6.35E+00	3.52	19.5	1.46E-01	5.09E+00
3.35	18.0	1.78E-01	5.76E+00	2.22	19.5	1.75E-01	4.70E+00
1.60	17.8	1.88E-01	5.05E+00	0.82	18.9	1.98E-01	4.19E+00
0.20	17.7	2.43E-01	4.47E+00	-0.68	18.8	2.33E-01	3.63E+00
-0.99	17.6	2.81E-01	4.15E+00	-2.01	18.7	2.61E-01	3.22E+00
-2.57	17.6	3.21E-01	3.51E+00	-3.23	18.5	2.93E-01	2.84E+00
-3.76	17.5	3.53E-01	3.07E+00	-4.49	18.2	3.27E-01	2.43E+00
-4.81	17.5	3.87E-01	2.78E+00	-5.75	18.1	3.61E-01	2.06E+00
-5.89	17.5	4.24E-01	2.43E+00	-7.12	18.0	4.06E-01	1.68E+00
-6.91	17.7	4.58E-01	2.14E+00	-8.38	17.9	4.69E-01	1.31E+00
-8.17	17.8	5.07E-01	1.79E+00	-9.88	17.9	5.11E-01	9.27E-01
-9.50	18.2	5.60E-01	1.36E+00	-11.18	17.8	5.68E-01	6.66E-01
-10.62	18.3	6.06E-01	1.09E+00	-12.54	17.8	6.30E-01	4.13E-01
-12.05	18.3	6.72E-01	7.48E-01	-13.42	17.9	6.77E-01	3.05E-01
-13.28	18.4	7.32E-01	4.31E-01	-14.33	18.0	7.45E-01	1.75E-01
-14.29	18.5	8.01E-01	3.05E-01	-15.02	18.0	7.97E-01	9.62E-02
-15.41	18.5	8.78E-01	1.28E-01	-15.97	18.0	8.78E-01	0.00E+00
-16.74	18.4	9.88E-01	0.00E+00				

Table B.1: Experimental data for single discharge (cont.)

Set No. 1 − 3 P_0 = 316 kPa ΔP = 40 kPa R = 984 $(kg.m)^{-1/2}$				Set No. 1 − 4 P_0 = 517 kPa ΔP = 235 kPa R = 1010 $(kg.m)^{-1/2}$			
h $[mm]$	T_o $[°C]$	$\dot{m}_G$ $[kg/min]$	$\dot{m}_L$ $[kg/min]$	h $[mm]$	T_o $[°C]$	$\dot{m}_G$ $[kg/min]$	$\dot{m}_L$ $[kg/min]$
12.94	18.5	0.00E+00	1.22E+01	18.80	19.7	0.00E+00	2.88E+01
11.51	19.5	9.07E-03	9.87E+00	17.39	21.9	1.28E-02	2.62E+01
10.28	20.1	1.53E-02	8.31E+00	16.09	22.9	2.39E-02	2.30E+01
9.09	20.4	2.64E-02	6.93E+00	14.72	23.4	4.74E-02	2.05E+01
7.90	20.5	3.56E-02	6.15E+00	13.38	24.0	7.36E-02	1.81E+01
6.71	20.6	5.04E-02	5.21E+00	11.90	24.1	1.01E-01	1.62E+01
5.27	20.7	6.81E-02	4.74E+00	10.61	24.1	1.30E-01	1.43E+01
3.94	20.9	9.25E-02	4.35E+00	9.27	24.2	1.67E-01	1.22E+01
2.75	20.8	1.13E-01	3.71E+00	7.73	23.8	2.07E-01	1.10E+01
1.38	20.7	1.37E-01	3.44E+00	6.29	23.4	2.40E-01	9.48E+00
0.09	20.5	1.65E-01	3.01E+00	4.40	23.2	2.93E-01	8.38E+00
-1.07	20.6	1.90E-01	2.69E+00	2.96	22.7	3.29E-01	7.91E+00
-2.65	20.7	2.13E-01	2.28E+00	2.02	22.2	3.78E-01	7.33E+00
-4.01	21.0	2.44E-01	1.85E+00	0.79	21.8	4.24E-01	6.74E+00
-5.38	21.1	2.67E-01	1.55E+00	-0.89	21.3	4.96E-01	5.76E+00
-6.78	21.3	3.07E-01	1.23E+00	-2.71	19.8	5.78E-01	4.98E+00
-7.90	21.4	3.36E-01	9.63E-01	-4.53	19.4	6.59E-01	4.39E+00
-8.71	21.7	3.77E-01	7.51E-01	-6.18	19.3	7.29E-01	3.51E+00
-9.97	21.7	4.24E-01	5.71E-01	-7.65	19.2	8.00E-01	3.14E+00
-11.09	21.6	4.76E-01	4.42E-01	-9.09	19.1	8.85E-01	2.49E+00
-12.31	21.6	5.29E-01	2.54E-01	-10.53	19.0	9.64E-01	1.97E+00
-13.36	21.5	5.78E-01	1.12E-01	-11.93	19.0	1.06E+00	1.44E+00
-15.04	21.7	6.72E-01	1.00E-04	-13.33	18.9	1.16E+00	1.12E+00
				-14.28	18.9	1.27E+00	8.37E-01
				-15.12	18.7	1.36E+00	5.71E-01
				-16.48	18.8	1.48E+00	3.27E-01
				-17.18	19.2	1.57E+00	1.76E-01
				-19.82	19.3	1.76E+00	0.00E+00

Table B.1: Experimental data for single discharge (cont.)

Set No. 1 – 5 P_0 = 517 kPa ΔP = 166 kPa R = 1006 $(kg.m)^{-1/2}$				Set No. 1 – 6 P_0 = 517 kPa ΔP = 97 kPa R = 1005 $(kg.m)^{-1/2}$			
h $[mm]$	T_o $[^oC]$	$\dot{m}_G$ $[kg/min]$	$\dot{m}_L$ $[kg/min]$	h $[mm]$	T_o $[^oC]$	$\dot{m}_G$ $[kg/min]$	$\dot{m}_L$ $[kg/min]$
17.24	22.8	0.00E+00	2.43E+01	15.61	20.8	0.00E+00	1.86E+01
15.94	23.1	1.35E-02	2.17E+01	14.56	21.0	1.31E-02	1.69E+01
14.99	23.1	1.95E-02	1.97E+01	13.64	21.4	1.67E-02	1.53E+01
13.45	22.9	4.98E-02	1.73E+01	12.48	21.8	3.44E-02	1.35E+01
12.43	22.7	7.01E-02	1.54E+01	11.32	21.9	5.44E-02	1.20E+01
11.17	22.5	9.42E-02	1.38E+01	10.23	21.8	7.19E-02	1.05E+01
10.12	20.7	1.14E-01	1.18E+01	9.18	21.6	9.21E-02	9.48E+00
8.57	20.4	1.45E-01	1.07E+01	7.92	21.4	1.15E-01	8.31E+00
7.49	20.3	1.75E-01	9.68E+00	6.76	21.2	1.43E-01	7.52E+00
6.43	20.2	2.02E-01	8.89E+00	5.15	21.0	1.82E-01	6.54E+00
5.21	20.1	2.24E-01	8.11E+00	3.67	20.6	2.08E-01	5.76E+00
4.02	20.1	2.61E-01	7.52E+00	2.24	20.3	2.50E-01	5.37E+00
2.44	20.0	3.07E-01	6.74E+00	0.76	19.8	2.93E-01	4.78E+00
1.21	19.9	3.51E-01	5.95E+00	-0.74	19.7	3.40E-01	4.31E+00
-0.50	19.8	4.17E-01	5.25E+00	-2.25	19.3	4.09E-01	3.84E+00
-1.84	19.7	4.82E-01	4.90E+00	-3.41	18.9	4.54E-01	3.55E+00
-3.41	19.3	5.45E-01	4.19E+00	-4.77	18.5	5.01E-01	2.93E+00
-5.02	19.2	6.06E-01	3.76E+00	-6.45	18.4	5.85E-01	2.45E+00
-6.28	19.0	6.64E-01	2.99E+00	-7.79	18.3	6.37E-01	2.06E+00
-8.00	19.0	7.55E-01	2.57E+00	-9.12	18.2	7.00E-01	1.60E+00
-9.26	19.0	8.13E-01	2.14E+00	-10.28	18.1	7.64E-01	1.25E+00
-10.49	18.9	8.78E-01	1.70E+00	-11.23	18.5	8.37E-01	8.91E-01
-11.61	18.8	9.49E-01	1.43E+00	-12.21	18.5	8.91E-01	7.30E-01
-12.77	18.7	1.05E+00	1.02E+00	-13.58	18.4	9.78E-01	4.76E-01
-13.66	19.2	1.11E+00	8.01E-01	-14.57	17.3	1.04E+00	2.84E-01
-14.53	19.2	1.17E+00	5.53E-01	-15.40	18.4	1.16E+00	1.63E-01
-15.23	19.3	1.27E+00	4.31E-01	-17.26	18.4	1.32E+00	0.00E+00
-15.96	19.3	1.36E+00	2.84E-01				
-16.80	19.2	1.44E+00	1.39E-01				
-18.31	19.2	1.60E+00	0.00E+00				

Table B.1: Experimental data for single discharge (cont.)

Set No. 1 − 7 P_0 = 316 kPa ΔP = 130 kPa R = 1017 $(kg.m)^{-1/2}$				Set No. 1 − 8 P_0 = 378 kPa ΔP = 123 kPa R = 990 $(kg.m)^{-1/2}$			
h [mm]	T_o [^oC]	$\dot{m}_G$ [kg/min]	$\dot{m}_L$ [kg/min]	h [mm]	T_o [^oC]	$\dot{m}_G$ [kg/min]	$\dot{m}_L$ [kg/min]
16.46	22.6	0.00E+00	2.13E+01	16.53	20.8	0.00E+00	2.13E+01
14.99	22.5	8.01E-03	1.86E+01	15.26	20.6	8.31E-03	1.89E+01
13.73	22.1	1.80E-02	1.58E+01	14.00	20.9	1.57E-02	1.65E+01
12.44	22.1	3.22E-02	1.37E+01	12.84	21.2	3.26E-02	1.46E+01
11.11	22.1	4.80E-02	1.16E+01	11.58	21.7	4.86E-02	1.26E+01
9.88	22.1	6.28E-02	1.01E+01	10.32	21.9	6.44E-02	1.10E+01
8.48	21.5	8.38E-02	8.81E+00	9.06	22.2	8.32E-02	9.68E+00
7.15	21.2	1.06E-01	7.72E+00	7.87	22.5	1.06E-01	8.70E+00
5.61	21.0	1.37E-01	6.93E+00	6.60	22.7	1.28E-01	7.72E+00
4.32	20.7	1.61E-01	6.23E+00	5.17	22.8	1.61E-01	6.74E+00
2.88	20.5	1.88E-01	5.72E+00	3.76	22.7	1.96E-01	6.35E+00
1.59	20.1	2.16E-01	5.09E+00	2.36	22.6	2.22E-01	5.72E+00
0.22	19.8	2.50E-01	4.66E+00	1.00	22.4	2.54E-01	4.98E+00
-1.07	19.7	2.87E-01	4.19E+00	-0.44	22.0	2.98E-01	4.51E+00
-2.50	19.5	3.32E-01	3.74E+00	-2.40	21.9	3.67E-01	3.97E+00
-3.76	19.3	3.65E-01	3.26E+00	-3.59	21.6	4.06E-01	3.53E+00
-4.92	19.2	4.03E-01	2.86E+00	-5.02	21.5	4.61E-01	3.01E+00
-6.25	19.1	4.54E-01	2.34E+00	-6.53	21.2	5.16E-01	2.49E+00
-7.79	19.0	5.11E-01	1.93E+00	-7.96	21.0	5.75E-01	2.01E+00
-9.08	18.9	5.54E-01	1.59E+00	-9.50	20.7	6.34E-01	1.55E+00
-10.52	18.9	6.06E-01	1.17E+00	-10.66	20.5	6.85E-01	1.23E+00
-11.85	18.9	6.67E-01	7.90E-01	-12.02	20.4	7.64E-01	8.55E-01
-13.17	19.1	7.35E-01	5.08E-01	-13.35	20.3	8.42E-01	5.53E-01
-14.19	19.1	8.03E-01	3.13E-01	-14.09	20.0	8.86E-01	4.38E-01
-15.13	19.7	8.62E-01	1.95E-01	-15.07	19.4	9.66E-01	2.31E-01
-15.98	20.7	9.18E-01	8.05E-02	-15.76	19.3	1.02E+00	1.36E-01
-16.96	20.6	1.01E+00	0.00E+00	-17.41	19.3	1.14E+00	0.00E+00

Table B.1: Experimental data for single discharge (cont.)

Set No. 1 − 9 P_0 = 448 kPa ΔP = 128 kPa R = 1006 $(kg.m)^{-1/2}$				Set No. 1 − 10 P_0 = 517 kPa ΔP = 128 kPa R = 1006 $(kg.m)^{-1/2}$			
h [mm]	T_o [^oC]	$\dot{m}_G$ [kg/min]	$\dot{m}_L$ [kg/min]	h [mm]	T_o [^oC]	$\dot{m}_G$ [kg/min]	$\dot{m}_L$ [kg/min]
16.57	21.4	0.00E+00	2.13E+01	16.69	19.2	0.00E+00	2.13E+01
15.48	21.2	9.37E-03	1.96E+01	15.29	19.3	1.34E-02	1.93E+01
14.60	20.7	1.53E-02	1.74E+01	14.06	19.4	2.56E-02	1.69E+01
13.30	20.4	3.85E-02	1.51E+01	12.83	19.7	4.84E-02	1.49E+01
12.29	20.4	5.14E-02	1.40E+01	11.32	19.9	7.25E-02	1.29E+01
10.95	20.2	6.87E-02	1.22E+01	9.88	20.9	1.04E-01	1.10E+01
9.80	20.2	8.96E-02	1.07E+01	8.37	20.4	1.33E-01	9.48E+00
8.46	20.4	1.15E-01	9.44E+00	7.00	20.5	1.70E-01	8.31E+00
7.10	20.5	1.43E-01	8.42E+00	5.60	20.3	1.96E-01	7.56E+00
5.87	21.0	1.75E-01	7.52E+00	4.29	20.5	2.22E-01	7.09E+00
4.43	21.0	2.01E-01	6.82E+00	2.75	20.0	2.71E-01	5.99E+00
3.21	21.0	2.24E-01	6.31E+00	1.46	19.8	3.13E-01	5.56E+00
1.73	21.2	2.67E-01	5.56E+00	-0.01	19.7	3.65E-01	5.13E+00
0.33	21.4	3.10E-01	5.17E+00	-1.42	19.7	4.21E-01	4.66E+00
-0.71	19.1	3.53E-01	4.70E+00	-2.85	19.5	4.87E-01	4.15E+00
-2.11	19.2	4.05E-01	4.19E+00	-4.15	19.4	5.37E-01	3.67E+00
-3.38	19.4	4.45E-01	3.74E+00	-5.62	19.4	5.91E-01	3.14E+00
-4.61	19.8	4.96E-01	3.32E+00	-7.02	19.3	6.58E-01	2.59E+00
-6.19	20.0	5.60E-01	2.78E+00	-8.28	19.2	7.16E-01	2.16E+00
-7.59	20.1	6.27E-01	2.32E+00	-9.72	19.2	7.97E-01	1.72E+00
-8.95	20.2	6.93E-01	1.91E+00	-11.07	21.2	8.83E-01	1.28E+00
-9.90	20.2	7.39E-01	1.60E+00	-12.30	21.1	9.58E-01	9.92E-01
-11.30	20.2	8.13E-01	1.18E+00	-13.70	21.1	1.05E+00	6.52E-01
-12.84	20.1	9.05E-01	7.58E-01	-15.17	21.2	1.17E+00	3.38E-01
-14.13	19.9	1.00E+00	4.66E-01	-16.40	21.1	1.28E+00	1.39E-01
-14.98	19.9	1.06E+00	3.35E-01	-17.69	21.0	1.41E+00	0.00E+00
-15.71	19.8	1.13E+00	2.03E-01				
-16.27	19.7	1.18E+00	1.12E-01				
-17.78	19.6	1.30E+00	0.00E+00				

Table B.1: Experimental data for single discharge (cont.)

Set No. 1 − 11 P_0 = 316 kPa ΔP = 123 kPa R = 1657 $(kg.m)^{-1/2}$				Set No. 1 − 12 P_0 = 316 kPa ΔP = 123 kPa R = 2951 $(kg.m)^{-1/2}$			
h [mm]	T_o [°C]	$\dot{m}_G$ [kg/min]	$\dot{m}_L$ [kg/min]	h [mm]	T_o [°C]	$\dot{m}_G$ [kg/min]	$\dot{m}_L$ [kg/min]
13.14	21.8	0.00E+00	1.27E+01	10.38	20.5	0.00E+00	7.13E+00
11.50	22.2	9.37E-03	1.03E+01	9.05	19.7	5.40E-03	5.76E+00
10.17	22.2	2.77E-02	8.31E+00	7.65	19.8	1.29E-02	4.70E+00
8.80	22.6	3.12E-02	7.05E+00	6.21	21.5	2.46E-02	4.00E+00
7.33	22.8	4.94E-02	5.95E+00	4.88	21.5	3.56E-02	3.38E+00
5.89	23.0	6.77E-02	5.17E+00	3.45	21.8	4.88E-02	2.81E+00
4.59	23.1	8.90E-02	4.55E+00	1.97	22.1	6.42E-02	2.29E+00
3.19	23.0	1.08E-01	4.04E+00	0.61	22.5	7.95E-02	1.91E+00
1.83	22.7	1.30E-01	3.59E+00	-0.87	23.2	1.00E-01	1.51E+00
0.46	22.7	1.57E-01	3.13E+00	-2.16	23.2	1.17E-01	1.22E+00
-0.97	22.6	1.82E-01	2.66E+00	-3.56	23.2	1.37E-01	9.63E-01
-2.37	21.6	2.05E-01	2.24E+00	-5.00	23.1	1.61E-01	7.12E-01
-3.73	20.7	2.30E-01	1.85E+00	-6.40	23.1	1.87E-01	5.52E-01
-5.03	20.1	2.64E-01	1.55E+00	-7.76	23.0	2.10E-01	3.87E-01
-6.22	20.0	2.93E-01	1.24E+00	-9.23	22.9	2.51E-01	2.23E-01
-7.69	19.9	3.36E-01	9.55E-01	-10.46	22.8	2.98E-01	1.16E-01
-9.15	19.6	3.87E-01	6.24E-01	-12.55	22.1	3.70E-01	4.60E-04
-10.48	19.1	4.45E-01	4.88E-01				
-11.25	18.6	4.82E-01	3.71E-01				
-12.37	18.5	5.40E-01	2.15E-01				
-13.28	18.4	5.85E-01	1.04E-01				
-14.85	18.2	6.53E-01	0.00E+00				

Table B.1: Experimental data for single discharge (cont.)

Set No. 1 − 13 P_0 = 517 kPa ΔP = 235 kPa R = 1605 $(kg.m)^{-1/2}$				*Set No.* 1 − 14 P_0 = 517 kPa ΔP = 235 kPa R = 3006 $(kg.m)^{-1/2}$			
h $[mm]$	T_o $[^oC]$	$\dot{m}_G$ $[kg/min]$	$\dot{m}_L$ $[kg/min]$	h $[mm]$	T_o $[^oC]$	$\dot{m}_G$ $[kg/min]$	$\dot{m}_L$ $[kg/min]$
15.56	20.2	0.00E+00	1.81E+01	11.82	19.6	0.00E+00	9.68E+00
14.06	19.4	1.22E-02	1.58E+01	10.45	19.4	1.06E-02	7.91E+00
12.72	18.9	2.79E-02	1.34E+01	9.15	19.4	2.09E-02	6.54E+00
11.32	18.6	4.94E-02	1.14E+01	7.85	19.4	3.75E-02	5.56E+00
9.99	18.2	7.11E-02	9.68E+00	6.38	19.5	5.78E-02	4.90E+00
8.38	18.0	9.83E-02	8.31E+00	4.87	19.8	7.77E-02	4.19E+00
7.01	17.8	1.26E-01	7.33E+00	3.46	19.9	9.79E-02	3.59E+00
5.64	19.3	1.55E-01	6.50E+00	2.02	20.2	1.20E-01	3.08E+00
4.30	19.2	1.80E-01	5.88E+00	0.65	20.5	1.42E-01	2.58E+00
2.90	19.1	2.05E-01	5.29E+00	-0.72	21.7	1.69E-01	2.10E+00
1.46	19.1	2.39E-01	4.70E+00	-2.20	21.7	1.98E-01	1.75E+00
0.06	19.2	2.77E-01	4.15E+00	-3.60	21.8	2.15E-01	1.38E+00
-1.27	19.2	3.11E-01	3.55E+00	-4.90	22.0	2.47E-01	1.10E+00
-2.75	19.2	3.59E-01	3.11E+00	-6.27	22.0	2.81E-01	8.48E-01
-4.11	19.2	4.09E-01	2.61E+00	-7.88	22.0	3.36E-01	5.60E-01
-5.48	19.0	4.63E-01	2.22E+00	-9.29	22.1	3.96E-01	4.08E-01
-6.99	19.0	5.25E-01	1.80E+00	-10.37	22.0	4.54E-01	2.80E-01
-8.35	18.9	5.88E-01	1.44E+00	-11.46	21.9	5.14E-01	1.63E-01
-9.79	18.9	6.61E-01	1.09E+00	-13.56	21.8	6.27E-01	2.40E-04
-11.26	18.9	7.48E-01	7.48E-01				
-12.74	18.8	8.45E-01	4.41E-01				
-13.79	18.8	9.14E-01	2.84E-01				
-14.73	18.9	9.86E-01	1.24E-01				
-15.92	18.9	1.06E+00	0.00E+00				

APPENDIX C

Experimental Data for Dual Discharge (Centerlines of Branches in the Same Horizontal Plane)

Table C.1: Experimental data for dual discharge
(Centerlines of branches in the same horizontal plane)

Set No. 2 − 1

$L/d =$	1.5	
$P_0 =$	316	kPa
$\Delta P =$	123	kPa
$R =$	1004	$(kg.m)^{-1/2}$

h	T_o	Right Branch		Left Branch	
		$\dot{m}_G$	$\dot{m}_L$	$\dot{m}_G$	$\dot{m}_L$
$[mm]$	$[^oC]$	$[kg/min]$	$[kg/min]$	$[kg/min]$	$[kg/min]$
21.37	23.2	0.00E+00	2.06E+01	0.00E+00	2.13E+01
19.24	23.5	7.55E-03	1.80E+01	7.55E-03	1.83E+01
16.75	23.4	2.40E-02	1.47E+01	2.55E-02	1.45E+01
14.58	23.5	4.30E-02	1.18E+01	4.29E-02	1.20E+01
12.51	23.5	6.33E-02	9.72E+00	6.22E-02	9.83E+00
10.45	23.5	8.51E-02	8.27E+00	8.41E-02	8.34E+00
8.32	20.0	1.13E-01	7.17E+00	1.12E-01	7.24E+00
6.22	20.6	1.42E-01	6.35E+00	1.44E-01	6.30E+00
4.19	21.0	1.81E-01	5.56E+00	1.81E-01	5.52E+00
2.05	21.3	2.10E-01	4.82E+00	2.24E-01	4.98E+00
-0.05	21.4	2.50E-01	4.35E+00	2.66E-01	4.35E+00
-2.19	21.6	2.93E-01	3.67E+00	3.07E-01	3.74E+00
-4.26	22.1	3.37E-01	3.13E+00	3.56E-01	3.15E+00
-6.39	22.6	3.92E-01	2.57E+00	3.97E-01	2.63E+00
-8.49	22.8	4.52E-01	2.07E+00	4.72E-01	2.14E+00
-10.59	23.0	4.99E-01	1.57E+00	5.29E-01	1.64E+00
-12.73	23.0	5.79E-01	1.13E+00	6.11E-01	1.13E+00
-14.79	22.9	6.63E-01	7.19E-01	7.01E-01	7.00E-01
-17.59	22.8	7.83E-01	3.54E-01	8.50E-01	2.81E-01
-21.01	22.3	1.01E+00	0.00E+00	1.05E+00	0.00E+00

Table C.1: Experimental data for dual discharge (cont.)
(Centerlines of branches in the same horizontal plane)

Set No. $2-2$
$L/d =$ 1.5
$P_0 =$ 316 kPa
$\Delta P =$ 82 kPa
$R =$ 1004 $(kg.m)^{-1/2}$

h	T_o	Right Branch		Left Branch	
		$\dot{m}_G$	$\dot{m}_L$	$\dot{m}_G$	$\dot{m}_L$
$[mm]$	$[^oC]$	$[kg/min]$	$[kg/min]$	$[kg/min]$	$[kg/min]$
19.63	20.8	0.00E+00	1.70E+01	0.00E+00	1.71E+01
17.53	22.1	8.16E-03	1.46E+01	6.63E-03	1.49E+01
14.97	22.5	2.74E-02	1.15E+01	2.50E-02	1.15E+01
12.87	22.6	4.46E-02	9.40E+00	4.09E-02	9.32E+00
10.77	22.7	6.66E-02	7.84E+00	6.11E-02	7.75E+00
8.67	22.6	8.94E-02	6.66E+00	8.51E-02	6.58E+00
6.53	22.5	1.13E-01	5.68E+00	1.12E-01	5.68E+00
4.50	22.9	1.45E-01	5.13E+00	1.42E-01	5.02E+00
2.36	23.1	1.83E-01	4.43E+00	1.82E-01	4.43E+00
-0.09	23.3	2.22E-01	3.86E+00	2.36E-01	3.87E+00
-2.23	23.3	2.75E-01	3.28E+00	2.64E-01	3.26E+00
-4.29	23.3	3.07E-01	2.81E+00	3.21E-01	2.81E+00
-6.39	23.3	3.53E-01	2.25E+00	3.74E-01	2.24E+00
-8.49	23.4	4.24E-01	1.78E+00	4.09E-01	1.81E+00
-10.56	23.5	4.69E-01	1.33E+00	4.84E-01	1.32E+00
-12.69	23.6	5.29E-01	9.27E-01	5.45E-01	9.04E-01
-14.79	23.6	6.03E-01	5.53E-01	6.23E-01	4.98E-01
-16.82	23.5	7.14E-01	3.01E-01	7.54E-01	2.21E-01
-19.97	23.3	9.14E-01	0.00E+00	9.32E-01	0.00E+00

Table C.1: Experimental data for dual discharge (cont.)
(Centerlines of branches in the same horizontal plane)

Set No. 2 − 3

$L/d = 1.5$

$P_0 = 316\ kPa$

$\Delta P = 40\ kPa$

$R = 983\ (kg.m)^{-1/2}$

h	T_o	Right Branch		Left Branch	
		$\dot{m}_G$	$\dot{m}_L$	$\dot{m}_G$	$\dot{m}_L$
$[mm]$	$[^oC]$	$[kg/min]$	$[kg/min]$	$[kg/min]$	$[kg/min]$
16.86	21.6	0.00E+00	1.21E+01	0.00E+00	1.23E+01
14.72	22.9	8.16E-03	9.87E+00	7.40E-03	9.87E+00
12.58	22.9	2.16E-02	7.91E+00	2.02E-02	7.87E+00
10.43	19.9	3.85E-02	6.39E+00	3.62E-02	6.38E+00
8.36	20.1	5.54E-02	5.29E+00	5.32E-02	5.33E+00
6.29	20.7	7.79E-02	4.55E+00	7.56E-02	4.55E+00
3.84	21.4	1.12E-01	3.83E+00	1.10E-01	3.82E+00
1.70	21.9	1.42E-01	3.27E+00	1.40E-01	3.25E+00
-0.40	23.1	1.81E-01	2.82E+00	1.83E-01	2.84E+00
-2.54	23.3	2.09E-01	2.33E+00	2.22E-01	2.35E+00
-4.61	23.4	2.48E-01	1.89E+00	2.58E-01	1.90E+00
-6.74	23.4	2.93E-01	1.50E+00	3.06E-01	1.51E+00
-8.84	23.4	3.36E-01	1.11E+00	3.51E-01	1.10E+00
-10.94	23.3	3.90E-01	7.16E-01	4.05E-01	7.14E-01
-13.04	23.2	4.67E-01	4.80E-01	4.85E-01	4.53E-01
-15.11	23.0	5.31E-01	2.03E-01	5.57E-01	1.81E-01
-17.83	22.7	6.77E-01	0.00E+00	6.97E-01	0.00E+00

Table C.1: Experimental data for dual discharge (cont.)
(Centerlines of branches in the same horizontal plane)

$Set\ No.\ 2-4$
$L/d =$ 1.5
$P_0 =$ 316 kPa
$\Delta P =$ 123 kPa
$R =$ 1618 $(kg.m)^{-1/2}$

h	T_o	Right Branch		Left Branch	
		$\dot{m}_G$	$\dot{m}_L$	$\dot{m}_G$	$\dot{m}_L$
$[mm]$	$[°C]$	$[kg/min]$	$[kg/min]$	$[kg/min]$	$[kg/min]$
17.28	22.5	0.00E+00	1.32E+01	0.00E+00	1.28E+01
15.01	23.0	8.01E-03	1.06E+01	5.87E-03	1.04E+01
12.90	23.3	1.95E-02	8.31E+00	1.91E-02	8.26E+00
10.80	23.4	3.71E-02	6.74E+00	3.67E-02	6.77E+00
8.67	21.3	5.80E-02	5.72E+00	5.76E-02	5.68E+00
6.60	21.5	8.13E-02	4.86E+00	7.63E-02	4.86E+00
3.80	21.8	1.13E-01	3.90E+00	1.12E-01	3.87E+00
1.73	22.2	1.37E-01	3.20E+00	1.41E-01	3.19E+00
-0.44	22.5	1.67E-01	2.60E+00	1.69E-01	2.66E+00
-2.57	22.4	2.01E-01	2.10E+00	2.06E-01	2.17E+00
-4.60	21.1	2.24E-01	1.70E+00	2.33E-01	1.73E+00
-6.70	21.1	2.66E-01	1.32E+00	2.73E-01	1.35E+00
-8.84	21.2	3.10E-01	9.55E-01	3.21E-01	9.87E-01
-10.94	21.3	3.68E-01	6.24E-01	3.80E-01	6.29E-01
-13.07	21.3	4.49E-01	4.08E-01	4.57E-01	3.93E-01
-15.13	21.4	5.28E-01	1.79E-01	5.45E-01	1.62E-01
-17.12	21.3	6.25E-01	0.00E+00	6.33E-01	0.00E+00

Table C.1: Experimental data for dual discharge (cont.)
(Centerlines of branches in the same horizontal plane)

$Set\ No.\ 2-5$ $L/d =$ 8.0 $P_0 =$ 316 kPa $\Delta P =$ 123 kPa $R =$ 2926 $(kg.m)^{-1/2}$					
h	T_o	Right Branch		Left Branch	
		$\dot{m}_G$	$\dot{m}_L$	$\dot{m}_G$	$\dot{m}_L$
$[mm]$	$[^oC]$	$[kg/min]$	$[kg/min]$	$[kg/min]$	$[kg/min]$
13.11	22.2	0.00E+00	7.21E+00	0.00E+00	7.16E+00
10.98	23.3	6.33E-03	5.56E+00	5.71E-03	5.56E+00
8.91	24.0	1.58E-02	4.35E+00	1.44E-02	4.24E+00
6.77	24.4	3.16E-02	3.46E+00	3.02E-02	3.46E+00
4.64	25.1	4.74E-02	2.76E+00	4.61E-02	2.77E+00
2.53	25.3	6.75E-02	2.20E+00	6.54E-02	2.20E+00
0.47	25.0	9.21E-02	1.73E+00	8.59E-02	1.75E+00
-1.63	25.0	1.12E-01	1.35E+00	1.10E-01	1.36E+00
-3.77	25.1	1.41E-01	9.99E-01	1.39E-01	1.00E+00
-5.87	25.1	1.73E-01	6.94E-01	1.69E-01	7.07E-01
-7.97	25.0	2.01E-01	4.84E-01	2.10E-01	4.84E-01
-10.77	24.9	2.64E-01	1.99E-01	2.75E-01	1.93E-01
-14.05	24.5	3.67E-01	0.00E+00	3.78E-01	0.00E+00

Table C.1: Experimental data for dual discharge (cont.)
(Centerlines of branches in the same horizontal plane)

Set No. 2 − 6					
$L/d =$ 1.5					
P_0 = 517 kPa					
ΔP = 235 kPa					
R = 993 $(kg.m)^{-1/2}$					
		Right Branch		Left Branch	
h [mm]	T_o [°C]	$\dot{m}_G$ [kg/min]	$\dot{m}_L$ [kg/min]	$\dot{m}_G$ [kg/min]	$\dot{m}_L$ [kg/min]
24.77	17.9	0.00E+00	2.91E+01	0.00E+00	2.94E+01
22.63	18.5	1.41E-02	2.60E+01	1.34E-02	2.65E+01
20.49	19.2	3.63E-02	2.22E+01	3.31E-02	2.23E+01
18.38	19.7	6.88E-02	1.91E+01	6.28E-02	1.91E+01
16.27	19.8	9.95E-02	1.63E+01	9.50E-02	1.64E+01
14.15	20.0	1.30E-01	1.42E+01	1.26E-01	1.41E+01
12.37	20.2	1.59E-01	1.27E+01	1.53E-01	1.26E+01
10.23	20.2	2.01E-01	1.09E+01	1.97E-01	1.08E+01
8.05	20.2	2.36E-01	9.48E+00	2.46E-01	9.36E+00
5.94	20.4	2.83E-01	8.38E+00	2.91E-01	8.26E+00
3.80	20.4	3.48E-01	7.52E+00	3.48E-01	7.44E+00
1.73	20.5	4.15E-01	6.74E+00	4.09E-01	6.62E+00
-0.41	20.5	4.84E-01	5.95E+00	4.84E-01	5.80E+00
-2.52	20.6	5.46E-01	5.21E+00	5.42E-01	5.09E+00
-4.56	20.8	6.16E-01	4.70E+00	6.06E-01	4.55E+00
-7.05	20.9	7.31E-01	3.87E+00	7.28E-01	3.75E+00
-9.15	21.1	8.02E-01	3.11E+00	8.14E-01	3.10E+00
-11.33	21.1	8.87E-01	2.43E+00	9.25E-01	2.47E+00
-13.40	21.1	9.93E-01	1.87E+00	1.04E+00	1.90E+00
-15.46	20.7	1.09E+00	1.36E+00	1.15E+00	1.34E+00
-17.64	20.7	1.23E+00	9.45E-01	1.31E+00	7.96E-01
-24.27	20.8	1.77E+00	0.00E+00	1.80E+00	0.00E+00

Table C.1: Experimental data for dual discharge (cont.)
(Centerlines of branches in the same horizontal plane)

Set No. 2 − 7
$L/d =$ 1.5
$P_0 =$ 517 kPa
$\Delta P =$ 166 kPa
$R =$ 990 $(kg.m)^{-1/2}$

h	T_o	Right Branch		Left Branch	
		$\dot{m}_G$	$\dot{m}_L$	$\dot{m}_G$	$\dot{m}_L$
$[mm]$	$[^oC]$	$[kg/min]$	$[kg/min]$	$[kg/min]$	$[kg/min]$
22.94	19.5	0.00E+00	2.46E+01	0.00E+00	2.47E+01
20.80	19.8	1.56E-02	2.18E+01	1.26E-02	2.21E+01
18.69	20.1	3.73E-02	1.86E+01	3.56E-02	1.84E+01
16.58	20.3	6.95E-02	1.58E+01	6.55E-02	1.57E+01
14.54	20.5	1.03E-01	1.35E+01	9.44E-02	1.35E+01
12.40	20.7	1.31E-01	1.18E+01	1.23E-01	1.16E+01
10.26	20.7	1.68E-01	9.95E+00	1.63E-01	9.79E+00
8.22	20.7	1.99E-01	8.70E+00	2.07E-01	8.62E+00
6.12	20.7	2.44E-01	7.72E+00	2.47E-01	7.56E+00
3.97	20.8	2.93E-01	6.74E+00	3.00E-01	6.81E+00
1.90	20.7	3.51E-01	5.99E+00	3.55E-01	6.03E+00
-0.20	20.8	4.23E-01	5.41E+00	4.26E-01	5.41E+00
-2.35	20.9	4.85E-01	4.78E+00	4.85E-01	4.70E+00
-4.45	20.9	5.49E-01	4.15E+00	5.49E-01	4.16E+00
-6.56	20.9	6.32E-01	3.46E+00	6.37E-01	3.46E+00
-8.63	20.9	7.06E-01	2.91E+00	7.20E-01	2.86E+00
-10.73	20.8	7.98E-01	2.30E+00	8.12E-01	2.32E+00
-12.91	20.8	8.85E-01	1.72E+00	9.15E-01	1.73E+00
-15.01	20.8	9.91E-01	1.22E+00	1.04E+00	1.16E+00
-17.08	20.7	1.13E+00	8.01E-01	1.19E+00	6.71E-01
-23.29	20.6	1.63E+00	0.00E+00	1.67E+00	0.00E+00

Table C.1: Experimental data for dual discharge (cont.)
(Centerlines of branches in the same horizontal plane)

$Set\ No.\ 2-8$
$L/d = 1.5$
$P_0 = 517\ kPa$
$\Delta P = 97\ kPa$
$R = 996\ (kg.m)^{-1/2}$

h	T_o	Right Branch		Left Branch	
		$\dot{m}_G$	$\dot{m}_L$	$\dot{m}_G$	$\dot{m}_L$
$[mm]$	$[^oC]$	$[kg/min]$	$[kg/min]$	$[kg/min]$	$[kg/min]$
20.37	19.6	0.00E+00	1.86E+01	0.00E+00	1.88E+01
18.20	19.9	1.56E-02	1.62E+01	1.31E-02	1.64E+01
16.09	20.2	4.15E-02	1.40E+01	3.89E-02	1.39E+01
13.98	20.6	6.75E-02	1.14E+01	6.16E-02	1.15E+01
11.84	20.9	9.77E-02	9.60E+00	9.21E-02	9.48E+00
9.77	20.8	1.28E-01	8.31E+00	1.20E-01	8.14E+00
7.66	20.8	1.67E-01	7.13E+00	1.61E-01	6.97E+00
5.55	20.9	2.06E-01	6.27E+00	2.01E-01	6.19E+00
3.45	20.9	2.40E-01	5.56E+00	2.53E-01	5.41E+00
1.31	21.0	3.07E-01	4.94E+00	2.96E-01	4.94E+00
-0.76	20.9	3.58E-01	4.55E+00	3.64E-01	4.43E+00
-2.87	20.9	4.12E-01	3.83E+00	4.23E-01	3.72E+00
-7.05	21.0	5.52E-01	2.65E+00	5.45E-01	2.65E+00
-9.19	21.1	6.22E-01	2,08E+00	6.40E-01	2.08E+00
-11.33	21.2	6.99E-01	1.57E+00	7.25E-01	1.58E+00
-13.40	21.2	8.07E-01	1.14E+00	8.21E-01	1.11E+00
-15.50	21.3	9.05E-01	7.12E-01	9.26E-01	6.36E-01
-21.33	21.2	1.36E+00	0.00E+00	1.39E+00	0.00E+00

Table C.1: Experimental data for dual discharge (cont.)
(Centerlines of branches in the same horizontal plane)

Set No. 2 − 9
$L/d =$ 1.5
$P_0 =$ 517 kPa
$\Delta P =$ 235 kPa
$R =$ 1600 $(kg.m)^{-1/2}$

h	T_o	Right Branch		Left Branch	
		$\dot{m}_G$	$\dot{m}_L$	$\dot{m}_G$	$\dot{m}_L$
$[mm]$	$[^oC]$	$[kg/min]$	$[kg/min]$	$[kg/min]$	$[kg/min]$
19.95	21.9	0.00E+00	1.83E+01	0.00E+00	1.80E+01
17.87	22.6	1.45E-02	1.55E+01	1.09E-02	1.53E+01
15.77	22.7	3.31E-02	1.30E+01	2.87E-02	1.28E+01
13.62	22.7	5.78E-02	1.07E+01	5.41E-02	1.05E+01
11.54	22.7	8.38E-02	9.01E+00	8.29E-02	8.93E+00
9.41	22.6	1.17E-01	7.60E+00	1.14E-01	7.60E+00
7.33	22.4	1.52E-01	6.42E+00	1.50E-01	6.42E+00
5.23	22.4	1.85E-01	5.56E+00	1.85E-01	5.56E+00
3.12	22.7	2.19E-01	4.82E+00	2.29E-01	4.86E+00
0.98	22.5	2.61E-01	4.27E+00	2.73E-01	4.24E+00
-1.13	22.7	3.04E-01	3.55E+00	3.16E-01	3.65E+00
-3.22	21.0	3.53E-01	2.96E+00	3.66E-01	2.99E+00
-5.29	21.0	4.08E-01	2.41E+00	4.23E-01	2.43E+00
-7.44	21.2	4.72E-01	1.91E+00	4.84E-01	1.94E+00
-9.51	21.4	5.42E-01	1.46E+00	5.45E-01	1.49E+00
-10.91	21.8	5.91E-01	1.21E+00	6.03E-01	1.21E+00
-13.05	22.0	6.69E-01	8.37E-01	6.96E-01	8.32E-01
-15.12	22.1	8.07E-01	4.94E-01	8.44E-01	4.45E-01
-19.49	22.1	9.25E-01	0.00E+00	9.43E-01	0.00E+00

Table C.1: Experimental data for dual discharge (cont.)
(Centerlines of branches in the same horizontal plane)

$Set\ No.\ 2-10$
$L/d = 1.5$
$P_0 = 517\ kPa$
$\Delta P = 235\ kPa$
$R = 2852\ (kg.m)^{-1/2}$

h [mm]	T_o [°C]	Right Branch $\dot{m}_G$ [kg/min]	Right Branch $\dot{m}_L$ [kg/min]	Left Branch $\dot{m}_G$ [kg/min]	Left Branch $\dot{m}_L$ [kg/min]
15.16	22.5	0.00E+00	1.03E+01	0.00E+00	1.01E+01
13.05	24.9	1.18E-02	8.03E+00	1.06E-02	8.14E+00
10.95	25.3	2.72E-02	6.35E+00	2.39E-02	6.27E+00
8.87	25.6	4.74E-02	5.17E+00	4.39E-02	5.06E+00
6.77	25.7	7.15E-02	4.39E+00	6.83E-02	4.24E+00
4.62	25.6	9.71E-02	3.58E+00	9.43E-02	3.52E+00
2.53	21.1	1.28E-01	2.89E+00	1.25E-01	2.90E+00
0.46	21.3	1.57E-01	2.37E+00	1.56E-01	2.36E+00
-1.68	21.4	1.91E-01	1.87E+00	1.92E-01	1.86E+00
-3.82	21.5	2.22E-01	1.45E+00	2.33E-01	1.45E+00
-5.89	21.6	2.66E-01	1.11E+00	2.75E-01	1.10E+00
-8.00	21.6	3.13E-01	7.41E-01	3.23E-01	7.43E-01
-10.21	21.5	3.81E-01	5.18E-01	3.95E-01	4.92E-01
-13.15	21.5	4.96E-01	1.91E-01	5.14E-01	1.89E-01
-15.53	21.5	6.14E-01	0.00E+00	6.22E-01	0.00E+00

Table C.1: Experimental data for dual discharge (cont.)
(Centerlines of branches in the same horizontal plane)

Set No. 2 − 11
$L/d =$ 2.0
$P_0 =$ 316 kPa
$\Delta P =$ 123 kPa
$R =$ 998 $(kg.m)^{-1/2}$

h	T_o	Right Branch		Left Branch	
		$\dot{m}_G$	$\dot{m}_L$	$\dot{m}_G$	$\dot{m}_L$
$[mm]$	$[^oC]$	$[kg/min]$	$[kg/min]$	$[kg/min]$	$[kg/min]$
20.87	26.5	0.00E+00	2.13E+01	0.00E+00	2.09E+01
18.60	26.5	9.52E-03	1.79E+01	8.91E-03	1.78E+01
16.50	26.5	2.38E-02	1.46E+01	2.11E-02	1.45E+01
14.40	26.5	4.15E-02	1.20E+01	3.80E-02	1.19E+01
12.30	26.5	5.94E-02	9.72E+00	5.71E-02	9.60E+00
10.20	25.7	8.28E-02	8.31E+00	8.09E-02	8.14E+00
8.10	25.7	1.16E-01	7.13E+00	1.09E-01	6.97E+00
6.00	25.9	1.48E-01	6.31E+00	1.41E-01	6.15E+00
3.90	26.1	1.87E-01	5.56E+00	1.81E-01	5.41E+00
1.80	26.2	2.19E-01	4.78E+00	2.22E-01	4.63E+00
-0.31	26.0	2.54E-01	4.19E+00	2.61E-01	4.08E+00
-2.41	26.0	3.01E-01	3.51E+00	3.03E-01	3.44E+00
-4.51	25.9	3.51E-01	2.81E+00	3.53E-01	2.81E+00
-6.61	25.8	4.00E-01	2.34E+00	4.06E-01	2.30E+00
-8.70	25.6	4.67E-01	1.83E+00	4.73E-01	1.81E+00
-10.80	25.6	5.28E-01	1.54E+00	5.29E-01	1.51E+00
-12.90	25.4	6.00E-01	9.19E-01	6.09E-01	9.69E-01
-15.00	25.0	6.75E-01	5.36E-01	7.04E-01	5.12E-01
-16.39	23.9	7.32E-01	4.17E-01	7.69E-01	3.85E-01
-20.13	23.8	9.71E-01	0.00E+00	9.78E-01	0.00E+00

Table C.1: Experimental data for dual discharge (cont.)
(Centerlines of branches in the same horizontal plane)

Set $No.$ 2 − 12
$L/d =$ 2.0
$P_0 =$ 316 kPa
$\Delta P =$ 82 kPa
$R =$ 1003 $(kg.m)^{-1/2}$

h	T_o	Right Branch		Left Branch	
		$\dot{m}_G$	$\dot{m}_L$	$\dot{m}_G$	$\dot{m}_L$
$[mm]$	$[^oC]$	$[kg/min]$	$[kg/min]$	$[kg/min]$	$[kg/min]$
19.06	25.4	0.00E+00	1.73E+01	0.00E+00	1.68E+01
16.89	25.6	9.67E-03	1.44E+01	9.37E-03	1.45E+01
14.96	25.6	2.15E-02	1.18E+01	1.97E-02	1.18E+01
12.82	25.7	3.87E-02	9.52E+00	3.58E-02	9.40E+00
10.72	25.7	5.86E-02	7.91E+00	5.50E-02	7.79E+00
8.66	25.2	8.37E-02	6.70E+00	7.94E-02	6.54E+00
6.52	25.4	1.17E-01	5.84E+00	1.09E-01	5.64E+00
4.42	25.5	1.52E-01	5.13E+00	1.43E-01	4.94E+00
2.36	25.6	1.86E-01	4.39E+00	1.78E-01	4.20E+00
0.22	25.7	2.15E-01	3.80E+00	2.20E-01	3.65E+00
-1.88	26.1	2.53E-01	3.14E+00	2.56E-01	3.10E+00
-3.98	25.6	2.96E-01	2.58E+00	3.03E-01	2.55E+00
-6.08	25.5	3.48E-01	2.09E+00	3.51E-01	2.05E+00
-8.18	25.4	4.05E-01	1.61E+00	4.11E-01	1.60E+00
-10.28	25.3	4.72E-01	1.17E+00	4.82E-01	1.16E+00
-12.38	25.0	5.40E-01	7.65E-01	5.51E-01	7.43E-01
-15.44	21.2	6.85E-01	3.67E-01	7.14E-01	3.43E-01
-19.15	21.3	9.39E-01	0.00E+00	9.41E-01	0.00E+00

Table C.1: Experimental data for dual discharge (cont.)
(Centerlines of branches in the same horizontal plane)

$Set\ No.\ 2-13$
$L/d = 2.0$
$P_0 = 316\ kPa$
$\Delta P = 40\ kPa$
$R = 995\ (kg.m)^{-1/2}$

h	T_o	Right Branch		Left Branch	
		$\dot{m}_G$	$\dot{m}_L$	$\dot{m}_G$	$\dot{m}_L$
$[mm]$	$[^oC]$	$[kg/min]$	$[kg/min]$	$[kg/min]$	$[kg/min]$
16.09	22.5	0.00E+00	1.22E+01	0.00E+00	1.20E+01
11.99	23.8	2.12E-02	7.60E+00	2.00E-02	7.56E+00
9.82	24.0	3.75E-02	6.11E+00	3.62E-02	5.99E+00
7.76	24.1	5.99E-02	5.17E+00	5.73E-02	5.02E+00
5.76	24.2	8.53E-02	4.39E+00	7.93E-02	4.24E+00
3.45	24.3	1.17E-01	3.76E+00	1.10E-01	3.62E+00
1.42	24.3	1.47E-01	3.14E+00	1.40E-01	3.01E+00
-0.65	24.4	1.78E-01	2.62E+00	1.74E-01	2.53E+00
-2.74	22.2	2.19E-01	2.20E+00	2.22E-01	2.15E+00
-4.84	22.5	2.53E-01	1.74E+00	2.61E-01	1.68E+00
-6.91	22.6	3.00E-01	1.31E+00	3.07E-01	1.30E+00
-9.04	22.6	3.52E-01	9.09E-01	3.65E-01	9.18E-01
-11.14	22.7	4.18E-01	5.57E-01	4.30E-01	5.79E-01
-14.15	22.7	5.23E-01	2.23E-01	5.48E-01	2.01E-01
-16.74	22.3	6.94E-01	0.00E+00	6.94E-01	0.00E+00

Table C.1: Experimental data for dual discharge (cont.)
(Centerlines of branches in the same horizontal plane)

Set No. 2 − 14 $L/d =$ 2.0 $P_0 =$ 316 kPa $\Delta P =$ 123 kPa $R =$ 1552 $(kg.m)^{-1/2}$					
		Right Branch		Left Branch	
h [mm]	T_o [^oC]	$\dot{m}_G$ [kg/min]	$\dot{m}_L$ [kg/min]	$\dot{m}_G$ [kg/min]	$\dot{m}_L$ [kg/min]
16.68	26.2	0.00E+00	1.38E+01	0.00E+00	1.33E+01
14.51	26.4	9.22E-03	1.07E+01	9.22E-03	1.06E+01
12.62	40.0	2.07E-02	8.50E+00	2.07E-02	8.54E+00
10.56	23.1	3.95E-02	7.13E+00	3.95E-02	6.97E+00
8.49	23.4	6.16E-02	5.80E+00	6.16E-02	5.68E+00
6.46	23.4	8.30E-02	4.98E+00	8.30E-02	4.90E+00
4.36	23.6	1.10E-01	4.23E+00	1.10E-01	4.16E+00
2.26	23.8	1.39E-01	3.51E+00	1.39E-01	3.38E+00
0.16	24.1	1.65E-01	2.81E+00	1.65E-01	2.75E+00
-1.98	24.4	1.96E-01	2.26E+00	1.96E-01	2.24E+00
-4.05	24.8	2.22E-01	1.77E+00	2.22E-01	1.75E+00
-6.29	25.2	2.67E-01	1.34E+00	2.67E-01	1.35E+00
-8.35	25.3	3.19E-01	9.73E-01	3.19E-01	9.69E-01
-10.45	25.4	3.81E-01	6.31E-01	3.81E-01	6.29E-01
-12.55	25.5	4.63E-01	4.21E-01	4.63E-01	4.27E-01
-14.68	25.2	5.45E-01	1.71E-01	5.45E-01	1.54E-01
-17.06	24.2	6.74E-01	0.00E+00	6.73E-01	0.00E+00

Table C.1: Experimental data for dual discharge (cont.)
(Centerlines of branches in the same horizontal plane)

$Set\ No.\ 2-15$					
$L/d =$ 2.0					
P_0 = 316 kPa					
ΔP = 123 kPa					
R = 2878 $(kg.m)^{-1/2}$					
		Right Branch		Left Branch	
h [mm]	T_o [^oC]	$\dot{m}_G$ [kg/min]	$\dot{m}_L$ [kg/min]	$\dot{m}_G$ [kg/min]	$\dot{m}_L$ [kg/min]
12.63	21.6	0.00E+00	7.33E+00	0.00E+00	7.28E+00
10.53	22.8	7.09E-03	5.52E+00	6.94E-03	5.41E+00
8.50	23.1	1.60E-02	4.35E+00	1.64E-02	4.24E+00
6.43	23.6	3.14E-02	3.38E+00	3.13E-02	3.34E+00
4.26	23.3	4.82E-02	2.68E+00	4.74E-02	2.67E+00
2.19	23.6	6.75E-02	2.08E+00	6.77E-02	2.09E+00
0.06	23.7	9.04E-02	1.58E+00	9.04E-02	1.60E+00
-2.08	23.8	1.16E-01	1.20E+00	1.17E-01	1.19E+00
-4.15	23.9	1.47E-01	8.73E-01	1.45E-01	8.61E-01
-6.28	23.9	1.86E-01	5.46E-01	1.82E-01	5.47E-01
-8.35	23.8	2.22E-01	3.50E-01	2.31E-01	3.30E-01
-10.48	23.7	2.78E-01	1.43E-01	2.91E-01	1.54E-01
-13.17	22.8	3.65E-01	0.00E+00	3.80E-01	0.00E+00

Table C.1: Experimental data for dual discharge (cont.)
(Centerlines of branches in the same horizontal plane)

$Set\ No.\ 2-16$
$L/d = 2.0$
$P_0 = 517\ kPa$
$\Delta P = 235\ kPa$
$R = 982\ (kg.m)^{-1/2}$

h	T_o	Right Branch		Left Branch	
		$\dot{m}_G$	$\dot{m}_L$	$\dot{m}_G$	$\dot{m}_L$
$[mm]$	$[^oC]$	$[kg/min]$	$[kg/min]$	$[kg/min]$	$[kg/min]$
23.83	22.9	0.00E+00	2.98E+01	0.00E+00	2.94E+01
21.69	23.8	2.02E-02	2.56E+01	1.71E-02	2.57E+01
19.58	23.9	4.15E-02	2.16E+01	3.81E-02	2.17E+01
17.47	24.0	7.05E-02	1.81E+01	6.56E-02	1.80E+01
15.33	24.1	9.92E-02	1.57E+01	9.41E-02	1.56E+01
13.26	24.1	1.33E-01	1.34E+01	1.28E-01	1.33E+01
11.17	22.0	1.67E-01	1.14E+01	1.61E-01	1.14E+01
9.02	22.5	2.05E-01	9.87E+00	2.08E-01	9.76E+00
6.92	22.6	2.50E-01	8.66E+00	2.50E-01	8.54E+00
4.81	23.0	3.03E-01	7.60E+00	3.03E-01	7.48E+00
2.73	23.2	3.56E-01	6.74E+00	3.58E-01	6.58E+00
0.63	23.3	4.24E-01	5.95E+00	4.21E-01	5.80E+00
-1.51	23.5	4.90E-01	5.21E+00	4.88E-01	5.06E+00
-3.62	23.5	5.55E-01	4.55E+00	5.54E-01	4.43E+00
-5.76	23.6	6.56E-01	3.93E+00	6.48E-01	3.79E+00
-7.86	23.6	7.38E-01	3.26E+00	7.40E-01	3.15E+00
-9.90	23.8	8.30E-01	2.55E+00	8.26E-01	2.57E+00
-12.04	23.6	9.32E-01	2.09E+00	9.44E-01	2.01E+00
-14.18	23.6	1.05E+00	1.55E+00	1.08E+00	1.48E+00
-16.21	23.6	1.18E+00	1.05E+00	1.23E+00	9.58E-01
-23.92	23.3	1.84E+00	0.00E+00	1.83E+00	0.00E+00

Table C.1: Experimental data for dual discharge (cont.)
(Centerlines of branches in the same horizontal plane)

$Set\ No.\ 2-17$
$L/d = 2.0$
$P_0 = 517\ kPa$
$\Delta P = 166\ kPa$
$R = 981\ (kg.m)^{-1/2}$

h	T_o	Right Branch		Left Branch	
		$\dot{m}_G$	$\dot{m}_L$	$\dot{m}_G$	$\dot{m}_L$
$[mm]$	$[^oC]$	$[kg/min]$	$[kg/min]$	$[kg/min]$	$[kg/min]$
22.10	24.1	0.00E+00	2.50E+01	0.00E+00	2.48E+01
19.96	24.3	1.97E-02	2.13E+01	1.70E-02	2.15E+01
17.86	24.5	4.15E-02	1.77E+01	3.75E-02	1.79E+01
15.86	24.5	6.71E-02	1.53E+01	6.28E-02	1.53E+01
13.72	24.7	9.67E-02	1.30E+01	7.26E-02	1.29E+01
11.68	24.8	1.29E-01	1.09E+01	1.24E-01	1.09E+01
9.50	24.8	1.67E-01	9.40E+00	1.62E-01	9.32E+00
7.53	25.1	2.03E-01	8.31E+00	2.00E-01	8.11E+00
5.34	22.2	2.50E-01	7.13E+00	2.51E-01	7.05E+00
3.23	22.3	3.06E-01	6.35E+00	3.07E-01	6.19E+00
1.12	22.8	3.61E-01	5.56E+00	3.64E-01	5.45E+00
-0.99	23.1	4.24E-01	4.90E+00	4.24E-01	4.74E+00
-3.09	23.4	4.85E-01	4.31E+00	4.92E-01	4.20E+00
-5.16	23.4	5.60E-01	3.61E+00	5.60E-01	3.50E+00
-7.30	23.3	6.61E-01	3.03E+00	6.58E-01	2.94E+00
-9.41	23.3	7.43E-01	2.43E+00	7.40E-01	2.37E+00
-11.51	23.2	8.46E-01	1.90E+00	8.60E-01	1.84E+00
-13.61	23.2	9.59E-01	1.35E+00	9.64E-01	1.30E+00
-15.72	23.0	1.09E+00	9.12E-01	1.13E+00	8.32E-01
-17.81	22.7	1.23E+00	5.32E-01	1.30E+00	4.24E-01
-22.76	22.5	1.68E+00	0.00E+00	1.67E+00	0.00E+00

Table C.1: Experimental data for dual discharge (cont.)
(Centerlines of branches in the same horizontal plane)

Set No. 2 − 18					
$L/d = 2.0$					
$P_0 = 517\ kPa$					
$\Delta P = 97\ kPa$					
$R = 990\ (kg.m)^{-1/2}$					
		Right Branch		Left Branch	
h [mm]	T_o [^oC]	$\dot{m}_G$ [kg/min]	$\dot{m}_L$ [kg/min]	$\dot{m}_G$ [kg/min]	$\dot{m}_L$ [kg/min]
19.62	23.2	0.00E+00	1.90E+01	0.00E+00	1.86E+01
17.48	23.5	1.90E-02	1.60E+01	1.70E-02	1.61E+01
15.37	23.7	4.20E-02	1.33E+01	3.97E-02	1.33E+01
13.23	23.9	6.75E-02	1.10E+01	6.38E-02	1.09E+01
11.12	24.0	9.58E-02	9.05E+00	9.04E-02	8.93E+00
9.05	24.1	1.31E-01	7.72E+00	1.25E-01	7.63E+00
6.91	24.2	1.75E-01	6.74E+00	1.65E-01	6.58E+00
4.81	22.6	2.08E-01	5.95E+00	2.15E-01	5.80E+00
2.67	22.6	2.54E-01	5.17E+00	2.56E-01	4.98E+00
0.60	22.6	3.09E-01	4.55E+00	3.07E-01	4.35E+00
-1.62	23.1	3.68E-01	3.95E+00	3.68E-01	3.80E+00
-3.72	23.2	4.36E-01	3.28E+00	4.38E-01	3.21E+00
-5.86	23.3	5.02E-01	2.69E+00	5.04E-01	2.63E+00
-8.00	23.4	5.75E-01	2.16E+00	5.75E-01	2.10E+00
-10.11	23.4	6.68E-01	1.63E+00	6.79E-01	1.59E+00
-12.18	23.5	7.65E-01	1.17E+00	7.69E-01	1.13E+00
-14.32	23.4	8.80E-01	7.48E-01	8.90E-01	7.00E-01
-17.08	23.0	1.07E+00	3.67E-01	1.12E+00	2.53E-01
-21.74	22.9	1.42E+00	0.00E+00	1.41E+00	0.00E+00

Table C.1: Experimental data for dual discharge (cont.)
(Centerlines of branches in the same horizontal plane)

$Set\ No.\ 2-19$
$L/d = 2.0$
$P_0 = 517\ kPa$
$\Delta P = 235\ kPa$
$R = 1528\ (kg.m)^{-1/2}$

h	T_o	Right Branch		Left Branch	
		$\dot{m}_G$	$\dot{m}_L$	$\dot{m}_G$	$\dot{m}_L$
$[mm]$	$[^oC]$	$[kg/min]$	$[kg/min]$	$[kg/min]$	$[kg/min]$
19.51	23.6	0.00E+00	1.93E+01	0.00E+00	1.87E+01
17.37	23.8	1.50E-02	1.58E+01	1.41E-02	1.57E+01
15.23	23.9	3.58E-02	1.30E+01	3.30E-02	1.29E+01
13.16	24.0	6.18E-02	1.07E+01	5.90E-02	1.05E+01
11.05	24.0	9.02E-02	9.05E+00	8.71E-02	8.93E+00
8.88	24.0	1.28E-01	7.52E+00	1.24E-01	7.36E+00
6.77	24.0	1.65E-01	6.42E+00	1.61E-01	6.38E+00
4.65	20.4	2.05E-01	5.60E+00	2.01E-01	5.41E+00
2.54	21.0	2.36E-01	4.78E+00	2.47E-01	4.67E+00
0.43	21.4	2.78E-01	4.04E+00	2.88E-01	4.00E+00
-1.68	21.9	3.21E-01	3.34E+00	3.36E-01	3.38E+00
-3.79	22.5	3.75E-01	2.79E+00	3.92E-01	2.79E+00
-5.90	22.9	4.39E-01	2.63E+00	4.54E-01	2.63E+00
-8.01	23.1	5.11E-01	1.74E+00	5.17E-01	1.75E+00
-10.08	23.2	6.13E-01	1.46E+00	6.05E-01	1.49E+00
-12.18	23.3	6.98E-01	9.09E-01	7.21E-01	9.04E-01
-14.31	23.3	8.11E-01	5.32E-01	8.42E-01	5.19E-01
-16.41	23.2	9.49E-01	3.01E-01	9.99E-01	2.21E-01
-19.04	21.1	1.14E+00	0.00E+00	1.14E+00	0.00E+00

Table C.1: Experimental data for dual discharge (cont.)
(Centerlines of branches in the same horizontal plane)

Set No. 2 − 20
$L/d =$ 2.0
$P_0 =$ 517 kPa
$\Delta P =$ 235 kPa
$R =$ 2863 $(kg.m)^{-1/2}$

h	T_o	Right Branch		Left Branch	
		$\dot{m}_G$	$\dot{m}_L$	$\dot{m}_G$	$\dot{m}_L$
$[mm]$	$[^oC]$	$[kg/min]$	$[kg/min]$	$[kg/min]$	$[kg/min]$
14.71	23.6	0.00E+00	1.02E+01	0.00E+00	1.01E+01
12.50	23.6	1.04E-02	7.91E+00	1.09E-02	8.07E+00
10.25	24.2	2.71E-02	5.95E+00	2.74E-02	6.03E+00
8.14	24.3	4.76E-02	4.82E+00	4.91E-02	4.90E+00
6.04	24.3	7.15E-02	4.00E+00	7.25E-02	4.00E+00
3.90	24.3	9.92E-02	3.30E+00	9.88E-02	3.29E+00
1.84	21.3	1.32E-01	2.65E+00	1.34E-01	2.67E+00
-0.23	21.5	1.65E-01	2.11E+00	1.68E-01	2.11E+00
-2.38	22.1	2.02E-01	1.64E+00	2.05E-01	1.66E+00
-4.49	22.4	2.39E-01	1.24E+00	2.50E-01	1.23E+00
-6.59	22.7	2.88E-01	8.73E-01	2.98E-01	8.68E-01
-8.70	23.0	3.49E-01	5.53E-01	3.58E-01	5.47E-01
-10.77	23.1	4.24E-01	3.46E-01	4.39E-01	3.26E-01
-12.87	23.1	5.17E-01	1.32E-01	5.43E-01	1.15E-01
-14.75	23.1	6.40E-01	0.00E+00	6.48E-01	0.00E+00

Table C.1: Experimental data for dual discharge (cont.)
(Centerlines of branches in the same horizontal plane)

Set No. 2 − 21
$L/d =$ 3.0
$P_0 =$ 316 kPa
$\Delta P =$ 123 kPa
$R =$ 968 $(kg.m)^{-1/2}$

h	T_o	Right Branch		Left Branch	
		$\dot{m}_G$	$\dot{m}_L$	$\dot{m}_G$	$\dot{m}_L$
$[mm]$	$[^oC]$	$[kg/min]$	$[kg/min]$	$[kg/min]$	$[kg/min]$
19.58	22.0	0.00E+00	2.18E+01	0.00E+00	2.17E+01
17.17	20.4	1.06E-02	1.82E+01	9.52E-03	1.81E+01
15.07	20.9	2.97E-02	1.51E+01	2.91E-02	1.49E+01
12.93	21.4	5.09E-02	1.23E+01	4.80E-02	1.21E+01
10.86	23.3	7.15E-02	1.03E+01	6.83E-02	9.95E+00
8.76	23.7	1.07E-01	8.66E+00	1.00E-01	8.42E+00
6.66	23.8	1.43E-01	7.84E+00	1.36E-01	7.52E+00
4.62	23.8	1.78E-01	6.31E+00	1.74E-01	6.15E+00
2.45	23.6	2.10E-01	5.37E+00	2.22E-01	5.21E+00
0.35	23.5	2.51E-01	4.70E+00	2.63E-01	4.51E+00
-2.10	23.5	3.07E-01	3.84E+00	3.16E-01	3.76E+00
-4.20	23.4	3.58E-01	3.16E+00	3.68E-01	3.10E+00
-6.26	23.3	4.18E-01	2.53E+00	4.36E-01	2.53E+00
-8.40	23.3	4.76E-01	1.94E+00	4.96E-01	1.96E+00
-10.46	23.2	5.45E-01	1.42E+00	5.68E-01	1.43E+00
-12.53	23.3	6.22E-01	9.41E-01	6.53E-01	9.11E-01
-14.66	23.7	7.34E-01	5.65E-01	7.71E-01	5.01E-01
-19.31	23.4	1.04E+00	0.00E+00	1.06E+00	0.00E+00

Table C.1: Experimental data for dual discharge (cont.)
(Centerlines of branches in the same horizontal plane)

Set No. 2 − 22
$L/d =$ 3.0
$P_0 =$ 316 kPa
$\Delta P =$ 82 kPa
$R =$ 980 $(kg.m)^{-1/2}$

h	T_o	Right Branch		Left Branch	
		$\dot{m}_G$	$\dot{m}_L$	$\dot{m}_G$	$\dot{m}_L$
$[mm]$	$[^oC]$	$[kg/min]$	$[kg/min]$	$[kg/min]$	$[kg/min]$
17.51	23.3	0.00E+00	1.76E+01	0.00E+00	1.73E+01
15.41	24.2	9.82E-03	1.50E+01	9.37E-03	1.49E+01
13.31	24.9	2.91E-02	1.21E+01	2.77E-02	1.20E+01
11.20	25.2	4.94E-02	9.80E+00	4.58E-02	9.68E+00
9.10	25.4	7.79E-02	8.07E+00	7.28E-02	7.75E+00
7.04	24.7	1.07E-01	6.74E+00	1.00E-01	6.58E+00
4.97	24.7	1.39E-01	5.68E+00	1.34E-01	5.52E+00
2.84	24.6	1.74E-01	4.86E+00	1.74E-01	4.70E+00
0.74	24.4	2.09E-01	4.58E+00	2.22E-01	4.51E+00
-1.40	24.4	2.51E-01	3.53E+00	2.64E-01	3.44E+00
-3.47	24.2	2.97E-01	2.85E+00	3.09E-01	2.84E+00
-5.63	23.4	3.55E-01	2.33E+00	3.71E-01	2.32E+00
-7.73	23.3	4.11E-01	1.79E+00	4.35E-01	1.79E+00
-9.76	23.2	4.84E-01	1.27E+00	5.02E-01	1.28E+00
-11.86	23.2	5.48E-01	8.15E-01	5.75E-01	7.96E-01
-13.96	23.6	6.34E-01	4.54E-01	6.69E-01	4.19E-01
-18.26	21.8	9.41E-01	0.00E+00	9.59E-01	0.00E+00

Table C.1: Experimental data for dual discharge (cont.)
(Centerlines of branches in the same horizontal plane)

		Set No. 2 − 23 $L/d =$ 3.0 $P_0 =$ 316 kPa $\Delta P =$ 40 kPa $R =$ 960 $(kg.m)^{-1/2}$			
h	T_o	Right Branch		Left Branch	
		$\dot{m}_G$	$\dot{m}_L$	$\dot{m}_G$	$\dot{m}_L$
$[mm]$	$[^oC]$	$[kg/min]$	$[kg/min]$	$[kg/min]$	$[kg/min]$
15.06	23.2	0.00E+00	1.25E+01	0.00E+00	1.25E+01
12.96	23.6	8.91E-03	1.01E+01	8.61E-03	1.01E+01
10.58	24.3	3.00E-02	7.87E+00	2.68E-02	7.75E+00
8.41	24.2	5.23E-02	6.23E+00	5.04E-02	6.11E+00
6.38	24.1	7.68E-02	5.17E+00	7.56E-02	5.06E+00
4.24	24.1	1.07E-01	4.39E+00	1.06E-01	4.28E+00
2.10	23.9	1.43E-01	3.71E+00	1.41E-01	3.64E+00
0.04	23.7	1.83E-01	3.07E+00	1.83E-01	3.08E+00
-2.06	23.5	2.15E-01	2.51E+00	2.27E-01	2.48E+00
-4.20	22.8	2.58E-01	1.98E+00	2.74E-01	2.00E+00
-6.30	22.9	3.07E-01	1.50E+00	3.09E-01	1.51E+00
-8.40	22.8	3.64E-01	1.04E+00	3.81E-01	1.06E+00
-10.46	23.7	4.23E-01	6.06E-01	4.43E-01	6.00E-01
-12.98	23.4	5.23E-01	3.05E-01	5.51E-01	2.77E-01
-16.27	23.3	6.97E-01	0.00E+00	6.99E-01	0.00E+00

Table C.1: Experimental data for dual discharge (cont.)
(Centerlines of branches in the same horizontal plane)

Set No. 2 − 24
$L/d =$ 3.0
$P_0 =$ 517 kPa
$\Delta P =$ 235 kPa
$R =$ 975 $(kg.m)^{-1/2}$

h	T_o	Right Branch		Left Branch	
[mm]	[^oC]	$\dot{m}_G$ [kg/min]	$\dot{m}_L$ [kg/min]	$\dot{m}_G$ [kg/min]	$\dot{m}_L$ [kg/min]
22.41	23.5	0.00E+00	2.99E+01	0.00E+00	2.97E+01
20.41	23.5	2.04E-02	2.56E+01	2.01E-02	2.59E+01
18.30	23.8	5.06E-02	2.21E+01	4.72E-02	2.20E+01
16.16	23.8	8.59E-02	1.86E+01	8.07E-02	1.81E+01
14.05	23.7	1.22E-01	1.59E+01	1.14E-01	1.55E+01
11.98	23.7	1.57E-01	1.34E+01	1.50E-01	1.33E+01
9.88	23.5	1.97E-01	1.16E+01	1.92E-01	1.15E+01
7.77	23.4	2.41E-01	1.01E+01	2.47E-01	9.91E+00
5.68	21.7	2.90E-01	9.01E+00	2.98E-01	8.81E+00
3.57	22.1	3.51E-01	7.87E+00	3.62E-01	7.67E+00
1.46	22.3	4.23E-01	6.82E+00	4.24E-01	6.62E+00
-0.64	22.4	4.87E-01	5.95E+00	4.88E-01	5.80E+00
-2.75	22.5	5.79E-01	5.17E+00	5.79E-01	5.02E+00
-4.85	22.5	6.52E-01	4.35E+00	6.52E-01	4.24E+00
-6.96	22.5	7.37E-01	3.59E+00	7.50E-01	3.50E+00
-9.09	22.5	8.43E-01	2.89E+00	8.46E-01	2.83E+00
-11.17	22.5	9.43E-01	2.21E+00	9.87E-01	2.20E+00
-13.30	22.2	1.05E+00	1.64E+00	1.09E+00	1.61E+00
-15.41	22.2	1.19E+00	1.09E+00	1.24E+00	1.03E+00
-17.16	22.2	1.34E+00	7.30E-01	1.43E+00	5.76E-01
-22.25	22.2	1.80E+00	0.00E+00	1.81E+00	0.00E+00

Table C.1: Experimental data for dual discharge (cont.)
(Centerlines of branches in the same horizontal plane)

Set No. 2 − 25					
$L/d =$ 3.0					
$P_0 =$ 517 kPa					
$\Delta P =$ 166 kPa					
$R =$ 974 $(kg.m)^{-1/2}$					
		Right Branch		Left Branch	
h [mm]	T_o [°C]	$\dot{m}_G$ [kg/min]	$\dot{m}_L$ [kg/min]	$\dot{m}_G$ [kg/min]	$\dot{m}_L$ [kg/min]
20.71	20.1	0.00E+00	2.52E+01	0.00E+00	2.49E+01
18.64	20.4	1.93E-02	2.16E+01	2.07E-02	2.15E+01
16.53	20.6	5.28E-02	1.81E+01	5.01E-02	1.78E+01
14.39	20.7	8.59E-02	1.52E+01	8.03E-02	1.51E+01
12.32	20.7	1.22E-01	1.30E+01	1.14E-01	1.29E+01
10.23	22.4	1.60E-01	1.10E+01	1.52E-01	1.09E+01
8.13	22.4	1.96E-01	9.56E+00	2.20E-01	9.36E+00
6.02	22.3	2.51E-01	8.31E+00	2.54E-01	8.14E+00
3.88	22.3	3.07E-01	7.21E+00	3.07E-01	7.01E+00
1.78	22.2	3.65E-01	6.42E+00	3.65E-01	6.19E+00
-0.33	22.2	4.27E-01	5.49E+00	4.36E-01	5.41E+00
-2.47	22.3	4.99E-01	4.74E+00	5.02E-01	4.63E+00
-4.54	22.1	5.87E-01	4.04E+00	5.92E-01	3.93E+00
-6.64	22.1	6.67E-01	3.30E+00	6.75E-01	3.30E+00
-8.71	22.0	7.51E-01	2.57E+00	7.56E-01	2.59E+00
-10.81	22.0	8.52E-01	1.99E+00	8.83E-01	1.98E+00
-12.99	22.0	9.60E-01	1.38E+00	1.00E+00	1.36E+00
-15.06	23.1	1.10E+00	9.73E-01	1.15E+00	8.68E-01
-17.13	23.1	1.25E+00	4.97E-01	1.33E+00	4.27E-01
-21.66	23.3	1.66E+00	0.00E+00	1.68E+00	0.00E+00

Table C.1: Experimental data for dual discharge (cont.)
(Centerlines of branches in the same horizontal plane)

Set No. 2 – 26
$L/d =$ 3.0
$P_0 =$ 517 kPa
$\Delta P =$ 97 kPa
$R =$ 984 $(kg.m)^{-1/2}$

h	T_o	Right Branch		Left Branch	
$[mm]$	$[^oC]$	$\dot{m}_G$ $[kg/min]$	$\dot{m}_L$ $[kg/min]$	$\dot{m}_G$ $[kg/min]$	$\dot{m}_L$ $[kg/min]$
18.60	20.7	0.00E+00	1.90E+01	0.00E+00	1.89E+01
16.35	20.9	1.81E-02	1.64E+01	1.80E-02	1.66E+01
14.25	21.2	4.79E-02	1.38E+01	4.48E-02	1.37E+01
12.14	21.3	8.09E-02	1.14E+01	7.56E-02	1.13E+01
10.03	21.3	1.18E-01	9.48E+00	1.11E-01	9.32E+00
7.93	21.4	1.56E-01	8.19E+00	1.52E-01	8.03E+00
5.82	21.4	2.06E-01	7.05E+00	1.96E-01	6.89E+00
3.75	21.5	2.43E-01	6.03E+00	2.48E-01	5.84E+00
1.61	21.6	2.96E-01	5.17E+00	3.01E-01	5.02E+00
-0.50	21.6	3.51E-01	4.55E+00	3.62E-01	4.47E+00
-2.74	21.6	4.21E-01	3.78E+00	4.36E-01	3.71E+00
-4.85	21.6	4.98E-01	3.14E+00	5.13E-01	3.10E+00
-7.02	21.5	5.95E-01	2.53E+00	6.06E-01	2.49E+00
-9.09	21.5	6.72E-01	1.91E+00	6.92E-01	1.90E+00
-10.69	21.4	7.52E-01	1.35E+00	7.73E-01	1.37E+00
-13.13	21.3	8.64E-01	8.73E-01	8.95E-01	8.86E-01
-15.23	21.3	1.00E+00	5.18E-01	1.04E+00	4.53E-01
-19.83	21.4	1.42E+00	0.00E+00	1.42E+00	0.00E+00

Table C.1: Experimental data for dual discharge
(Centerlines of branches in the same horizontal plane)

$Set\ No.\ 2-27$
$L/d = 8.0$
$P_0 = 316\ kPa$
$\Delta P = 123\ kPa$
$R = 997\ (kg.m)^{-1/2}$

h $[mm]$	T_o $[^oC]$	Right Branch $\dot{m}_G$ $[kg/min]$	Right Branch $\dot{m}_L$ $[kg/min]$	Left Branch $\dot{m}_G$ $[kg/min]$	Left Branch $\dot{m}_L$ $[kg/min]$
16.81	25.6	0.00E+00	2.12E+01	0.00E+00	2.09E+01
14.71	25.8	1.29E-02	1.73E+01	1.13E-02	1.77E+01
12.51	25.8	3.55E-02	1.34E+01	3.16E-02	1.37E+01
10.30	25.9	5.56E-02	1.06E+01	5.86E-02	1.07E+01
8.16	25.8	9.21E-02	8.46E+00	8.71E-02	8.62E+00
6.17	24.3	1.23E-01	7.13E+00	1.18E-01	7.16E+00
4.07	24.5	1.68E-01	5.95E+00	1.65E-01	5.87E+00
1.97	24.6	2.36E-01	5.17E+00	2.43E-01	5.02E+00
-0.13	24.7	2.61E-01	4.47E+00	2.64E-01	4.32E+00
-2.27	24.9	3.23E-01	3.67E+00	3.23E-01	3.69E+00
-4.37	25.0	3.87E-01	2.98E+00	3.89E-01	2.98E+00
-6.47	25.0	4.60E-01	2.32E+00	4.54E-01	2.31E+00
-8.60	24.9	5.40E-01	1.61E+00	5.29E-01	1.64E+00
-10.67	24.8	6.40E-01	1.09E+00	6.29E-01	1.07E+00
-12.76	22.6	7.41E-01	5.53E-01	7.35E-01	5.83E-01
-14.85	22.5	8.83E-01	2.44E-01	8.92E-01	2.41E-01
-16.77	22.4	1.05E+00	0.00E+00	1.06E+00	0.00E+00

Table C.1: Experimental data for dual discharge (cont.)
(Centerlines of branches in the same horizontal plane)

Set No. $2-28$					
$L/d = 8.0$					
$P_0 = 316 \; kPa$					
$\Delta P = 82 \; kPa$					
$R = 995 \; (kg.m)^{-1/2}$					
		Right Branch		Left Branch	
h [mm]	T_o [°C]	$\dot{m}_G$ [kg/min]	$\dot{m}_L$ [kg/min]	$\dot{m}_G$ [kg/min]	$\dot{m}_L$ [kg/min]
15.49	23.9	0.00E+00	1.73E+01	0.00E+00	1.71E+01
13.32	24.1	1.37E-02	1.38E+01	1.10E-02	1.42E+01
11.22	24.5	3.36E-02	1.06E+01	2.97E-02	1.07E+01
9.12	24.5	5.52E-02	8.27E+00	5.29E-02	8.38E+00
7.01	24.7	8.59E-02	6.74E+00	8.13E-02	6.66E+00
4.88	24.6	1.23E-01	5.64E+00	1.19E-01	5.56E+00
2.74	24.7	1.65E-01	4.82E+00	1.61E-01	4.74E+00
0.71	24.6	2.05E-01	4.15E+00	2.10E-01	4.08E+00
-1.38	22.6	2.53E-01	3.46E+00	2.63E-01	3.46E+00
-3.49	22.8	3.07E-01	2.77E+00	3.11E-01	2.79E+00
-5.59	23.0	3.81E-01	2.14E+00	3.81E-01	2.13E+00
-7.69	23.2	4.54E-01	1.56E+00	4.52E-01	1.56E+00
-9.79	23.3	5.29E-01	1.02E+00	5.25E-01	1.01E+00
-12.06	23.3	6.20E-01	4.90E-01	6.19E-01	5.12E-01
-14.16	23.4	7.69E-01	2.03E-01	7.70E-01	1.97E-01
-15.97	22.6	9.23E-01	0.00E+00	9.29E-01	0.00E+00

Table C.1: Experimental data for dual discharge (cont.)
(Centerlines of branches in the same horizontal plane)

$Set\ No.\ 2-29$
$L/d = 8.0$
$P_0 = 316\ kPa$
$\Delta P = 40\ kPa$
$R = 986\ (kg.m)^{-1/2}$

h	T_o	Right Branch		Left Branch	
$[mm]$	$[^oC]$	$\dot{m}_G$ $[kg/min]$	$\dot{m}_L$ $[kg/min]$	$\dot{m}_G$ $[kg/min]$	$\dot{m}_L$ $[kg/min]$
13.32	22.8	0.00E+00	1.22E+01	0.00E+00	1.21E+01
9.15	23.6	2.77E-02	6.89E+00	2.52E-02	6.97E+00
6.98	23.7	5.34E-02	5.52E+00	5.04E-02	5.52E+00
4.92	23.9	8.32E-02	4.74E+00	7.91E-02	4.63E+00
2.82	23.8	1.17E-01	3.92E+00	1.13E-01	3.81E+00
0.71	23.7	1.58E-01	3.24E+00	1.55E-01	3.22E+00
-1.39	23.6	2.00E-01	2.54E+00	1.98E-01	2.55E+00
-3.49	23.6	2.47E-01	2.04E+00	2.51E-01	2.07E+00
-5.59	23.5	3.04E-01	1.57E+00	3.07E-01	1.60E+00
-7.69	23.4	3.62E-01	1.05E+00	3.67E-01	1.07E+00
-9.79	23.2	4.38E-01	5.85E-01	4.45E-01	6.18E-01
-11.84	21.6	5.16E-01	2.96E-01	5.26E-01	3.10E-01
-14.57	21.6	6.69E-01	0.00E+00	6.77E-01	0.00E+00

Table C.1: Experimental data for dual discharge (cont.)
(Centerlines of branches in the same horizontal plane)

Set No. 2 – 30
$L/d =$ 8.0
$P_0 =$ 517 kPa
$\Delta P =$ 235 kPa
$R =$ 985 $(kg.m)^{-1/2}$

h	T_o	Right Branch		Left Branch	
		$\dot{m}_G$	$\dot{m}_L$	$\dot{m}_G$	$\dot{m}_L$
$[mm]$	$[^oC]$	$[kg/min]$	$[kg/min]$	$[kg/min]$	$[kg/min]$
19.50	24.7	0.00E+00	2.97E+01	0.00E+00	2.93E+01
17.29	25.1	1.87E-02	2.56E+01	1.87E-02	2.59E+01
15.00	25.3	5.92E-02	2.06E+01	5.92E-02	2.09E+01
12.89	25.4	9.84E-02	1.69E+01	9.84E-02	1.68E+01
10.79	25.4	1.39E-01	1.43E+01	1.39E-01	1.41E+01
8.68	25.3	1.86E-01	1.21E+01	1.86E-01	1.20E+01
6.57	25.2	2.31E-01	1.01E+01	2.31E-01	9.99E+00
4.48	22.0	2.97E-01	8.70E+00	2.97E-01	8.54E+00
2.38	22.2	3.42E-01	7.48E+00	3.42E-01	7.36E+00
0.27	22.4	4.54E-01	6.35E+00	4.54E-01	6.27E+00
-1.84	22.4	5.45E-01	5.41E+00	5.45E-01	5.25E+00
-3.94	22.5	6.46E-01	4.51E+00	6.46E-01	4.39E+00
-6.05	22.6	7.46E-01	3.66E+00	7.46E-01	3.58E+00
-8.15	22.6	8.62E-01	2.81E+00	8.62E-01	2.80E+00
-10.26	23.0	1.01E+00	2.06E+00	1.01E+00	2.09E+00
-12.36	22.9	1.14E+00	1.35E+00	1.14E+00	1.38E+00
-14.46	22.8	1.32E+00	7.51E-01	1.32E+00	7.61E-01
-16.56	23.0	1.52E+00	3.46E-01	1.52E+00	3.43E-01
-19.54	22.9	1.79E+00	0.00E+00	1.79E+00	0.00E+00

Table C.1: Experimental data for dual discharge (cont.)
(Centerlines of branches in the same horizontal plane)

Set No. 2 − 31
$L/d =$ 8.0
$P_0 =$ 517 kPa
$\Delta P =$ 166 kPa
$R =$ 992 $(kg.m)^{-1/2}$

h	T_o	Right Branch		Left Branch	
		$\dot{m}_G$	$\dot{m}_L$	$\dot{m}_G$	$\dot{m}_L$
$[mm]$	$[^oC]$	$[kg/min]$	$[kg/min]$	$[kg/min]$	$[kg/min]$
17.79	22.7	0.00E+00	2.48E+01	0.00E+00	2.44E+01
15.89	23.1	1.95E-02	2.09E+01	1.71E-02	2.14E+01
13.78	23.2	5.78E-02	1.73E+01	4.74E-02	1.73E+01
11.72	21.4	9.21E-02	1.40E+01	8.30E-02	1.41E+01
9.96	22.0	1.28E-01	1.21E+01	1.19E-01	1.21E+01
7.82	22.4	1.76E-01	9.99E+00	1.68E-01	9.91E+00
5.74	22.7	2.22E-01	8.38E+00	2.24E-01	8.34E+00
3.60	23.3	2.81E-01	7.25E+00	2.91E-01	7.16E+00
1.49	23.4	3.56E-01	6.27E+00	3.61E-01	6.19E+00
-0.62	23.5	4.35E-01	5.33E+00	4.38E-01	5.33E+00
-2.69	23.5	5.16E-01	4.58E+00	5.16E-01	4.55E+00
-4.83	23.6	6.30E-01	3.76E+00	6.24E-01	3.67E+00
-6.97	23.6	7.28E-01	2.89E+00	7.07E-01	2.85E+00
-9.07	23.6	8.38E-01	2.10E+00	8.14E-01	2.12E+00
-11.14	23.5	9.66E-01	1.46E+00	9.48E-01	1.48E+00
-13.24	23.5	1.13E+00	8.76E-01	1.13E+00	9.04E-01
-15.34	21.9	1.32E+00	4.88E-01	1.34E+00	4.79E-01
-18.84	21.9	1.61E+00	0.00E+00	1.62E+00	0.00E+00

Table C.1: Experimental data for dual discharge (cont.)
(Centerlines of branches in the same horizontal plane)

Set No. 2 − 32
$L/d =$ 8.0
$P_0 =$ 517 kPa
$\Delta P =$ 97 kPa
$R =$ 996 $(kg.m)^{-1/2}$

h	T_o	Right Branch		Left Branch	
		$\dot{m}_G$	$\dot{m}_L$	$\dot{m}_G$	$\dot{m}_L$
$[mm]$	$[^oC]$	$[kg/min]$	$[kg/min]$	$[kg/min]$	$[kg/min]$
15.99	23.9	0.00E+00	1.89E+01	0.00E+00	1.86E+01
14.13	23.9	1.71E-02	1.62E+01	1.53E-02	1.64E+01
12.03	23.9	5.34E-02	1.30E+01	4.66E-02	1.31E+01
9.95	23.9	8.68E-02	1.04E+01	8.15E-02	1.05E+01
7.85	22.3	1.26E-01	8.42E+00	1.19E-01	8.50E+00
5.71	22.5	1.75E-01	7.13E+00	1.69E-01	7.05E+00
3.60	22.6	2.20E-01	5.95E+00	2.23E-01	5.91E+00
1.46	22.7	2.80E-01	5.17E+00	2.86E-01	5.06E+00
-0.61	22.8	3.81E-01	4.39E+00	3.84E-01	4.24E+00
-2.75	22.9	4.26E-01	3.63E+00	4.42E-01	3.67E+00
-4.82	23.1	4.87E-01	2.96E+00	4.99E-01	2.94E+00
-6.93	23.0	6.19E-01	2.30E+00	6.22E-01	2.28E+00
-9.07	23.0	7.31E-01	1.60E+00	7.26E-01	1.63E+00
-11.17	22.9	8.43E-01	9.81E-01	8.30E-01	1.00E+00
-13.24	22.7	1.01E+00	5.15E-01	1.00E+00	5.40E-01
-15.33	22.2	1.18E+00	2.03E-01	1.19E+00	2.02E-01
-17.11	21.1	1.37E+00	0.00E+00	1.39E+00	0.00E+00

APPENDIX D

Experimental Data for Dual Discharge (Centerlines of Branches in the Same Vertical Plane)

Table D.1: Experimental data for dual discharge
(Centerlines of branches in the same vertical plane)

Set No. 3 − 1 $L/d =$ 1.5 $P_0 =$ 316 kPa $\Delta P =$ 123 kPa $R =$ 1028 $(kg.m)^{-1/2}$							
Upper Branch				Lower Branch			
h_A [mm]	T_o [^oC]	$\dot{m}_G$ [kg/min]	$\dot{m}_L$ [kg/min]	h_B [mm]	T_o [^oC]	$\dot{m}_G$ [kg/min]	$\dot{m}_L$ [kg/min]
18.79	25.0	0.00E+00	2.04E+01	9.92	21.6	0.00E+00	2.05E+01
16.83	24.4	1.21E-02	1.63E+01	7.95	23.1	3.38E-03	1.90E+01
14.73	23.8	4.74E-02	1.26E+01	6.03	23.3	6.48E-03	1.60E+01
12.63	23.5	8.79E-02	9.48E+00	3.94	23.1	2.42E-02	1.33E+01
10.46	22.9	1.41E-01	7.13E+00	2.05	22.8	4.27E-02	1.09E+01
8.33	22.6	1.99E-01	5.56E+00	0.09	22.6	6.85E-02	8.93E+00
6.30	23.0	2.71E-01	4.19E+00	-2.02	24.4	1.12E-01	6.93E+00
4.13	23.3	3.65E-01	2.88E+00	-4.12	24.2	1.83E-01	5.02E+00
2.07	22.3	4.81E-01	1.64E+00	-6.22	24.0	2.67E-01	3.89E+00
0.85	19.7	5.66E-01	9.99E-01	-8.33	23.8	3.54E-01	2.90E+00
-1.25	23.1	7.00E-01	5.01E-01	-10.43	23.5	4.55E-01	1.94E+00
-3.18	23.3	7.37E-01	3.46E-01	-13.19	23.2	6.14E-01	9.51E-01
-5.27	23.1	8.26E-01	1.91E-01	-15.33	22.8	7.49E-01	4.45E-01
-7.16	22.8	8.86E-01	9.22E-02	-17.08	22.5	9.21E-01	1.12E-01
-10.95	24.4	9.94E-01	0.00E+00	-17.95	21.6	1.00E+00	0.00E+00

Table D.1: Experimental data for dual discharge (cont.)
(Centerlines of branches in the same vertical plane)

Set No. 3 − 2

$L/d =$ 1.5

$P_0 =$ 316 kPa

$\Delta P =$ 82 kPa

$R =$ 1046 $(kg.m)^{-1/2}$

Upper Branch				Lower Branch			
h_A $[mm]$	T_o $[^oC]$	$\dot{m}_G$ $[kg/min]$	$\dot{m}_L$ $[kg/min]$	h_B $[mm]$	T_o $[^oC]$	$\dot{m}_G$ $[kg/min]$	$\dot{m}_L$ $[kg/min]$
17.06	19.2	0.00E+00	1.63E+01	9.12	20.6	0.00E+00	1.64E+01
15.17	18.9	1.18E-02	1.31E+01	7.09	20.1	4.63E-03	1.49E+01
13.14	18.9	4.30E-02	9.87E+00	4.99	20.0	1.22E-02	1.21E+01
11.39	18.8	7.07E-02	8.19E+00	2.86	20.0	2.97E-02	9.99E+00
9.26	20.7	1.20E-01	5.88E+00	1.29	19.9	4.55E-02	8.22E+00
7.15	20.9	1.74E-01	4.70E+00	-0.78	19.7	7.15E-02	6.77E+00
5.05	20.7	2.39E-01	3.46E+00	-2.89	20.0	1.25E-01	4.94E+00
2.95	20.7	3.24E-01	2.26E+00	-4.99	20.0	1.95E-01	3.78E+00
0.82	20.6	4.46E-01	1.27E+00	-7.05	20.0	2.78E-01	2.75E+00
-0.72	20.6	5.23E-01	6.27E-01	-9.19	19.9	3.65E-01	1.94E+00
-2.12	20.1	6.06E-01	4.71E-01	-11.29	19.8	4.83E-01	1.26E+00
-4.21	20.0	6.69E-01	3.05E-01	-13.39	19.8	5.93E-01	6.22E-01
-6.35	20.0	7.37E-01	1.55E-01	-15.49	19.7	7.33E-01	2.41E-01
-11.11	19.6	8.75E-01	0.00E+00	-16.47	19.6	8.45E-01	5.82E-02
				-17.10	19.0	9.00E-01	0.00E+00

Table D.1: Experimental data for dual discharge (cont.)
(Centerlines of branches in the same vertical plane)

Set No. 3 − 3
$L/d =$ 1.5
$P_0 =$ 316 kPa
$\Delta P =$ 40 kPa
$R =$ 1017 $(kg.m)^{-1/2}$

Upper Branch				Lower Branch			
h_A [mm]	T_o [^oC]	$\dot{m}_G$ [kg/min]	$\dot{m}_L$ [kg/min]	h_B [mm]	T_o [^oC]	$\dot{m}_G$ [kg/min]	$\dot{m}_L$ [kg/min]
14.54	20.8	0.00E+00	1.18E+01	7.51	20.3	0.00E+00	1.18E+01
12.44	21.9	1.60E-02	8.85E+00	5.51	19.9	6.17E-03	9.68E+00
10.34	22.0	3.85E-02	6.39E+00	3.42	19.7	1.83E-02	7.79E+00
8.24	22.1	7.36E-02	5.05E+00	1.49	19.5	3.32E-02	6.19E+00
6.10	22.0	1.23E-01	3.96E+00	-0.64	19.5	5.96E-02	4.74E+00
4.00	21.7	1.84E-01	3.40E+00	-2.71	19.5	1.11E-01	3.39E+00
1.90	20.9	2.50E-01	1.91E+00	-4.84	19.5	1.78E-01	2.45E+00
-0.20	20.5	3.49E-01	1.10E+00	-6.95	19.5	2.50E-01	1.86E+00
-2.33	20.2	4.43E-01	4.71E-01	-9.02	19.9	3.29E-01	1.21E+00
-3.69	19.9	4.84E-01	3.42E-01	-11.12	19.9	4.08E-01	7.25E-01
-5.79	19.7	5.48E-01	1.75E-01	-13.22	19.8	5.13E-01	3.30E-01
-7.72	19.5	6.09E-01	6.88E-02	-14.62	19.7	6.06E-01	8.14E-02
-11.18	19.4	6.70E-01	0.00E+00	-15.53	19.4	7.03E-01	0.00E+00

Table D.1: Experimental data for dual discharge (cont.)
(Centerlines of branches in the same vertical plane)

Set No. 3 − 4

$L/d =$ 1.5
$P_0 =$ 316 kPa
$\Delta P =$ 123 kPa
$R =$ 1588 $(kg.m)^{-1/2}$

Upper Branch				Lower Branch			
h_A $[mm]$	T_o $[^oC]$	$\dot{m}_G$ $[kg/min]$	$\dot{m}_L$ $[kg/min]$	h_B $[mm]$	T_o $[^oC]$	$\dot{m}_G$ $[kg/min]$	$\dot{m}_L$ $[kg/min]$
15.31	20.8	0.00E+00	1.34E+01	8.70	20.1	0.00E+00	1.30E+01
13.31	20.8	1.16E-02	1.00E+01	6.04	19.5	8.61E-03	1.06E+01
11.14	20.7	3.75E-02	7.21E+00	3.95	19.3	1.74E-02	8.54E+00
9.11	20.6	7.13E-02	5.56E+00	1.85	19.3	3.48E-02	6.77E+00
7.01	20.5	1.11E-01	4.23E+00	-0.25	19.2	6.38E-02	5.09E+00
4.84	20.4	1.63E-01	2.97E+00	-2.35	19.1	1.09E-01	3.85E+00
2.74	20.2	2.20E-01	1.93E+00	-4.10	19.1	1.52E-01	2.81E+00
0.68	20.2	3.07E-01	1.13E+00	-6.17	19.1	2.16E-01	1.94E+00
-1.42	19.7	4.36E-01	5.01E-01	-8.31	19.1	2.78E-01	1.22E+00
-3.16	19.5	4.84E-01	3.42E-01	-10.41	19.0	3.62E-01	6.89E-01
-5.26	19.3	5.45E-01	1.71E-01	-12.54	19.0	4.78E-01	3.85E-01
-7.36	19.3	6.06E-01	7.27E-02	-14.47	18.9	6.06E-01	8.52E-02
-10.93	19.1	6.50E-01	0.00E+00	-15.10	18.7	6.59E-01	0.00E+00

Table D.1: Experimental data for dual discharge (cont.)
(Centerlines of branches in the same vertical plane)

Set No. 3 − 5 $L/d =$ 1.5 $P_0 =$ 316 kPa $\Delta P =$ 123 kPa $R =$ 3007 $(kg.m)^{-1/2}$							
Upper Branch				Lower Branch			
h_A $[mm]$	T_o $[^oC]$	$\dot{m}_G$ $[kg/min]$	$\dot{m}_L$ $[kg/min]$	h_B $[mm]$	T_o $[^oC]$	$\dot{m}_G$ $[kg/min]$	$\dot{m}_L$ $[kg/min]$
11.39	19.5	0.00E+00	7.05E+00	7.47	19.6	0.00E+00	6.93E+00
9.40	19.5	8.31E-03	5.33E+00	4.99	19.3	6.63E-03	5.41E+00
7.30	19.6	2.81E-02	3.46E+00	3.21	19.1	1.41E-02	4.43E+00
5.20	19.6	4.96E-02	2.55E+00	1.14	19.1	3.18E-02	3.32E+00
3.13	19.6	8.14E-02	1.81E+00	-0.68	19.5	5.74E-02	2.40E+00
1.03	19.7	1.26E-01	1.13E+00	-2.71	19.5	9.31E-02	1.60E+00
-1.07	19.7	1.92E-01	5.18E-01	-4.81	19.6	1.31E-01	1.04E+00
-2.85	19.5	2.37E-01	2.44E-01	-6.91	19.6	1.79E-01	5.90E-01
-4.22	19.3	2.71E-01	1.71E-01	-9.01	19.7	2.37E-01	3.39E-01
-6.00	19.1	3.07E-01	7.66E-02	-11.11	19.6	3.07E-01	1.08E-01
-9.88	19.5	3.68E-01	0.00E+00	-12.37	19.5	3.71E-01	0.00E+00

Table D.1: Experimental data for dual discharge (cont.)
(Centerlines of branches in the same vertical plane)

Set No. 3 − 6

$L/d = 1.5$

$P_0 = 517 \; kPa$

$\Delta P = 235 \; kPa$

$R = 1025 \; (kg.m)^{-1/2}$

Upper Branch				Lower Branch			
h_A $[mm]$	T_o $[^oC]$	$\dot{m}_G$ $[kg/min]$	$\dot{m}_L$ $[kg/min]$	h_B $[mm]$	T_o $[^oC]$	$\dot{m}_G$ $[kg/min]$	$\dot{m}_L$ $[kg/min]$
21.41	22.0	0.00E+00	2.82E+01	10.06	22.2	0.00E+00	2.85E+01
19.38	22.0	1.97E-02	2.34E+01	7.86	22.1	1.16E-02	2.65E+01
17.23	22.0	7.54E-02	1.82E+01	5.82	22.5	2.48E-02	2.22E+01
15.55	22.1	1.26E-01	1.51E+01	3.65	22.6	4.98E-02	1.85E+01
13.34	22.0	2.07E-01	1.18E+01	1.62	22.6	8.86E-02	1.53E+01
11.27	22.0	2.98E-01	9.09E+00	-0.52	22.6	1.29E-01	1.28E+01
9.13	22.0	3.95E-01	6.93E+00	-2.49	22.4	1.96E-01	1.03E+01
7.06	22.3	5.26E-01	5.45E+00	-4.75	22.9	2.98E-01	7.20E+00
5.02	22.3	6.72E-01	3.88E+00	-6.89	22.8	4.13E-01	5.80E+00
2.85	22.2	8.62E-01	2.21E+00	-8.96	22.4	5.55E-01	4.47E+00
0.86	22.2	1.08E+00	1.05E+00	-11.11	22.8	6.86E-01	3.23E+00
-1.35	22.1	1.32E+00	5.01E-01	-13.25	22.8	8.62E-01	2.22E+00
-3.38	22.5	1.39E+00	3.67E-01	-15.32	22.8	1.06E+00	1.38E+00
-5.56	22.6	1.48E+00	2.11E-01	-17.46	22.8	1.29E+00	5.90E-01
-7.59	22.6	1.57E+00	8.83E-02	-20.97	22.5	1.72E+00	0.00E+00
-11.70	22.4	1.69E+00	0.00E+00				

Table D.1: Experimental data for dual discharge (cont.)
(Centerlines of branches in the same vertical plane)

$$Set\ No. 3-7$$
$$L/d = 1.5$$
$$P_0 = 517\ kPa$$
$$\Delta P = 166\ kPa$$
$$R = 1018\ (kg.m)^{-1/2}$$

Upper Branch				Lower Branch			
h_A [mm]	T_o [°C]	$\dot{m}_G$ [kg/min]	$\dot{m}_L$ [kg/min]	h_B [mm]	T_o [°C]	$\dot{m}_G$ [kg/min]	$\dot{m}_L$ [kg/min]
19.84	21.9	0.00E+00	2.39E+01	9.00	22.4	0.00E+00	2.40E+01
17.59	21.9	2.57E-02	1.89E+01	6.52	23.4	1.38E-02	2.13E+01
15.48	21.9	8.36E-02	1.50E+01	4.40	21.2	3.24E-02	1.73E+01
13.38	21.9	1.47E-01	1.16E+01	2.31	23.2	6.12E-02	1.47E+01
11.27	21.9	2.10E-01	9.09E+00	0.21	22.9	1.00E-01	1.21E+01
9.20	21.8	2.98E-01	8.85E+00	-1.92	22.7	1.56E-01	9.28E+00
7.06	21.4	4.17E-01	5.49E+00	-4.10	21.8	2.48E-01	6.97E+00
4.78	21.6	5.63E-01	3.93E+00	-6.15	21.7	3.46E-01	5.41E+00
2.71	21.8	7.16E-01	2.37E+00	-8.25	21.6	4.84E-01	4.24E+00
0.57	22.1	9.11E-01	1.25E+00	-10.43	21.6	6.26E-01	3.06E+00
-1.01	23.3	1.10E+00	5.60E-01	-12.43	21.2	7.59E-01	2.05E+00
-2.69	23.4	1.21E+00	4.50E-01	-14.61	21.1	9.46E-01	1.28E+00
-4.79	20.9	1.31E+00	2.76E-01	-16.68	21.1	1.17E+00	5.65E-01
-6.89	23.2	1.39E+00	1.32E-01	-18.68	21.2	1.45E+00	1.73E-01
-12.05	22.2	1.58E+00	0.00E+00	-20.19	21.2	1.59E+00	0.00E+00

Table D.1: Experimental data for dual discharge (cont.)
(Centerlines of branches in the same vertical plane)

Set No. 3 − 8

$L/d =$ 1.5
$P_0 =$ 517 kPa
$\Delta P =$ 97 kPa
$R =$ 1035 $(kg.m)^{-1/2}$

Upper Branch				Lower Branch			
h_A [mm]	T_o [°C]	$\dot{m}_G$ [kg/min]	$\dot{m}_L$ [kg/min]	h_B [mm]	T_o [°C]	$\dot{m}_G$ [kg/min]	$\dot{m}_L$ [kg/min]
17.49	21.7	0.00E+00	1.79E+01	7.78	22.4	0.00E+00	1.81E+01
15.49	22.5	1.93E-02	1.46E+01	5.75	22.0	1.28E-02	1.61E+01
13.41	23.0	6.84E-02	1.14E+01	3.61	21.8	2.89E-02	1.32E+01
11.27	23.2	1.24E-01	8.70E+00	1.58	21.6	6.34E-02	1.08E+01
9.16	23.2	1.96E-01	6.74E+00	-0.56	21.5	9.69E-02	8.54E+00
7.09	23.2	2.64E-01	5.21E+00	-2.81	21.4	1.70E-01	6.30E+00
4.99	22.8	3.75E-01	4.00E+00	-4.79	22.1	2.50E-01	4.70E+00
2.88	22.7	5.05E-01	2.77E+00	-6.89	22.0	3.55E-01	3.76E+00
0.78	22.6	6.50E-01	1.62E+00	-8.99	22.0	4.84E-01	2.70E+00
-1.43	22.4	8.57E-01	6.24E-01	-11.10	22.1	6.10E-01	1.87E+00
-3.46	22.0	9.74E-01	3.61E-01	-13.21	22.0	7.59E-01	1.15E+00
-12.01	21.4	1.31E+00	0.00E+00	-15.35	22.0	9.41E-01	5.12E-01
				-17.59	22.0	1.23E+00	8.34E-02
				-18.47	21.9	1.32E+00	0.00E+00

Table D.1: Experimental data for dual discharge (cont.)
(Centerlines of branches in the same vertical plane)

$$Set\ No.\ 3-9$$
$$L/d = 1.5$$
$$P_0 = 517\ kPa$$
$$\Delta P = 235\ kPa$$
$$R = 1631\ (kg.m)^{-1/2}$$

Upper Branch				Lower Branch			
h_A $[mm]$	T_o $[^oC]$	$\dot{m}_G$ $[kg/min]$	$\dot{m}_L$ $[kg/min]$	h_B $[mm]$	T_o $[^oC]$	$\dot{m}_G$ $[kg/min]$	$\dot{m}_L$ $[kg/min]$
17.49	20.8	0.00E+00	1.78E+01	8.45	20.9	0.00E+00	1.78E+01
15.52	20.9	1.83E-02	1.45E+01	6.11	21.5	1.34E-02	1.55E+01
13.39	21.3	5.54E-02	1.07E+01	4.01	21.6	3.16E-02	1.27E+01
11.31	20.9	1.06E-01	8.11E+00	1.91	21.6	6.10E-02	1.01E+01
9.17	21.0	1.67E-01	6.15E+00	-0.16	21.4	1.05E-01	7.75E+00
7.07	20.9	1.99E-01	4.66E+00	-1.95	21.4	1.57E-01	6.15E+00
4.96	20.9	3.19E-01	3.25E+00	-4.08	21.7	2.34E-01	4.51E+00
2.86	20.9	4.40E-01	2.11E+00	-6.18	21.5	3.20E-01	3.34E+00
0.72	20.9	6.06E-01	1.16E+00	-8.29	21.5	4.17E-01	2.33E+00
-1.35	20.8	7.98E-01	4.48E-01	-10.36	21.4	5.40E-01	1.53E+00
-3.10	21.5	8.62E-01	3.42E-01	-12.50	21.4	6.77E-01	9.15E-01
-5.20	21.6	9.43E-01	1.75E-01	-14.64	21.4	8.60E-01	4.07E-01
-7.30	21.6	1.01E+00	7.27E-02	-16.43	21.3	1.05E+00	7.36E-02
-11.16	21.4	1.06E+00	0.00E+00	-17.03	21.2	1.11E+00	0.00E+00

Table D.1: Experimental data for dual discharge (cont.)
(Centerlines of branches in the same vertical plane)

Set No. 3 − 10 $L/d = 1.5$ $P_0 = 517\ kPa$ $\Delta P = 235\ kPa$ $R = 2966\ (kg.m)^{-1/2}$							
Upper Branch				Lower Branch			
h_A [mm]	T_o [^oC]	$\dot{m}_G$ [kg/min]	$\dot{m}_L$ [kg/min]	h_B [mm]	T_o [^oC]	$\dot{m}_G$ [kg/min]	$\dot{m}_L$ [kg/min]
13.31	21.2	0.00E+00	9.87E+00	8.24	20.5	0.00E+00	9.72E+00
11.31	21.2	1.21E-02	7.25E+00	5.83	20.4	7.70E-03	8.46E+00
9.20	21.1	4.18E-02	5.17E+00	3.69	20.8	2.16E-02	6.58E+00
7.10	20.9	8.09E-02	4.00E+00	1.55	20.8	4.44E-02	5.02E+00
4.96	20.8	1.29E-01	2.89E+00	-0.90	20.9	9.46E-02	3.52E+00
2.89	20.6	1.91E-01	1.96E+00	-2.98	21.2	1.47E-01	2.48E+00
0.75	20.5	2.66E-01	1.13E+00	-5.12	21.1	2.19E-01	1.63E+00
-1.28	20.4	3.80E-01	4.73E-01	-7.19	21.1	2.73E-01	1.07E+00
-3.38	20.4	4.70E-01	2.60E-01	-9.33	21.1	3.49E-01	6.11E-01
-5.52	20.8	5.37E-01	1.16E-01	-11.44	21.0	4.58E-01	2.93E-01
-10.11	20.9	6.22E-01	0.00E+00	-12.88	20.9	5.49E-01	8.52E-02
				-13.69	20.9	6.22E-01	0.00E+00

Table D.1: Experimental data for dual discharge (cont.)
(Centerlines of branches in the same vertical plane)

Set No. 3 − 11 $L/d =$ 2.0 $P_0 =$ 316 kPa $\Delta P =$ 123 kPa $R =$ 1023 $(kg.m)^{-1/2}$							
Upper Branch				Lower Branch			
h_A $[mm]$	T_o $[^oC]$	$\dot{m}_G$ $[kg/min]$	$\dot{m}_L$ $[kg/min]$	h_B $[mm]$	T_o $[^oC]$	$\dot{m}_G$ $[kg/min]$	$\dot{m}_L$ $[kg/min]$
18.29	22.4	0.00E+00	2.06E+01	10.38	21.1	0.00E+00	2.05E+01
16.39	22.4	9.82E-03	1.68E+01	8.94	20.9	5.71E-03	1.86E+01
14.36	19.9	2.99E-02	1.29E+01	6.70	20.8	1.84E-02	1.49E+01
12.37	21.8	5.64E-02	9.72E+00	4.81	21.8	3.62E-02	1.22E+01
10.26	20.8	9.73E-02	7.48E+00	3.13	19.7	5.50E-02	1.01E+01
8.16	20.4	1.51E-01	5.84E+00	1.41	19.5	8.18E-02	8.31E+00
6.41	20.1	2.06E-01	4.78E+00	-0.65	21.2	1.26E-01	6.46E+00
4.42	20.8	2.75E-01	3.73E+00	-2.65	20.9	1.87E-01	5.17E+00
2.46	20.9	3.53E-01	2.58E+00	-4.74	20.7	2.50E-01	4.04E+00
0.89	21.1	4.42E-01	1.71E+00	-6.84	20.5	3.17E-01	3.00E+00
-0.44	20.7	5.29E-01	1.12E+00	-8.94	20.2	4.10E-01	2.15E+00
-1.81	21.1	6.41E-01	6.22E-01	-11.04	20.1	5.10E-01	1.42E+00
-3.53	20.9	7.40E-01	3.55E-01	-13.07	19.9	6.17E-01	8.01E-01
-5.77	20.8	8.29E-01	2.21E-01	-15.13	19.7	7.77E-01	4.04E-01
-7.66	17.3	8.67E-01	1.50E-01	-16.80	19.6	9.21E-01	1.12E-01
-9.34	19.7	9.28E-01	6.38E-02	-17.68	19.6	1.03E+00	0.00E+00
-12.10	19.5	9.98E-01	0.00E+00				

Table D.1: Experimental data for dual discharge (cont.)
(Centerlines of branches in the same vertical plane)

Set No. 3 − 12							
$L/d = 2.0$							
$P_0 = 316 \; kPa$							
$\Delta P = 82 \; kPa$							
$R = 1025 \; (kg.m)^{-1/2}$							
Upper Branch				Lower Branch			
h_A $[mm]$	T_o $[^oC]$	$\dot{m}_G$ $[kg/min]$	$\dot{m}_L$ $[kg/min]$	h_B $[mm]$	T_o $[^oC]$	$\dot{m}_G$ $[kg/min]$	$\dot{m}_L$ $[kg/min]$
16.29	20.7	0.00E+00	1.66E+01	9.71	18.9	0.00E+00	1.67E+01
14.47	20.1	1.19E-02	1.32E+01	8.56	21.3	5.09E-03	1.53E+01
12.41	20.0	3.49E-02	9.32E+00	6.81	21.5	1.22E-02	1.30E+01
10.24	19.8	6.42E-02	7.16E+00	5.06	21.4	2.44E-02	1.09E+01
8.17	19.5	1.03E-01	5.68E+00	3.31	21.1	4.15E-02	8.85E+00
6.07	19.2	1.58E-01	4.51E+00	1.38	20.2	6.75E-02	6.97E+00
4.00	19.1	2.33E-01	3.52E+00	-0.37	19.9	1.08E-01	5.60E+00
1.90	19.1	3.06E-01	2.47E+00	-2.64	19.9	1.74E-01	4.31E+00
-0.23	19.0	4.11E-01	1.45E+00	-4.70	19.5	2.23E-01	3.25E+00
-1.95	18.9	5.23E-01	7.68E-01	-6.84	19.5	2.93E-01	2.37E+00
-3.91	21.3	6.06E-01	4.45E-01	-8.94	19.4	3.65E-01	1.64E+00
-5.66	21.5	6.69E-01	2.57E-01	-10.97	19.4	4.54E-01	1.02E+00
-7.41	21.4	7.48E-01	1.50E-01	-12.79	19.3	5.67E-01	4.93E-01
-9.16	21.1	8.13E-01	7.77E-02	-14.85	19.2	7.10E-01	1.99E-01
-11.68	19.9	8.91E-01	0.00E+00	-16.18	19.1	8.30E-01	6.88E-02
				-16.74	19.1	9.07E-01	0.00E+00

Table D.1: Experimental data for dual discharge (cont.)
(Centerlines of branches in the same vertical plane)

Set No. 3 – 13							
$L/d =$ 2.0							
$P_0 =$ 316 kPa							
$\Delta P =$ 40 kPa							
$R =$ 984 $(kg.m)^{-1/2}$							
Upper Branch				Lower Branch			
h_A $[mm]$	T_o $[^oC]$	$\dot{m}_G$ $[kg/min]$	$\dot{m}_L$ $[kg/min]$	h_B $[mm]$	T_o $[^oC]$	$\dot{m}_G$ $[kg/min]$	$\dot{m}_L$ $[kg/min]$
14.05	23.1	0.00E+00	1.22E+01	8.59	19.7	0.00E+00	1.22E+01
12.02	22.8	1.26E-02	8.58E+00	8.66	19.0	0.00E+00	1.22E+01
9.92	22.8	3.16E-02	6.23E+00	6.81	19.0	8.46E-03	9.56E+00
7.84	22.5	5.90E-02	4.82E+00	5.06	18.9	1.66E-02	7.91E+00
5.89	22.2	9.42E-02	3.97E+00	3.31	18.8	3.16E-02	6.39E+00
3.79	21.7	1.45E-01	3.10E+00	1.21	18.7	6.08E-02	4.90E+00
1.69	20.4	2.10E-01	2.16E+00	-0.89	20.8	1.05E-01	3.71E+00
-0.23	19.9	2.98E-01	1.52E+00	-2.99	20.6	1.63E-01	2.87E+00
-2.30	19.9	3.68E-01	7.96E-01	-5.09	20.5	2.08E-01	2.10E+00
-3.56	19.7	4.54E-01	4.42E-01	-7.12	20.4	2.61E-01	1.48E+00
-5.66	19.0	5.25E-01	2.17E-01	-9.12	20.3	3.21E-01	9.63E-01
-7.41	18.9	5.82E-01	1.35E-01	-11.25	20.1	4.15E-01	5.98E-01
-11.61	18.9	6.85E-01	0.00E+00	-13.14	20.0	5.07E-01	2.60E-01
				-14.50	19.9	5.86E-01	8.44E-02
				-15.24	19.9	6.85E-01	0.00E+00

Table D.1: Experimental data for dual discharge (cont.)
(Centerlines of branches in the same vertical plane)

Set No. 3 − 14							
$L/d = 2.0$							
$P_0 = 316$ kPa							
$\Delta P = 123$ kPa							
$R = 1580$ $(kg.m)^{-1/2}$							
Upper Branch				Lower Branch			
h_A [mm]	T_o [^oC]	$\dot{m}_G$ [kg/min]	$\dot{m}_L$ [kg/min]	h_B [mm]	T_o [^oC]	$\dot{m}_G$ [kg/min]	$\dot{m}_L$ [kg/min]
14.65	22.3	0.00E+00	1.33E+01	9.29	22.6	0.00E+00	1.33E+01
12.58	22.4	1.15E-02	9.83E+00	7.51	21.6	6.33E-03	1.11E+01
10.45	22.5	3.17E-02	7.32E+00	5.41	21.9	1.53E-02	8.70E+00
8.38	22.4	5.92E-02	5.45E+00	3.31	22.0	3.25E-02	6.74E+00
6.21	22.6	1.00E-01	4.24E+00	1.17	22.7	6.75E-02	4.94E+00
4.21	22.7	1.37E-01	3.27E+00	-0.90	22.6	1.07E-01	3.84E+00
2.01	22.6	1.95E-01	2.28E+00	-3.00	22.6	1.54E-01	2.77E+00
-0.02	22.7	2.67E-01	1.41E+00	-5.10	22.6	2.05E-01	2.01E+00
-2.09	22.7	3.74E-01	7.03E-01	-7.20	22.6	2.48E-01	1.40E+00
-3.59	20.9	4.70E-01	3.89E-01	-9.30	22.6	3.20E-01	8.66E-01
-4.96	21.6	5.08E-01	3.02E-01	-11.43	22.5	4.16E-01	4.83E-01
-10.84	22.3	6.56E-01	0.00E+00	-13.50	22.5	5.38E-01	2.41E-01
				-14.79	22.3	6.63E-01	0.00E+00

Table D.1: Experimental data for dual discharge (cont.)
(Centerlines of branches in the same vertical plane)

$$\begin{array}{lcll} & Set\ \ No.\ 3-15 & & \\ L/d = & 2.0 & & \\ P_0 = & 316 & kPa & \\ \Delta P = & 123 & kPa & \\ R = & 2983 & (kg.m)^{-1/2} & \end{array}$$

Upper Branch				Lower Branch			
h_A [mm]	T_o [^oC]	$\dot{m}_G$ [kg/min]	$\dot{m}_L$ [kg/min]	h_B [mm]	T_o [^oC]	$\dot{m}_G$ [kg/min]	$\dot{m}_L$ [kg/min]
11.00	22.1	0.00E+00	6.97E+00	8.24	23.3	0.00E+00	7.13E+00
8.90	22.2	9.97E-03	4.98E+00	6.14	21.9	6.33E-03	5.56E+00
6.80	22.4	2.60E-02	3.58E+00	3.97	22.0	1.63E-02	4.19E+00
4.67	22.6	4.95E-02	2.72E+00	1.90	22.6	3.90E-02	3.05E+00
2.92	23.0	7.28E-02	2.09E+00	-0.20	22.7	6.81E-02	2.18E+00
0.81	23.1	1.03E-01	1.51E+00	-2.30	22.7	9.55E-02	1.49E+00
-1.29	23.2	1.43E-01	9.04E-01	-4.43	22.7	1.36E-01	1.05E+00
-3.42	23.3	2.22E-01	4.03E-01	-6.53	22.7	1.75E-01	6.41E-01
-5.45	23.3	2.90E-01	2.32E-01	-8.60	22.8	2.19E-01	3.61E-01
-9.40	22.1	3.86E-01	0.00E+00	-10.73	22.5	2.80E-01	2.10E-01
				-12.48	22.5	3.70E-01	0.00E+00

Table D.1: Experimental data for dual discharge (cont.)
(Centerlines of branches in the same vertical plane)

Set No. 3 − 16

$L/d =$ 2.0

$P_0 =$ 517 kPa

$\Delta P =$ 235 kPa

$R =$ 1008 $(kg.m)^{-1/2}$

Upper Branch				Lower Branch			
h_A $[mm]$	T_o $[^oC]$	$\dot{m}_G$ $[kg/min]$	$\dot{m}_L$ $[kg/min]$	h_B $[mm]$	T_o $[^oC]$	$\dot{m}_G$ $[kg/min]$	$\dot{m}_L$ $[kg/min]$
20.76	23.2	0.00E+00	2.89E+01	11.22	22.9	0.00E+00	2.88E+01
18.69	23.4	2.14E-02	2.39E+01	8.97	22.6	1.25E-02	2.62E+01
16.51	23.5	6.30E-02	1.85E+01	6.51	24.6	3.56E-02	2.11E+01
14.40	23.5	1.17E-01	1.47E+01	4.37	24.5	6.79E-02	1.75E+01
12.33	23.5	1.81E-01	1.15E+01	2.30	24.3	1.10E-01	1.42E+01
10.19	23.3	2.64E-01	8.93E+00	0.54	24.1	1.56E-01	1.19E+01
8.12	23.3	3.65E-01	7.16E+00	-1.57	24.0	2.25E-01	8.89E+00
6.01	23.2	4.98E-01	5.41E+00	-3.71	24.0	3.21E-01	7.09E+00
3.91	23.1	6.34E-01	4.16E+00	-5.78	23.8	4.42E-01	5.56E+00
1.73	23.1	8.13E-01	2.58E+00	-7.85	23.7	5.66E-01	4.39E+00
-0.30	23.0	1.03E+00	1.36E+00	-10.02	23.6	6.98E-01	3.26E+00
-2.46	25.0	1.34E+00	5.12E-01	-12.12	23.5	8.43E-01	2.28E+00
-4.55	23.1	1.39E+00	4.62E-01	-14.18	21.6	1.02E+00	1.51E+00
-5.96	24.6	1.50E+00	3.12E-01	-16.32	21.5	1.23E+00	8.19E-01
-11.93	24.1	1.78E+00	0.00E+00	-20.73	21.2	1.80E+00	0.00E+00

Table D.1: Experimental data for dual discharge (cont.)
(Centerlines of branches in the same vertical plane)

Set No. 3 − 17

$L/d =$ 2.0

$P_0 =$ 517 kPa

$\Delta P =$ 166 kPa

$R =$ 1016 $(kg.m)^{-1/2}$

Upper Branch				Lower Branch			
h_A $[mm]$	T_o $[^oC]$	$\dot{m}_G$ $[kg/min]$	$\dot{m}_L$ $[kg/min]$	h_B $[mm]$	T_o $[^oC]$	$\dot{m}_G$ $[kg/min]$	$\dot{m}_L$ $[kg/min]$
19.25	21.9	0.00E+00	2.40E+01	10.42	22.2	0.00E+00	2.40E+01
17.22	22.1	2.01E-02	2.00E+01	8.35	21.0	1.38E-02	2.17E+01
15.11	22.1	5.82E-02	1.57E+01	6.21	21.6	2.97E-02	1.85E+01
12.94	22.2	1.09E-01	1.20E+01	4.06	22.0	6.08E-02	1.50E+01
10.83	22.3	1.72E-01	9.28E+00	1.99	22.2	9.87E-02	1.22E+01
8.76	22.3	2.50E-01	7.36E+00	-0.05	22.6	1.52E-01	9.48E+00
6.62	22.2	3.51E-01	5.84E+00	-2.26	22.8	2.26E-01	7.17E+00
4.58	22.3	4.72E-01	4.59E+00	-4.37	22.8	3.26E-01	5.76E+00
2.48	22.3	6.06E-01	3.33E+00	-6.47	22.7	4.34E-01	4.55E+00
0.34	22.3	7.67E-01	1.99E+00	-7.84	22.7	5.19E-01	3.81E+00
-2.05	22.2	1.06E+00	7.61E-01	-9.91	22.7	6.35E-01	2.79E+00
-4.12	21.0	1.21E+00	4.42E-01	-12.09	22.7	7.92E-01	1.94E+00
-6.26	21.6	1.35E+00	3.02E-01	-13.45	22.8	9.04E-01	1.44E+00
-12.13	22.6	1.62E+00	0.00E+00	-15.56	22.6	1.09E+00	8.01E-01
				-17.73	22.5	1.36E+00	3.27E-01
				-20.07	22.3	1.64E+00	0.00E+00

Table D.1: Experimental data for dual discharge (cont.)
(Centerlines of branches in the same vertical plane)

Set No. 3 − 18

$L/d =$ 2.0

$P_0 =$ 517 kPa

$\Delta P =$ 97 kPa

$R =$ 981 $(kg.m)^{-1/2}$

Upper Branch				Lower Branch			
h_A [mm]	T_o [^oC]	$\dot{m}_G$ [kg/min]	$\dot{m}_L$ [kg/min]	h_B [mm]	T_o [^oC]	$\dot{m}_G$ [kg/min]	$\dot{m}_L$ [kg/min]
16.97	22.7	0.00E+00	1.81E+01	9.25	23.1	0.00E+00	1.82E+01
14.76	22.6	2.39E-02	1.47E+01	7.22	23.3	1.34E-02	1.65E+01
12.65	22.7	6.09E-02	1.09E+01	5.11	23.4	3.34E-02	1.34E+01
10.58	22.8	1.07E-01	8.18E+00	3.04	23.5	6.19E-02	1.09E+01
8.44	22.8	1.69E-01	6.54E+00	0.97	23.6	9.91E-02	8.62E+00
6.40	22.3	2.44E-01	5.17E+00	-1.22	25.0	1.65E-01	6.35E+00
4.30	22.5	3.33E-01	4.24E+00	-3.34	22.0	2.42E-01	4.98E+00
2.12	22.7	4.51E-01	3.14E+00	-5.41	22.0	3.37E-01	4.00E+00
0.08	22.9	5.75E-01	2.13E+00	-7.42	22.2	4.45E-01	3.00E+00
-2.02	23.0	7.48E-01	1.05E+00	-9.52	22.2	5.55E-01	2.13E+00
-3.49	23.1	9.14E-01	4.77E-01	-11.66	22.2	6.78E-01	1.41E+00
-5.25	23.3	1.03E+00	3.51E-01	-13.77	22.2	8.48E-01	7.94E-01
-12.34	23.6	1.35E+00	0.00E+00	-15.90	22.2	1.05E+00	3.44E-01
				-18.18	22.0	1.35E+00	0.00E+00

Table D.1: Experimental data for dual discharge (cont.)
(Centerlines of branches in the same vertical plane)

Set No. 3 − 19

$L/d = 2.0$

$P_0 = 517\ kPa$

$\Delta P = 235\ kPa$

$R = 1592\ (kg.m)^{-1/2}$

Upper Branch				Lower Branch			
h_A [mm]	T_o [°C]	$\dot{m}_G$ [kg/min]	$\dot{m}_L$ [kg/min]	h_B [mm]	T_o [°C]	$\dot{m}_G$ [kg/min]	$\dot{m}_L$ [kg/min]
16.90	22.3	0.00E+00	1.80E+01	9.72	21.5	0.00E+00	1.85E+01
14.87	22.4	1.86E-02	1.45E+01	7.64	22.6	1.28E-02	1.62E+01
12.69	22.4	5.22E-02	1.07E+01	5.46	23.1	3.02E-02	1.27E+01
10.55	22.4	9.62E-02	8.22E+00	3.39	23.4	5.93E-02	1.01E+01
8.44	22.5	1.52E-01	6.38E+00	1.00	24.4	1.13E-01	7.52E+00
6.34	22.5	2.22E-01	5.02E+00	-1.14	25.0	1.77E-01	5.60E+00
4.27	22.5	2.98E-01	3.81E+00	-3.29	25.0	2.40E-01	4.39E+00
2.09	22.5	4.00E-01	2.59E+00	-5.43	25.0	3.22E-01	3.23E+00
0.06	21.0	5.42E-01	1.60E+00	-7.54	24.9	4.16E-01	2.35E+00
-2.08	21.3	7.16E-01	7.78E-01	-9.64	24.9	5.22E-01	1.64E+00
-4.16	22.5	8.95E-01	3.37E-01	-11.75	24.8	6.51E-01	1.05E+00
-11.47	24.4	1.13E+00	0.00E+00	-13.85	24.5	8.14E-01	5.18E-01
				-15.98	24.4	1.01E+00	1.36E-01
				-17.05	23.8	1.13E+00	0.00E+00

Table D.1: Experimental data for dual discharge (cont.)
(Centerlines of branches in the same vertical plane)

$$\begin{array}{lcll} & Set\ \ No. & 3-20 & \\ L/d = & 2.0 & & \\ P_0 = & 517 & kPa & \\ \Delta P = & 235 & kPa & \\ R = & 2925 & (kg.m)^{-1/2} & \end{array}$$

Upper Branch				Lower Branch			
h_A $[mm]$	T_o $[^oC]$	$\dot{m}_G$ $[kg/min]$	$\dot{m}_L$ $[kg/min]$	h_B $[mm]$	T_o $[^oC]$	$\dot{m}_G$ $[kg/min]$	$\dot{m}_L$ $[kg/min]$
12.73	21.9	0.00E+00	9.79E+00	8.97	23.1	0.00E+00	1.01E+01
10.65	22.1	1.56E-02	7.32E+00	6.86	23.0	9.82E-03	8.31E+00
8.48	22.4	4.44E-02	5.37E+00	4.72	23.3	2.37E-02	6.35E+00
6.34	22.5	7.91E-02	4.16E+00	2.68	23.5	4.67E-02	4.78E+00
4.20	22.6	1.23E-01	3.14E+00	0.54	24.8	9.21E-02	3.57E+00
2.09	22.7	1.74E-01	2.26E+00	-1.57	24.3	1.40E-01	2.60E+00
0.02	22.8	2.39E-01	1.45E+00	-3.67	24.3	1.87E-01	1.83E+00
-2.09	22.9	3.03E-01	7.11E-01	-5.81	24.3	2.39E-01	1.46E+00
-3.49	23.1	4.24E-01	3.72E-01	-7.88	24.3	3.04E-01	7.90E-01
-5.60	23.0	5.14E-01	2.36E-01	-9.28	24.2	3.57E-01	5.18E-01
-10.10	23.8	6.37E-01	0.00E+00	-11.42	24.2	4.72E-01	2.85E-01
				-13.93	23.9	6.39E-01	0.00E+00

Table D.1: Experimental data for dual discharge (cont.)
(Centerlines of branches in the same vertical plane)

Set No. 3 – 21

$L/d =$ 3.0
$P_0 =$ 316 kPa
$\Delta P =$ 123 kPa
$R =$ 1024 $(kg.m)^{-1/2}$

Upper Branch				Lower Branch			
h_A $[mm]$	T_o $[^oC]$	$\dot{m}_G$ $[kg/min]$	$\dot{m}_L$ $[kg/min]$	h_B $[mm]$	T_o $[^oC]$	$\dot{m}_G$ $[kg/min]$	$\dot{m}_L$ $[kg/min]$
17.46	25.3	0.00E+00	2.06E+01	11.84	23.8	0.00E+00	2.05E+01
15.64	25.4	5.25E-03	1.66E+01	10.26	23.4	9.26E-03	1.78E+01
13.54	25.2	3.28E-02	1.35E+01	8.23	23.2	2.75E-02	1.42E+01
11.40	24.7	6.10E-02	1.02E+01	6.21	24.0	5.34E-02	1.09E+01
9.27	24.3	9.67E-02	8.14E+00	4.11	23.8	9.68E-02	8.15E+00
7.17	24.0	1.40E-01	6.62E+00	2.01	23.5	1.49E-01	6.50E+00
5.03	23.7	1.93E-01	5.45E+00	-0.09	23.2	2.08E-01	5.25E+00
2.93	25.3	2.51E-01	4.39E+00	-2.19	22.9	2.61E-01	4.39E+00
0.86	25.3	3.16E-01	3.57E+00	-4.29	22.7	3.22E-01	3.51E+00
-1.20	25.2	4.02E-01	2.65E+00	-6.39	21.4	3.91E-01	2.69E+00
-3.30	25.1	5.07E-01	1.69E+00	-8.49	22.3	4.72E-01	1.94E+00
-5.06	25.0	6.11E-01	9.40E-01	-10.55	22.2	5.56E-01	1.27E+00
-6.60	24.3	7.45E-01	3.97E-01	-12.72	22.0	6.77E-01	6.94E-01
-8.56	23.4	8.98E-01	1.38E-01	-14.78	21.7	8.13E-01	2.80E-01
-11.53	24.2	1.02E+00	0.00E+00	-16.18	21.5	9.51E-01	6.88E-02
				-16.66	20.8	1.02E+00	0.00E+00

Table D.1: Experimental data for dual discharge (cont.)
(Centerlines of branches in the same vertical plane)

Set No. 3 – 22
$L/d = 3.0$
$P_0 = 316\ kPa$
$\Delta P = 82\ kPa$
$R = 1029\ (kg.m)^{-1/2}$

Upper Branch				Lower Branch			
h_A [mm]	T_o [°C]	$\dot{m}_G$ [kg/min]	$\dot{m}_L$ [kg/min]	h_B [mm]	T_o [°C]	$\dot{m}_G$ [kg/min]	$\dot{m}_L$ [kg/min]
16.36	18.9	0.00E+00	1.67E+01	11.48	18.6	0.00E+00	1.65E+01
14.37	19.1	1.13E-02	1.37E+01	10.43	18.8	5.56E-03	1.52E+01
12.23	19.0	3.16E-02	1.06E+01	9.06	18.8	1.37E-02	1.30E+01
10.17	19.0	5.72E-02	8.14E+00	6.96	19.0	3.32E-02	1.03E+01
8.07	18.9	8.97E-02	6.58E+00	4.83	19.0	6.67E-02	7.33E+00
5.97	18.9	1.32E-01	5.33E+00	2.76	18.9	1.09E-01	5.84E+00
3.90	18.9	1.79E-01	4.55E+00	0.59	18.8	1.65E-01	4.82E+00
1.80	18.9	2.36E-01	3.77E+00	-1.47	18.7	2.03E-01	4.00E+00
0.01	18.8	2.93E-01	3.03E+00	-3.57	18.6	2.57E-01	3.11E+00
-2.05	18.4	3.70E-01	2.24E+00	-5.67	18.5	3.27E-01	2.39E+00
-4.19	18.4	4.66E-01	1.37E+00	-7.77	18.5	3.97E-01	1.75E+00
-6.22	18.7	5.88E-01	5.93E-01	-9.87	18.5	4.77E-01	1.12E+00
-8.39	18.8	7.34E-01	2.01E-01	-11.97	18.5	5.73E-01	6.17E-01
-9.75	18.8	7.98E-01	1.00E-01	-13.93	18.4	7.00E-01	2.44E-01
-12.17	18.9	8.91E-01	0.00E+00	-15.19	18.3	8.10E-01	7.27E-02
				-16.03	18.4	8.89E-01	0.00E+00

Table D.1: Experimental data for dual discharge (cont.)
(Centerlines of branches in the same vertical plane)

Set No. 3 − 23							
$L/d = 3.0$ $P_0 = 316$ kPa $\Delta P = 40$ kPa $R = 997$ $(kg.m)^{-1/2}$							
Upper Branch				Lower Branch			
h_A $[mm]$	T_o $[^oC]$	$\dot{m}_G$ $[kg/min]$	$\dot{m}_L$ $[kg/min]$	h_B $[mm]$	T_o $[^oC]$	$\dot{m}_G$ $[kg/min]$	$\dot{m}_L$ $[kg/min]$
13.77	19.1	0.00E+00	1.21E+01	10.46	19.3	0.00E+00	1.20E+01
11.67	18.9	1.40E-02	8.89E+00	8.96	19.0	7.09E-03	9.87E+00
9.57	18.8	3.39E-02	6.70E+00	6.86	19.0	2.42E-02	7.44E+00
7.64	18.9	5.61E-02	5.41E+00	4.79	19.0	5.16E-02	5.45E+00
5.54	18.9	8.77E-02	4.39E+00	3.11	19.1	8.09E-02	4.43E+00
3.48	18.8	1.27E-01	3.61E+00	1.64	19.1	1.22E-01	3.71E+00
1.41	18.8	1.77E-01	2.98E+00	-1.09	19.1	1.65E-01	2.97E+00
-0.72	19.2	2.22E-01	2.30E+00	-3.19	19.1	2.08E-01	2.26E+00
-2.79	19.4	2.78E-01	1.64E+00	-5.29	19.0	2.51E-01	1.73E+00
-4.89	19.4	3.48E-01	1.05E+00	-7.39	19.0	3.09E-01	1.18E+00
-6.99	19.3	4.54E-01	4.49E-01	-9.49	18.9	3.80E-01	6.87E-01
-9.16	19.0	6.05E-01	8.24E-02	-11.41	18.7	4.69E-01	4.17E-01
-11.65	19.0	6.85E-01	0.00E+00	-13.34	18.6	5.74E-01	1.04E-01
				-14.66	18.2	6.81E-01	0.00E+00

Table D.1: Experimental data for dual discharge (cont.)
(Centerlines of branches in the same vertical plane)

Set No. 3 − 24
$L/d =$ 3.0
$P_0 =$ 517 kPa
$\Delta P =$ 235 kPa
$R =$ 1008 $(kg.m)^{-1/2}$

Upper Branch				Lower Branch			
h_A $[mm]$	T_o $[^oC]$	$\dot{m}_G$ $[kg/min]$	$\dot{m}_L$ $[kg/min]$	h_B $[mm]$	T_o $[^oC]$	$\dot{m}_G$ $[kg/min]$	$\dot{m}_L$ $[kg/min]$
20.08	23.6	0.00E+00	2.90E+01	13.17	23.9	0.00E+00	2.87E+01
17.97	24.4	2.16E-02	2.43E+01	11.45	23.5	1.35E-02	2.60E+01
15.86	24.7	5.54E-02	1.98E+01	9.34	23.2	3.71E-02	2.17E+01
13.79	25.1	1.04E-01	1.59E+01	7.24	23.1	8.03E-02	1.84E+01
11.65	25.2	1.56E-01	1.33E+01	5.14	23.5	1.38E-01	1.47E+01
9.54	25.3	2.23E-01	1.05E+01	3.10	23.7	2.12E-01	1.15E+01
7.44	25.6	3.04E-01	8.81E+00	0.89	23.7	2.77E-01	8.89E+00
5.37	25.5	3.92E-01	7.16E+00	-1.18	23.8	3.74E-01	7.21E+00
3.26	25.4	4.99E-01	5.72E+00	-3.21	23.7	4.76E-01	6.07E+00
1.09	25.2	6.22E-01	4.51E+00	-5.28	23.6	5.83E-01	4.94E+00
-0.98	25.0	7.64E-01	3.18E+00	-7.42	23.5	6.95E-01	4.00E+00
-3.13	24.1	9.61E-01	1.92E+00	-9.56	23.4	8.13E-01	2.89E+00
-5.20	24.1	1.20E+00	8.97E-01	-11.70	23.2	9.55E-01	1.99E+00
-7.37	23.5	1.45E+00	3.76E-01	-13.77	23.0	1.10E+00	1.25E+00
-9.47	23.2	1.60E+00	1.38E-01	-15.79	22.7	1.30E+00	6.10E-01
-12.84	23.3	1.77E+00	0.00E+00	-17.75	22.6	1.55E+00	2.15E-01
				-19.61	22.5	1.76E+00	0.00E+00

Table D.1: Experimental data for dual discharge (cont.)
(Centerlines of branches in the same vertical plane)

Set No. 3 – 25

$L/d =$ 3.0
$P_0 =$ 517 kPa
$\Delta P =$ 166 kPa
$R =$ 1006 $(kg.m)^{-1/2}$

Upper Branch				Lower Branch			
h_A [mm]	T_o [°C]	$\dot{m}_G$ [kg/min]	$\dot{m}_L$ [kg/min]	h_B [mm]	T_o [°C]	$\dot{m}_G$ [kg/min]	$\dot{m}_L$ [kg/min]
18.69	22.4	0.00E+00	2.44E+01	12.34	21.6	0.00E+00	2.41E+01
16.58	22.5	2.14E-02	2.06E+01	10.30	22.0	1.62E-02	2.14E+01
14.44	22.5	5.94E-02	1.62E+01	8.20	21.3	4.57E-02	1.76E+01
12.40	22.4	1.01E-01	1.32E+01	6.10	21.2	9.02E-02	1.45E+01
10.26	22.3	1.57E-01	1.07E+01	3.99	21.1	1.54E-01	1.11E+01
8.09	22.2	2.24E-01	8.73E+00	1.92	22.2	2.12E-01	8.85E+00
5.81	22.0	3.09E-01	7.01E+00	-0.25	21.5	2.98E-01	6.89E+00
3.81	22.0	3.89E-01	5.87E+00	-2.36	21.5	3.87E-01	5.64E+00
1.70	21.9	4.90E-01	4.63E+00	-4.43	21.7	4.82E-01	4.70E+00
-0.44	21.7	5.95E-01	3.63E+00	-6.54	21.8	5.75E-01	3.79E+00
-2.55	21.7	7.32E-01	2.43E+00	-8.58	24.0	7.03E-01	2.81E+00
-4.62	21.6	9.11E-01	1.38E+00	-10.79	23.5	8.19E-01	1.96E+00
-6.48	21.6	1.13E+00	5.47E-01	-12.83	23.4	9.62E-01	1.27E+00
-8.52	22.0	1.33E+00	2.81E-01	-15.00	23.3	1.16E+00	6.06E-01
-13.67	21.1	1.61E+00	0.00E+00	-17.06	23.1	1.39E+00	1.95E-01
				-19.06	22.9	1.62E+00	0.00E+00

Table D.1: Experimental data for dual discharge (cont.)
(Centerlines of branches in the same vertical plane)

Set No. 3 − 26

$L/d =$ 3.0

$P_0 =$ 517 kPa

$\Delta P =$ 97 kPa

$R =$ 1024 $(kg.m)^{-1/2}$

Upper Branch				Lower Branch			
h_A $[mm]$	T_o $[^oC]$	$\dot{m}_G$ $[kg/min]$	$\dot{m}_L$ $[kg/min]$	h_B $[mm]$	T_o $[^oC]$	$\dot{m}_G$ $[kg/min]$	$\dot{m}_L$ $[kg/min]$
16.33	25.9	0.00E+00	1.82E+01	11.29	22.3	0.00E+00	1.82E+01
14.32	26.2	1.95E-02	1.53E+01	8.90	22.5	2.01E-02	1.54E+01
12.22	26.4	5.56E-02	1.18E+01	6.76	22.5	5.53E-02	1.27E+01
10.15	26.6	9.98E-02	9.36E+00	4.69	22.5	1.05E-01	9.80E+00
8.40	22.8	1.47E-01	7.75E+00	2.58	22.1	1.57E-01	7.68E+00
6.19	22.8	2.13E-01	6.58E+00	0.48	22.1	2.26E-01	6.11E+00
4.19	22.8	2.75E-01	5.41E+00	-1.66	22.1	3.02E-01	5.13E+00
2.05	22.8	3.49E-01	4.47E+00	-3.77	22.1	3.89E-01	4.04E+00
-0.02	22.8	4.46E-01	3.58E+00	-5.81	21.9	4.82E-01	3.18E+00
-2.16	22.7	5.46E-01	2.59E+00	-8.02	22.5	5.87E-01	2.27E+00
-4.27	22.6	6.77E-01	1.64E+00	-10.09	22.5	6.91E-01	1.62E+00
-6.34	22.4	8.63E-01	7.86E-01	-12.19	22.4	8.10E-01	1.00E+00
-8.17	22.6	1.08E+00	2.93E-01	-14.29	22.3	9.90E-01	4.80E-01
-9.92	22.5	1.21E+00	1.38E-01	-18.25	21.9	1.34E+00	0.00E+00
-13.57	22.5	1.40E+00	0.00E+00				

Table D.1: Experimental data for dual discharge
(Centerlines of branches in the same vertical plane)

Set No. 3 − 27							
$L/d = 8.0$							
$P_0 = 316\ kPa$							
$\Delta P = 123\ kPa$							
$R = 1027\ (kg.m)^{-1/2}$							
Upper Branch				Lower Branch			
h_A [mm]	T_o [°C]	$\dot{m}_G$ [kg/min]	$\dot{m}_L$ [kg/min]	h_B [mm]	T_o [°C]	$\dot{m}_G$ [kg/min]	$\dot{m}_L$ [kg/min]
16.58	22.7	0.00E+00	2.05E+01	16.77	19.4	0.00E+00	2.05E+01
14.80	22.9	7.85E-03	1.72E+01	15.09	19.1	9.37E-03	1.75E+01
13.54	22.4	2.44E-02	1.43E+01	12.99	21.9	2.70E-02	1.35E+01
11.89	21.7	4.26E-02	1.17E+01	11.24	22.0	4.19E-02	1.17E+01
9.86	21.0	6.71E-02	9.40E+00	9.38	23.1	6.46E-02	9.09E+00
7.83	20.6	9.73E-02	7.75E+00	7.66	23.1	8.79E-02	7.76E+00
5.80	20.2	1.36E-01	6.58E+00	5.74	23.1	1.20E-01	6.74E+00
3.84	18.8	1.81E-01	5.68E+00	4.06	23.0	1.53E-01	5.88E+00
2.02	18.5	2.22E-01	4.98E+00	2.27	22.9	1.98E-01	5.09E+00
0.03	17.9	2.71E-01	4.24E+00	0.45	22.7	2.29E-01	4.39E+00
-2.11	17.9	3.33E-01	3.52E+00	-1.37	22.5	2.80E-01	3.80E+00
-4.21	20.6	3.95E-01	2.99E+00	-3.12	21.9	3.29E-01	3.24E+00
-6.24	20.5	4.57E-01	2.28E+00	-5.04	21.8	3.91E-01	2.61E+00
-8.34	20.5	5.29E-01	1.64E+00	-6.96	21.8	4.55E-01	2.10E+00
-10.47	20.1	6.22E-01	1.02E+00	-8.75	21.7	5.24E-01	1.55E+00
-12.08	20.1	6.93E-01	6.00E-01	-10.46	21.6	6.04E-01	1.07E+00
-13.42	20.1	7.67E-01	3.64E-01	-12.00	21.6	6.76E-01	6.87E-01
-14.57	20.0	8.49E-01	1.81E-01	-13.43	21.5	7.51E-01	4.63E-01
-15.87	21.6	9.93E-01	0.00E+00	-14.97	21.4	8.71E-01	1.91E-01
				-15.67	21.2	9.32E-01	1.00E-01
				-16.54	21.0	1.02E+00	0.00E+00

Table D.1: Experimental data for dual discharge (cont.)
(Centerlines of branches in the same vertical plane)

Set No. 3 – 28

$L/d =$ 8.0
$P_0 =$ 316 kPa
$\Delta P =$ 82 kPa
$R =$ 1025 $(kg.m)^{-1/2}$

Upper Branch				Lower Branch			
h_A [mm]	T_o [°C]	$\dot{m}_G$ [kg/min]	$\dot{m}_L$ [kg/min]	h_B [mm]	T_o [°C]	$\dot{m}_G$ [kg/min]	$\dot{m}_L$ [kg/min]
15.82	21.8	0.00E+00	1.66E+01	15.41	18.1	0.00E+00	1.67E+01
13.75	20.3	1.35E-02	1.32E+01	13.70	18.1	1.09E-02	1.40E+01
11.89	20.1	3.22E-02	1.05E+01	11.53	18.1	2.83E-02	1.05E+01
9.86	19.9	5.30E-02	8.34E+00	9.50	18.0	4.82E-02	8.23E+00
7.93	19.8	7.87E-02	6.97E+00	7.68	18.0	7.17E-02	6.82E+00
5.83	19.6	1.14E-01	5.80E+00	5.58	17.9	1.05E-01	5.76E+00
3.87	19.6	1.53E-01	5.02E+00	3.41	17.9	1.42E-01	4.90E+00
1.70	19.5	1.97E-01	4.32E+00	1.38	17.8	1.81E-01	4.15E+00
-0.31	19.2	2.43E-01	3.61E+00	-0.72	17.8	2.23E-01	3.49E+00
-2.31	20.0	2.93E-01	3.08E+00	-2.82	18.0	2.73E-01	2.79E+00
-4.23	20.3	3.51E-01	2.43E+00	-4.92	18.4	3.30E-01	2.20E+00
-6.26	20.3	4.06E-01	1.82E+00	-7.02	18.6	3.95E-01	1.61E+00
-8.29	19.6	4.84E-01	1.27E+00	-9.09	18.9	4.99E-01	1.10E+00
-10.36	18.9	5.60E-01	7.25E-01	-11.08	18.9	5.84E-01	6.59E-01
-11.90	18.7	6.37E-01	4.92E-01	-12.62	19.0	6.66E-01	4.21E-01
-13.51	18.5	7.31E-01	2.17E-01	-14.47	19.0	8.01E-01	1.20E-01
-15.58	19.5	8.86E-01	0.00E+00	-15.45	19.0	8.99E-01	0.00E+00

Table D.1: Experimental data for dual discharge (cont.)
(Centerlines of branches in the same vertical plane)

Set No. 3 – 29 $L/d =$ 8.0 $P_0 =$ 316 kPa $\Delta P =$ 40 kPa $R =$ 996 $(kg{\cdot}m)^{-1/2}$							
Upper Branch				Lower Branch			
h_A [mm]	T_o [°C]	$\dot{m}_G$ [kg/min]	$\dot{m}_L$ [kg/min]	h_B [mm]	T_o [°C]	$\dot{m}_G$ [kg/min]	$\dot{m}_L$ [kg/min]
13.96	21.5	0.00E+00	1.21E+01	13.33	19.8	0.00E+00	1.20E+01
12.28	20.8	7.85E-03	9.76E+00	11.34	19.7	1.22E-02	9.09E+00
10.18	20.6	2.54E-02	7.56E+00	9.24	19.7	2.77E-02	6.74E+00
8.07	20.3	4.55E-02	5.87E+00	7.31	19.7	4.74E-02	5.37E+00
6.32	20.1	6.48E-02	4.94E+00	5.39	19.6	7.05E-02	4.58E+00
4.36	19.8	9.62E-02	4.20E+00	3.33	19.5	1.05E-01	3.96E+00
2.33	22.3	1.32E-01	3.67E+00	1.33	19.6	1.36E-01	3.21E+00
0.51	21.6	1.67E-01	3.02E+00	-0.35	19.5	1.74E-01	2.74E+00
-1.45	21.3	2.17E-01	2.49E+00	-2.41	19.5	2.08E-01	2.27E+00
-3.44	21.0	2.57E-01	1.96E+00	-4.34	19.5	2.50E-01	1.69E+00
-5.54	20.4	3.07E-01	1.45E+00	-6.33	19.5	3.00E-01	1.24E+00
-6.87	20.2	3.65E-01	9.69E-01	-8.32	19.5	3.62E-01	8.01E-01
-9.04	20.0	4.29E-01	6.18E-01	-10.11	19.6	4.26E-01	4.76E-01
-10.73	19.8	4.92E-01	4.10E-01	-11.59	22.4	4.95E-01	3.25E-01
-12.09	19.7	5.54E-01	2.09E-01	-12.88	22.4	5.81E-01	1.36E-01
-13.21	19.6	6.09E-01	8.52E-02	-14.21	22.4	6.92E-01	0.00E+00
-14.47	19.6	6.81E-01	0.00E+00				

Table D.1: Experimental data for dual discharge (cont.)
(Centerlines of branches in the same vertical plane)

Set No. 3 − 30

$L/d =$ 8.0
$P_0 =$ 517 kPa
$\Delta P =$ 235 kPa
$R =$ 1013 $(kg.m)^{-1/2}$

Upper Branch				Lower Branch			
h_A $[mm]$	T_o $[^oC]$	$\dot{m}_G$ $[kg/min]$	$\dot{m}_L$ $[kg/min]$	h_B $[mm]$	T_o $[^oC]$	$\dot{m}_G$ $[kg/min]$	$\dot{m}_L$ $[kg/min]$
18.81	23.2	0.00E+00	2.85E+01	18.66	23.5	0.00E+00	2.89E+01
12.56	24.2	9.21E-02	1.58E+01	16.63	23.8	2.26E-02	2.44E+01
10.47	22.6	1.39E-01	1.30E+01	14.56	23.9	5.55E-02	2.00E+01
8.29	23.0	1.87E-01	1.09E+01	12.24	23.9	9.31E-02	1.62E+01
6.22	23.3	2.50E-01	9.32E+00	10.31	23.9	1.36E-01	1.34E+01
4.11	23.5	3.10E-01	7.79E+00	8.24	23.9	1.86E-01	1.12E+01
2.04	23.6	3.87E-01	6.73E+00	6.06	23.7	2.28E-01	9.36E+00
-0.10	23.7	4.79E-01	5.80E+00	3.92	23.7	2.93E-01	8.07E+00
-2.20	23.7	5.62E-01	4.90E+00	1.85	23.7	3.66E-01	6.89E+00
-4.31	23.2	6.61E-01	4.16E+00	-0.29	23.7	4.44E-01	5.92E+00
-6.42	23.5	7.45E-01	3.21E+00	-2.36	23.5	5.40E-01	5.05E+00
-8.53	23.4	8.58E-01	2.51E+00	-4.47	23.5	6.36E-01	4.19E+00
-10.60	23.5	9.78E-01	1.81E+00	-6.54	23.5	7.34E-01	3.42E+00
-12.74	23.6	1.17E+00	1.14E+00	-8.68	23.5	8.62E-01	2.63E+00
-14.84	23.7	1.36E+00	5.83E-01	-10.79	23.6	9.99E-01	1.96E+00
-18.00	23.2	1.76E+00	0.00E+00	-12.92	23.6	1.17E+00	1.31E+00
				-14.92	23.6	1.34E+00	6.94E-01
				-16.74	23.6	1.55E+00	2.76E-01
				-18.69	23.2	1.78E+00	0.00E+00

Table D.1: Experimental data for dual discharge (cont.)
(Centerlines of branches in the same vertical plane)

$Set\ No. 3-31$
$L/d = 8.0$
$P_0 = 517\ kPa$
$\Delta P = 166\ kPa$
$R = 1020\ (kg.m)^{-1/2}$

Upper Branch				Lower Branch			
h_A $[mm]$	T_o $[^oC]$	$\dot{m}_G$ $[kg/min]$	$\dot{m}_L$ $[kg/min]$	h_B $[mm]$	T_o $[^oC]$	$\dot{m}_G$ $[kg/min]$	$\dot{m}_L$ $[kg/min]$
17.56	21.2	0.00E+00	2.37E+01	17.52	22.2	0.00E+00	2.41E+01
15.56	21.5	1.90E-02	2.00E+01	15.23	22.7	2.58E-02	2.00E+01
13.46	21.9	5.32E-02	1.61E+01	13.13	22.7	6.02E-02	1.62E+01
11.39	22.1	8.79E-02	1.35E+01	11.02	22.2	9.61E-02	1.34E+01
9.21	22.2	1.32E-01	1.08E+01	8.95	22.6	1.36E-01	1.10E+01
7.11	22.4	1.84E-01	8.85E+00	6.84	22.6	1.87E-01	9.09E+00
5.07	22.5	2.41E-01	7.56E+00	4.63	22.6	2.36E-01	7.60E+00
2.89	22.5	3.07E-01	6.46E+00	2.52	22.6	2.97E-01	6.54E+00
0.72	22.4	3.80E-01	5.48E+00	0.42	23.4	3.67E-01	5.56E+00
-1.32	22.3	4.69E-01	4.70E+00	-1.62	22.5	4.46E-01	4.78E+00
-3.46	22.3	5.60E-01	4.04E+00	-3.79	22.5	5.46E-01	4.08E+00
-5.53	22.3	6.50E-01	3.22E+00	-5.90	22.3	6.39E-01	3.22E+00
-7.64	22.2	7.45E-01	2.45E+00	-7.97	22.2	7.45E-01	2.51E+00
-9.81	22.2	8.75E-01	1.79E+00	-10.07	22.1	8.70E-01	1.83E+00
-11.85	20.8	9.00E-01	1.12E+00	-12.18	22.1	1.03E+00	1.22E+00
-13.95	20.9	1.19E+00	6.18E-01	-14.28	22.1	1.20E+00	6.24E-01
-16.06	21.2	1.40E+00	2.33E-01	-16.34	22.0	1.42E+00	2.78E-01
-17.25	21.8	1.61E+00	0.00E+00	-17.99	22.0	1.59E+00	0.00E+00

Table D.1: Experimental data for dual discharge (cont.)
(Centerlines of branches in the same vertical plane)

Set No. 3 – 32 $L/d = 8.0$ $P_0 = 517\ kPa$ $\Delta P = 97\ kPa$ $R = 1020\ (kg.m)^{-1/2}$							
Upper Branch				Lower Branch			
h_A [mm]	T_o [^oC]	$\dot{m}_G$ [kg/min]	$\dot{m}_L$ [kg/min]	h_B [mm]	T_o [^oC]	$\dot{m}_G$ [kg/min]	$\dot{m}_L$ [kg/min]
15.66	22.8	0.00E+00	1.80E+01	15.73	21.2	0.00E+00	1.85E+01
13.97	22.8	1.88E-02	1.56E+01	13.66	21.2	2.07E-02	1.53E+01
11.83	22.6	5.14E-02	1.24E+01	11.52	21.1	5.22E-02	1.22E+01
9.94	22.4	8.18E-02	9.52E+00	9.42	19.9	8.34E-02	9.72E+00
7.83	22.4	1.22E-01	7.87E+00	7.28	19.9	1.27E-01	7.87E+00
5.73	22.4	1.69E-01	6.73E+00	5.10	20.0	1.76E-01	6.62E+00
3.61	19.4	2.29E-01	5.60E+00	3.03	20.1	2.18E-01	5.56E+00
1.50	20.7	2.78E-01	4.82E+00	0.85	20.3	2.77E-01	4.74E+00
-0.61	20.7	3.58E-01	4.08E+00	-1.19	20.5	3.43E-01	4.04E+00
-2.71	21.0	4.39E-01	3.40E+00	-3.29	20.6	4.31E-01	3.34E+00
-4.85	21.1	5.28E-01	2.75E+00	-5.50	20.7	5.23E-01	2.66E+00
-6.97	21.2	6.06E-01	2.14E+00	-7.51	20.8	6.17E-01	2.03E+00
-9.04	21.4	7.07E-01	1.54E+00	-9.58	20.8	7.13E-01	1.43E+00
-11.14	21.4	8.27E-01	9.69E-01	-11.78	20.8	8.68E-01	8.76E-01
-13.22	21.4	9.78E-01	4.66E-01	-13.89	20.9	1.04E+00	4.25E-01
-15.36	21.2	1.13E+00	1.54E-01	-15.60	20.8	1.23E+00	1.04E-01
-16.30	21.1	1.33E+00	0.00E+00	-16.44	20.6	1.34E+00	0.00E+00

APPENDIX E

Experimental Data for the Semicircular Duct

Table E.1: Experimental data for the semicircular duct

Set No. 4 − 1 Branch A Only P_0 = 316 kPa ΔP = 123 kPa R = 1016 $(kg.m)^{-1/2}$				Set No. 4 − 2 Branch A Only P_0 = 316 kPa ΔP = 40 kPa R = 1000 $(kg.m)^{-1/2}$				Set No. 4 − 3 Branch A Only P_0 = 517 kPa ΔP = 235 kPa R = 1003 $(kg.m)^{-1/2}$			
h_A $[mm]$	T_o $[^oC]$	$\dot{m}_G$ $[kg/min]$	$\dot{m}_L$ $[kg/min]$	h_A $[mm]$	T_o $[^oC]$	$\dot{m}_G$ $[kg/min]$	$\dot{m}_L$ $[kg/min]$	h_A $[mm]$	T_o $[^oC]$	$\dot{m}_G$ $[kg/min]$	$\dot{m}_L$ $[kg/min]$
15.93	22.1	0.00E+00	2.07E+01	12.46	24.2	0.00E+00	1.20E+01	18.00	25.7	0.00E+00	2.90E+01
13.93	21.9	1.53E-02	1.66E+01	10.36	24.3	1.50E-02	9.13E+00	15.79	26.1	2.39E-02	2.53E+01
11.80	22.5	4.34E-02	1.38E+01	8.37	24.3	3.36E-02	7.05E+00	13.69	26.4	6.75E-02	2.07E+01
9.66	22.0	8.38E-02	1.17E+01	6.20	24.5	6.54E-02	5.84E+00	11.62	26.7	1.24E-01	1.72E+01
7.59	22.7	1.29E-01	9.83E+00	4.13	24.7	1.05E-01	5.02E+00	9.51	26.6	1.92E-01	1.47E+01
5.49	22.7	1.78E-01	8.34E+00	1.96	25.0	1.58E-01	4.35E+00	7.37	26.3	2.64E-01	1.32E+01
3.46	22.7	2.33E-01	6.97E+00	-0.07	25.2	2.09E-01	3.65E+00	5.26	26.3	3.43E-01	1.11E+01
1.40	22.7	2.81E-01	5.99E+00	-2.24	25.3	2.64E-01	2.92E+00	3.16	26.1	4.35E-01	9.44E+00
-0.81	22.7	3.48E-01	4.94E+00	-4.31	25.4	3.10E-01	2.20E+00	1.06	25.8	5.19E-01	7.83E+00
-3.05	22.8	4.14E-01	3.91E+00	-6.41	25.5	3.65E-01	1.51E+00	-1.05	25.7	6.15E-01	6.58E+00
-5.18	22.9	4.83E-01	2.96E+00	-8.51	25.6	4.39E-01	1.01E+00	-3.12	25.5	7.20E-01	5.41E+00
-7.29	22.8	5.44E-01	2.17E+00	-10.61	25.8	5.03E-01	6.54E-01	-5.23	25.5	7.94E-01	4.24E+00
-9.49	22.3	6.26E-01	1.42E+00	-12.71	25.8	6.00E-01	2.09E-01	-7.37	25.2	9.05E-01	3.28E+00
-11.56	22.8	7.20E-01	8.86E-01	-15.86	25.8	6.75E-01	0.00E+00	-9.44	25.1	1.03E+00	2.41E+00
-13.83	22.7	8.50E-01	4.23E-01					-11.62	24.9	1.17E+00	1.64E+00
-18.31	22.6	1.03E+00	0.00E+00					-13.69	24.7	1.32E+00	9.94E-01
								-15.83	24.6	1.48E+00	4.49E-01
								-17.55	24.4	1.62E+00	1.66E-01
								-20.71	24.0	1.72E+00	0.00E+00

Table E.1: Experimental data for the semicircular duct (cont.)

Set No. 4 – 4
Branch B Only
P_0 = 316 kPa
ΔP = 123 kPa
R = 1012 $(kg.m)^{-1/2}$

h_B [mm]	T_o [^oC]	$\dot{m}_G$ [kg/min]	$\dot{m}_L$ [kg/min]
19.24	23.2	0.00E+00	2.08E+01
17.15	23.1	1.98E-02	1.68E+01
15.05	22.9	5.98E-02	1.37E+01
12.91	23.2	1.30E-01	1.13E+01
10.85	23.0	2.08E-01	9.28E+00
8.75	23.0	2.78E-01	7.56E+00
6.65	23.2	3.53E-01	6.07E+00
4.58	23.0	4.36E-01	4.86E+00
2.41	23.2	5.13E-01	3.75E+00
0.38	22.9	6.09E-01	2.81E+00
-1.72	22.9	7.04E-01	1.81E+00
-3.86	22.8	8.13E-01	1.01E+00
-5.92	22.7	9.45E-01	3.30E-01
-7.44	22.7	1.04E+00	0.00E+00

Set No. 4 – 5
Branch B Only
P_0 = 316 kPa
ΔP = 40 kPa
R = 1000 $(kg.m)^{-1/2}$

h_B [mm]	T_o [^oC]	$\dot{m}_G$ [kg/min]	$\dot{m}_L$ [kg/min]
15.02	22.5	0.00E+00	1.20E+01
12.96	22.5	1.95E-02	8.93E+00
10.82	22.5	5.06E-02	6.70E+00
8.76	22.9	1.05E-01	5.41E+00
6.69	23.3	1.83E-01	4.63E+00
4.55	23.4	2.50E-01	3.70E+00
2.45	23.6	3.08E-01	2.71E+00
0.32	24.0	3.80E-01	1.94E+00
-1.78	24.0	4.65E-01	1.27E+00
-3.81	24.1	5.41E-01	6.96E-01
-5.95	24.2	6.40E-01	2.29E-01
-7.35	24.2	7.04E-01	0.00E+00

Set No. 4 – 6
Branch B Only
P_0 = 517 kPa
ΔP = 235 kPa
R = 1003 $(kg.m)^{-1/2}$

h_B [mm]	T_o [^oC]	$\dot{m}_G$ [kg/min]	$\dot{m}_L$ [kg/min]
21.82	24.6	0.00E+00	2.90E+01
19.71	25.2	3.39E-02	2.47E+01
17.60	26.3	1.05E-01	2.05E+01
15.53	26.4	1.96E-01	1.70E+01
13.36	26.5	2.94E-01	1.49E+01
11.32	26.6	3.96E-01	1.25E+01
9.18	26.8	5.07E-01	1.01E+01
7.08	26.9	6.21E-01	8.07E+00
4.97	26.9	7.36E-01	6.38E+00
2.86	26.5	8.56E-01	5.02E+00
0.79	26.4	1.01E+00	3.83E+00
-1.35	26.3	1.17E+00	2.73E+00
-3.56	26.3	1.34E+00	1.58E+00
-5.91	26.1	1.54E+00	5.47E-01
-7.44	25.9	1.74E+00	0.00E+00

Table E.1: Experimental data for the semicircular duct (cont.)

Set No. 4 − 7 *Branch C Only* P_0 = 316 kPa ΔP = 123 kPa R = 1017 $(kg.m)^{-1/2}$				*Set No. 4 − 8* *Branch C Only* P_0 = 316 kPa ΔP = 40 kPa R = 992 $(kg.m)^{-1/2}$				*Set No. 4 − 9* *Branch C Only* P_0 = 517 kPa ΔP = 235 kPa R = 1010 $(kg.m)^{-1/2}$			
h_C $[mm]$	T_o $[^oC]$	$\dot{m}_G$ $[kg/min]$	$\dot{m}_L$ $[kg/min]$	h_C $[mm]$	T_o $[^oC]$	$\dot{m}_G$ $[kg/min]$	$\dot{m}_L$ $[kg/min]$	h_C $[mm]$	T_o $[^oC]$	$\dot{m}_G$ $[kg/min]$	$\dot{m}_L$ $[kg/min]$
20.74	22.6	0.00E+00	2.07E+01	15.14	25.4	0.00E+00	1.21E+01	22.59	26.3	0.00E+00	2.88E+01
17.97	23.5	7.40E-03	1.88E+01	13.04	25.4	1.61E-02	9.32E+00	20.48	26.1	1.70E-02	2.61E+01
15.84	24.0	3.71E-02	1.49E+01	10.24	25.9	8.79E-02	6.19E+00	18.38	26.0	6.14E-02	2.10E+01
13.74	24.3	1.05E-01	1.17E+01	8.11	25.9	1.90E-01	4.59E+00	16.27	26.0	1.52E-01	1.68E+01
11.60	24.5	2.06E-01	8.81E+00	6.04	27.2	2.78E-01	3.12E+00	14.17	26.0	2.65E-01	1.41E+01
9.57	24.6	3.08E-01	6.58E+00	3.94	26.0	3.83E-01	1.71E+00	12.10	26.1	4.26E-01	1.06E+01
7.50	24.4	4.26E-01	4.63E+00	2.19	26.1	4.98E-01	7.43E-01	9.99	26.1	6.09E-01	7.99E+00
5.33	24.5	5.47E-01	2.94E+00	0.65	26.3	6.09E-01	1.31E-01	7.89	26.1	7.68E-01	5.80E+00
3.23	24.4	6.91E-01	1.45E+00	0.00	26.3	7.04E-01	0.00E+00	5.71	26.2	9.64E-01	3.89E+00
1.24	24.3	8.42E-01	3.60E-01					3.67	26.1	1.16E+00	2.20E+00
0.00	24.2	1.04E+00	0.00E+00					1.46	26.2	1.40E+00	7.25E-01
								0.00	26.2	1.73E+00	0.00E+00

Table E.1: Experimental data for the semicircular duct (cont.)

Set No. 4 – 10 Branches A and B Active P_0 = 316 kPa ΔP = 123 kPa							
Branch A R = 1026 $(kg.m)^{-1/2}$				Branch B R = 1026 $(kg.m)^{-1/2}$			
h_A $[mm]$	T_o $[^oC]$	$\dot{m}_G$ $[kg/min]$	$\dot{m}_L$ $[kg/min]$	h_B $[mm]$	T_o $[^oC]$	$\dot{m}_G$ $[kg/min]$	$\dot{m}_L$ $[kg/min]$
17.53	23.6	0.00E+00	2.05E+01	17.18	23.5	0.00E+00	2.05E+01
15.32	23.6	1.76E-02	1.62E+01	15.00	24.0	1.68E-02	1.80E+01
13.15	23.7	5.35E-02	1.35E+01	12.94	25.0	4.27E-02	1.49E+01
11.12	23.7	1.05E-01	1.09E+01	10.81	23.8	9.06E-02	1.25E+01
8.99	23.7	1.65E-01	8.77E+00	6.46	24.5	2.38E-01	8.14E+00
6.89	24.2	2.33E-01	6.97E+00	4.54	24.1	3.10E-01	6.50E+00
4.82	23.6	3.07E-01	5.41E+00	2.47	24.1	3.98E-01	4.82E+00
2.65	23.9	4.06E-01	3.75E+00	0.30	24.1	4.89E-01	3.64E+00
0.55	23.6	5.31E-01	2.17E+00	-1.80	24.1	5.87E-01	2.49E+00
-1.13	23.5	6.72E-01	1.05E+00	-5.93	23.6	8.24E-01	5.83E-01
-2.96	24.0	7.52E-01	7.61E-01	-7.44	23.8	9.76E-01	0.00E+00
-5.02	25.0	8.45E-01	4.49E-01				
-7.15	23.8	9.17E-01	2.09E-01				
-11.50	23.9	1.02E+00	0.00E+00				

Table E.1: Experimental data for the semicircular duct (cont.)

Set No. 4 – 11 *Branches A and B Active* P_0 = 316 kPa ΔP = 40 kPa							
Branch A R = 992 $(kg.m)^{-1/2}$				*Branch B* R = 976 $(kg.m)^{-1/2}$			
h_A $[mm]$	T_o $[^oC]$	$\dot{m}_G$ $[kg/min]$	$\dot{m}_L$ $[kg/min]$	h_B $[mm]$	T_o $[^oC]$	$\dot{m}_G$ $[kg/min]$	$\dot{m}_L$ $[kg/min]$
14.12	20.3	0.00E+00	1.21E+01	14.07	22.8	0.00E+00	1.23E+01
12.12	20.7	1.18E-02	9.79E+00	11.90	22.4	1.68E-02	1.01E+01
10.05	21.0	3.48E-02	7.71E+00	9.80	22.6	3.97E-02	7.75E+00
8.02	21.2	6.71E-02	6.07E+00	7.67	22.7	8.01E-02	6.19E+00
5.85	21.4	1.24E-01	5.06E+00	5.57	22.7	1.53E-01	4.63E+00
3.40	22.1	1.86E-01	4.16E+00	3.47	24.3	2.37E-01	4.16E+00
1.30	22.1	2.36E-01	3.30E+00	1.44	24.9	3.06E-01	3.06E+00
-0.81	22.3	3.08E-01	2.22E+00	-0.67	25.2	3.75E-01	2.09E+00
-2.95	22.8	3.97E-01	1.07E+00	-2.80	25.3	4.62E-01	1.32E+00
-5.01	23.2	5.24E-01	4.70E-01	-4.97	27.2	5.49E-01	5.83E-01
-7.11	22.4	5.94E-01	2.65E-01	-6.76	25.5	6.46E-01	1.23E-01
-11.84	20.4	6.77E-01	0.00E+00	-7.44	25.1	6.80E-01	0.00E+00

Table E.1: Experimental data for the semicircular duct (cont.)

Set No. 4 – 12 *Branches A and B Active* P_0 = 517 kPa ΔP = 235 kPa							
Branch A R = 1020 $(kg.m)^{-1/2}$				*Branch B* R = 1010 $(kg.m)^{-1/2}$			
h_A $[mm]$	T_o $[^oC]$	$\dot{m}_G$ $[kg/min]$	$\dot{m}_L$ $[kg/min]$	h_B $[mm]$	T_o $[^oC]$	$\dot{m}_G$ $[kg/min]$	$\dot{m}_L$ $[kg/min]$
20.49	23.0	0.00E+00	2.85E+01	19.17	24.8	0.00E+00	2.88E+01
18.42	23.3	2.15E-02	2.43E+01	17.43	23.3	1.52E-02	2.55E+01
16.34	23.7	7.56E-02	1.96E+01	15.29	23.3	5.79E-02	2.28E+01
14.20	24.1	1.52E-01	1.64E+01	13.22	23.5	1.11E-01	2.00E+01
12.09	24.3	2.27E-01	1.39E+01	11.12	23.8	1.78E-01	1.72E+01
9.95	24.5	3.26E-01	1.14E+01	8.98	24.0	2.68E-01	1.47E+01
7.87	24.8	4.44E-01	8.73E+00	6.91	24.1	3.78E-01	1.21E+01
5.76	25.0	5.93E-01	6.42E+00	4.76	25.1	5.14E-01	9.32E+00
3.66	25.2	7.55E-01	4.43E+00	2.69	25.4	6.50E-01	7.13E+00
1.52	24.3	9.71E-01	2.43E+00	0.58	25.6	7.86E-01	5.29E+00
-0.53	23.3	1.10E+00	1.66E+00	-1.56	25.7	9.50E-01	3.79E+00
-2.67	23.3	1.26E+00	1.03E+00	-3.78	25.6	1.13E+00	2.24E+00
-4.74	23.5	1.39E+00	5.47E-01	-6.27	25.6	1.36E+00	7.07E-01
-6.84	23.8	1.51E+00	2.33E-01	-7.44	25.2	1.58E+00	0.00E+00
-11.08	24.8	1.63E+00	0.00E+00				

Table E.1: Experimental data for the semicircular duct (cont.)

Set No. 4 − 13 *Branches A and C Active* P_0 = 316 kPa ΔP = 123 kPa							
Branch A R = 1026 $(kg.m)^{-1/2}$				*Branch C* R = 1007 $(kg.m)^{-1/2}$			
h_A $[mm]$	T_o $[^oC]$	$\dot{m}_G$ $[kg/min]$	$\dot{m}_L$ $[kg/min]$	h_C $[mm]$	T_o $[^oC]$	$\dot{m}_G$ $[kg/min]$	$\dot{m}_L$ $[kg/min]$
16.65	23.6	0.00E+00	2.05E+01	20.03	25.6	0.00E+00	2.09E+01
14.62	23.8	1.25E-02	1.70E+01	17.57	25.2	1.27E-02	1.74E+01
12.45	23.9	4.10E-02	1.40E+01	15.47	25.1	5.17E-02	1.37E+01
10.41	24.9	8.69E-02	1.17E+01	13.37	24.9	1.16E-01	1.12E+01
8.25	25.8	1.30E-01	1.01E+01	11.24	24.8	2.03E-01	8.93E+00
6.21	25.3	1.78E-01	8.54E+00	9.29	23.4	2.74E-01	6.97E+00
4.08	25.4	2.36E-01	7.05E+00	7.08	23.4	3.95E-01	4.78E+00
1.98	25.9	2.90E-01	5.80E+00	4.98	23.1	5.18E-01	3.20E+00
-0.12	25.6	3.49E-01	4.86E+00	2.88	23.3	6.32E-01	1.64E+00
-2.22	26.0	4.18E-01	3.71E+00	1.13	23.2	7.63E-01	5.30E-01
-3.94	26.0	4.86E-01	2.93E+00	0.00	23.2	9.66E-01	0.00E+00
-6.08	25.5	5.81E-01	1.55E+00				
-7.83	25.2	6.59E-01	1.08E+00				
-9.93	25.1	7.54E-01	7.36E-01				
-12.03	24.9	8.54E-01	3.01E-01				
-15.52	23.4	9.89E-01	0.00E+00				

Table E.1: Experimental data for the semicircular duct (cont.)

Set No. 4 – 14 *Branches A and C Active* P_0 = 316 kPa ΔP = 40 kPa							
Branch A R = 1008 $(kg.m)^{-1/2}$				*Branch C* R = 992 $(kg.m)^{-1/2}$			
h_A $[mm]$	T_o $[^oC]$	$\dot{m}_G$ $[kg/min]$	$\dot{m}_L$ $[kg/min]$	h_C $[mm]$	T_o $[^oC]$	$\dot{m}_G$ $[kg/min]$	$\dot{m}_L$ $[kg/min]$
13.38	21.9	0.00E+00	1.19E+01	15.02	26.0	0.00E+00	1.21E+01
11.24	22.2	9.82E-03	9.32E+00	12.99	26.1	1.46E-02	9.72E+00
9.14	22.6	3.24E-02	7.36E+00	10.90	26.2	5.56E-02	6.97E+00
6.93	23.0	6.52E-02	6.07E+00	8.83	26.1	1.17E-01	5.29E+00
4.83	23.5	1.03E-01	5.06E+00	6.77	26.9	2.23E-01	3.91E+00
2.69	24.1	1.54E-01	4.39E+00	4.56	26.9	3.24E-01	2.40E+00
0.55	24.3	2.01E-01	3.85E+00	2.50	27.1	4.24E-01	1.07E+00
-1.48	24.4	2.33E-01	2.99E+00	0.85	27.1	5.33E-01	2.81E-01
-3.65	24.8	2.89E-01	2.31E+00	0.00	27.1	6.67E-01	0.00E+00
-5.68	24.9	3.37E-01	1.67E+00				
-7.82	25.3	4.03E-01	1.10E+00				
-9.96	26.0	4.98E-01	5.47E-01				
-12.41	26.1	6.25E-01	8.52E-02				
-15.16	26.9	6.60E-01	0.00E+00				

Table E.1: Experimental data for the semicircular duct (cont.)

Set No. 4 – 15
Branches A and C Active
P_0 = 517 kPa
ΔP = 235 kPa

Branch A $R = 1010$ $(kg.m)^{-1/2}$				Branch C $R = 1010$ $(kg.m)^{-1/2}$			
h_A $[mm]$	T_o $[^oC]$	$\dot{m}_G$ $[kg/min]$	$\dot{m}_L$ $[kg/min]$	h_C $[mm]$	T_o $[^oC]$	$\dot{m}_G$ $[kg/min]$	$\dot{m}_L$ $[kg/min]$
19.25	19.2	0.00E+00	2.88E+01	22.33	22.7	0.00E+00	2.88E+01
17.18	19.6	1.87E-02	2.45E+01	20.12	23.6	2.84E-02	2.45E+01
15.11	20.0	6.14E-02	2.03E+01	18.01	23.8	7.21E-02	2.03E+01
13.00	20.7	1.19E-01	1.74E+01	15.91	24.0	1.49E-01	1.70E+01
10.89	20.7	1.87E-01	1.53E+01	13.74	24.1	2.56E-01	1.44E+01
8.78	21.1	2.51E-01	1.33E+01	11.68	24.2	3.71E-01	1.17E+01
6.67	21.5	3.89E-01	1.11E+01	9.65	24.2	5.00E-01	9.13E+00
4.56	21.9	4.14E-01	9.24E+00	7.55	24.4	6.63E-01	6.58E+00
2.45	22.0	5.10E-01	7.63E+00	5.43	25.8	7.96E-01	4.51E+00
0.34	22.3	6.09E-01	5.87E+00	3.29	25.7	9.88E-01	2.62E+00
-3.07	22.7	8.01E-01	3.02E+00	0.72	25.6	1.25E+00	7.25E-01
-5.28	23.6	9.40E-01	1.99E+00	0.00	25.5	1.53E+00	0.00E+00
-7.39	23.8	1.07E+00	1.59E+00				
-9.49	24.0	1.22E+00	1.05E+00				
-11.66	24.1	1.38E+00	5.59E-01				
-13.72	24.2	1.52E+00	1.66E-01				
-16.85	25.1	1.59E+00	0.00E+00				

Table E.1: Experimental data for the semicircular duct (cont.)

Set No. 4 – 16 Branches B and C Active P_0 = 316 kPa ΔP = 123 kPa							
Branch B R = 1026 $(kg.m)^{-1/2}$				Branch C R = 1012 $(kg.m)^{-1/2}$			
h_B $[mm]$	T_o $[^oC]$	$\dot{m}_G$ $[kg/min]$	$\dot{m}_L$ $[kg/min]$	h_C $[mm]$	T_o $[^oC]$	$\dot{m}_G$ $[kg/min]$	$\dot{m}_L$ $[kg/min]$
21.80	23.8	0.00E+00	2.05E+01	21.29	23.7	0.00E+00	2.08E+01
19.56	23.8	1.61E-02	1.64E+01	18.95	23.7	1.83E-02	1.68E+01
17.49	23.8	8.63E-02	1.27E+01	16.88	23.7	5.16E-02	1.37E+01
15.36	24.5	1.85E-01	9.13E+00	14.78	24.0	1.12E-01	1.15E+01
13.33	24.6	3.01E-01	6.03E+00	12.68	23.9	1.91E-01	9.32E+00
11.51	23.7	3.51E-01	5.33E+00	10.58	23.8	2.61E-01	7.56E+00
9.44	23.7	4.26E-01	4.24E+00	8.52	24.4	3.34E-01	5.80E+00
7.34	24.0	5.16E-01	3.14E+00	6.38	23.6	4.28E-01	4.24E+00
5.24	23.9	6.25E-01	2.17E+00	4.35	23.5	5.27E-01	2.98E+00
3.14	23.8	7.24E-01	1.41E+00	2.21	23.4	6.60E-01	1.43E+00
1.08	24.4	8.16E-01	8.32E-01	0.43	23.1	7.88E-01	4.06E-01
-1.06	23.6	9.03E-01	4.10E-01	0.00	23.4	9.59E-01	0.00E+00
-5.61	23.4	9.90E-01	0.00E+00				

Table E.1: Experimental data for the semicircular duct (cont.)

Set No. 4 – 17 Branches B and C Active P_0 = 316 kPa ΔP = 40 kPa							
Branch B R = 1000 $(kg.m)^{-1/2}$				Branch C R = 1000 $(kg.m)^{-1/2}$			
h_B $[mm]$	T_o $[^oC]$	$\dot{m}_G$ $[kg/min]$	$\dot{m}_L$ $[kg/min]$	h_C $[mm]$	T_o $[^oC]$	$\dot{m}_G$ $[kg/min]$	$\dot{m}_L$ $[kg/min]$
17.23	20.2	0.00E+00	1.20E+01	16.62	22.4	0.00E+00	1.20E+01
15.06	21.1	1.15E-02	9.76E+00	15.14	23.0	1.23E-02	9.72E+00
12.96	21.8	5.74E-02	7.32E+00	13.00	23.3	3.96E-02	7.60E+00
10.86	22.4	1.40E-01	5.37E+00	10.94	22.2	9.66E-02	6.11E+00
7.70	23.0	2.36E-01	3.22E+00	8.84	22.7	1.64E-01	4.82E+00
5.56	23.3	2.92E-01	2.32E+00	6.35	23.3	2.64E-01	3.46E+00
3.50	22.2	3.96E-01	1.63E+00	4.29	23.4	3.50E-01	2.20E+00
1.40	22.7	4.77E-01	9.94E-01	2.47	23.5	4.27E-01	1.10E+00
-1.09	23.3	5.63E-01	3.97E-01	0.79	23.6	5.34E-01	2.49E-01
-3.15	23.4	6.29E-01	1.00E-01	0.00	23.6	6.75E-01	0.00E+00
-6.12	23.6	6.57E-01	0.00E+00				

Table E.1: Experimental data for the semicircular duct (cont.)

Set No. 4 – 18 *Branches B and C Active* P_0 = 517 kPa ΔP = 235 kPa							
Branch B R = 1010 $(kg.m)^{-1/2}$				*Branch C* R = 1021 $(kg.m)^{-1/2}$			
h_B $[mm]$	T_o $[^oC]$	$\dot{m}_G$ $[kg/min]$	$\dot{m}_L$ $[kg/min]$	h_C $[mm]$	T_o $[^oC]$	$\dot{m}_G$ $[kg/min]$	$\dot{m}_L$ $[kg/min]$
25.14	24.5	0.00E+00	2.88E+01	24.38	26.3	0.00E+00	2.85E+01
23.03	25.0	2.83E-02	2.38E+01	22.56	26.4	2.53E-02	2.59E+01
20.92	25.4	1.24E-01	1.81E+01	20.47	25.6	6.78E-02	2.19E+01
18.81	25.7	2.47E-01	1.38E+01	18.32	25.6	1.37E-01	1.81E+01
17.23	26.1	3.96E-01	1.09E+01	16.25	25.6	2.23E-01	1.61E+01
15.12	26.4	5.47E-01	8.50E+00	14.11	25.8	3.18E-01	1.37E+01
13.03	25.6	6.48E-01	6.73E+00	12.04	25.9	4.15E-01	1.13E+01
10.88	25.5	7.53E-01	5.37E+00	9.93	26.0	5.30E-01	9.05E+00
8.81	25.6	8.91E-01	4.16E+00	7.90	26.1	6.40E-01	6.97E+00
6.67	25.8	1.03E+00	3.18E+00	5.73	26.1	7.84E-01	5.02E+00
4.60	25.9	1.14E+00	2.38E+00	3.66	26.1	9.35E-01	3.26E+00
2.49	26.0	1.25E+00	1.56E+00	0.80	25.9	1.20E+00	1.05E+00
0.46	26.1	1.35E+00	9.76E-01	0.00	25.7	1.57E+00	0.00E+00
-1.71	26.1	1.44E+00	4.77E-01				
-3.78	26.1	1.50E+00	1.81E-01				
-7.44	25.7	1.54E+00	0.00E+00				

Table E.1: Experimental data for the semicircular duct (cont.)

Set No. 4 – 19
Branches A, B and C Active
$P_0 = 316 \; kPa$
$\Delta P = 123 \; kPa$

Branch A, $R = 1026 \; (kg.m)^{-1/2}$				Branch B, $R = 1032 \; (kg.m)^{-1/2}$				Branch C, $R = 1007 \; (kg.m)^{-1/2}$			
h_A $[mm]$	T_o $[^oC]$	$\dot{m}_G$ $[kg/min]$	$\dot{m}_L$ $[kg/min]$	h_B $[mm]$	T_o $[^oC]$	$\dot{m}_G$ $[kg/min]$	$\dot{m}_L$ $[kg/min]$	h_C $[mm]$	T_o $[^oC]$	$\dot{m}_G$ $[kg/min]$	$\dot{m}_L$ $[kg/min]$
18.30	23.2	0.00E+00	2.05E+01	20.19	23.5	0.00E+00	2.04E+01	20.28	23.2	0.00E+00	2.09E+01
16.13	23.2	9.67E-03	1.66E+01	18.29	23.8	1.21E-02	1.69E+01	19.40	23.2	1.01E-02	1.85E+01
14.24	23.6	4.34E-02	1.37E+01	16.30	24.0	5.13E-02	1.45E+01	17.30	23.2	3.49E-02	1.53E+01
12.10	23.3	9.42E-02	1.12E+01	14.69	24.2	1.05E-01	1.11E+01	15.31	23.3	7.64E-02	1.33E+01
10.07	23.4	1.52E-01	8.93E+00	12.59	24.0	2.00E-01	8.34E+00	13.35	23.3	1.32E-01	1.13E+01
7.94	23.4	2.36E-01	6.93E+00	10.49	23.8	2.69E-01	6.77E+00	11.00	23.3	2.05E-01	9.28E+00
5.80	23.4	3.20E-01	5.02E+00	8.43	23.6	3.54E-01	5.41E+00	8.94	23.4	2.71E-01	6.97E+00
3.74	24.3	4.41E-01	2.96E+00	6.36	23.5	4.59E-01	4.04E+00	6.88	23.3	3.49E-01	5.41E+00
1.67	24.1	6.09E-01	1.34E+00	4.19	23.4	5.52E-01	2.78E+00	5.09	23.2	4.32E-01	4.04E+00
-0.12	24.1	7.20E-01	8.07E-01	2.09	23.5	6.63E-01	1.83E+00	0.00	22.6	9.46E-01	0.00E+00
-2.11	24.1	8.43E-01	4.40E-01	-0.04	23.2	7.40E-01	1.03E+00				
-4.32	24.0	9.21E-01	2.21E-01	-2.11	23.1	8.25E-01	5.47E-01				
-8.62	23.7	9.64E-01	0.00E+00	-4.20	22.9	8.97E-01	2.49E-01				
				-7.44	22.9	9.60E-01	0.00E+00				

Table E.1: Experimental data for the semicircular duct (cont.)

Set No. 4 – 20
Branches A, B and C Active
$P_0 = 316 \ kPa$
$\Delta P = 82 \ kPa$

Branch A, $R = 1023 \ (kg.m)^{-1/2}$				Branch B, $R = 1022 \ (kg.m)^{-1/2}$				Branch C, $R = 1022 \ (kg.m)^{-1/2}$			
h_A $[mm]$	T_o $[^oC]$	$\dot{m}_G$ $[kg/min]$	$\dot{m}_L$ $[kg/min]$	h_B $[mm]$	T_o $[^oC]$	$\dot{m}_G$ $[kg/min]$	$\dot{m}_L$ $[kg/min]$	h_C $[mm]$	T_o $[^oC]$	$\dot{m}_G$ $[kg/min]$	$\dot{m}_L$ $[kg/min]$
16.80	22.2	0.00E+00	1.68E+01	18.38	22.4	0.00E+00	1.68E+01	19.46	19.0	0.00E+00	1.68E+01
14.80	22.8	1.06E-02	1.40E+01	16.52	23.1	9.72E-03	1.45E+01	17.29	18.9	1.58E-02	1.39E+01
13.05	22.5	3.95E-02	1.16E+01	14.52	23.7	4.87E-02	1.14E+01	15.19	19.1	4.62E-02	1.15E+01
11.20	23.8	7.56E-02	9.64E+00	12.42	23.6	1.31E-01	8.14E+00	13.02	19.5	9.50E-02	9.32E+00
9.13	24.6	1.26E-01	7.83E+00	10.32	23.6	2.09E-01	6.38E+00	10.92	19.8	1.60E-01	7.79E+00
7.10	25.2	1.99E-01	6.23E+00	8.18	23.5	2.98E-01	4.63E+00	8.85	20.0	2.44E-01	6.19E+00
4.61	26.2	2.93E-01	4.59E+00	5.95	23.1	3.91E-01	3.42E+00	6.75	20.3	3.26E-01	4.74E+00
2.55	26.4	3.80E-01	2.88E+00	3.85	21.9	5.05E-01	2.22E+00	4.62	20.6	4.19E-01	3.26E+00
0.93	26.9	4.99E-01	1.56E+00	1.75	21.9	6.14E-01	1.38E+00	2.52	20.8	5.24E-01	1.69E+00
-1.13	27.1	6.40E-01	6.18E-01	-0.39	22.4	6.91E-01	7.61E-01	0.77	21.0	6.83E-01	4.14E-01
-3.20	27.0	7.98E-01	2.61E-01	-2.48	20.4	7.77E-01	3.34E-01	0.00	21.1	8.48E-01	0.00E+00
-10.10	25.8	8.82E-01	0.00E+00	-6.08	19.2	8.47E-01	0.00E+00				

Table E.1: Experimental data for the semicircular duct (cont.)

Set No. 4 – 21 *Branches A, B and C Active* P_0 = 316 *kPa* ΔP = 40 *kPa*											
Branch A R = 1000 $(kg.m)^{-1/2}$				*Branch B* R = 1000 $(kg.m)^{-1/2}$				*Branch C* R = 992 $(kg.m)^{-1/2}$			
h_A $[mm]$	T_o $[^oC]$	$\dot{m}_G$ $[kg/min]$	$\dot{m}_L$ $[kg/min]$	h_B $[mm]$	T_o $[^oC]$	$\dot{m}_G$ $[kg/min]$	$\dot{m}_L$ $[kg/min]$	h_C $[mm]$	T_o $[^oC]$	$\dot{m}_G$ $[kg/min]$	$\dot{m}_L$ $[kg/min]$
14.14	23.4	0.00E+00	1.20E+01	15.13	20.8	0.00E+00	1.20E+01	16.51	21.7	0.00E+00	1.21E+01
12.11	23.6	7.70E-03	9.40E+00	12.81	21.6	2.40E-02	9.13E+00	14.37	21.9	1.74E-02	9.28E+00
9.34	24.1	4.58E-02	6.93E+00	10.75	22.2	8.84E-02	6.58E+00	12.38	22.2	4.57E-02	7.36E+00
7.28	24.4	8.38E-02	5.60E+00	8.64	22.6	1.77E-01	4.24E+00	10.20	22.5	9.44E-02	5.80E+00
5.17	25.2	1.41E-01	4.70E+00	6.58	23.0	2.40E-01	3.30E+00	8.07	22.7	1.67E-01	4.63E+00
3.04	25.7	2.22E-01	3.95E+00	4.54	23.3	3.09E-01	2.36E+00	6.00	22.8	2.52E-01	3.46E+00
0.94	25.7	2.87E-01	2.83E+00	2.48	23.4	3.97E-01	1.59E+00	3.87	23.0	3.38E-01	2.17E+00
-1.17	26.1	3.67E-01	1.41E+00	0.33	19.0	5.03E-01	8.32E-01	2.26	23.0	4.14E-01	1.12E+00
-3.27	26.2	5.59E-01	3.47E-01	-1.70	18.9	5.97E-01	3.64E-01	0.72	23.0	5.21E-01	2.81E-01
-5.33	26.3	6.39E-01	9.27E-02	-5.34	18.4	6.78E-01	0.00E+00	0.00	23.0	6.44E-01	0.00E+00
-9.40	26.3	6.91E-01	0.00E+00								

Table E.1: Experimental data for the semicircular duct (cont.)

Set No. 4 – 22 *Branches A, B and C Active* P_0 = 517 kPa ΔP = 123 kPa											
Branch A R = 1012 $(kg.m)^{-1/2}$				*Branch B* R = 1007 $(kg.m)^{-1/2}$				*Branch C* R = 993 $(kg.m)^{-1/2}$			
h_A $[mm]$	T_o $[^oC]$	$\dot{m}_G$ $[kg/min]$	$\dot{m}_L$ $[kg/min]$	h_B $[mm]$	T_o $[^oC]$	$\dot{m}_G$ $[kg/min]$	$\dot{m}_L$ $[kg/min]$	h_C $[mm]$	T_o $[^oC]$	$\dot{m}_G$ $[kg/min]$	$\dot{m}_L$ $[kg/min]$
19.10	20.8	0.00E+00	2.08E+01	20.56	21.7	0.00E+00	2.09E+01	21.12	20.3	0.00E+00	2.12E+01
17.03	21.1	1.63E-02	1.84E+01	18.84	21.5	1.52E-02	1.88E+01	19.04	20.6	2.61E-02	1.84E+01
14.96	21.4	6.14E-02	1.51E+01	16.73	22.2	7.31E-02	1.54E+01	16.97	21.2	6.47E-02	1.54E+01
12.78	21.9	1.29E-01	1.26E+01	14.65	22.4	1.61E-01	1.18E+01	14.90	21.7	1.31E-01	1.34E+01
10.71	22.1	2.08E-01	1.02E+01	12.58	23.1	2.76E-01	8.93E+00	12.76	22.2	2.14E-01	1.13E+01
8.63	23.4	3.10E-01	8.14E+00	10.40	23.1	3.70E-01	7.40E+00	10.62	22.7	3.14E-01	9.32E+00
6.49	23.5	4.44E-01	5.87E+00	8.26	23.1	5.01E-01	5.72E+00	8.59	23.2	4.04E-01	7.36E+00
4.38	23.5	6.09E-01	3.95E+00	6.20	23.1	6.17E-01	4.43E+00	6.48	23.4	5.02E-01	5.48E+00
2.31	23.5	8.17E-01	1.73E+00	4.13	23.1	7.59E-01	2.99E+00	4.35	23.6	6.26E-01	3.80E+00
0.24	23.3	9.84E-01	9.40E-01	2.03	23.1	8.66E-01	1.94E+00	1.90	23.6	7.80E-01	1.82E+00
-2.32	23.1	1.14E+00	5.10E-01	-0.15	23.0	9.88E-01	1.12E+00	0.77	23.6	8.85E-01	1.07E+00
-4.53	22.9	1.22E+00	2.05E-01	-2.21	22.9	1.10E+00	5.62E-01	0.00	23.5	1.22E+00	0.00E+00
-8.67	20.8	1.28E+00	0.00E+00	-4.27	22.5	1.19E+00	2.41E-01				
				-7.44	22.5	1.22E+00	0.00E+00				